Long-term plasticity of excitatory inputs onto identified hippocampal neurons in the anaesthetized rat

---

A thesis submitted for the degree of
Doctor of Philosophy
Michaelmas Term 2015



Petrina, Yau Pok, Lau

Somerville College

University of Oxford

For Hau Shing Lau

Abstract

Long-term plasticity of excitatory synapses onto identified hippocampal neurons in anaesthetized rat

Petrina, Yau-Pok, Lau

Somerville College, University of Oxford

Thesis submitted for the degree of *Doctor of Philosophy* in Michaelmas Term 2015

Use-dependent long-term plasticity in synaptic connections represents the cellular substrate for learning and memory. The hippocampus is the most thoroughly investigated brain area for long-term synaptic plasticity, long-term potentiation (LTP) and long-term depression (LTD) are both well characterized in glutamatergic excitatory connections between hippocampal principal cells *in vitro* and *in vivo*. An increasing number of studies based on acute brain slice preparations report LTP and LTD in excitatory synapses onto postsynaptic hippocampal GABAergic inhibitory interneurons. However, a systematic study of activity-induced long-term plasticity in excitatory synaptic connections to inhibitory GABAergic interneurons *in vivo* is missing. To determine whether LTP and LTD occur in excitatory synaptic connections to the hippocampal CA1 area GABAergic interneurons types in intact brain, I have used juxtacellular recording to measure synaptically evoked short-delay postsynaptic action potential probability in identified CA1 neurons in the urethane-anaesthetized rats.

Plasticity in excitatory synaptic connections to CA1 cell types was measured as a change of afferent pathway stimulation-evoked postsynaptic spike probability and delay. In

the study only experiments with monosynaptic-like short-delay (range 3-12 ms) postsynaptic spikes phase-locked to afferent stimulation were used. Afferent fibres were stimulated from the CA1 area of the hippocampus at the contralateral (left) side to avoid simultaneous monosynaptic activation of GABAergic fibres and to exclude antidromic spikes in recorded CA1 cells (in right hemisphere). Plasticity in pathways was tested using theta-burst high-frequency stimulation (TBS, 100 pulses), which is one of the most common synaptic plasticity induction protocols in acute brain slice studies.

I discovered that TBS elicited permanent potentiation in single shock-evoked postsynaptic spike probability with shortening or no change in evoked spike latency in various postsynaptic neuron types including three identified pyramidal cells and parvalbumin-expressing (PV+) interneurons. Most fast-spiking PV+ cells showed LTP including an axo-axonic cell and one bistratified cell, whereas two identified basket cells exhibited LTD in similar experimental conditions. In addition, I discovered diverse plasticity in non-fast spiking interneurons, reporting LTP in an ivy cell, and LTD in three incompletely identified regular-spiking CA1 interneurons. I report that the underlying brain state, defined as theta oscillation (3-6 Hz) or non-theta in local field potential, failed to explain whether LTP, LTD or no plasticity was generated in interneurons.

The results show that activity-induced potentiation and depression similar to LTP and LTD also occur in excitatory synaptic pathways to various CA1 interneurons types *in vivo*. I propose that long-term plasticity in excitatory connections to inhibitory interneurons may be take place in learning and memory processes in the hippocampus.

Total word counts about 45, 000

Declaration

The work described in this thesis was carried out in the MRC Anatomical Neuropharmacology Unit and at the Department of Pharmacology, University of Oxford, between October 2010 and January 2015 under the supervision of Dr Karri Lamsa and co-supervision of Dr Peter Magill. The research presented in this thesis is my own original work, with the exceptions outlined below.

Mr Ben Micklem (MRC, Anatomical Neuropharmacology Unit, University of Oxford, *UK*) helped assembling the DAB reconstruction drawings presented in Chapter 3, figure 3.7C. Dr Joseph Somogyi (MRC, Anatomical Neuropharmacology Unit, Oxford University) helped me to do semi-quantitative fluorophore spectral analysis of the measurements I performed by myself.

I adopted the theta oscillation analysis script created by Dr John Tukker (MRC Anatomical Neuropharmacology unit, Oxford, *UK*), with the permission, to define significant LFP theta oscillations described in Chapter 2.4.2.

No part of this thesis has been submitted for any other publication.

Acknowledgement

I would like to express my sincere gratitude to my primary supervisor, Dr Karri Lamsa, for his patience and guidance through every stage of this research project, and my secondary supervisor, Prof. Peter Magill for his ideas, advice, and encouragement. This project would have not achieved the present stage without their constant support and supervision. I also would like to thank Prof. Peter Somogyi for sharing his enthusiasm and deep understanding for science. I sincerely thank all of them for their genuine interest in my project and in my personal development.

I am grateful to have the opportunity to engage in intellectually curious Neuroscience Community in Oxford, the discussions with different members have been most fruitful and they aided my growth in science and in person. Secondly, I would like to thank my advisors Profs. Peter Somogyi and Trevor Sharp for their critical reviews on the project, in the middle of my study. Their advice assured me to progress and encouraged me to continue and pursue this exciting and challenging project. I thank all my supervisors and advisors sincerely for intellectual scientific discussions during my training, which has had enormous impact in personal development in the past few years.

I am very thankful for Prof. Paul Bolam for his smiling face of encouragement and taking many aspect of this project administration under his wings selflessly. I would also like to thank Profs. Peter Somogyi, Paul Bolam, Pete Magill and Jozsef Csicsvari and members of their group for generously sharing their lab equipment and expertise during the whole course of this project. In particular, I thank Drs Kouichi *Nakamura*, Andrew Sharott, and Nicolas Mallet for their valuable demonstrations of juxtacellular recording and thank Drs Tim Viney and Linda Katona on sharing their knowledge on local field oscillation analysis.

Special thank goes to Drs Peter Flaxman and Henrike Hartung for their contributions on developing stimulation electrodes that I have relied on throughout my study. I have benefited enormously from Dr Joseph Somogyi's meticulous demonstration on confocal microscopy and I thank him, and I thank Drs Gunes Unal, Ms Wendy Tynan, and Mrs Kristina Wagner, for their knowledge and support on immunohistochemical processing and evaluation. I am also grateful for Dr. Andras Szabo and Ms Kathryn Newton for getting me started in the anatomical aspects of my project and assisting in daily practical routines.

Sincere thanks to Mrs Liz Norman and her team in the animal unit. Last but not least, I thank all the supporting staff in the Department of Pharmacology and the MRC Anatomical Neuropharmacology Unit for their helps in many small, but significant practical issues.

Personally, I would like to express my sincere gratitude to my friends, Siron, Wiebke, Esther, Timothy, Jamie, Dimitrios, Judith, Kristina, Linda, Leo, Terry, May, Samuel, Harvey, Hayley, Tony, Bolton, and KJ, for their constant support and cheering. I am forever grateful to my parents, who always believed in me and have given me chance to explore my passion in science.

Contents

Abstract.....

Declaration ..... **iii**

Acknowledgement.....**iv**

Contents.....**vi**

Abbreviations ..... **xii**

1. Introduction.....**1**

1.1. Synaptic plasticity in the hippocampus as a cellular substrate for learning and memory **1**

1.1.1. Hebbian postulate of associative learning and NMDA receptor as a co-incidence detector1

1.1.2. *In vivo* evidence for the hippocampal LTP as a memory storage mechanism.....4

1.1.3. Parallel LTP and LTD in inhibitory interneurons in acute brain slice experiments …….. 6

1.2. The roles of GABAergic inhibition in principal cells network function in the hippocampus.....**10**

1.2.1. Disynaptic inhibition regulates the temporal fidelity of CA1 pyramidal cells input-output operation.....10

1.2.2. Interneurons are pivotal for the gamma, theta and sharp wave oscillations in the hippocampal CA1 area.....12

1.2.3. Compromised synaptic inhibition generates pathological synchronous neuronal activity ……. 17

1.3. Context of this study.....**20**

1.3.1. Previous findings on interneuron long-term plasticity *in vitro*.....20

1.3.2. Aims of this research and content of chapters 21

2. Materials and methods 24

2.1. Experimental animals and anaesthesia 25

2.2. Surgical procedures 26

2.3. Electrophysiological experiments 28

2.3.1. Microelectrode recording of the LFP and extracellular spikes 28

2.3.2. Afferent electrical stimulation to evoke synaptic responses 30

2.3.3. Recording postsynaptic spikes and juxtacellular cell labelling 32

2.4. Electrophysiology data acquisitions and analyses 34

2.4.1. Single spike sorting 34

2.4.2. Spontaneous oscillations in the LFP 36

2.4.3. Analyses of single cell spike firing phase during the LFP theta oscillation 38

2.4.4. Plasticity analyses of stimulus-evoked postsynaptic spike 39

2.4.5. Data analyses and statistics 40

2.5. Anatomical processes and analyses 42

2.5.1. Perfusion of rat brain and fixation 42

2.5.2. Fixed brain sectioning and neurobiotin-filled cell visualization 43

2.5.2.1. Freeze and thaw 44

2.5.3. Immunohistochemistry 45

2.5.3.1. Immunohistological staining 46

2.5.4. Acquisition and evaluation of fluorescence images 47

2.5.5. Digital fluorescence image reconstruction 50

2.5.5.1. DAB reaction and image reconstruction 51

2.5.6. Figures and tables 55

3. Synaptic excitation of distinct CA1 area neuron types by stimulation from contralateral hippocampus 67

3.1. Introduction.....68

3.2. Results.....70

3.2.1. Defining putative monosynaptic excitatory connection to CA1 hippocampal neurons when electrically stimulating contralateral hippocampus 70

3.2.2. Synaptic excitation of CA1 pyramidal cells by contralateral stimulation 74

3.2.2.1. Pyramidal cells exhibit low level of spontaneous firing in the anaesthetised rat 76

3.2.2.2. CA1 area pyramidal cell firing is phase-coupled to the trough of local field potential theta cycles.....76

3.2.2.3. Pyramidal cells have slow action potential kinetics 77

3.2.2.4. Pyramidal cells exhibit occasionally short-interval action potential bursts known as complex spikes.....78

3.2.2.5. Juxtacellular labelling and post hoc visualization confirms pyramidal cell identity .... …….. 79

3.2.3. Synaptic excitation of postsynaptic CA1 area interneurons from the contralateral side 80

3.2.3.1. Subpopulation of interneurons is revealed by fast postsynaptic action potential kinetics ……..80

3.2.3.2. PV+ interneurons show high rate of spontaneous firing or coupling to LFP theta cycles that differ from pyramidal cells.....81

3.2.3.3. Other electrophysiological properties that indicate CA1 interneuron but were not used here to categorise neurons.....83

3.2.3.4. Confirming non-pyramidal cell anatomical structure in post hoc analysis of juxtalabelled cells.....84

3.3. Discussion 85

3.3.1. Electrical stimulation from the contralateral hippocampus elicits fEPSP and postsynaptic spike in the CA1 area with monosynaptic transmission characteristics 85

3.3.2. Excitatory connections from contralateral hippocampus with monosynaptic characteristics target CA1 pyramidal cells and various type of interneurons.....87

3.3.3. Anatomical pathways behind monosynaptic connections between the left and right CA1 areas 89

3.4. Figure and table 90

4. Activity-induced long-term potentiation in excitatory hippocampal fibres to CA1 area pyramidal cells *in vivo* 105

4.1. Introduction 106

4.2. Results 107

4.2.1. A common LTP-induction paradigm elicits long-term potentiation of excitatory synaptic connection to CA1 pyramidal cells *in vivo* 107

4.2.1.1. Synaptically-evoked postsynaptic action potentials during baseline and following TBS 110

4.2.1.2. Pyramidal cell spontaneous firing and brain states during plasticity experiments 112

4.3. Discussion 113

4.3.1. Robust LTP in excitatory synaptic connections to CA1 pyramidal cells 114

4.3.2. Synaptically-evoked spike distribution in the pre- and post-TBS supports observations on monosynaptically evoked spike 116

4.4. Figures and table 118

5. Afferent excitatory pathway long-term plasticity in CA1 fast-spiking PV+ interneurons 125

5.1. Introduction 126

5.2. Results 128

5.2.1. Long-term plasticity study in fast-piking postsynaptic PV+ interneurons 128

5.2.2. Plastic change in synaptically evoked postsynaptic action potentials following TBS 130

5.2.2.1. Spontaneous firing properties of postsynaptic PV+ cells in the plasticity experiments 132

5.2.2.2. Identification of postsynaptic fast-spiking interneuron types in plasticity experiments 134

5.2.2.3. Plasticity in identified perisomatic-targeting PV+ basket- and axo-axonic cells ...135

5.2.2.4. Plasticity in other fast-spiking PV+ interneurons ...137

5.3. Discussion ...138

5.3.1. Plasticity in identified PV+ cell types *in vivo* ...139

5.3.2. Possible factors affecting polarity of long-term plasticity in PV-expressing interneurons ...141

5.4. Tables and figures ...143

6. Excitatory pathway long-term plasticity to other CA1 neuron types ...157

6.1. Introduction ...158

6.2. Results ...160

6.2.1. Long-term plasticity in anatomically analysed non-fast spiking CA1 interneurons ...160

6.2.1.1. LTP in an ivy cell ...161

6.2.1.2. LTD in unidentified regular-spiking CA1 interneuron ...162

6.2.1.3. LTD in CA1 non-fast spiking interneurons lacking anatomical analysis and cell type identity ...163

6.3. Discussion ...165

6.3.1. Diversity of long-term plasticity results in non-fast spiking CA1 interneurons *in vivo* ...165

6.4. Table and figures ...168

7. Contribution of brain state and postsynaptic firing level to plasticity in the CA1 area neurons ...180

7.1. Introduction ...181

7.2. Results ...182

7.2.1. Potential impact of postsynaptic cell spontaneous firing level and hippocampal brain state on the excitatory pathway long-term plasticity ...183

7.2.1.1. Spontaneous firing level of postsynaptic cells in the plasticity experiments ...184

7.2.1.2. Brain states during the TBS determined by LFP oscillations 184

7.2.2. Postsynaptic cell excitation level and action potential discharge during the TBS 185

7.2.2.1. Quantifying postsynaptic cell action potential firing during the TBS 186

7.2.2.2. Comparison of afferent pathway strength and plasticity 187

7.3. Discussion 187

7.3.1. Robust brain state-independent plasticity in pyramidal cells 188

7.3.2. Qualitative differences in the interneuron plasticity are poorly explained by brain states or target cell firing level 189

7.4. Figures 192

8. General Discussion 198

8.1. Summary of findings 199

8.2. Functional implications of use-dependent LTP and LTD in excitatory input to interneurons 204

8.2.1. Possible role in hippocampus-based learning and spatial memory 205

8.2.2. Interneuron LTP and LTD in pathological processes 207

8.3. Other mechanisms contributing to long-term changes in CA1 interneurons input-output function 209

8.4. Future directions 211

8.5. Final conclusions 213

9. Reference 214

Abbreviations

DAB	3,3'-Diaminobenzidine tetra-hydrochloride
AAC	axo-axonic cell
AMPA(R)	α-amino-3-hydroxy-5-methylisoxazole-4-propionic acid (receptor)
ANOVA	analysis of variance
BC	basket cell
CA	cornu ammonis
CB1R	cannabinoid receptor 1
CCK	cholecystokinin
DG	dentate gyrus
EC	entorhinal cortex
(f)EPSP	(field) excitatory postsynaptic potential
GABA	gamma-aminobutyric acid
ISI	interspike interval
LTP	long-term potentiation
NGS	normal goat serum
NHS	normal horse serum
NMDA(R)	*N*-methyl-D-aspartate (receptor)
nNOS	neuronal nitric oxide synthase
NPY	neuropeptide Y
O-LM	oriens-lacunosum moleculare
PB	phosphate buffer
PBS	phosphate buffered saline
PV	parvalbumin
str.luc.	stratum lucidum
str.l.-m.	stratum lacunosum-moleculare
str.ori.	stratum oriens
SOM	somatostatin
str.pyr.	stratum pyramidale
str.rad.	stratum radiatum
str.	stratum
TBS	Theta modulated high frequency burst afferent fibre stimulation
TBSa	0.1 M Trizma® based saline with 0.03% Azide
TBS-Tx	Tris-buffered saline with 0.3% Triton X-100

1. Introduction

1.1. Synaptic plasticity in the hippocampus as a cellular substrate for learning and memory

1.1.1. Hebbian postulate of associative learning and NMDA receptor as a co-incidence detector

A Canadian psychologist and neuroscientist Donald Hebb published his famous theory of cellular mechanisms of learning in 1949. Although this famous postulate did not reveal any actual molecular or biological mechanism behind learning processes in the brain, it established an idea that associative function of neurons involved in learning process triggers a biological process, which specifically and selectively leads to strengthening of communication between these cells. This postulate is known as "Hebbian theory" and it has ever since has become one of the most cited statements in literature of cellular neuroscience. Below is a quote to Hebb's original text published in 1949.

"Let us assume that the persistence or repetition of a reverberatory activity (or "trace") tends to induce lasting cellular changes that add to its stability… When an axon of cell A is near enough to excite a cell B and repeatedly or persistently takes part in firing it, some growth process or metabolic change takes place in one or both cells such that A's efficiency, as one of the cells firing B, is increased."

Experiments in cellular neuroscience have demonstrated that Hebb's postulate generally describes well what happens in neuronal circuits during learning processes at the synaptic level. More than six decades of investigation have been able to identify key biological processes where associative firing of pre- and postsynaptic neuron results in permanent potentiation of the synapses activated between them. For simplicity, I will focus here on the history of studies in the hippocampus.

A key step in understanding cellular processes that underlie learning and memory was made in late 1960s in work by Drs Terje Lømo, Per Andersen, and Tim Bliss in the University of Oslo, Norway. They discovered that activating the perforant path axons to dentate granule cells with brief trains of electrical stimuli in anaesthetized rabbits resulted in increased efficiency of transmission in these synapses that could last for hours (Bliss and Lomo, 1973, Lomo, 2003). Their work resulted in a publication reporting long-term potentiation (LTP) in excitatory perforant pathway synapses to dentate gyrus area (Bliss and Lomo, 1973).

Importantly, a series of studies soon after discovered that activation of co-incidence detector, identified as postsynaptic glutamate *N*-methyl *D*-aspartate receptor (NMDAR), has a central role in LTP induction in hippocampal glutamatergic excitatory synapses (Bliss and Collingridge, 1993, Liu et al., 2004). The glutamate NMDAR-dependent LTP has become a standard model for memory formation, and it exhibits several properties of Hebbian rule;

input specificity, associativity, co-operatively, and persistence (Hebb, 1949). First, activation of postsynaptic NMDARs requires associative activity of pre- and postsynaptic cell(s) in order to release extracellular magnesium ion (Mg^{2+}) block of NMDARs by postsynaptic cell depolarization, driven by repetitive release of glutamate from presynaptic cell(s) (Nowak et al., 1984). Second, this mechanism is restricted to active synapses only hence it is input specific (Mcnaughton et al., 1978). Third, it is co-operative, since postsynaptic NMDAR activation can be achieved by simultaneous activity of several weak excitatory inputs, which would be too weak to depolarize the postsynaptic cell enough to release Mg^{2+} block alone (Ault et al., 1980, Mayer and Westbrook, 1984, Nowak et al., 1984). Fourth, it is persistent and experiments in rodents have demonstrated it can last up to several months, but possibly even longer (Abraham, 2003).

Although NMDAR-dependent LTP has an established role as cellular substrate for learning and memory, it is important to note that it does not represent the only activity-induced synaptic potentiation mechanism in the hippocampus. For instance, NMDAR-dependent LTP is the main synaptic long-term potentiation mechanism in glutamatergic CA1 pyramidal cell synapses, but synaptic long-term plasticity mechanisms in synapses to CA1 interneurons are in most cases NMDAR-independent (Lamsa et al., 2007b, Kullmann and Lamsa, 2011). In addition, hippocampal mossy fibres from dentate gyrus glutamatergic granule cells to CA3 pyramidal cells exhibit NMDAR-independent LTP (Nicoll and Schmitz, 2005, Galvan et al., 2008).

1.1.2. *In vivo* evidence for the hippocampal LTP as a memory storage mechanism

Perhaps most compelling evidence for glutamate NMDARs playing role in persistent memory formation came from behavioural experiments in which the function of these receptors is compromised or blocked either pharmacologically or using genetic approaches. In a series of studies in 1980s and 1990s Dr Richard Morris used the Morris water maze to study spatial learning and memory in rats (Morris, 1984). In these experiments rats were placed to swim in a water pool filled with murky water until they found an underwater hidden platform to rest. Repositioning of the hidden platform was used to test learning skills. In one group of animals, a highly specific NMDAR antagonist APV hippocampus was applied into hippocampus, and the APV-treated animals showed significantly impaired learning of novel platform positions in the pool, as compared to their controls (Morris et al., 1986). Applying the drug in the hippocampus was relevant because this brain area comprises neuronal circuits for spatial learning and memory (O'Keefe and Nadel, 1978) (see Chapter 1.2.2.). The CA1 area in hippocampus contains so called place cells, pyramidal neurons that are active as a unique combination in specific loci of an environment that the animal is familiar with and in which it has learned to navigate (O'Keefe and Nadel, 1978). A paper by McHugh and colleagues in 1996 demonstrated that genetic ablation of NMDAR (via GluN1 knock-out) in the hippocampal CA1 region impaired generation of these place cell combinations in novel environments (McHugh et al., 1996). They found that place cell representations of spatial loci were less specific in the mice with genetically compromised NMDARs in CA1 pyramidal cells. These mice also exhibited poor spatial long-term learning in novel environments.

NMDAR-mediated LTP's role in hippocampal memory function has gained further support from experiments where critical biochemical steps in LTP, triggered by activation of NMDARs but independent of them once activated, have been genetically compromised. Early key studies in this regard were experiments, which demonstrated impaired spatial long-term learning skills in mice with genetically compromised CamKII enzyme (Cho et al., 1998, Giese et al., 1998). Activation of CamKII is a prerequisite for establishment of synaptic long-term potentiation in CA1 pyramidal cells, and this is triggered by NMDAR-mediated calcium influx into pyramidal cells spines (Sanhueza and Lisman, 2013).

As a summary various results in the literature convincingly show that LTP in pyramidal cells involving NMDAR-activation plays a central role in learning processes in the hippocampus. However, it is also noteworthy that the same behavioural tests that showed dependence of spatial learning and place cell formation on NMDARs, reported that the processes are not fully dependent on this mechanisms (Tsien et al., 1996, Nakazawa et al., 2004). This indicates that in addition, some other pharmacologically and molecularly distinct processes operate in memory encoding in parallel with NMDAR-dependent LTP in pyramidal cells.

1.1.3. Parallel LTP and LTD in inhibitory interneurons in acute brain slice experiments

In addition to LTP in excitatory synapses to pyramidal cells, similar or analogous activity-induced potentiation mechanisms have been shown to occur in the CA1 area excitatory synapses to inhibitory GABAergic interneurons (Lawrence and McBain, 2003, Laezza and Dingledine, 2011). However, studies on long-term plasticity in hippocampal interneurons have given diverse results, which have been confusing in a sense that although significant LTP or LTD have been reported in CA1 interneurons, results were often inconsistent when studied in large populations of CA1 interneurons (Kullmann and Lamsa, 2007). It has been demonstrated that one explanation for inconsistent LTP results in the CA1 area interneurons is cell type specificity (Nissen et al., 2010). Postsynaptic CA1 interneurons identified by their anatomical features and molecular expression properties exhibit different long-term plasticity in their glutamatergic afferents. Plasticity results in similar identified postsynaptic CA1 area interneuron types are consistent (Perez et al., 2001, Nissen et al., 2010, Szabo et al., 2012, Camire and Topolnik, 2014) although may still vary depending on loci of excitatory inputs to the cell tested (Sambandan et al., 2010, Le Roux et al., 2013) and the cells activity history, which can lead to internalization of plasticity-regulating receptors (Pelkey et al., 2008, Sambandan et al., 2010). The hippocampal interneuron population represents a diverse group of neurons and the CA1 area alone comprises more than 20 identified cell types according to their anatomical and molecular properties (Freund and Buzsaki, 1996, Somogyi and Klausberger, 2005). These neurons developmentally emerge

from at least three different brain sub-regions during early ontogeny (Butt et al., 2005, DeFelipe et al., 2013, Matta et al., 2013, Kepecs and Fishell, 2014).

A picture emerging from hippocampal acute brain slice studies is that although glutamate NMDAR-dependent LTP does occur also in some CA1 area interneurons, it is not the only prevalent synaptic LTP mechanism in these cells (Moreau and Kullmann, 2013). On the contrary, in most synapses LTP is independent of NMDAR. However, NMDAR-LTP has been reported in at least in a subset of synapses innervating CA1 area fast-spiking (putative PV+) basket cells (Le Roux et al., 2013). Similarly, it has been reported that glutamatergic axon collaterals in *stratum radiatum* (likely to represent Schaffer collaterals from the CA3 pyramidal cells) exhibit NMDAR-dependent LTP in a subset of interneurons whose soma locate in that layer (Lamsa et al., 2005, Lamsa et al., 2007a). However, unlike in pyramidal cells their NMDAR-dependent LTP in interneurons does not require the alpha CaMKII isoform (Lamsa et al., 2007a).

In most CA1 area interneurons LTP is evoked by high-frequency stimulation in the presence of full NMDAR blockade (Perez et al., 2001, Le Roux et al., 2013, Camire and Topolnik, 2014) . The most commonly used stimulation paradigm for LTP induction in these experiments has been theta modulated high frequency burst afferent fibre stimulation (TBS) (Kullmann and Lamsa, 2011). Stimulating glutamatergic fibres with this stimulation paradigm has been reported to result in LTP in identified CA1 interneuron types in slices; Oriens-

lacunosum moleculare (O-LM) cells, PV+ expressing basket and axo-axonic cells, neuronal nitric oxide synthase (nNOS), and neuropeptide-Y (NPY) expressing ivy cells. On the other hand, the paradigm failed to elicit LTP in similar conditions in cholecystokinin (CCK) expressing CA1 interneuron types including CCK+ basket cells and Schaffer collateral expressing cells (Perez et al., 2001, Oren et al., 2009, Nissen et al., 2010, Szabo et al., 2012, Campanac et al., 2013). In addition, the TBS-induced potentiation of synaptic input strength can be associated with an increase intrinsic excitability of target cell. This has been reported at least in some CA1 area interneurons (Ross and Soltesz, 2001, Campanac et al., 2013).

Importantly, plasticity experiments in the CA1 area have also revealed that LTP induction in pyramidal cells and interneurons can be washed-out by dialyzing cell cytoplasm in whole-cell recording conditions, which is the most common state-of-the-art technique currently used in LTP experiments (Isaac et al., 1996, Lamsa et al., 2005). Hence, an objective approach to study LTP would be to use minimally dialyzing recording methods such as the perforated-patch whole cell technique (Lamsa et al., 2007a), or extracellular recording of the cell input-output relation (Buzsaki and Eidelberg, 1982b).

Another feature of long-term plasticity in glutamatergic synapses in CA1 interneurons is that TBS and other high-frequency afferent stimulation patterns can also elicit LTD is some interneurons (Nissen et al., 2010, Peterfi et al., 2012). Although it not entirely clear why this happens, there are some explanations offered by previous studies. First, some identified CA1

interneuron types in slices regularly generate LTD rather than LTP although afferent stimulation and postsynaptic parameters are kept similar in all tested cells. As an example, PV+ bistratified cells in the CA1 area failed to show LTP in a slice study, and only exhibited LTD even when studied using a minimally dialyzing perforated patch recording technique (Nissen et al., 2010). Second, different activation of endogenous modulators by distinct stimulation pattern may result in different plasticity. A recent study demonstrated that activation of cannabinoid receptors in glutamatergic terminals to PV+ cells by endocannabinoids, generates LTD. Importantly, the same study showed that LTD is not restricted to bistratified cells, but in addition occurs in PV+ basket cells (Peterfi et al., 2012). Third, the outcome of a plasticity induction experiment may depend on recent activity history of the cell. This has been most thoroughly demonstrated in CA3 area interneurons (Pelkey et al., 2008) in which a preceding high-frequency stimulation can lead to internalization of the group III metabotropic glutamate receptor mGluR7 in synapses leading to a switch of direction in plasticity elicited when the same afferent stimulation is applied again (Pelkey et al., 2008). However, the significance of this switch to hippocampal function is not clear.

Some recent studies using whole cell recording in the hippocampal CA1 area, putative O-LM cells showed that intense postsynaptic cell spiking can result in long-lasting potentiation of glutamatergic synapses to these cells too (Nicholson and Kullmann, 2014). Overall, slice experiments show that CA1 inhibitory interneurons have evolved with various mechanisms for long-term plasticity of afferent excitatory synapses. However, what remains

still unknown is whether any of these or other similar forms of plasticity take place in the CA1 interneuron types in the intact brain of a living animal.

1.2. The roles of GABAergic inhibition in principal cells network function in the hippocampus

1.2.1. Disynaptic inhibition regulates the temporal fidelity of CA1 pyramidal cells input-output operation

Acute slice work allows simple experiments to demonstrate the computational role of inhibitory GABAergic transmission in the hippocampal CA3-CA1 area neuronal network. A simple experimental design in hippocampal slice preparations with two afferent pathway stimulations demonstrated a critical role for the feed-forward inhibition in input-output function of the CA1 pyramidal cells (Pouille and Scanziani, 2001, Lamsa et al., 2005, Pavlov et al., 2011b). Excitatory CA3 axon collaterals that monosynaptically innervate postsynaptic CA1 pyramidal cells also activate feed-forward GABAergic inhibitory interneurons in the CA1 area. Consequently, strong disynaptic inhibition shortly follows monosynaptic excitatory input in CA1 pyramidal cells and reduces the time window for excitation to a few milliseconds (Pouille and Scanziani, 2001, Lamsa et al., 2005). The disynaptic IPSC follows the EPSP with 3-5 ms delay and it is associated with prominent shunting conductance that

drops excitability of the postsynaptic cell just a few milliseconds after EPSP peak (Pouille and Scanziani, 2001, Pavlov et al., 2011b). A short time window for effective synaptic excitation determined by the EPSP-IPSC sequence defines temporal resolution for summation of excitatory inputs to the cell and their transformation to an output signal (i.e. firing) (Pouille and Scanziani, 2001). Compromising CA1 inhibitory interneuron activity or strength of GABAergic inhibitory synapses compromises this fast-operating clockwork-like mechanism (Kullmann and Lamsa, 2007). Experiments in slices have demonstrated that temporal integration of excitatory signalling in CA1 pyramidal cells and its transformation to CA1 pyramidal cell firing, shifts from high-resolution co-incidence detection to integration of EPSPs over a broad time window if GABAergic transmission is compromised (Pouille and Scanziani, 2001, Lamsa et al., 2005). Importantly, the same happens if excitatory glutamatergic input into CA1 interneurons is compromised selectively (Lamsa et al., 2005). When disynaptic inhibition is elicited in physiological conditions, fast disynaptic inhibition sets high-resolution temporal encoding of excitatory inputs to CA1 pyramidal cells in narrow time windows, and is responsible for their precise conversion to output signals (Pouille and Scanziani, 2001, Pavlov et al., 2011b). Thus, powerful disynaptic inhibition maintains high throughput in information processing through CA1 pyramidal cells.

Hence, given that fast computational capacity of neuronal networks is considered a parameter of intelligence, these simple experiments on the input integration in brain slices suggest that accuracy of disynaptic inhibition could define a temporal capacity to process input information and transform it to output signals at a high rate (Pouille and Scanziani,

2001). In this situation, it is important that the capacity for fast throughput in information processing is not compromised during the reorganization of synaptic circuits (Kullmann and Lamsa, 2007). Therefore, it has been suggested that synaptic weights should change to balance disynaptic inhibition in hippocampal CA1 circuits in parallel with strengthened pyramidal cell-to-pyramidal cell communication during learning and memory processes to meet these requirements. One possible mechanism to provide dynamic disynaptic inhibition in the CA1 area is activity-induced long-term plasticity in excitatory synapses onto CA1 interneurons (Kullmann and Lamsa, 2007, Dupret et al., 2013). However, it has not been studied whether such plasticity also occurs in intact hippocampus *in vivo*.

1.2.2. Interneurons are pivotal for the gamma, theta and sharp wave oscillations in the hippocampal CA1 area

GABAergic inhibitory interneurons play a pivotal role in the generation and maintenance of coordinated synchronous principal cell activity patterns in neocortex and hippocampus (Hajos and Paulsen, 2009, Lisman and Jensen, 2013). These brain areas exhibit different coordinated synchronous activity patterns in the normal physiological function of the brain (Draguhn et al., 2014). Synchronous oscillatory activities vary according to the behavioural task but the three major oscillation patterns, gamma (30-80 Hz), theta (4-8 Hz) (O'Keefe and Nadel, 1978, Buzsaki, 2002) and sharp wave ripple complexes (SPW-R) mostly occur during cognitive task performances in awake animals and humans, as well as during

sleep (Inostroza and Born, 2013, Gulyas and Freund, 2014). These patterns of coordinated synchronous neuronal activity are associated with learning and memory processing such as memory recall in the hippocampus (Sadowski et al., 2011). Since the hippocampal CA1 area comprises of the storage area for the spatial cognitive map, these activity patterns are well described in the context of spatial memory function (Hartley et al., 2014). Gamma oscillations occur in all cortical areas, whereas theta and sharp waves ripple complexes are specific to the hippocampus and its neighbouring areas (Buzsáki, 2006). Interestingly, in the CA1 area, interneurons have been shown to exhibit cell type specific firing patterns during these oscillation patterns (Somogyi and Klausberger, 2005). Cell type specific firing behaviour during these activity patterns with highly specialized anatomical features of each interneuron type strongly suggests that the distinct GABAergic interneuron types have division of labour in structuring coordinated network activities in the hippocampus (Soltesz, 2006).

The rhythmogenic role of inhibitory interneurons in neuronal networks has been well characterized in the hippocampus (Hajos et al., 2004, Hajos and Paulsen, 2009). Hippocampal PV+ perisoma-targetting inhibitory basket cells generate and maintain coordinated synchronous activity of pyramidal cells at gamma frequency (30-80 Hz) (Penttonen et al., 1998, Butler and Paulsen, 2014). The hippocampal CA3 area contains “gamma generating circuitry”, making hippocampus a good area to investigate cellular mechanisms of network gamma oscillations (Hajos and Paulsen, 2009). Robust gamma oscillations can also be induced in acute hippocampal slice preparations with moderate pharmacological facilitation of neuronal excitability (Whittington et al., 1995, Fisahn et al., 1998). An individual CA3-

CA1 area basket cell targets to about 3000 CA1 pyramidal neurons in rodent hippocampus, and is able to simultaneously entrain large population of pyramidal cells into gamma frequency firing though inhibitory IPSPs (Cobb et al., 1995, Oren et al., 2006, Oren et al., 2010). An important role of PV+ basket cells in the generation of gamma oscillations has been proven with genetic modulations selectively compromising PV+ function (Korotkova et al., 2010). In these experiments, hippocampal gamma oscillations during spatial navigation task have shown altered properties in volume and temporal features (Wulff et al., 2009).

In addition, gamma frequency activity in the hippocampus is also entrained by the excitatory input from entorhinal cortex (Cunningham et al., 2004). In the CA1 area the two gamma activity patterns are focused on distinct laminar layers, revealed by current sink and source analyses (Lasztoczi and Klausberger, 2014). Gamma oscillations in the CA3-CA1 regions most commonly occur in the hippocampus together with theta rhythm (Buzsáki, 2006). Experiments with targeted modulation of the excitatory input to PV+ interneurons have shown that PV+ inhibitory cells contribute to both gamma and theta oscillations (Vreugdenhil et al., 2003, Curley and Lewis, 2012).

Theta oscillations (4-8 Hz) characteristically occur in the hippocampal CA1 area during spatial navigation tasks (O'Keefe and Nadel, 1978, Buzsaki, 2002). Theta rhythm has its origin in the extrahippocampal inputs mainly from two sources; from entorhinal cortex and septum (Kramis et al., 1975, Charpak et al., 1995). These two forms are often referred to as

type 1 and 2 as they have slightly different physical and pharmacological properties (Kramis et al., 1975). Type 1 has higher average frequency (8 Hz) and presumably because it is generated mainly by glutamatergic inputs, it is insensitive to anticholinergic drug atropine. Type 1 is well characterized during locomotion and REM sleep. Type 2 (4-7 Hz) predominates under anaesthesia (including urethane anaesthesia), and anticholinergic compounds pharmacologically block the theta rhythm originated from the septum (Sainsbury et al., 1987).

In the hippocampus, movements are associated with theta and specific features of theta oscillation EEG and pyramidal cells firing during the rhythm have been shown to encode information in the cognitive spatial map (Lisman and Jensen, 2013, Hartley et al., 2014). The hippocampal CA1 and the entorhinal cortex circuitry together comprised the cognitive map of spatial environment (Sasaki et al., 2014). Principal cells in the CA1 area that activated in specific loci of learned spatial environment are called place cells (O'Keefe and Nadel, 1978). The combination of active place cells is unique to each locus of a familiar environment. Interestingly, when animal explores a novel environment learning its way through it, remapping of spatial cognitive map takes place. This is associated with the generation of new place cells (Dragoi and Tonegawa, 2014). New place formation is to take place through cellular mechanisms for memory recording and storage, possibly via synaptic long-term potentiation (O'Keefe and Nadel, 1978, Blum and Abbott, 1996, Muller et al., 1996). Indeed, compromising LTP pharmacologically or using a genetic approach compromises spatial learning in novel environment (Giese et al., 1998, Shapiro, 2001, Cacucci et al., 2007). Most

schematics of hippocampal memory storage have focused to explain learning with plasticity between hippocampal pyramidal cells. However, results in a recent study indicate that in addition some pyramidal cell connections to local fast-spiking interneurons change weight during remapping process (Dupret et al., 2013).

The hippocampal sharp wave ripple (SPW-R) complex is the highest frequency (100-200 Hz) physiological oscillation pattern in hippocampal EEG and LFP (Draguhn et al., 2000). The SPW-Rs are short (50 ms) episodes that occur in the hippocampal CA3-CA1 are during moments of immobility when animal performs a spatial navigation task (Ylinen et al., 1995, Csicsvari et al., 1999, Gulyas and Freund, 2014). Experiments on spatial learning and memory have shown that SPW-Rs in the CA1 area are involved in memory consolidation (Csicsvari and Dupret, 2014). These activity patterns are characterized by organized sequential firing of CA1 pyramidal cells that encode spatial memory (Diba and Buzsaki, 2007) and playing CA1 place cells in reverse order in respect to recent navigation history (Foster and Wilson, 2006, Carr et al., 2011). However, SPW-Rs have also been suggested to play “imaginary spatial fields” predicting possible spatial environment and performing novel place cell pre-play when an animal enters an unknown environment (Dragoi and Tonegawa, 2014). SPW-Rs network oscillations are the most synchronous physiological patterns in the brain, and the memory consolidation process during the episodes is thought to activate LTP type processes in communication between CA1 cells (Buzsaki et al., 1990). In addition to gamma and theta frequency oscillations, PV+ cell activity may play an important role in

triggering hippocampal sharp wave ripples (Klausberger et al., 2003, Ellender et al., 2010, Schlingloff et al., 2014).

1.2.3. Compromised synaptic inhibition generates pathological synchronous neuronal activity

This rhythmogenic neuronal machinery with fine-tuned division of labour of specialized interneuron types (Soltesz, 2006) has its Achille's heel. The pivotal role of the interneurons to pattern and organize neocortical and hippocampal network activities also means that dysfunction of inhibitory neuronal circuits readily results in pathological features in spatial-temporal properties of coordinated activity of pyramidal cells (Buzsaki and Watson, 2012, Hu et al., 2014). A well-known example is the generation of hippocampal epileptiform activity by pharmacological inhibition of the GABAergic inhibitory system. Application of $GABA_A$ receptor antagonist triggers hypersynchronous pathological discharge of CA3-CA1 pyramidal cells (Tasker and Dudek, 1991). Characteristically the volume of synchronously firing pyramidal cells is substantially above the magnitude observed in physiological oscillations (Margineanu, 2010). In the absence of effective inhibition, synchronous pyramidal cells lose the ability to encode relevant information in their activity (Lisman and Buzsaki, 2008). The "bewildered" activity periods of pyramidal cell discharge uncontrollably propagate in the hippocampus causing excitotoxic cell damage (Fujikawa, 2005). Importantly, the pathological

discharges are able to hijack activity-induced synaptic plasticity mechanisms such as LTP, which have evolved to be activated by physiological activity patterns. Thus, epileptogenesis abuses physiological plasticity mechanisms of learning and memory such as the NMDAR-dependent LTP to facilitate progression of the disease in the hippocampus (Scimemi et al., 2006, Meador, 2007).

Another example of inhibitory interneuron dysfunction in pathological conditions comes from studies of cognitive dysfunction in inheritable neuropsychiatric diseases which might have, at least partially, their roots in developmental failure of cortical interneurons (Lisman and Buzsaki, 2008). Although the causal connection between mild congenital interneuron dysfunction and cognitive impairment in humans has not been directly demonstrated, an increasing number of studies with genetically manipulated rodent lines indicate that indeed altering PV+ cortical interneurons cause behavioural changes related to psychiatric diseases. These symptoms include cognitive decline with impaired performance in spatial navigation and learning tasks (Fuchs et al., 2007, Bannerman et al., 2014).

An important element in this interneuronopathy-hypothesis is a link between malfunctioning PV+ interneurons and alterations in cortical oscillatory activity, often associated with impaired cognitive function (Lewis et al., 2012). As I reviewed above, oscillations in EEG and LFP reflect coordinated synchronous neuronal activity in the hippocampus during behaviour-related cognitive tasks. Although EEG traces only represent

population activity of neurons, small abnormal features in the oscillatory activity waveforms, frequency, or other patterning can reflect dysfunction in the spatial-temporal organization of neurons during this activity. Hence, cortical oscillations have been closely studied in human patients with cognitive impairment, such as Alzheimer disease or schizophrenia-associated cognitive symptoms. In neuropsychiatric diseases cognitive impairment correlates with specific alterations in cortical gamma oscillations most commonly seen in patients as reduced oscillation amplitude or altered frequency (Narayanan and Johnston, 2007, Williams and Boksa, 2010). Moreover, experiments on rodent models of genetic disease or targeted transgenic modulation of PV+ interneurons often show alterations in neocortical (and hippocampal) gamma- and theta oscillations with impaired cognitive performance in behavioural tests (Korotkova et al., 2010, Marin, 2012).

As a summary, moderate dysfunction of specific inhibitory interneurons in the hippocampus may allow normal brain function and EEG without epileptiform activity. However, if these subtle changes compromise the input-output operation of inhibitory neurons minor alterations in EEG or LFP can emerge in physiological oscillation patterns in the cortex and hippocampus during specific behavioural tasks. These mild oscillatory abnormalities may be also associated with compromised performance in challenging cognitive tasks revealed by specific behavioural tests.

1.3. Context of this study

1.3.1. Previous findings on interneuron long-term plasticity *in vitro*

Experiments on acute and cultured hippocampal slice preparations have demonstrated that high-frequency afferent firing of glutamatergic axons can elicit long-lasting potentiation or –depression in synapses onto inhibitory interneurons. The specific outcome for plasticity depends on the postsynaptic interneuron type (Nissen et al., 2010), brain state (Pelkey et al., 2008) and firing activity of pre-and postsynaptic cells (Lamsa et al., 2007a). However studies showing that these or similar plasticity processes take place between glutamatergic hippocampal fibres and specific postsynaptic interneuron types *in vivo* have hitherto been missing.

The contextual significance for use-dependent LTP and LTD in specific pyramidal cell to interneuron synapses can be justified by conditions presented in the Chapter 1.2. Theoretically the strength between pyramidal cell and interneuron communications would be expected to balance in parallel with learning-associated LTP in pyramidal cells in the CA1 area (Kullmann and Lamsa, 2007). According to slice experiments the LTP observed of the interneuron is needed to rescue temporal fidelity of CA1 pyramidal cells input-output function in the face of memory recordings in the CA1 circuits (Lamsa et al., 2005). A recent study by Dupret et al. (2013) , demonstrated in drug-free animals using tetrode recordings that establishment of novel CA1 area place cells is associated with permanent changes in communication between pyramidal cells and fast-spiking interneurons. Whether LTP-like

mechanisms, as reported earlier in acute hippocampal slices, could explain such changes and potentiate transmission from excitatory fibers to identified PV+ CA1 interneuron types *in vivo* is not known.

1.3.2. Aims of this research and content of chapters

The overall aim of this study is to investigate whether LTP or LTD-like potentiation or depression in transmission from excitatory glutamatergic fibres to identified CA1 interneuron types also occur *in vivo* in the hippocampus. Experiments on slice preparation have reported that LTP and LTD in interneurons also depends on the postsynaptic cell membrane potential and the degree of postsynaptic firing during afferent pathway activity (Pelkey et al., 2008, Oren et al., 2009, Szabo et al., 2012). I therefore aim to compare plasticity results with postsynaptic cell spontaneous firing level, their firing during plasticity induction and in the hippocampal brain state defined during an LFP oscillation pattern.

Chapter 2 explains methods and resources used in this study. In Chapter 3, I will introduce the experimental design of the study, and define criteria for monosynaptic excitatory responses when stimulating in left hippocampus whilst recording in the right hemisphere CA1 area. These analyses also reveal the difficulty of the experiments with less than every fifth spontaneously active CA1 neurons showed stimulation-evoked excitatory

input monosynaptic transmission features. This chapter also explains why the experimental approach was chosen. Juxtacellular recording of the postsynaptic cell avoids recorded cell cytoplasmic dialysis, which can compromise plasticity (Isaac et al., 1996, Lamsa et al., 2005). Stimulation and recording from contralateral CA1 areas also avoids antidromic spike generation in postsynaptic cells. The chapter also describes how postsynaptic cell types are analysed using both electrophysiological features of juxtacellularly recorded cells and results from anatomical and immunohistochemical analyses of these neurons following labelling with neurobiotin. Chapter 4 introduces the experimental paradigm and monosynaptic pathways transmission strength analyses in three experiments on identified postsynaptic CA1 pyramidal cells. These neurons show robust LTP as expected from numerous experiments *in vitro* and *in vivo* (Bliss et al., Anwyl, 1999, Cooke and Bliss, 2006). The results demonstrate that the experimental design and paradigm can be reliably used to measure long-term plasticity in the excitatory synaptic pathway to identified CA1 neurons *in vivo*. Chapter 5 reports the first evidence on the activity-induced long-term plasticity in the excitatory synaptic inputs to identified hippocampal interneurons in intact living brain. Both LTP and LTD are reported in identified PV+ fast-spiking cells, and the results show specificity to cell type. Chapter 6 introduces results from similar experiments in electrophysiologically and anatomically analysed non-fast spiking interneurons. In chapter 7, I analyse the spontaneous firing level of recorded neurons during experiments, their firing during electrical afferent stimulation (i.e. TBS) used to test plasticity and the general brain state defined as theta (3 - 6 Hz) or non-theta oscillation in hippocampal LFP. I compare these parameters with the plasticity outcome in each experiment. Finally, in Chapter 8 I discuss how these findings relate to our knowledge

based on the literature and results from acute brain slice preparations. I discuss the possible role of CA1 area interneuron plasticity in spatial learning processes.

2. Materials and methods

2.1. Experimental animals and anaesthesia

Experiments were carried out on adult male Sprague-Dawley rats (Charles River, Margate, *UK*), according to the Animal (Scientific Procedures) Act, 1986 (United Kingdom), and the European Communities council Directive (86/609/EEC). Electrophysiological recordings were made in 103 rats, weight between 280 and 350 g. Anaesthesia was induced with isoflurane (Isoflo, Schering-Plough, Welwyn Garden City, UK) by inhalation (4% v/v in Oxygen, Isoflurane Vapouriser Std. Fill 5%, Vet-Tech Solutions, Ltd., UK), then maintained by intraperitoneal injection (i.p.) of urethane (1.25 - 1.3 g/kg ethyl carbamate in 0.9% saline, Sigma-Aldrich, St. Louis, UK).

The depth of anaesthesia was continuously monitored by following the respiratory and heart rates and testing corneal reflex and hind leg withdrawal reflex to a paw pinch. If an animal showed either paw pinch withdrawal reflex or rapid vibrational whisker movements accompanied by an increase in average heart rate and breathing, I gave an additional dose of 0.1 – 0.2 ml of urethane. Small supplemental doses of ketamine (30 mg/kg i.p.; Ketaset, Willows Francis, Crawley, UK) and xylazine (3 mg/kg i.p.; Rompun, Bayer, *Germany*) were used to maintain a desired anesthesia level (defined by recorded cortical electrical activity, see Chapter 2.2.) throughout the experiment (Magill et al., 2001).

2.2. Surgical procedures

Before craniotomy, I shaved head of the animal and fixed it firmly in a stereotaxic frame (David Kopf Instruments, Tujunga, CA, USA) at 3 points, i.e. ears and nose. Body parts of the animal in direct contact with clamping bars i.e. ears bars and nose lever, were covered with local anaesthetic (lidocaine gel, 2% m/v; Biorex Laboratories Ltd., Enfield, UK). Body temperature of experimental animals was maintained at 37 ^{o}C ± 0.5 ^{o}C (Harvard Apparatus, Edinburg, UK), using a homeothermic heating mattress with an external abdominal temperature measurement probe with feedback to the heating pad. Hypromellose eye drop and eye gel (Norton Pharmaceuticals, Harlow, UK) were applied to avoid corneal dehydration. I monitored the electrocardiogram continuously using two wires placed subcutaneously to the forelimb and hind limb on the same side of its body. I assessed anaesthesia level by monitoring LFP in cortical areas (with inserted metal wire) and by monitoring vibrational whisker movement and respiration rate (as described above in Chapter 2.1.). Saline-based glucose (10 % w/v glucose in 0.9 % w/v normal saline) solution was injected subcutaneously (0.2 ml / 2 h) to compensate fluid loss from the animal during experiment.

All wound margins were first disinfected and infiltrated with local anaesthetic, bupivacaine (0.75 % w/v, subcutaneous injection; Astra, Kings Langley, UK). About 20 min after injection of bupivacaine, a rostrocaudal incision was performed to expose the skull, the

muscles and periosteum were detached with the back of surgical blade and the skin was kept apart with haemostats. The skull surface was cleaned with bone scraper under a diagnostic microscope (4 to 25 x magnification, Leica Microsystems Ltd., Milton Keynes, UK) and bleeding was stopped by cotton bud and bone wax. The coordinates of Bregma were recorded after cleaning. Then, I marked the Bregma position with a black dot using a permanent marker pen on the skull. The stereotaxic coordinates of the target recording area were calculated from the marked Bregma point (Paxinos and Watson, 2007). The Bregma position is a more stable reference point than the Interaural junction as a reference point because weight differences in adult male Sprague-Dawley rats can change the Interaural junction. Surgical windows, i.e. craniotomies, were made in the skull above the right and left dorsal hippocampal CA1 area by drilling through the skull with a dental drill. Remaining bone pieces from drilling were cleared away by fine forceps and dust was removed with saline-soaked cotton bud. Extra fine surgical forceps were used to remove the dura mater to minimize possible damage to the brain surface and blood vessels. The openings were then cleaned and a wall of dental cement was built to protect that from possible peripheral bleeding, 0.9% w/v saline solution was applied regularly to areas of exposed brain surface to prevent dehydration. For accurate measurement of the depth of penetration, saline solution was dried before inserting electrodes into the brain. Finally, the operation windows were covered with warm paraffin wax to maintain hydration (Sigma, Aldrich, St Louise, USA; no 76228 solidification point 44 - 46°C) once the electrodes were lowered into the brain.

2.3. Electrophysiological experiments

2.3.1. Microelectrode recording of the LFP and extracellular spikes

Extracellular LFPs and action potentials were recorded at the following coordinates; 3.0 mm (posterior to Bregma ± 300 μm), 3.6 mm from midline (lateral to Bregma ± 500 μm), and depth 2.2 mm (ventral to the brain surface ± 300 μm) by a glass microelectrode (Paxinos and Watson, 2007). Microelectrodes were fine glass electrodes pulled from borosilicate glass capillaries with inner lining filaments (1.2 mm outer, 0.69 mm inner diameter; GC120F-10, Harvard Apparatus, Edinburgh, UK). Electrodes were pulled using a vertical puller (PE-2, Narashige, Tokyo, *Japan*). Tips were adjusted by touching the microelectrodes with a curved end of a glass rod under a light microscope (60 x magnifications) to achieve a 1-1.5 μm external diameter. The glass electrode was filled with 0.5 M NaCl (in ddH_2O) with 1.5% to 3% (w/v) Neurobiotin™ tracer (N-(2-aminoethyl) biotinamide hydrochloride, FW 322.8, Vector Laboratories, Peterborough, *UK*). The recording electrode was placed in a micro-drive holder (EXFO-8200 Inchworm Motor Microdrive System, Quebec, *Canada*) that could be controlled manually or by a computer-controlled stepping interphase, which allows fine movements (up to 0.5 μm resolution) in dorsal-ventral axis. A silver wire with silver-chloride coating was inserted and connected to a head-stage and bridge amplifier (DPA-2FS, Axon Instruments, Union City, CA, *USA*) where the extracellular potential was amplified (10 x) before it differentially filtered to simultaneously monitor LFP and individual action potentials. The extracellular potential for LFP was amplified further 100 x (NL-106 AC-DC Amp, Digitimer™, Welwyn Garden City, *UK*) before band-pass filtering between 0.3 Hz and 3 kHz

(NL125 filters, Digitimer™, Welwyn Garden City, *UK*). Extracellular deflections corresponding to individual action potentials in neurons, called spike thereafter, were recorded following AC-coupling and amplified (100 x; NL-105, Digitimer™, Welwyn Garden City, *UK*) before band-pass filtering (between 300 Hz and 5 kHz; NL125, Digitimer™, Welwyn Garden City, *UK*). "Notch filters", humbug units, (Quest Scientific, Vancouver, *Canada*) were used in both channels to eliminate noise at 50 Hz (Brown et al., 2002, Magill et al., 2004).

Recording electrodes with input resistance (measured by injecting positive current to 1 nA at 10 Hz) between 15 and 21 MΩ were made. Input resistance in the brain tissues measured between 13 and 26 MΩ during recordings. A high frequency short pulse was applied to generate resonance on the recording electrode tip to clear the accumulated cellular debris, if the impedance increased to above 23 MΩ outside hippocampus. The rat hippocampus roughly located between 2000 μm and 2600 μm dorsal to the brain surface. The impedance of the recording electrodes was consistently monitored during penetration at multiple depths i.e. at 200 μm, 900 μm, 1600 μm, and before entering the hippocampus at 1600 to 1950 μm (depending on the level of brain swelling). The recording electrodes were lowered into the hippocampal CA1 at a speed of 20 μm/s, reducing speed to 5 μm/s after reaching the hippocampus and when searching for postsynaptic neurons responding to afferent stimulation generating an action potential. The electrode movement was reduced to a speed of 0.5 μm/s, when the electrode is approaching a spontaneously firing cell. At this

stage, detected action potentials can be increased up to 1.5 mV when the electrode moved closer, recordings were made typically at about 0.4 - 0.5 mV spike amplitude.

2.3.2. Afferent electrical stimulation to evoke synaptic responses

Concentric bipolar stimulating electrodes (epoxylite insulted platinum electrodes with about 30 degree tip angle, 125 µm tip diameter, 25 µm inner pole and 125 µm outer pole; FHC Inc., Main, United States) were first implanted into the left CA1 to allow sufficient time for brain tissue to recover after the implantation. Single, double, and triple stimulation electrodes were used. In most experiments parallel double electrodes or triple concentric electrodes (with tip separation of 150 - 200 µm) were positioned simultaneously in the left CA1 area to increase probability of finding an active synaptic connection to a recording area in contralateral CA1. The stimulation electrodes were lowered to *stratum oriens* (*str. ori*.) of the contralateral CA1 region by a stereotaxic arm, 3000 to 3200 µm posterior and 3.0 to 4.0 mm lateral to the bregma and a depth of 2100 - 2500 µm from the brain surface (Buzsaki and Eidelberg, 1982b). In order to locate the tip of the stimulating electrode, a lesion in the brain tissue was created by passing a large current pulse (500 µA, 200 ms) to the stimulation electrode at the end of each experiment. The position of the lesion could then be determined in *post hoc* analysis of the fixed brain tissue. Initial stimulation was given as monophasic constant-current pulses (0.1ms, 800 nA) at a frequency of 0.2 Hz when the electrode reaches

2000 µm depth from the brain surface. The length of each stimulation pulse was kept constant throughout all experiments while its polarity and intensity were adjusted in the beginning via an independent constant current stimulation isolator. Each of the stimulation electrodes were tested individually by turning on and off their stimulation isolators and altering stimulation intensity and polarity individually in the first and last penetration, 1000 µm ventral to the brain surface in the neocortex above the hippocampal CA1 area. The stimulation electrode was then lowered into the hippocampus CA1 area (Swanson, 1981, Buzsaki and Eidelberg, 1982a, b) (Figure 2.1 A). At this stage, I focused on evaluating a likely monosynaptic stimulation response by analysing the evoked response jitter and consistent delay to stimulation (Deadwyler et al., 1975, Berry and Pentreath, 1976, Buzsaki and Eidelberg, 1982b, Andersen et al., 2007, Royer et al., 2012). The final localization of stimulating electrodes in the CA1 was adjusted by monitoring the field excitatory postsynaptic potential (fEPSP) in local field-potential (LFP) (Buzsaki and Eidelberg, 1982b, Andersen et al., 2007) (Figure 2.2B). The evoked fEPSP was either a positive or a negative deflection, its polarity depending on recorded hippocampal CA1 area lamina (Figure 2.2 B). Eliciting the field EPSP in the beginning of the experiment indicated successful activation of excitatory projection axons targeting the recording area from the contralateral stimulation (Buzsaki and Czeh, 1981, Buzsaki and Eidelberg, 1982b).

2.3.3. Recording postsynaptic spikes and juxtacellular cell labelling

Continuous recording of stimulation-evoked LFP responses with postsynaptic spikes that matched monosynaptic criteria were recorded for at least 10 min (every 5 s) i.e. baseline, before applying a theta-burst stimulation (see below, TBS) to the stimulation pathway. The afferent stimulation-evoked postsynaptic action potential probability and delay in the evoked spike were used as measures of the excitatory synaptic input strength (Figure 2.2). The TBS was used to induce long-term plasticity in the single-shock activated excitatory synaptic pathway. The TBS-pattern a plasticity-induction pattern that commonly used in experiments with acute brain slices to elicit long-term plasticity in excitatory glutamatergic synapses onto CA1 area interneurons and pyramidal cells (Capocchi et al., 1992, Huang et al., 2005, Di Lazzaro et al., 2008, Nissen et al., 2010). A train of TBS consisted of 100 pulses, delivered in 20 bursts of 5 stimuli at 100 Hz, at 200 ms intervals (theta frequency, i.e. 5 Hz). Following TBS, LFP recording including the stimulation responses continued for at least 20 min, typically 30 – 45 min (in some rare cases, putative interneurons were recorded for several hours). At the end of the plasticity recording the microelectrode was taken closer to the monitored cell (refer to Chapter 1.3.2 for details) and the juxtacellular labelling method was applied to label the cell with Neurobiotin^{TM} tracer (FW 322.8, Vector Laboratories, Peterborough, UK) as described in Pinault (1996). Neurobiotin-filled recording electrodes were advanced to juxtaposition to the cell slowly (0.5 μm/s) until the spike amplitude reached about 0.7 mV (Figure 2.2). The Neurobiotin^{TM} (FW 322.8, Vector Laboratories, Peterborough, *UK*) was delivered onto the target cell iontophoretically applying a series of

high intensity (10 – 50 nA) positive square current pulses at 200 ms on/off cycle (Pinault, 1996).

The current intensity was adjusted manually while monitoring firing of the labelled cell. Labelling a neuron is most effective when current injection is associated with action potential firing of the neuron with extracellularly applied current pulses. Length of overall labelling period with active modulation of the labelled cell varied from a few periods of 30 s episodes to 5 - 10 min continuous modulation, however typically lasting 2 to 3 minutes. The physiological condition of target cells was closely monitored during the labelling, and current injection was stopped if any sign of cellular damage might occur. Any sudden increase of action potential width and increased spontaneous firing frequency could indicate cellular damage (Pinault, 1996). When the electrode tip was localized in *stratum pyramidale* (*str. pyr.*), where neuronal somata are densely packed together, extra care was taken to verify that the modulated cell action potential properties (i.e. extracellular spike kinetics, see Figure 2.3 and 2.4) corresponded to the action potential properties of the cell recorded during plasticity experiment (see Figure 2.2). Following successful labelling and modulation, a recovery period (1h to 5h) allowed the injected neurobiotin to diffuse inside the labelled cell (Figure 3.6 C and 3.7 A).

2.4. Electrophysiology data acquisitions and analyses

Extracellular potential recordings were differentially filtered for LFP and unit activity signals (see 1.3.2 above) and were acquired at 1 kHz and 20 kHz, respectively using Spike2 (version 7.0; Cambridge Electronic Design, Cambridge, *UK*) acquisition and analysis software. The data was analysed using Spike2 (version 7.0; Cambridge Electronic Design, Cambridge, *UK*) and further processed with Microsoft Excel (2007, 2010), KyPlot (Version 2.0, beta 13, 32 bit), SigmaPlot® (10.0.1), MATLAB® (R2013b), Graphpad prism (v. 6, 2014), and presented in Inkscape (Version 2, 1991), Microsoft PowerPoint and Word (2010).

2.4.1. Single spike sorting

The extracellular spike shape, width and amplitude were carefully monitored throughout the experiment and compared at different stages of the recording, during and after the labelling procedure (see Chapter 1.3.3. for detail juxtacellular labelling procedures) to confirm that the same cell (by the same extracellular spike properties) was analysed (Figure 2.2 C). Spikes generated by the target cell during spontaneous activity and in response to electrical stimulation were recognized in the filtered unit channel from their temporal and amplitude properties, set for spike detection by Spike2 software (as shown in Figure 2.4). In some experiments (in particular for cells recorded in *str. pyr.*) multiple neuronal firings were

occasionally seen in spontaneous activity or in stimulus-evoked response or during labelling. Caution was taken to isolate firing of the target cells from spontaneously active neurons around it (see Chapter 1.3.3) and to avoid contamination from surrounding cells. To ensure spikes were from the same cell, Principal Component Analysis (PCA) on Spike 2 (version 7.0; Cambridge Electronic Design, Cambridge, *UK*) was used to identify spontaneous spikes with similar action potential properties to the pre-set evoked spike in the cell. The PCA in Spike2 (version 7.0; Cambridge Electronic Design, Cambridge, UK) runs spike templates detected in a specified time (x-axis) and amplitude (y-axis) window against recording data in the unit channel (Figure 2.4B). By matching the spike amplitude and waveform features within the set window, spikes detected within the set window were either grouped into an existing template that had a matching waveform or a new template was formed based on that new spike waveform (Figure 2.4B). The critical waveform isolated spikes from different cells based on features include amplitude, delay to stimulation, area under waveform curves and slopes. For most sets of critical spike waveforms only the first few components are useful, the rest corresponding to noise. Cluster analysis in Spike2 (version 7.0; Cambridge Electronic Design, Cambridge, *UK*) was used to extract the top three factors that separate the spikes by correlation (a sample cluster plot was shown in Figure 2.4 C). Visual inspection was carried out to ensure spike homogeneity within each cluster. In the example cluster plot shown in Figure 2.4 C (data from cell PL310812, baseline recording) each dot represents one spike detected in the recording. The cluster plot sorted out recorded spikes into different categories based on spike templates (Figure 2.4B) by matching the peak and trough amplitudes, rising and descending slopes automatically (Spike2 vis. 7.0, C.E.D, Cambridge, *UK*). In Figure 2.4C, the blue cluster represents the evoked and spontaneous spikes that share very similar

waveforms, the light green cluster is the stimulation artefact and black dots represent noise detected in the recording. The spike sorting success rate depends on the signal-to-noise ratio i.e. how representative templates are depends on how well the PCA can isolate spikes from background noise. Therefore, spontaneous spikes and evoked spikes were extracted to a new waveform channel for comparison and verification by comparing spontaneous spike against the closest evoked spike in the data file to ensure accuracy of the sorting. Recognition of evoked and spontaneous spikes on individual neurons was based on this newly updated template thereafter. The PCA and cluster analysis result were then visually scanned against the closest evoked spike to check the accuracy of the sorting and extracted individual waveforms in a new channel for comparison and verification purposes. Analyses of evoked and spontaneous spiking patterns for individual neurons were based on this newly formed channel. After spike sorting, spike width was calculated from the onset to the end of waveforms, and in some cases, the action potential half-width (measured from onset to trough) was measured instead because of small signal-to-noise ratio (Figure 2.4.).

2.4.2. Spontaneous oscillations in the LFP

The brain state varies depending on the anaesthesia level. Slow wave activity (SWA) in the LFP mostly occurs during deep anaesthesia (less than 2 Hz) (Buzsaki et al., 1983). Oscillation in theta frequency (3 - 6 Hz in anaesthetized rats) represents a more active brain

state. It occurs naturally in a lighter anaesthesia state. Common oscillation patterns including slow-wave and theta activity (see Chapter 1.4.2 above) were first recognized during recording and later verified off-line in analysis with Spike2 (version 7.0; Cambridge Electronic Design, Cambridge, UK). In my experiments using urethane based anaesthesia (1.25 - 1.3 g/kg ethyl carbamate in 0.9% saline, Sigma-Aldrich, St. Louis, UK) maintained by injection of low-doses of ketamine-xylazine (30 mg/kg i.p.; Ketaset, Willows Francis, Crawley, *UK* and 3 mg/kg i.p.; Rompun, Bayer, *Germany*, respectively) and slow-wave oscillation of less than 2 Hz occurred naturally, usually 5 – 15 min after ketamine-xylazine injection. This oscillation may continue for 30 min to 120 min (Klausberger et al., 2003b). Theta oscillation is characterised by a small amplitude (less than 0.5mV) regular sinusoidal wave at a frequency from 3 to 6 Hz.

Quantitative analysis of theta frequency was performed by a Spike2 script created by Dr John Tukker (MRC Anatomical Neuropharmacology unit, Oxford, *UK*) (Tukker et al., 2007). The unit recording channel was down sized by 20 times and band-pass filtered (3 – 6 Hz). The Spike2 script defines significant theta oscillations when at least 3 consecutive cycles of oscillation at 3 – 6 Hz occur. A theta cycle was identified when a significant (> 4 times) ratio between a power of theta and delta (2 – 3 Hz) frequency band was detected in a 2 s time window using a fast fourier transform with 1024 points (Tukker et al., 2007). The start and end point of theta cycles were checked and redefined manually by visual inspection of field potential waveform over a longer period. Troughs of theta oscillation cycles were identified in order to develop a phase relationship between spontaneous spiking pattern and theta cycles.

Sharp wave-associated high-frequency ripples (90-200 Hz in anaesthetized animals) occasionally occurred in the CA1 area of the hippocampus (Foster and Wilson, 2006; Tukker et al., 2007). The duration of episodes was typically less than 100 ms (Ylinen et al., 1995; Csicsvari et al., 1999). Ripple oscillations were detected by visual inspection of the field potential after band-passed filtering at 90 to 200 Hz in the downsized (4 times) unit recording channel. The results were then visually checked to confirm if ripple cycles were associated with slow-wave deflection (Buzsáki et al., 1983).

2.4.3. Analyses of single cell spike firing phase during the LFP theta oscillation

Hippocampal CA1 neuron types fire action potentials in a cell type-specific manner during oscillations in LFP (Klausberger et al., 2005, 2003a). A Spike2 script created by Dr John Tukker (MRC Anatomical Neuropharmacology unit, Oxford, *UK*) was used to isolate theta oscillations quantitatively and for analyse of single neuron action potential phase during theta oscillation (Tukker et al., 2007). Theta oscillation was first isolated as described above in Chapter 2.4.2 using the Spike2 script. Phase preference in the LFP for spontaneously fired action potentials during theta oscillation is a valid parameter to identify specific CA1 interneuron types or subpopulations (Klausberger et al., 2003b; Tukker et al., 2007; Klausberger and Somogyi, 2008; Dupret et al., 2008; Viney et al., 2013). The spontaneous

activity of a recorded cell was considered to be modulated by theta oscillation when a non-uniform distribution of spiking was shown using the Raleign's test ($p \leq 0.05$) (Zar, 1999). The strength of modulation was indicated by 3 variables, 1) the preferred phase angle, 2) angle deviation (like standard deviation in Gaussian distribution), and 3) depth of the modulation, shown by normalized vector (refer to as r in statistics, value between 0 and 1, no modulation when $r = 0$ and spiking concentrated at one angle when $r = 1$) (Zar, 1989). Phase histograms with 360 degree bin size are used to show the phase coupling of recorded cell spike to its hippocampal theta oscillation (see Chapter 2.4.5. for details).

2.4.4. Plasticity analyses of stimulus-evoked postsynaptic spike

Spikes evoked by contralateral single shock electrical stimulation and generated by the postsynaptic target neurons were identified as described above in Chapter 2.4.1. Evoked spikes were considered monosynaptic when spikes were phase-locked to the presynaptic afferent stimulation and the spike delay was between 9 ms and 15 ms from stimulation artefacts as reported in previous studies with projection afferent pathway stimulation (Buzsaki and Czeh, 1981, Buzsaki and Eidelberg, 1982b). Evoke response extraction was set between 3 ms and 20 ms for unbiased detection. Spike probability and latency are the principal parameters used to analyse synaptic efficacy. Probability of spiking or P(Spike) is the occurrence of the evoked spike divided by the total number of stimulation cycles within the

analysed time windows. The spike latency was defined as delay between the stimuli given and post-synaptic response onset.

A semi-automatic spike detection program was set up in Spike2 (C.E.D., Cambridge, *UK*) to detect delay between evoked spike and timing of afferent stimulation. In histograms shown in figures, failures to evoke a spike are indicated as "F" next to abscissa 0 time point. Latency of spikes was plotted against time to illustrate changes in synaptic efficiency in each experiment presented. The stimulus-evoked spike data were shown together with occurrence of spontaneous spiking activity of the same cell, the data for spontaneous firing were pooled from 1 s time windows immediately preceding stimulation in each cycle ever 5 s.

Spike delay (latency) distributions are shown in 20 ms stimulus histograms with various temporal bins. To compare synaptic responses between baseline and post-TBS in Chapters 4 to 6, histograms were constructed from spontaneous firing of postsynaptic neurons in a 1s time window preceding stimulation in each cycle.

2.4.5. Data analyses and statistics

The major read-outs for synaptic strength before and after the plasticity induction protocol with TBS are (1) evoked spike probability in response to the contralateral afferent

stimulations, i.e. P(Spike), and (2) delay between the stimulation and the post-synaptic responses, i.e. spike latency. In addition the spontaneous firing rate of individual target cell, and the local LFPs were analysed and quantified during the plasticity recordings because of its association with intrinsic excitability of the target cells. Data analyses protocol used in identification of specific oscillation patterns in the LFP were described above in Chapter 2.4.2.

To minimise the effect of varying spontaneous firing rate on the plasticity measurements, statistical comparisons of P(Spike) and spike latency between the pre- and post-TBS periods were made in time windows that showed the most similar spontaneous firing rates (Klausberger et al., 2004, Klausberger et al., 2005). The P(Spike) was calculated in each selected windows and the Chi-square test was used to test if the pre-TBS and post-TBS P(Spike) values differed statistically. Correspondingly, a difference between the stimulus-evoked spike latency between the pre- and post-TBS period was statistically tested. If the data showed Gaussian distribution ($p > 0.05$, Kolmogorov-Smirnov test) the Student's t-test was used (Zar, 1989). When the data failed the normality test, the Mann-Whitney test was used (Graphpad prism 6.0, GraphPad Software, Inc. La Jolla, USA).

The probability and delay of stimulus-evoked spikes in all recordings were plotted in histograms showing data in the standard time points; baseline (pre-TBS), post-TBS 0 – 15 min, 15 – 30 min, and in some cases 30 – 45 min and > 45 min periods. Histograms on

selected time windows were illustrated for all individual experiments in the results chapter. The Raleigh's test was used to analyse their spontaneous firing preference during the LFP theta oscillations cycles (see Chapter 2.4.2.). The mean angle of the firing was calculated by transforming directional data into rectangular polar coordinates (Zar, 1989). Variations from the mean angle were represented by the angle deviation. The depth of modulation measured dispersion (symbolized by *r*, in a range of 0 to 1), which represents a spectrum between uniform dispersion to concentration in one direction (Zar, 1989).

2.5. Anatomical processes and analyses

2.5.1. Perfusion of rat brain and fixation

After recovery period, animals were injected with an overdose (0.3 – 0.5 ml for rats weighted between 280 and 350 g) of ketamine and xylazine mixture (ketamine 30 mg/kg and xylazine 3 mg/kg, i.p.) and perfused via circulation system from ascending aorta or sinistral ventricle with 200 ml 0.1 M phosphate buffered saline solution (PBS, pH 7.4, at 22-24 ^{o}C) followed by 300 – 400 ml fixative. The fixative composed of 4 % w/v paraformaldehyde (PFA) and 15 % v/v saturated picric acid solution (#74069, Fluka, *Switzerland*), in 0.1 M phosphate buffer (PB) with freshly added 0.05 % glutaraldehyde (distilled grade, TAAB laboratories Equipment, Aldermaston, *UK*). The brain was dissected out and put for post-fixation in 4 % paraformaldehyde in 0.1 M PB, at 4 ^{o}C overnight. Samples were then stored in

0.1 M PB with 0.05% azide (103692K, VWR International Ltd., Poole, *UK*) at 4 ^{o}C. The fixed brain was washed in 0.1 M PB solution before sectioning (see Chapter 2.5.2).

2.5.2. Fixed brain sectioning and neurobiotin-filled cell visualization

The frontal cortex and cerebellum were cut from the fixed brain with a razor blade or scalpel. The rostral cut side was glued to the cutting stage of a vibratome (VT1000S; Leica Microsystems, Milton Keynes, *UK*) for serial sectioning (60 μm thick) in cold standard PB solution. All collected sections (between Bregma -2.8 and -4.6 mm) were washed in 0.1 M PB solution (10 min, 3 times). Details on the buffering solution used in this project are listed in Table 2.1. Sections were divided in 3 or 4 series. One of the series was selected for visualization of the labelled cell using standard protocols and the rest were stored in 0.1M PB solution with 0.05 % (w/v) Azide (103692K, VWR International Ltd., Poole, *UK*) in a 24 well-plate (Greiner bio-one Ltd., Stonehouse, *UK*) at 4 ^{o}C.

The visualization process of labelled cells started with washing in 0.1M PB for 3 times (10 min each), on shaker under room temperature (22-24 ^{o}C). The sections were then incubated in Alexa FluorTM 488 conjugated streptavidin (1:1000, Life Technologies, Sigma-Aldrich Inc., St. Louis, USA) in 0.1 M Trizma® based saline (TBSa, pH 7.4, Trizma base and

Trizma HCL, Sigma-Aldrich Inc., St. Louis, *USA*, T4661 and T3253 in 0.9 % NaCl solution) buffer with 0.3 % Triton™ X-100 (X-100, Sigma-Aldrich Inc., St. Louis, *USA*) overnight on shaker at 4 ^{o}C, to improve binding of streptavidin to the neurobiotin. The incubation process was carried out in the dark to avoid ambient light degrading the fluorescence signals. Sections were washed using standard steps (VWR International ltd., Leuven, *Belgium*). Samples were mounted and air-dried on glass slides before sealing with Vectashield mounting medium (Vector Laboratories Inc, Burlingame, *USA*) and cover slips for the examination under epifluorescence microscope (AxioImager Z1, 43HE filter set, 20× magnification).

2.5.2.1. Freeze and thaw

Some sections were processed using freeze and thaw treatment, which is a more delicate way to permeabilize the cell membrane compared to detergent, hence it improved visualization of delicate structures, such as axon, in the fixed brain. Permeabilization is based on making cell membranes porous by rapid freezing while leaving the cellular compartment more intact. To preserve neuron morphology during freeze and thaw cycles, the brain slices were first immersed in freshly prepared 20 % sucrose in TBS overnight at 4°C in the dark until sections sank to the bottom of the well on a shaking plate. The sections were then transferred and flattened on the bottom of a 6-well plate (Greiner bio-one Ltd., Stonehouse, *UK*, 657160) one by one with a cleaned burst pen. Excessive sucrose was dried up by a glass

Pasteur pipette and a dried brush pen. Then, the plate was dipped into excessive liquid nitrogen until sections were frozen, indicated by colour change from yellow to ivory and finally to white. The well was then thawed rapidly by pipetting room temperature (22-24 ^{o}C) 0.1 M PB into the well and rubbing the bottom of the well, on the outside of the plate with a finger. The freeze and thaw steps were repeated once in well-fixed tissue. The sections were washed in PB and twice in TBS (20 min each) on a shaker at room temperature (22-24 ^{o}C) to remove sucrose before further immunohistological processing. The sections then underwent the same neurobiotin visualisation process with streptavidin as described above (Chapter 2.5.2) except that TBST was replaced by TBS. Sections expected to contain recorded neuron soma and extensive axon arborisations were particularly selected for freeze and thaw permeabilization. Visualization of recorded cell structures was followed by standard immunohistological staining or conversion to 3,3'-Diaminobenzidine tetra-hydrochloride (DAB) reaction (see Chapter 2.5.3.) to either analyse the presence of specific cellular proteins or to maximize visualization of fine morphological structures of the recorded cells.

2.5.3. Immunohistochemistry

Interneuron types in the hippocampal CA1 area can be partly or in some cases fully identified by their somato-dendritic structure and axon distribution. However additional criteria for cell type identification can be provided by intracellular marker protein and

membrane protein immunohistochemical analyses (Somogyi and Klausberger, 2005). Immunohistochemical staining for specific key proteins was chosen based on previous published results (Freund and Buzsaki, 1996, Shepherd and Grillner, 2010).

2.5.3.1. Immunohistological staining

Primary antibodies against specific markers were selected to study the presence of marker proteins in sections with streptavidin-fluorophore visualized structures of recorded neurons. Then secondary antibodies binding to primary antibodies were selected based on their origin and conjugated fluorophore.

Brain sections with relevant streptavidin-visualized cellular structures of the labelled neuron were selected for further immunohistochemistry processing. Primary antibodies for immunohistochemical reactions were selected on the basis of electrophysiological, like fast action potential kinetics of PV+ interneurons, and anatomical features, such as somatodendritic and axon properties (Hu et al., 2014), (Somogyi and Klausberger, 2005). Sections were either free-floating or dismounted from the glass slides under 10 x magnification stereomicroscope or washed in 0.1 M PB, 5 timesfor 10 min each round on shaker. Primary and secondary antibodies used in this project are listed in detail in tables 2.3 and 2.4 respectively. Free-floating sections were washed in TBST (or TBS for freeze and

thaw sections) with standard washes 3 times at room temperature for 15 min each, before putting them in 20 % blocking solution for at least 2 h in room temperature (22-24 ^{o}C) or put on a shaker in the dark at 4°C. Blocking serum was normal horse serum or goat serum (NHS, Vector Laboratories, Peterborough, UK) in TBS(T) depending on the species in which primary antibodies were raised. Other blocking reagents, including BSA, gelatine, and milk were used to test improvement of blocking background staining in some studies. The sections were incubated in appropriate primary antibodies diluted in 1 % serum in TBS(T) for over 48 hours at 4 ^{o}C while shaking in the dark (see Table 2.3, primary antibodies list). Following standard washing procedures, the sections were put in relevant fluorochrome-conjugated secondary antibodies in 1 % of the selected blocking serum in TBS(T) and kept overnight at 4 ^{o}C or 2 – 4 h at room temperature (22 - 24 ^{o}C) on a shaker in the dark. Then, unbound secondary antibodies were washed out with TBS (or TBST when membrane permeabilization was achieved by using freeze and thaw method) 20 min repeating it 3 times. Finally sections were mounted on glass slides as described above to fix the brain sections and protecting them from drying out. Mounted sections were covered by cover slip and sealed with nail polish.

2.5.4. Acquisition and evaluation of fluorescence images

After mounting and drying, I first examined the immunohistochemical staining results with either 20 x or 63 x magnification objectives (PL Fluotar 20x/ 0.5, PL apochromat 63x/

1.40 oil objectives, Leica Microsystems Ltd., UK) in an epifluorescent microscope (DM5000 B, Leica Microsystems Ltd., UK) using appropriate filter setting L5, Y3 or Y5 (Leica Microsystems Ltd., UK) for fluorochromes Alexa 488, Cy3, and Alexa 647/ Alexa 649/ DyLight 649/ Cy5, respectively. After the initial examination, sections with good staining in relevant structures were forwarded for further analysis using a laser-scanning confocal microscope (LSM 710, Carl Zeiss AG, Cambridge, UK). Immunohistological images were analysed and captured for illustration purpose either by an ORCA-ER CCD camera (Hamamatsu) attached to DM5000 B epifluorescent microscope (Leica Microsystems Ltd., UK) or by Zen software in Zeiss confocal microscope software (version 2008, Carl Zeiss AG, Cambridge, UK). In the latter, one laser was applied to the section at a time using a sequential multitrack single channel operation mode with Zen software (version 2008, Carl Zeiss AG). Confocal scanning images were viewed and captured under triple band primary beam splitter (LSM710, Carl Zeiss AG, Cambridge, UK) using either a sequential multi-tracks single channel operation mode (one laser was applied to the section at a time) or a spectral filtered multichannel (two channels were excited at the same time but the collection of their emission profile was gated to ensure no cross-talk between emission) with Zen software (version 2008, Carl Zeiss AG). Exposure time and pinhole size were set for each channel separately before scanning. Both modes avoided cross talk between channels with overlapping immunofluorophore emission profile. Micrographs were not manipulated except in adjustment in exposure time, contrast, and size.

Immunoreactions were defined positive while neurobiotin signal co-labelled with marker(s) of interest in a relevant cellular compartment. It was considered to be negative when fluorescence was not detected in a relevant neurobiotin-labelled cell, but immunopositivity was detected in surrounding unfilled cells. At least two separate regions with successful antibody staining were evaluated. Another round of immunohistochemical processing could be repeated on well-documented immunonegative channel. In case of weak signals, a semi-quantitative fluorophore spectral analysis method was used to evaluate immunoreactivity, measuring the specific spectral component of emission light and comparing its intensity between relevant subcellular domains and selected control areas such as nucleus of the same cell, cytoplasm or nucleus of nearby neurons, and extracellular space. This eliminates signal cross-talk and recognizes genuine weak fluorophore emission (Somogyi et al., 2012). Channel separation was first tested by spectral identification using Zeiss Axio Imager (the QUASAR spectral detector on Zeiss Axio Imager on confocal microscope, Z1-LSM 710, Carl Zeiss AG, Cambridge, UK) and ZEN software (version 2008, Carl Zeiss AG, Cambridge, UK). Images were captured in lambda mode to record full emission spectra from 400 to 730 nm for each fluorophore(s) by stimulating them individually with relevant laser (Somogyi et al., 2012). Fluorophore-specific narrow emission spectral band was selected for Alexa488, Cy3, and Cy5 fluorophores for the present project (Somogyi et al., 2012). The emission spectrum was set to detect non-overlapped emission peaks at relevant narrow ranges. Then, the emission profile was obtained in marker relevant subcellular domain and compared to surrounding background and internal positive control under detection setting. A signal was considered positive if the fluorophore emission peak amplitude from area of interest was at least 1.5 times larger than the background and

comparable to the internal control in signal intensity and expression patterns (Somogyi et al., 2012).

2.5.5. Digital fluorescence image reconstruction

For reconstruction of cellular structures visualized with streptavidin-fluorophore a stack of images along the z-axis was captured using AxioImager Z1 on laser scanning confocal microscope and ZEN software. Reconstructed was carried out using the ImageJ software (developed by Wayne Rasband, the Research Services Branch, National Institute of Mental Health, Bethesda, Maryland, USA). Single micrograph, exposure time and pinhole size were set for each channel separately before z-stack scanning. Channel tracks were switched in sequence of excitation wavelengths for each scanning layer one by one. A stack image was assembled at optical thickness of about 1.2 μm (in principle, less than half the thickness of the optical slice based on Nyquist-Shannon sampling theorem), the depth covered by each scan depended on how much streptavidin Alexa 488 -visualized axon and/or dendrites needed to be visualized in each section. ImageJ collapsed the z-stack images into one flat image by maximal projection.

I reconstructed an overall structural image of each cell in digital fluorescence images for illustration. Reconstruction was performed based on collapsed Z-stack images and using confocal micrographs as a reference for subsequent drawing in ImageJ (the Research Services Branch, National Institute of Mental Health, Bethesda, Maryland, USA) with plugin NeuronJ (version 1.4.2., http://www.imagescience.org/meijering/software/neuronj/). Neurites of the target cells were traced semi-automatically by NeuronJ plugin, in a 3-pixel thick line, on a colour-inverted image reconstructed by ImageJ. Then drawings from different sections were aligned by GIMP software (ver. 2.6.11; http://www.gimp.org/), including dendrites, main axon, hippocampal *strata* locations, microglia and blood vessels. The drawings were not manipulated except in orienting.

2.5.5.1. DAB reaction and image reconstruction

In addition to visualization of neurobiotin-filled neurons with streptavidin, sections from some cells were processed with a DAB (approx. 97 %, Sigma-Aldrich Inc., St. Louis, USA) precipitation reaction following freeze and thaw treatment. This process is by far the most sensitive method for detecting neurobiotin in thin neurites such as in the labelled axon. Therefore it was primarily used here to visualize the axon of recorded neurons. DAB (approx. 97 %, Sigma-Aldrich Inc., St. Louis, USA) visualization is based on avidin-biotin reaction (ABC reaction). First, selected sections underwent a biotin [solution B in TBS(T), 1:100,

Vectastain ABC kit, Vector Laboratories Inc, Burilngame, USA] reaction for over 48 hours in 4 ^{o}C, in 24-well plate on a shaker, in the dark. The next step involved, mixing avidin and biotin (1:100, solution A and B from Vectastain ABC kit, Vector Laboratories Inc, Burilngame, USA) in 0.1M TBS or TBST buffer for more than 30 min before reacting with the section at room temperature (22-24 ^{o}C). The sections were then incubated in this pre-mixed avidin-biotin solution overnight at 4 ^{o}C or 4 h in room temperature (22-24 ^{o}C) on a shaker in the dark.

Oxidization of the DAB (approx. 97 %, Sigma-Aldrich Inc., St. Louis, USA) produces an insoluble brown precipitation. To control this relatively rapid reaction, an enzymatic reaction was used to produce peroxide, which can oxidizes DAB in a slower rate, to produce a permanent deposit on neurobiotin labelled cells and is visible by the naked eyes. The DAB solution used in the processes here composed of DAB, 0.2 M PB, 20 % Glucose (BDH Laboratory Supplies, Poole, *UK*), ammonium nickel sulphate (0.05% w/v; BDH Laboratory Supplies, Poole, *UK*) and 0.4 % ammonium chloride (Sigma-Aldrich Inc., St. Louis, USA, A-4514-100G) in distilled water (see the Table 2.2 for details). Concentrations varied depending on streptavidin signal strength and background staining.

Selected sections were transferred to glass vials after washing them by standard steps in PB and then incubated in 1 – 2 ml DAB solution for 15 to 40 min at room temperature (22-24 ^{o}C) in the fume hood, depending on the preliminary colour change observed by visual

inspection. Following the incubation, 2 – 4 µl glucose-oxidase (0.00542 g / ml, Sigma-Aldrich Inc., St. Louis, USA) was added to the DAB solution and upon oxidase reaction, hydrogen peroxide was produced converting DAB to an insoluble brown precipitate (Hsu and Soban, 1982). The precipitation process was monitored closely by checking the colour development under a light microscope at 10 x magnification every 10 min. Reaction was stopped between 10 min to 2 h to optimise staining to the background ratio. Sections were then washed thoroughly to stop the peroxide reaction and incubated in osmium tetroxide (4 % w/v solution, TAAB Laboratories Equipment Ltd., Reading, *UK*) in 0.1 PB for about 30 – 50 min. The amount of osmium varied from 0.5 to 2 % depending on signal to background level after the DAB reaction. Finally, the sections were washed with standard steps in PB and flattened on the bottom of the glass vial before undergoing a series of dehydration process by ascending concentration ethanol (VWR International Ltd., Poole, *UK*) steps (50%, 70%, 90%, 95%, repeated twice in absolute ethanol and in propylene oxide) (VWR International Ltd., Poole, UK), each 10 min at room temperature (22-24 ^{o}C). Embedding medium resin was freshly prepared by mixing components A (44611), B (44612), C (44613) and D (44614) from the Durcupan ACM Fluka kit (Sigma-Aldrich Chemie GmbH, Steinheim, *Germany*) in a 10 : 10 : 0.3 : 0.3 ratio. The mixture was left in room temperature (22-24 ^{o}C) for more than 20 min to let the bubbles disappear before transferring to immersion bowl. Dehydrated sections were immersed in resin for at least 4 h (in some cases overnight) at room temperature (22-24 ^{o}C) before mounting them on glass slides and covering with cover slips (VWR International Limited, Pennsylvania USA). The slides were incubated at 60 ºC for 48 hours to let the components polymerize and harden (Halasy et al., 1996).

Features of DAB-filled cells were then drawn from representative sections showing soma and axo-dendritic arborisations using a drawing tube on a light microscope (63 x magnification) and semi-transparent tracing pad. Each section formed by individual drawing were first mounted according to surrounding visual markers and then photographed. The assembled image was then captured by digital camera, stacked, and size adjusted to give a reconstruction using Adobe Photoshop (Adobe system, San Jose, *USA*) with the help of Mr. Ben Micklem (MRC, Anatomical Neuropharmacology Unit, Oxford, *UK*) (Zsuppan, 1984).

2.5.6. Figures and tables

Figure 2.1.

A

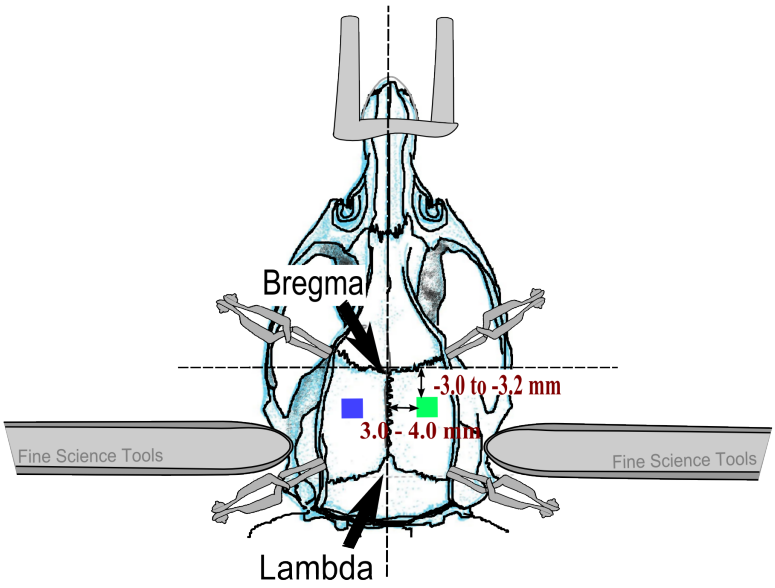

B

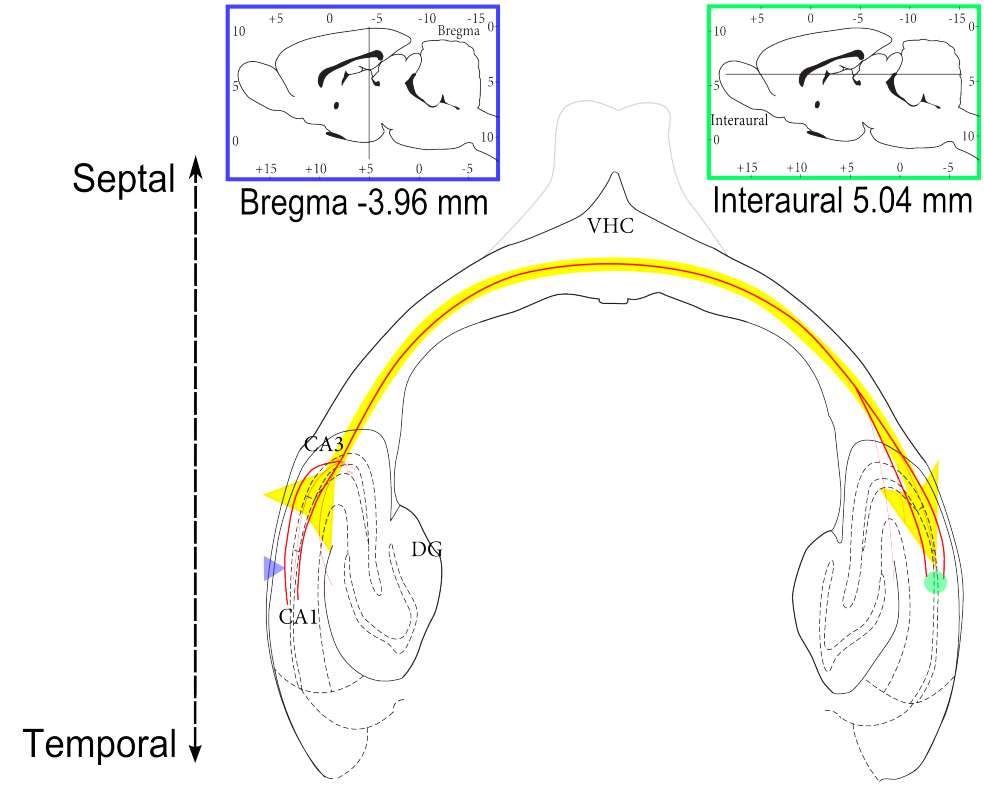

Figure 2.1. Experimental design to stimulate excitatory glutamatergic projection fibres between left and right hippocampus. The extracellular stimulus electrode was positioned in left hemisphere hippocampal CA1 area and stimulation responses recorded in the contralateral hippocampal CA1 area.

(A) A schematic of skull of anaesthetised rat clamped in stereotaxic frame and shown from top. In all experiments stimulation electrode was positioned in the left hemisphere dorsal hippocampus using the coordinates described previously (scaled craniotomy illustrated in picture as a blue square); caudal from Bregma (range 3.0 to 3.2 mm), lateral (range) 3.0 – 4.0 mm, depth range 2.1 – 2.5 mm. Juxtacellular and local field potential (LFP) recordings were performed with a glass microelectrode in dorsal hippocampal CA1 area of right hemisphere (scaled craniotomy area highlighted in green, AP, Bregma -3.2 mm; ML, Bregma -4.0 mm; Depth 2.1 mm ± 300 μm).

(B) A schematic of connectivity from left hippocampal CA1 area to right hippocampal CA1 area. Glutamatergic monosynaptic excitation is mediated both via the orthodromic stimulation of commissural CA1-CA3 fibres from the left hippocampus and antidromic stimulation of right hippocampus commissural fibres. The purple triangles indicate the position of the stimulus electrode positions. The green spots illustrate positioning of the recording glass electrodes. Red lines show the two types of glutamatergic axons originating from left hemisphere CA3 pyramidal cells, modified from Swanson et al. (1981). Because commissural fibres and Schaffer collaterals are axonal branches from the same pyramidal cells, stimulation of these connections generate monosynaptic response in the right hippocampal CA1 area (Buzsaki and Czeh, 1981, Buzsaki and Eidelberg, 1982a, b). Insets show sagittal sections of approximate position of the large schematic left side (left inset) and right side (right inset).

Figure 2.2.

A

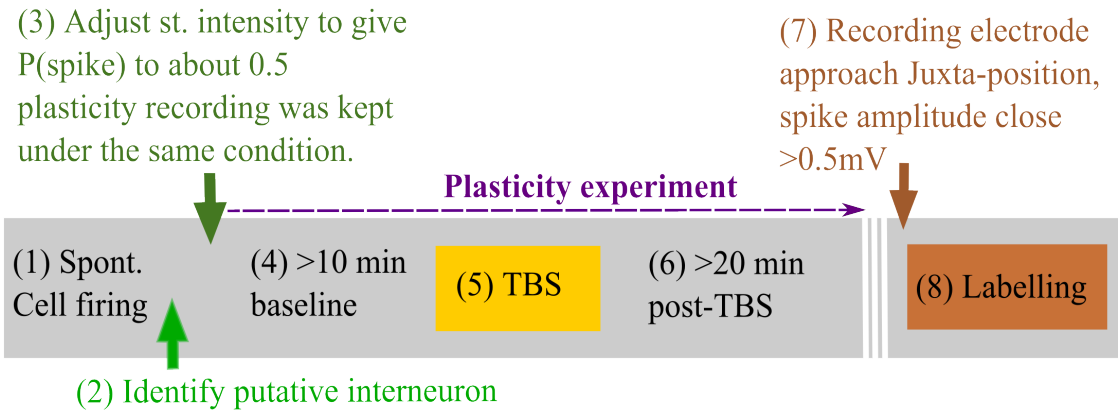

B

B1

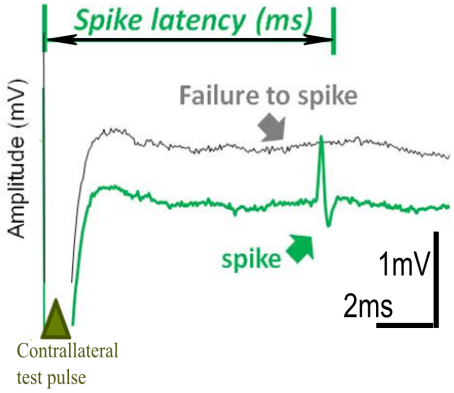

B2

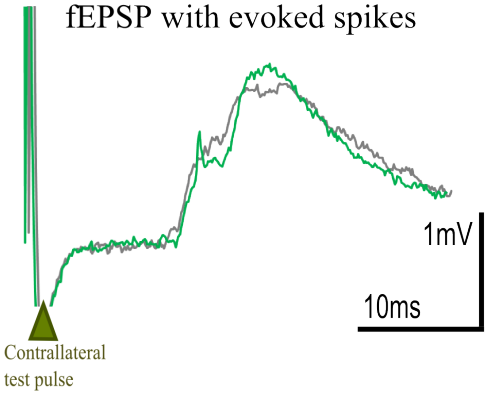

Figure 2.2. Full experimental protocol. First to record afferent electrical simulation-evoked postsynaptic action potential, then test plasticity in the evoked pathway and finally label the recorded cell with neurobiotin using the juxtacellular labelling method described above in 2.3.3.

(A) A schematic drawing shows eight steps of a full experiment in a urethane-xylazine-ketamine anesthetised rat. Following positioning of the stimulation electrode in the left dorsal hippocampal (dHC) CA1 area, saline-neurobiotin-filled glass-capillary electrode was positioned in the right dHC CA1 (see Figure 1). Stimulation and recording electrodes were placed in their correct final stereotaxic position, and a single shock stimulus was delivered every 5 s at 0.8 – 1 mA to test if stimulation electrode can elicit a capacitive transient i.e. stimulation artefact in recording electrode. Stimulation electrode location was adjusted until it evoked field potential EPSP in the right side dHC. If not, stimulation electrode positioning was readjusted again. The recording microelectrode was moved in dHC CA1 systematically to find a spontaneous firing cell that responds with a short-delay spike to the contralateral stimulation. The actual recording process starts by (1) detecting a spontaneously firing neuron in the CA1 area. (2) Classification of neurons by spontaneously firing pattern (see Chapter 2.3.3.). (3) Afferent pathway stimulation was used to find if the cell responds to contralateral single-shock stimulation with a spike with short delay. If yes, intensity was adjusted to elicit the spike in the cell with approximately 50 % of stimulation cycles (see Chapter 3.). (4) Following a stable baseline of at least 10 min, (5) theta-modulated high-frequency stimulation pattern (TBS) was delivered via the stimulation electrode to the pathway to test long-term plasticity in the evoked spike probability. (6) Following the TBS, single shock stimulation was resumed for at least 20 min. (7) Following plasticity experiment, the recording electrode was moved into close proximity of recorded cell and (8) recorded cell was subjected to juxtacellular labelling. Current injections described in Figure 2.3. were used to facilitate cell spontaneous firing and to apply the marker molecule (neurobiotin) to juxtaposition of the cell. After labelling, the neuron was left to recover for at least 60 min (but up to 6 h) to allow time for neurobiotin to diffuse through the cell.

(B) Sample traces show a postsynaptic spike with a monosynaptic delay in CA1 neurons in response to contralateral electrical stimulation. (B1) Juxtacellular recording responses with a spike (green trace) and another cycle with failure to evoke spike (grey) shown in unit channel (band-bass filtered 300 Hz – 5 kHz). Deflection on left (dark green arrowhead) is stimulation artefact. (B2) Stimulus-evoked traces in LFP channel (band-passed filtered at 0.3 Hz to 3 kHz). Green trace shows stimulation cycle with a post-synaptic spike, black trace illustrates next cycle with a failure to spike under the same conditions (single shock stimulus intensity 800 μA). Slow waveform in LFP traces of this cell shows an uncommon underlying field EPSP (fEPSP duration, amplitude and initial slope are defined in the trace).

Figure 2.3.

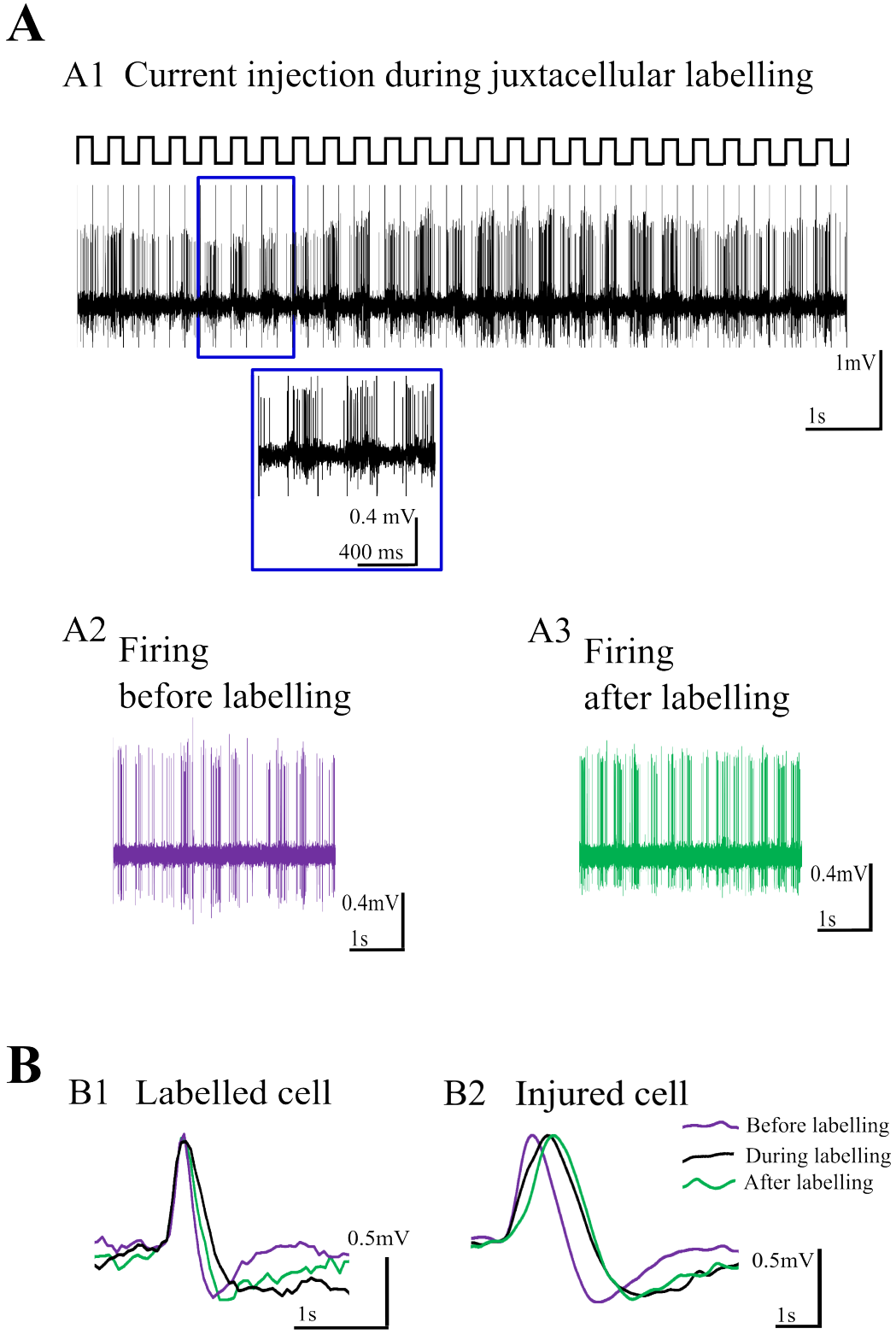
A
A1 Current injection during juxtacellular labelling
1mV
1s
0.4 mV
400 ms
A2 Firing before labelling
0.4mV
1s
A3 Firing after labelling
0.4mV
1s
B
B1 Labelled cell
0.5mV
1s
B2 Injured cell
Before labelling
During labelling
After labelling
0.5mV
1s

Figure 2.3. Juxtacellular labelling of recorded cell with neurobiotin through spiking modulation.

(A) Sample traces showing firing in a recorded cell in band-passed filtered (300 Hz – 5 kHz) unit channel. The traces show spontaneous spiking activity of the cell (PL190912) before juxtacellular labelling (A2), during modulation (A1) and after modulation (A3) (see 2.4.1. for details on how the identification of evoked and spontaneous spikes belong to the same cell was achieved). (A1) Steps of positive current (<10 nA) were applied into the recording electrode in a 200 ms on/off square pulse cycles (current pulses shown on top) (Pinault, 1996) to facilitate spontaneous firing of the recorded neuron. Facilitation of firing is seen in a sample period shown (marked and shown in blue rectangles) with higher temporal resolution. Note bimodal firing of the cell during current step protocol. Modulation in recorded cell varied from 30 s to 10 min, typically lasting around 2 to 5 min. A recovery period of up to 6 hours allowed the applied neurobiotin to diffuse throughout the labelled cell, (A2-A3) Spontaneous firing pattern reminded unchanged after the modulation as illustrated in the two sample traces before and after labelling.

B) Superimposed action potentials recorded juxtacellularly from a two sample cells before, during and after labelling protocol. B1) A healthy sample cell showing similar extracellular spike kinetics before labelling (taken 2 min before start of modulation, in purple), during modulation (black trace), and immediately after modulation (in green). Action potentials extracted from a fast spiking interneuron (PL311012) with narrow spike kinetics. Extracellular spike kinetics remained unchanged indicating the cell was healthy. In most of cases good labelling was achieved even when spike waveform was modestly changed i.e. half time and spike width increase < 20%, if its spontaneous firing level remained unchanged. (B2) Superimposed action potentials extracted from a sample regular spiking cell in which labelling was unsuccessful. The cell starts showing wider spikes with longer spike waveform after modulation indicating that the cell was damaged during the labelling process. Damaged cells are less likely to become visualised. This may be caused by cell death during the long recovery period that normally follows the labelling. Therefore quick perfusion was considered for these cells, which resulted in partial staining of the cell so that only soma and proximal dendrites are visualised *post hoc*.

Figure 2.4.

A Spike Width

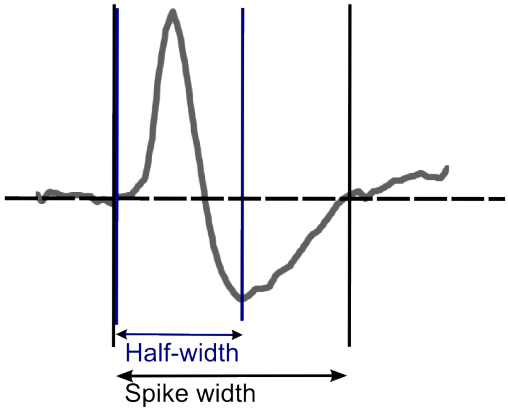

B Principle component analysis

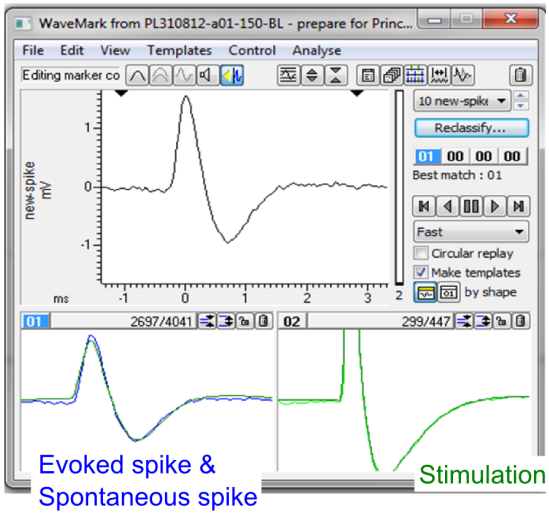

C Cluster analysis

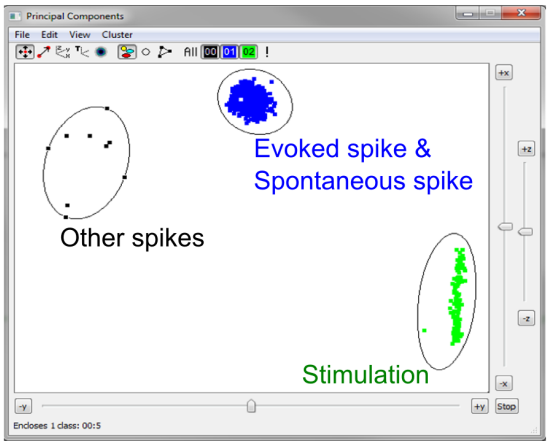

Figure 2.4. Single spike sorting. Waveform features were used to confirm that spontaneous and synaptically-evoked spikes were generated by the same cell (A) Spike width and half width. Action potential duration was measured from the onset to the end of waveform, and its half-width as a time from the onset to trough.

(B) Spontaneous and evoked spikes were isolated from a filtered unit channel with set time scale and amplitude by Spike2 software (see 2.4.1 for details). The software detected and isolated spikes by principle component analysis and cluster analysis.

(C). The principle component analysis (PCA) used parameters including (1) peak amplitude and its time point, (2) interception with y-axis when spike waveform is at zero value, (3) half height position between the (1) and the (2). Then, extracted spikes underwent correlation analysis. The PCA and cluster analysis results were then visually scanned against the closest evoked spike and if matched, extracted as a template waveform to recognise all spikes with same features.

Table 2.1. Buffer solutions.

Solution type	pH	Chemical	Concentration (mM)	Molecular Weight (g/l)	Producer
0.1 M PB	7.39	Na_2HPO_4 x $2H_2O$	80	177.99	Sigma–Aldrich, Gillingham, *UK*
		NaH_2PO_4 x H_2O	20	137.99	
0.2 M PB		Na_2HPO_4 x $2H_2O$	160	177.99	
		NaH_2PO_4 x H_2O	40	137.99	
0.1 M PBS		PB	100	315.98	
		NaCl	0.9% w/v	58.44	
PB plus Azide		PB	100	315.98	VWR International Ltd., Poole, *UK*
		Sodium Azide	0.05% w/v	65.01	
TBS	7.4	Trizma HCl	42	157.6	Sigma–Aldrich, Gillingham, *UK*
		Trizma Base	8	121.14	
		NaCl	0.9% w/v	58.44	
TBST		TBS	1	337.18	
		Triton X-100	0.3% w/v	625	

Table 2.2. DAB protocol.

Solution type	Solutions/ Solute	Amount of solutions used		
		Quarter	***Half***	***Full***
Pre-incubation mixture	1% w/v Ammonium Nickel (II) sulphate in dH2O (µl)	3700	3600	3400
	dH2O (µl)	100	200	400
	0.4% w/v Ammonium Chloride in dH2O (µl)	100	100	100
	20% w/v glucose in 0.1M PB (µl)	100	100	100
	0.5mg/ml DAB (µl)	1000	1000	1000
	0.2M PB (µl)	500	500	500
DAB reaction	Glucose oxdiase (µm)	4		
	dH2O (ml)	2		
Post-staining fixation		**Amount of Osmium tetroxide used**		
		0.5%		***1%***
	4% Osmium tetroxide in dH2O (µl)	500		1000
	0.2M PB (µl)	1000		1000
	0.1M PB (µl)	2000		2000
Standard washing between DAB reaction steps: 0.1M PB				
Resin Durcupan™ Components	A: M epoxy resin (g)	10		
	B: Hardener 964 (g)	10		
	C: Accelerator 960 (g)	0.3		
	D: Plasticizer (g)	0.3		

Table 2.3. List of primary antibodies.

Primary Antibodies					
Antigen	**Species**	**Type** [a]	**Supplier**	**Product number**	**Dilution** [c]
Calbindin	Rabbit	M	Swant, gift from Prof. Somogyi, MRC ANU, Oxford	CB-38	1:500
CB1	Guinea pig	P	Frontier Science	Cb1-GP-Af530-1	1:1000
PV	Rabbit	P	Swant	PV-28	1:1000
	Guinea pig	P	Synaptic Systems	195004	1:2000
	Goat	P	Swant	PVG 214	1:1000
Pro-CCK	Rabbit	P [b]	Gift from Prof. Watanabe to Prof. Somogyi then to us.	1090	1:500
NOS	Mouse	M	Sigma	1167	1:500
NPY	Rabbit	P	Immunostar	22940	1:4000
SAT B1	Rabbit	P	Abcam	ab70004	1:400
SAT B1	Goat	P	Santa Cruz	sc-5989	1:1000
SOM	Mouse	M	GeneTex Incorporates	gtx71935	1:200

[a] M: monocolonal; P: polyclonal

[b] Polyclonal rabbit antiserum raise to the c-terminal nonapeptide of pro-CCK coupled keyhole limpet hemocyanin (Morino et al., 1994, Viney et al., 2013)

[c] Dilution in Tris-BS or Tris-BST containing 1% NHS or NGS.

Table 2.4. Secondary antibodies and streptavidin conjugates.

Secondary Antibodies				
Conjugate	**Species**	**Supplier**	**Product code**	**Dilution [a]**
Alexa405	Donkey anti-Mouse	Abcam, gift from Prof. Somogyi, (MRC ANU, Oxford)	ab175658	1:250
Cy3	Donkey anti-Goat	Jackson	705-165-147	1:400
Cy3	Donkey anti-Guinea pig	Jackson	706-165-148	1:400
Cy3	Donkey anti-Mouse	Jackson	715-165-151	1:400
Cy3	Donkey anti-Rabbit	Jackson	711-165-152	1:400
Cy5	Donkey anti-Rabbit	Jackson	712-175-153	1:250
Cy5/ Dylight649 / Alexa647	Donkey anti-Guinea pig	Jackson	706-175-148	1:250
DyLight 649/ Alexa649	Donkey anti-Rabbit	Jackson	711-175-152 or 711-497-003	1:250

Streptavidin Conjugates			
Conjugate	**Supplier**	**Product code**	**Dilution**
Alexa 488	Invitrogen	S-32354	1:1000

[a] Dilution in Tris-BS or Tris-BST containing 1% NHS or NGS.

3. Synaptic excitation of distinct CA1 area neuron types by stimulation from contralateral hippocampus

3.1. Introduction

The Schaffer collateral fibres that originate from CA3 pyramidal cells provide one of the major excitatory synaptic inputs to CA1 area neurons. The CA3 pyramidal cell axons follow both transverse and oblique orientations forming connections to CA1 pyramidal cells apical dendrites in the *stratum radiatum* and basal dendrites in the *stratum oriens* (Blackstad, 1956, Ishizuka et al., 1990, Andersen et al., 2007, Szirmai et al., 2012). In addition, many CA3 pyramidal cells send axon collaterals to the hippocampus of the contralateral site where they innervate CA3 and CA1 area neurons comprising the commissural pathway (Figure 2.1.) (Swanson et al., 1981). The majority of cortical synaptic plasticity studies have utilised excitatory hippocampal synapses between the CA3 and CA1 areas (Bliss et al., Andersen et al., 2007).

Transmission properties in this pathway, including NMDA receptor-dependent long-term potentiation, represent a stereotype of "a common glutamatergic cortical synapse". In addition, the hippocampal CA3-CA1 circuit has become a popular synaptic plasticity study model for two other, more practical reasons. First, preparation of acute slices from rodent or rabbit dorsal hippocampus is straight forward, since simply slicing coronal sections of these animal brains allows good preservation of the Schaffer collateral pathway in dorsal hippocampus. Second, glutamatergic synapses in the CA1 area show laminar organisation, which allows relatively selective activation of specific projection pathways to the CA1 area

by aiming the stimulation to a specific laminar layer (Andersen et al., 2000, Andersen et al., 2007). In my thesis project I have studied activity-induced long-term plasticity of excitatory glutamatergic synapses in the hippocampal CA1 area *in vivo*. In these recordings the exact localisation of the stimulation and recording electrodes was verified *post hoc* by analysing electrode tracks and marker-labelled postsynaptic cells in the tissue.

I have used juxtacellular recording of postsynaptic spike generation probability as the main index of excitatory synaptic connection strength. Therefore, in the experimental design it is important to avoid co-activation of monosynaptic local inhibitory fibres, which could seriously mask the extracellularly measured evoked spike properties. In slice experiments such co-activation of the two different fibres can be revealed by blockade of GABA receptors pharmacologically. However, *in vivo* conditions GABA receptor blockade is usually lethal. Therefore, I have placed the stimulation electrode far away from the recording site to avoid monosynaptic activation of local GABAergic synapses in the recording area. Stimulation of glutamatergic fibres in the contralateral hippocampus avoids direct stimulation of GABAergic interneuron axons in the recording area. Hence I have chosen commissural pathway stimulation to study the long-term plasticity properties of excitatory synaptic input to hippocampal CA1 neuron types.

Using juxtacellular recording in these experiments has an important advantage compared to intracellular recordings. It allows stable long-term recording without dialysing

the postsynaptic cell cytoplasm. This is an important aspect because acute slice experiments have demonstrated that cytoplasmic dialysis significantly compromises LTP in the CA1 area pyramidal cells (Isaac et al., 1996) and in many interneurons (Lamsa et al., 2005). In addition, choosing juxtacellular recording had another advantage as I found that most tested neurons in the CA1 area failed to show firing in response to excitatory pathway stimulation from the contralateral site. Using juxtacellular recording I was able to avoid unnecessary labelling a numerous "deaf neurons" in recorded areas. By choosing the juxtacellular recording and labelling technique, I was able to label and visualise only the recorded cells, which was advantageous for cell type identification based anatomical analyses of the visualised cell structure. These 14 cells exhibited the excitatory synaptic response defined as a putative monosynaptic spike as described below in Chapter 3.2.1.

3.2. Results

3.2.1. Defining putative monosynaptic excitatory connection to CA1 hippocampal neurons when electrically stimulating contralateral hippocampus

In this study, I aimed to establish that electrical stimulation from the left hemisphere hippocampus elicits excitatory synaptic responses in the right hippocampal CA1 area. Synchronous activation of commissural fibres with single-shock electrical stimulation in the

contralateral hemisphere produces a field excitatory postsynaptic potential (fEPSP) in the target region of these axons (Buzsaki and Eidelberg, 1982b, Royer et al., 2010). At the beginning of each experiment, I first confirmed that electrical stimulation elicits synaptic fEPSP in the contralateral CA1 area (Figure 2.2-B2). At this stage, the repositioning of the stimulation electrode in the left hippocampus was often executed if stimulation failed to evoked fEPSP with standard stimulation intensity (800 - 1000μA, max 2500 μA) (Buzsaki and Eidelberg, 1982b). I confirmed that single shock stimulus-evoked fEPSP polarity reversed when the recording electrode proceeded deeper from most superficial CA1 layer *stratum oriens (str. ori.)* to *stratum pyramidale (str. pyr.)* and from *str. pyr* to *stratum radiatum (str. rad.)* (Andersen et al., 2007). This provided useful additional information (in addition to stereotaxic co-ordinates) to estimate the exact laminar position of the recording electrode in the hippocampus during the experiment. At this stage of the experiment, the recording microelectrode was primarily used to detect fEPSP in the CA1 while stimulating in the other hemisphere. The fEPSP deflection of positive polarity was observed in *str. ori.* and *pyr.*, the fEPSP polarity turned to a negative deflection in *str. rad*. Recording of local field potential (LFP) and individual postsynaptic neuron action potentials in juxtacellular mode were aimed at following co-ordinates: 3.0 - 3.4 mm posterior; 3.9 - 4.1 mm lateral to Bregma and the depth 2.2 - 2.5 mm from brain surface (Paxinos and Watson, 2007). Correspondingly, stimulation electrode in left hippocampal CA1 was positioned at 3.0 to 3.2 mm posterior and 3.0 to 4.0 mm lateral to the bregma and a depth of 2.1 - 2.5 mm from the brain surface as described in Chapter 2.3.1. (Buzsaki and Eidelberg, 1982b). Experimental animals were anaesthetized by urethane; the depth of anaesthesia was monitored through oscillatory

activities in the LFP, and via other parameters described in Chapter 2.1., and it is maintained by topping up with xylazine and ketamine.

Individual postsynaptic neuron action potentials were measured extracellularly by placing the microelectrode close to a target neuron. Afferent stimulus-evoked postsynaptic action potential probability and a delay from electrical stimulation were used to measure the excitatory synaptic input strength (Figure 2.2). Labelling at the end of the recording was performed by advancing the microelectrode to juxtaposition of the target neuron, as described in Methods 2.3.3 (Klausberger et al., 2004, Magill et al., 2004, Klausberger et al., 2005, Magill et al., 2006, Tukker et al., 2007). I considered spikes that were synaptically-evoke and putatively monosynaptic when evoked action potentials fulfilled the following criteria. First, evoked spikes were phase-locked to the timing of the presynaptic afferent stimulation with a short delay that corresponds to the propagation of signal via monosynaptic pathway from the contralateral hemisphere (Buzsaki and Czeh, 1981, Buzsaki and Eidelberg, 1982b, Andersen et al., 2007, Royer et al., 2012). When the delay was 5 - 20 ms (measured from stimulation artefact) the evoked spike was considered putatively monosynaptic. The action potential travels at speeds between 0.27 – 1.37 m/s via the Schaffer collaterals (Berry and Pentreath, 1976) and synaptic release from presynaptic terminals takes a few milliseconds. The timing of postsynaptic action potential depends on postsynaptic cell membrane time constant and the distance of the cell membrane potential from the action potential firing threshold (Hille, 1992). Postsynaptic action potentials generated by polysynaptic connections show a longer spike delay and a larger cycle-by-cycle variability in the delay (Deadwyler et al., 1975).

Therefore, only strictly phase-locked action potentials with a short delay can be considered the monosynaptically evoked. The criteria correspond to values previously reported with projection pathway stimulation and juxtacellular recording in the hippocampus (Buzsaki and Czeh, 1981, Buzsaki and Eidelberg, 1982b). Importantly, there are no excitatory connections directly from the CA1 to the CA1 area between hemispheres, which eliminates the possibility of antidromic action potentials in the stimulus-evoked spikes (Buzsaki and Czeh, 1981, Buzsaki and Eidelberg, 1982a, b). For every postsynaptic neuron that generated a spike to afferent stimulation, I tested various stimulation intensities to alter spike probability from zero (subthreshold) to its maximum. Finally, if the connection was judged monosynaptic, I reset the stimulation intensity close to half-maximal spike probability (i.e. postsynaptic spike generated in 50 % of single-shock stimuli delivered at 5 s intervals).

To illustration the delay and probability of stimulus-evoked extracellular deflections that correspond to postsynaptic action potentials. I prepared peri-stimulus histogram (PSTH) for each recorded cell (see Chapters 4, 5 and 6). The PSTH illustrates evoked postsynaptic cell action potentials for up to 20 ms from stimulation artefact. The evoked spikes typically clustered at 9 - 12 ms from stimulation. For each histogram, I pooled 100 (but in some experiments with low spiking probability 200) consecutive stimulation cycles. The PSTHs illustrate clearly for each cell the temporal distribution of stimulation-evoked spikes, their delay and evoked spike data coherence and how much spontaneous firing existed in the background (Berry and Pentreath, 1976). The mean spike latency in all experiments presented ($n = 14$) was 9.95 ± 0.43 ms (mean ± SEM of individual cell mean values) and in individual

experiments they distribute within a relatively narrow temporal window, i.e. in 3 ms between 8.863 ms and 11.50 ms. The probability of an evoked spike in the experiments was 52% calculated by counting the number of evoked action potentials divided by the total number of stimulation cycles during baseline period. I used a semi-automatic spike detection program in Spike2 to measure the delay between spikes and stimulation (described in Methods 2.4.2).

To summarise, I first established glutamatergic synaptic connectivity from left hippocampus to the right hemisphere CA1 area using the microelectrode for fEPSP recording. Then, I aimed to find a postsynaptic neuron in the CA1 area that is excited by the pathway stimulation to generate an action potential, which fulfils the criteria above for monosynaptic transmission (see for details Chapters 4 and 5).

3.2.2. Synaptic excitation of CA1 pyramidal cells by contralateral stimulation

In the CA1 area, pyramidal cells and GABAergic inhibitory interneurons can often be identified by their electrophysiological behaviour (Buzsaki and Eidelberg, 1982b, Csicsvari et al., 1999). When observed with juxtacellular measurement, these two neuron populations in many cases show distinct action potential properties (Csicsvari et al., 1999, Klausberger et al., 2004, Klausberger et al., 2005). This was highly advantageous in my project studying contralateral connectivity to hippocampal CA1 area neurons because it allowed the identification of post-synaptic neuron type, at least in some cases, when *post hoc* anatomical

analyses were not sufficient enough to confirm the cell identity.

Pyramidal cell discharge at a lower rate (in my experiments at 1.4 ± 0.01 Hz) and have slower action potential kinetics, than most GABAergic interneurons (Csicsvari et al., 1999, Csicsvari et al., 2003). In contrast, action potentials from parvalbumin-expressing interneurons have distinctively short spike width (< 1 ms) and high spontaneous firing rates (Klausberger et al., 2005). Analysing spontaneous action potential firing allows identification of a pyramidal cell when it shows at least two of the following criteria: (1) Juxtacellularly recorded cell exhibits complex spikes which are characteristic for pyramidal cells (Csicsvari et al., 1999); (2) cell shows slow action potential kinetics with low (about 1-4 Hz) spontaneous firing frequency during theta oscillation; (3) firing of the cell is phase locked to the trough of LFP theta oscillation (Klausberger et al., 2004, Klausberger et al., 2005). However, pyramidal cells and some interneurons can show fairly similar extracellularly measured action potential kinetics and their spontaneous firing behaviour in urethane anaesthetized rat can sometimes be difficult to distinguish (detail describe below). Therefore direct anatomical verification of the cell type required successful visualization of the cell after juxtacellular labelling with neurobiotin (Pinault, 1996, Klausberger et al., 2003).

3.2.2.1. Pyramidal cells exhibit low level of spontaneous firing in the anaesthetised rat

Many CA1 pyramidal cells fire irregularly and at a frequency lower than 4 Hz in urethane-anaesthetized rat most of the time except during sharp wave ripple episodes (Klausberger et al., 2004). I analysed the spontaneous firing rate of three pyramidal cells selected because these cells either showed identifiable anatomical structures after juxtacellular labelling or complex spikes, or both. I stimulated contralateral afferents every 5 s and I analysed spontaneous firing activity in 1 s periods taken just before delivering stimulation pulses. The three putative pyramidal cells fired all at an averaged frequency below 4 Hz throughout the analysis. The average firing frequencies of the cells in baseline conditions were 3.78 Hz, 1.11 HZ, and 2.43 Hz (Figures 3.3. - 3.5. and Chapter 4, Table 4.1.). Two of the three cells with clear theta and non-theta periods also showed higher spontaneous firing rate during theta than non-theta (2.94 Hz vs. 1.11 Hz and 2.96 Hz vs. 2.43 Hz, respectively).

3.2.2.2. CA1 area pyramidal cell firing is phase-coupled to the trough of local field potential theta cycles

Spontaneous action potential coupling to synchronous hippocampal oscillations can be used to differentiate pyramidal cells from some interneurons (Klausberger et al., 2004, Klausberger et al., 2005). In all three cells theta-oscillation activity was detected during baseline conditions, I analysed the timing of their spontaneous action potential in relation to

the LFP oscillation theta cycle, measured simultaneously with the same microelectrode. In all three cells theta coupling analysis showed preferred firing at the trough of theta cycles (Kamondi et al., 1998). However, in one cell the number of analysed theta cycles were lower (cell 2 above had only 43 theta cycles for the analysis) than in the other two (n = 1184 and 1278, respectively for PyC1 and PyC3), which explains the less clear statistical coupling result (see Chapter 4, Table 4.1.).

3.2.2.3. Pyramidal cells have slow action potential kinetics

Due to their longer action potential kinetics than in many interneurons, pyramidal cells also have wider extracellularly recorded action potential waveform than many interneurons (Csicsvari et al., 1999). Although, in this study I used action potential kinetics only as a criterion to discriminate fast-spiking parvalbumin neurons from other neuron types (as I will describe below in chapter 3.2.3.), waveform values in the three pyramidal cells were all in line with what has been reported previously (Csicsvari et al., 1999). Pyramidal cells in this study showed long spike duration measured from the onset to the end of spike waveform. Mean ± SEM of extracellularly recorded spike duration was 1.76 ± 0.18 ms and from the beginning of action potential to the trough (half width) was 0.86 ± 0.17 ms. The averaged spike duration is statistically much longer than sub-millisecond spike duration from onset to the end, measured in fast-spiking interneurons and reported in Chapter 3.2.3.

3.2.2.4. Pyramidal cells exhibit occasionally short-interval action potential bursts known as complex spikes

Pyramidal cells are known to fire complex spikes occasionally in a burst of two to several spikes. Complex spikes are usually prominent during sharp wave ripple episodes and these also occur in the transition from the slow-wave to theta oscillations in drug-free animals (Ranck, 1973, Fox and Ranck, 1981, Csicsvari et al., 1999). Complex spikes also occur in the urethane anaesthetized rodent hippocampus (Csicsvari et al., 1999). Because their occurrence can be quite infrequent in the anaethetised animal brain, the presence of complex spikes is best seen in action potential autocorrelation function and inter-spike interval histograms. Since pyramidal cells fire otherwise with irregular intervals, complex spike firing with fixed intervals (3- 5 ms) generates a clear peak at < 10 ms interval in these analyses (Csicsvari et al., 1999, Royer et al., 2012).

In both analytical approaches, firing of high-frequency complex spikes in pyramidal cells gives a different outcome than for interneurons, which can also fire at high frequency. This is because pyramidal cell firing autocorrelogram show a distinct a peak at short (3-10 ms) interval and the rest of its firing is comprised of irregular intervals, whereas interneurons show diversely various short spike intervals. Interneurons lack 'the fixed interval complex spike pattern and their firing frequency is more smoothly modulated. For example, in cell PL260313 a clear peak with an 8 ms interval with a low proportion of spike intervals close to the peak indicate that the recorded cell is an irregular spiking neuron with occasional high-

frequency bursts with short and almost fixed interval (Figure 3.2., 6.2., 6.3., and 6.4.). However, if complex spikes are rare in firing periods available for the analysis, a peak can be less evident. Here I observed complex spikes also in cell PL240113 and the firing analysis showed a clear peak at 8 ms in the interspike interval (ISI) histogram (Figure 3.3.B). However, the rare occurrence of complex spikes may fail to show clearly in this analysis as I found in the cell PL120811, which only had a few complex spikes during baseline recording (Figure 3.4.B).

In summary, the combination of three independent electrophysiology criteria, a firing rate, occurrences of complex spikes and spike duration, together with information on spike coupling to field potential during theta oscillation revealed CA1 pyramidal cells from other CA1 area neuron types.

3.2.2.5. Juxtacellular labelling and post hoc visualization confirms pyramidal cell identity

By injecting a step-wise positive current in the recorded pyramidal cells (methods described in Chapter 2.3.2 and illustrated in Figure 2.2A), microiontophoresis was achieved and led to labelling and visualization of two out of the three pyramidal cells above (Figures 3.3. – 3.5.). The two visualized CA1 area pyramidal cells showed branches of spiny dendrites in *stratum radiatum* and *stratum lacunosum-moleculare* and basal dendrites in *stratum oriens*

(Pyapali et al., 1998). One pyramidal cell (PL260313) failed to show successfully visualized structures that would have enabled anatomical identification. To summarize, three CA1 pyramidal cells receiving excitatory synaptic input from contralateral hippocampus were identified by functional criteria described above and in addition two of those cells were anatomically confirmed as pyramidal cells by successful *post hoc* visualization.

3.2.3. Synaptic excitation of postsynaptic CA1 area interneurons from the contralateral side

Stimulation of fibres in the hippocampus of the left hemisphere triggered the excitatory post-synaptic response in a diverse group of CA1 non-pyramidal cell neurons in the right hemisphere. Most distinctively I identified postsynaptic neurons with fast spike kinetics and relatively high spontaneous firing rates (Martina and Jonas, 1997, Jonas et al., 2004).

3.2.3.1. Subpopulation of interneurons is revealed by fast postsynaptic action potential kinetics

Fast spiking cells (FSC) in the hippocampus express the neurochemical marker parvalbumin (PV), hence they are called PV+ interneurons (Martina and Jonas, 1997). In juxtacellular microelectrode recordings their extracellularly measured action potentials are as short as 1 ms in duration (see definition of spike kinetics in Methods Chapter 2.3.3.1.). The

PV+ hippocampal CA1 area interneurons can be classified further and divided into individual types based on their anatomical characteristics (Klausberger et al., 2004, Klausberger et al., 2005). I recorded contralateral stimulation-evoked spikes (as defined above in 3.2.1.) in 16 postsynaptic cells with fast postsynaptic spike kinetics. Among these, stable plasticity recording was performed in seven cells and five were fully identified as specific cell types (refer to Method Chapter 2.4).

In these seven fast spiking neurons, the extracellularly recorded postsynaptic spike had a average width of 1.1 ms or less (half-width less than 0.6 ms) in all except FSC7 (PL030412), in which the action potential was most likely recorded from proximal dendrite rather than in the soma (Pyapali et al., 1998, Hu et al., 2010). In that cell an average spike width of 1.17 ms was measured. The cell showed a high spontaneous firing rate typical of PV+ CA1 area interneurons (please see 3.2.3.2. below and Chapter 5 for details and identification of the cells).

3.2.3.2. PV+ interneurons show high rate of spontaneous firing or coupling to LFP theta cycles that differ from pyramidal cells

In addition to fast spike kinetics, PV+ interneurons exhibit other electrophysiological features in juxtacellular recording that distinguish them from other interneurons and pyramidal cells. As an example, PV+ CA1 area interneurons show a high spontaneous firing

level and characteristically specific PV+ cell types fire action potentials phase-locked to (or close to) LFP theta cycle peak (Kamondi et al., 1998, Klausberger et al., 2004, Klausberger et al., 2005). The fast spiking postsynaptic cells here exhibited much higher spontaneous firing level than the pyramidal cells I presented in Chapter 3.2.2.1 (Buzsaki and Eidelberg, 1982b, Kamondi et al., 1998, Klausberger et al., 2004, Klausberger et al., 2005).

An average spiking frequency of the fast spiking neurons was 14.40 ± 2.61 Hz and their firing rate increased to average 17.35 ± 3.82 Hz during theta oscillation (mean ± SEM., n = 7). The spiking rates were statistically higher than the firing rate of the identified pyramidal cells reported above ($p < 0.05$, Student's *t*-test). These recorded neurons belong to a subpopulation that is distinctive from pyramidal cell and it is very likely that they are PV+ interneurons, because of their high spontaneous activity level and fast spike kinetics (Martina and Jonas, 1997, Csicsvari et al., 1999, Jonas et al., 2004).

In addition to high average spontaneous firing rate, certain PV+ interneuron types in the CA1 area exhibit very distinctive timing of action potential firing during hippocampal theta oscillation cycles (Klausberger et al., 2004, Klausberger et al., 2005). PV+ perisoma-targeting basket cells (BC) and axon initial segment-targeting axo-axonic cells (AAC) discharge action potentials at the opposite phase to the LFP theta cycles than pyramidal cells (Klausberger et al., 2004, Klausberger et al., 2005). Spiking of PV+ BCs and AACs is phase-locked close to the theta oscillation cycle peak rather than trough (Klausberger et al., 2005). PV-expressing

basket cells fire with a preference to the descending phase from LFP theta cycle peak, whereas AACs are strongly phase-locked to spike at the peak of theta oscillations (Klausberger et al., 2003, Somogyi and Klausberger, 2005). I analysed theta phase coupling in all putative interneurons in this study and found four cells with spike not coupling to the troughs of theta cycles (Kamondi et al., 1998, Klausberger et al., 2004).

3.2.3.3. Other electrophysiological properties that indicate CA1 interneuron but were not used here to categorise neurons

In addition to the electrophysiological features above, juxtacellular recordings in an earlier study reported other electrophysiological properties, which may be more common in interneurons than in pyramidal cells (Buzsaki and Eidelberg, 1982b). However, I have excluded them here as cell classification criteria, because I consider them too elusive and uncertain markers under my experimental conditions.

In line with previous studies I found that stimulus-evoked postsynaptic firing was elicited in CA1 interneurons by small stimulation intensities, which barely evoked a distinguishable field EPSP (fEPSP) in LFP (Buzsaki and Czeh, 1981, Buzsaki and Eidelberg, 1982b). Similar findings have been reported previously in the activation of hippocampal feed-forward inhibition (Turner, 1990). Although I did not systematically quantify evoked spike

probability and the fEPSP amplitude ratio in this work mainly because many interneuron recordings completely lack of the fEPSP (see Chapters 4, 5 and 6).

Second, synaptically evoked spikes in interneurons, when fEPSP is visible, occur at the onset or the early rising phase of the fEPSP signal, similar to what has been reported earlier (Buzsaki and Eidelberg, 1982b). This indicates that interneuron mediating feed-forward inhibition fire earlier than pyramidal cells. Pyramidal cells fire mainly at fEPSP peak or during fEPSP decay (Buzsaki and Eidelberg, 1982b).

3.2.3.4. Confirming non-pyramidal cell anatomical structure in post hoc analysis of juxtalabelled cells

Similar to my pyramidal cell juxtacellular recordings above, I also systematically aimed to label recorded interneurons with neurobiotin at the end of electrophysiological experiment (see Chapters 4, 5 and 6). In 7 stable recordings that were electrophysiologically defined as nonpyramidal cells, 5 revealed CA1 nonpyramidal cell structures. My principal criteria to confirm that a labelled postsynaptic cell was a CA1 area GABAergic interneuron is clearly visualized aspiny dendrites (Freund and Buzsaki, 1996, Spruston, 2008, Bezaire and Soltesz, 2013). These cells were then further analysed for detailed interneuron type identification in Chapters 5 and 6.

3.3. Discussion

The work described in this chapter aimed to establish criteria to judge a monosynaptic excitatory transmission response in the CA1 neurons to stimulation of commissural fibres with a microelectrode implanted in the contralateral hippocampus (Buzsaki and Czeh, 1981, Buzsaki and Eidelberg, 1982a, b). Stimulation was delivered from the CA1 area to avoid antidromic action potentials in recorded interneurons (Buzsaki and Czeh, 1981, Buzsaki and Eidelberg, 1982a). Hippocampal CA1 area excitatory neurons do not send axons to the contralateral CA1 area (Berry and Pentreath, 1976, Sik et al., 1994, Jinno et al., 2007, Ropireddy et al., 2011). Another aim in this chapter was to study whether contralateral stimulation also widely excites distinct CA1 interneuron types in addition to pyramidal cells (Blackstad, 1956). These two aims were studied here by recording monosynaptic excitatory responses (as defined above) from identified right hemisphere CA1 area postsynaptic cells. In this chapter, I also presented criteria to identify (at least partially) postsynaptic cell types by their electrophysiological parameters.

3.3.1. Electrical stimulation from the contralateral hippocampus elicits fEPSP and postsynaptic spike in the CA1 area with monosynaptic transmission characteristics

I confirmed in various recordings that single-shock electrical stimulation from the left hemisphere hippocampal CA1 area elicited the fEPSP in the right hippocampal CA1 area. The fEPSPs were systematically screened in the beginning of each experiment to confirm synaptic connectivity between the stimulation and recording areas. fEPSPs showed characteristic hippocampal fEPSP shape with a phase-locked onset and a reversed polarity in deep hippocampal layers (see Chapter 3.2.1.). During stimulus-evoked postsynaptic spike recordings from interneurons the fEPSP were often absent or negligible (see Chapter 3.2.3.3.).

In all recordings included in this study the synaptically-mediated postsynaptic spikes in right hemisphere CA1 area occurred with a short delay. The delay values in our experiments are consistent with previous reports on transmission via the monosynaptic glutamatergic projection pathway to the hippocampus (Buzsaki and Eidelberg, 1982b). Furthermore, an additional factor indicates that the postsynaptic spikes were likely to be elicited by monosynaptic excitatory EPSPs rather than polysynaptically driven synaptic excitation. The evoked postsynaptic spike delay showed little cycle-per-cycle variations, i.e. a few milliseconds (Deadwyler et al., 1975). This is an additional characteristic of monosynaptically driven postsynaptic signalling (Berry and Pentreath, 1976, Buzsaki and Czeh, 1981, Andersen et al., 2000, Andersen et al., 2007). Spikes phase-locked to stimulation and their narrow temporal distribution with small cycle-by-cycle variations are clearly seen in spike-distribution histograms I have prepared for every recorded cell in this study (see Chapters 4, 5 and 6). The above-mentioned parameters are good indicators, because spikes induced by polysynaptic excitatory events show large variability in cycle-by-cycle delay (Deadwyler et

al., 1975, Berry and Pentreath, 1976, Debanne et al., 1998). I also discovered that alterations in transmission strength (i.e. changing stimulation intensity) in the excitatory pathway increased and decreased spike probability with a small change in delay (Berry and Pentreath, 1976, Buzsaki and Eidelberg, 1982b). This relationship is demonstrated in a sample cell in Chapter 4. Spikes evoked by polysynaptic postsynaptic activity are likely to show large changes in delay when probability alters by increased or decreased stimulation strength. It seems that I am unable to directly address whether activation of the associative polysynaptic loop in the CA3 area contributes to single-shock evoked synaptic transmission between the hemispheres here. However, my results on consistent spike delay with small delay variability, and the relation of probability and delay values with altered stimulation strength indicate that the phase-locked postsynaptic spikes analysed in the 14 cells were generated by a monosynaptic excitatory connection (Deadwyler et al., 1975, Berry and Pentreath, 1976, Buzsaki and Czeh, 1981, Buzsaki and Eidelberg, 1982b). Antidromic (non-synaptic) action potentials can be excluded in this study because CA1 areas are not directly interconnected via excitatory axons (Blackstad, 1956, Buzsaki and Czeh, 1981, Buzsaki and Eidelberg, 1982a).

3.3.2. Excitatory connections from contralateral hippocampus with monosynaptic characteristics target CA1 pyramidal cells and various type of interneurons

Analyses of postsynaptic cell firing behaviour in juxtacellular recordings can be used to identify and categorise synaptically excited postsynaptic cell types or neuron subpopulations in the CA1. Thus analysing "background" spontaneous firing activity brought valuable information for cell type identification of neurons in which I recorded stimulus-evoked spikes. I managed to distinguish pyramidal cells from interneurons by the electrophysiological properties including action potential kinetics, their general firing level and complex spike activity (Csicsvari et al., 1999, Jonas et al., 2004). Spontaneous firing data provided useful material for analyses of interneurons, in particular the PV+ interneuron types. Action potential firing preference during hippocampal theta oscillation partially revealed PV+ interneuron types in this specific group. I briefly mention these analyses here in Chapter 3 and these are fully described in Chapter 5. Figures 3.4. - 3.5. illustrate individual sample cells to show how electrophysiological data complement anatomical analyses for full interneurons.

Thus, even without anatomical or immunohistochemical cell type analyses I was able to categorise recorded postsynaptic CA1 neurons to pyramidal cells and fast-spiking GABAergic interneurons. I conclude that contralateral stimulation elicits spikes in right hippocampal CA1 pyramidal cells and in non-pyramidal cells including various different interneuron types.

3.3.3. Anatomical pathways behind monosynaptic connections between the left and right CA1 areas

Although my experiments here do not directly show an anatomical monosynaptic pathway connecting the stimulation and recording area, previously published work can used to support this. Electrical stimulation in the left hemisphere CA1 area antidromically activates pyramidal cell somata, which are located either on the ipsilateral or contralateral CA3 area (Buzsaki and Eidelberg, 1982a, Andersen et al., 2007, Bezaire and Soltesz, 2013). In other words, a synaptic response detected in right side CA1 neurons comes from activation of left side CA3 pyramidal cell commissural fibres that directly innervate right side CA1 cells. In addition left side CA1 stimulation antidromically activates right side CA3 pyramidal cells, which then innervate CA1 area via Schaffer collaterals. Stimulus-evoked responses in this study emerge from activation of one or both of these monosynaptic pathways. The two pathways are illustrated in a schematic in Methods Figure 2.1B.

3.4. Figure and table

Figure 3.1

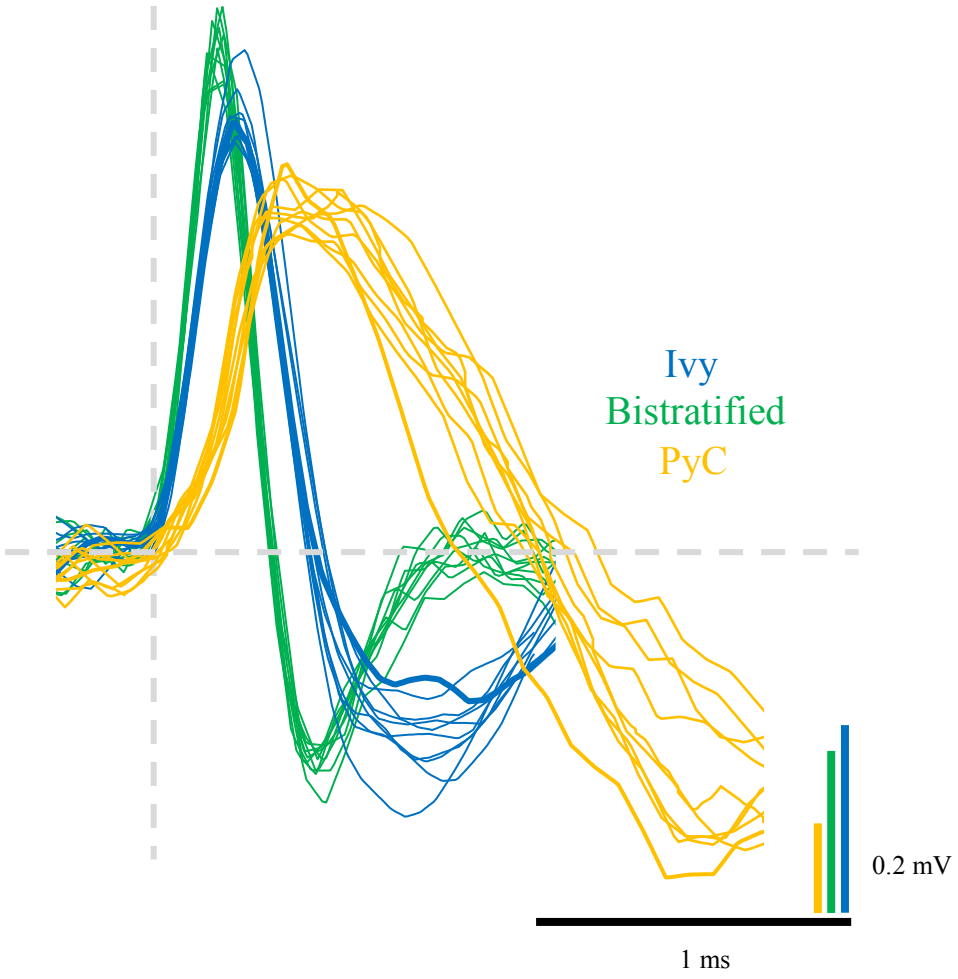

Figures 3.1. Extracellularly recorded action potentials of different CA1 neuron types. To illustrate spike waveforms of distinct CA1 neuron types, I superimposed 10 consecutive action potentials from a fast spiking PV+ bistratified cell (green), from regular spiking ivy (blue), and from a pyramidal cell (yellow). Figure demonstrates spike width from early onset (aligned to start where black vertical line is) to trough (shown by coloured dotted line for each cell type). Values defined this way are referred to as half-width in the text. Half spike width for the illustrated bistratified cell, ivy cell, and pyramidal cell are 0.384 ms ± 0.020 ms, 0.72 ms ± 0.023 ms, and 1.17 ms ± 0.018ms, respectively.

Figure 3.2.

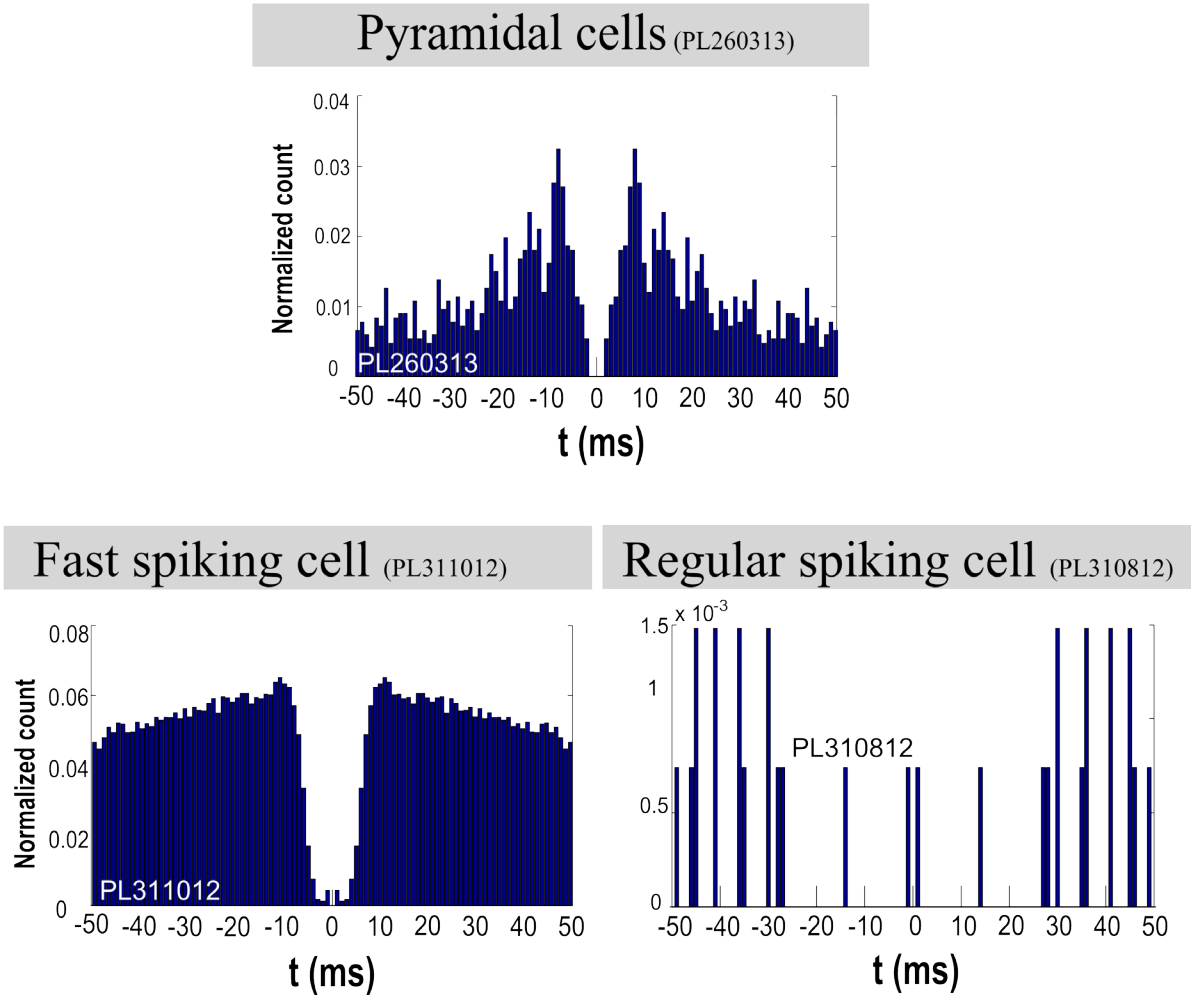

Figure 3.2. Sample spike autocorrelograms for spontaneous spiking of an identified pyramidal cell (above), a fast spiking interneurons (lower panel, left) and a regular spiking interneuron (lower panel, right). Spike autocorrelograms plot of normalized count against interspike intervals 50 ms before and after each spontaneous spike. Pyramidal cells showed a peak at 8 ms due to complex spikes, which is absent in both fast spiking and regular spiking interneurons (above).

Figure 3.3.

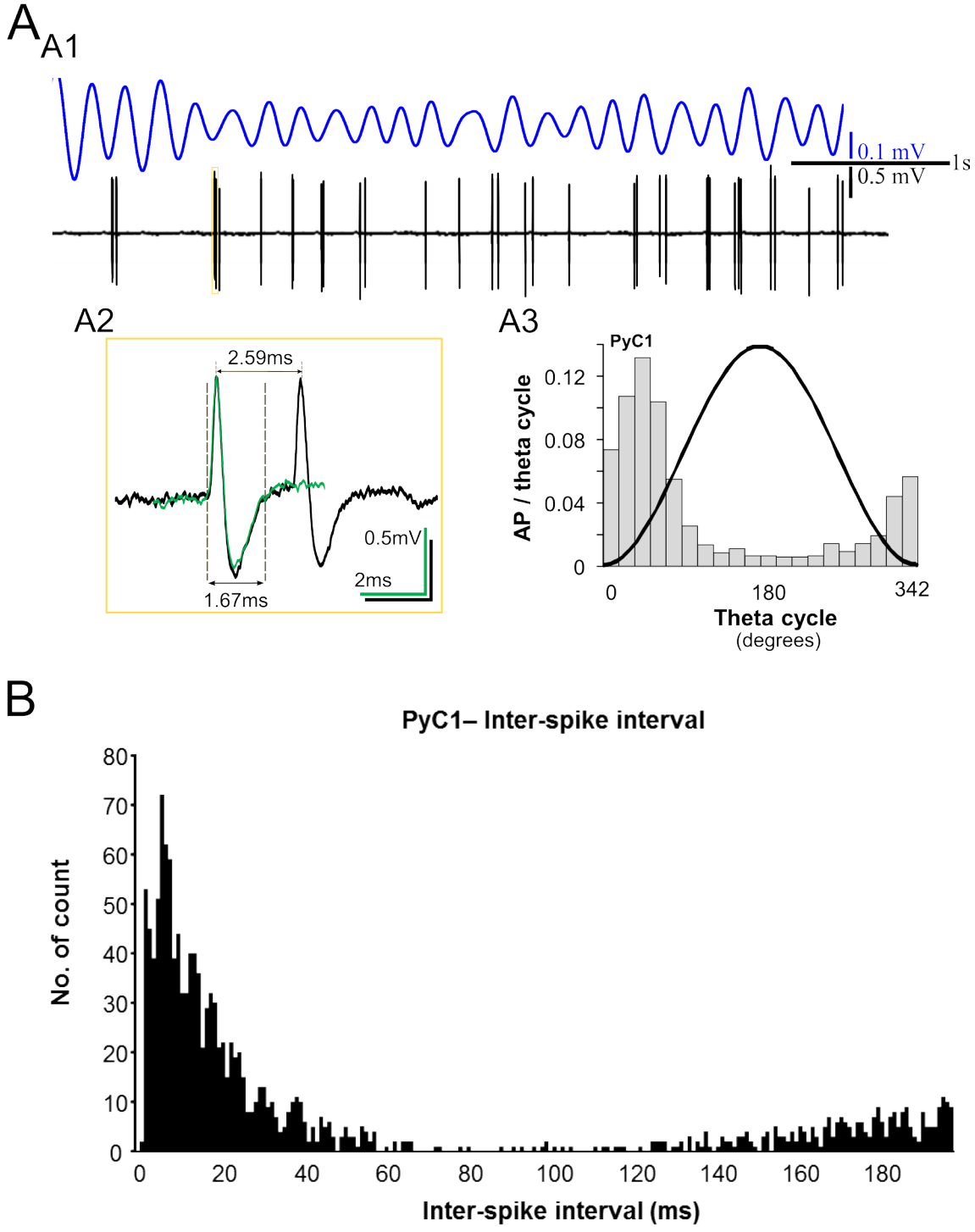
A
A1
0.1 mV
0.5 mV
1s
A2
2.59ms
1.67ms
0.5mV
2ms
A3
PyC1
AP / theta cycle
0.12
0.08
0.04
0
0
180
342
Theta cycle
(degrees)
B
PyC1– Inter-spike interval
No. of count
80
70
60
50
40
30
20
10
0
0
20
40
60
80
100
120
140
160
180
Inter-spike interval (ms)

Figure 3.3. Pyramidal cell PL240113. The cell was also anatomically identified, but not illustrated here. (A1) Sample traces of juxtacellularly recorded spontaneous action potential firing from pyramidal cell PL240113. Above (in blue) filtered local field potential (LFP) shows extracellular theta oscillation (3 – 6 Hz) recorded in the CA1 *stratum pyramidale*. Below (in black) is band-pass filtered unit trace showing juxtacellularly recorded firing of the pyramidal cell with same microelectrode. The pyramidal cell spontaneous discharge shows characteristic irregular firing on consecutive theta cycles. (A2) Superimposed sample traces of a spontaneous complex spike (black) and a synaptic stimulation-evoked spike (green) triggered by contralateral stimulation. Spikes have slow action potential kinetics (1.67 ms width) typical of pyramidal cells. In addition, short inter-spike interval complex spikes characteristic of pyramidal cells occur in this cells. (A3) Action potential firing preference of the pyramidal cell during theta oscillation is close to trough of LFP theta cycle (Klausberger et al., 2003). Vertical axis of the histogram indicates number of spikes counted during an average LFP theta cycle (theta cycle shown in black).

(B) Analysis of inter-spike interval (ISI) of spontaneously-fired action potentials reveals occurrence of short-interval complex spikes (<10 ms) in the recorded cell (Csicsvari et al., 1999). Histogram indicates irregular firing pattern with occasional short-interval spike bursts with highly regular 8 ms interval. Otherwise irregular firing of "non-complex" spikes is seen as fast decay after the peak in the ISI histogram.

Figure 3.4.

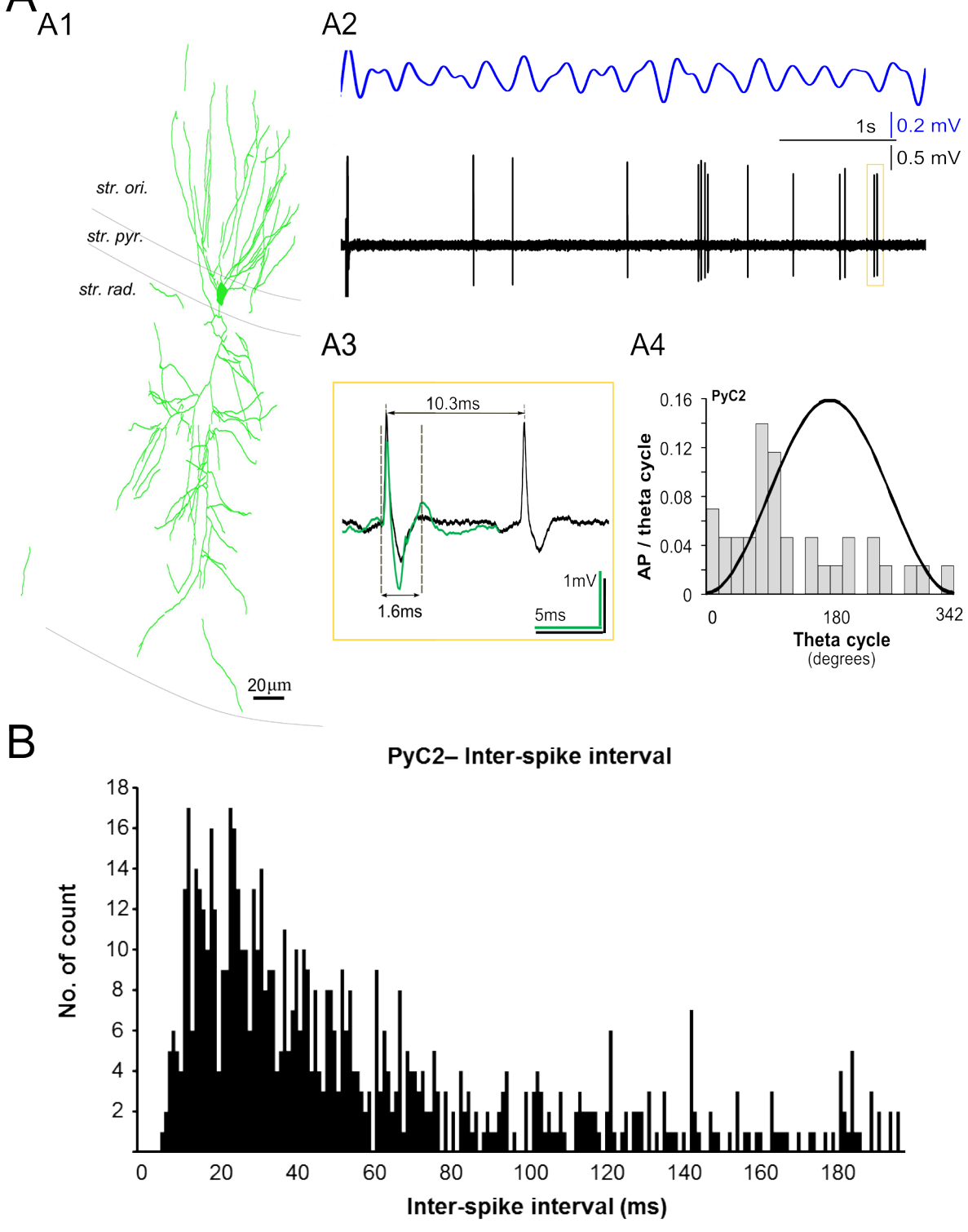
A
A1
A2
str. ori.
str. pyr.
str. rad.
20μm
1s
0.2 mV
0.5 mV
A3
10.3ms
1.6ms
1mV
5ms
A4
PyC2
AP / theta cycle
0.16
0.12
0.08
0.04
0
0
180
342
Theta cycle
(degrees)
B
PyC2– Inter-spike interval
No. of count
18
16
14
12
10
8
6
4
2
0
20
40
60
80
100
120
140
160
180
Inter-spike interval (ms)

Figure 3.4. Pyramidal cell PL120811 with anatomical verification illustrated. (A1) An illustration of the somato-dendritic structure of a labelled pyramidal cell (green), reconstructed in Image-J software with NeuroJ plug-in, under 20x magnifications. It is a representatio of a collapsed z-stack confocal fluorescence image of neurobiotin labelled neuronal structures, visualized by streptavidin conjugated with Alexa488, in one 60 μm thick section. (A2) Sample traces show LFP in blue and juxtacellularly recorded action potential firing of the cell in black. Area marked in yellow frame is illustrated in next panel. (A3) Spikes have pyramidal cell-like slow action potential kinetics (average width 1.6 ms). However, clear complex spikes with short (< 10 ms) inter-spike interval were not regularly observed in this cell, although occasionally closely packed second spikes with decreased in amplitude were seen (black) in spontaneous firing of PL120811. A sample post-synaptic spike evoked by contralateral stimulation is superimposed and shown in green. (A4) Spontaneous spike timing histogram of the recorded cell during LFP theta. In this cell the phase-preference at a theta cycle trough is less clear than in the other two pyramidal cells because of the low number of spontaneous action potentials available for analysis during theta (n = 43 compared to n = 1184 in PL240113 and n = 1278 in PL260313).

(B) Statistical analysis of inter-spike interval (ISI) fails to show a clear peak at 3 - 9 ms that reflects complex spikes, but indicates irregular low frequency firing that is also typical for CA1 pyramidal cells.

Figure 3.5.

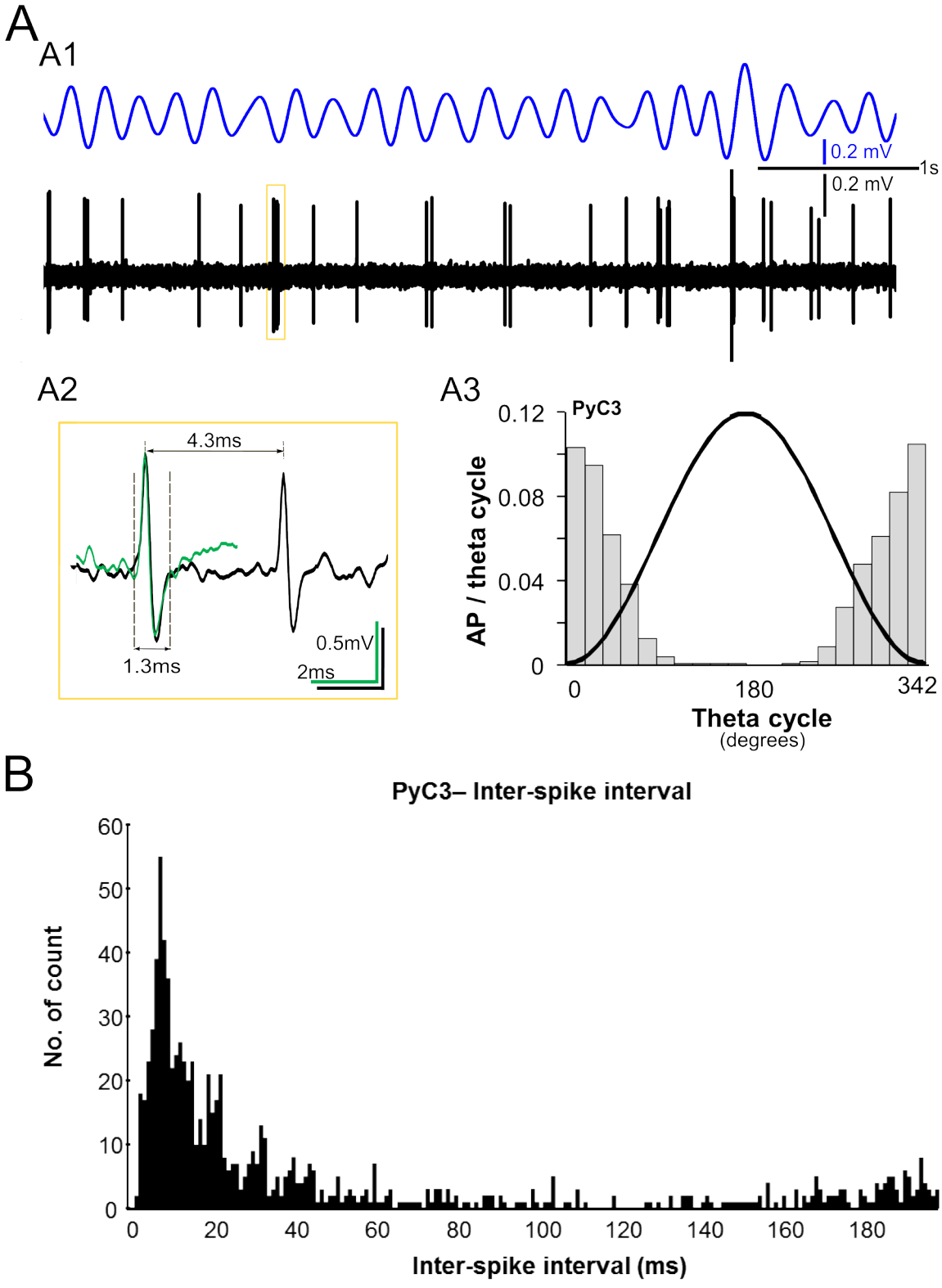
A
A1
0.2 mV
1s
0.2 mV
A2
4.3ms
1.3ms
0.5mV
2ms
A3
PyC3
0.12
0.08
0.04
0
AP / theta cycle
0
180
342
Theta cycle
(degrees)
B
PyC3– Inter-spike interval
No. of count
60
50
40
30
20
10
0
0
20
40
60
80
100
120
140
160
180
Inter-spike interval (ms)

Figure 3.5. Pyramidal cell PL260313. (A1) Sample traces during spontaneous firing of the cell (black trace) showing LFP theta oscillation at 4 Hz (in blue). Pyramidal shows irregular firing at consecutive cycles. (A2) A sample trace of extracellularly recorded spontaneous complex spike (black) and an afferent stimulation-evoked postsynaptic spike (green). The spikes show slow action potential kinetics. The cell identity could not be confirmed anatomically because of its unsuccessful labelling. (A3) Preference of spontaneous spiking during theta oscillation is clearly phase-locked to theta cycle trough.

(B) Inter-spike interval of spontaneous action potential activity shows a peak at 8 ms. Fast decay after the peak indicates otherwise irregular low frequency firing pattern.

Figures 3.6, 3.7. and 3.8. Three examples of fully identified CA1 interneuron types, which showed monosynaptic-like excitatory synaptic input to afferent stimulation from contralateral hippocampus. Samples demonstrate how electrophysiological data uncover interneurons and complement the anatomical analysis to reveal the full identity of interneuron type.

Figure 3.6.

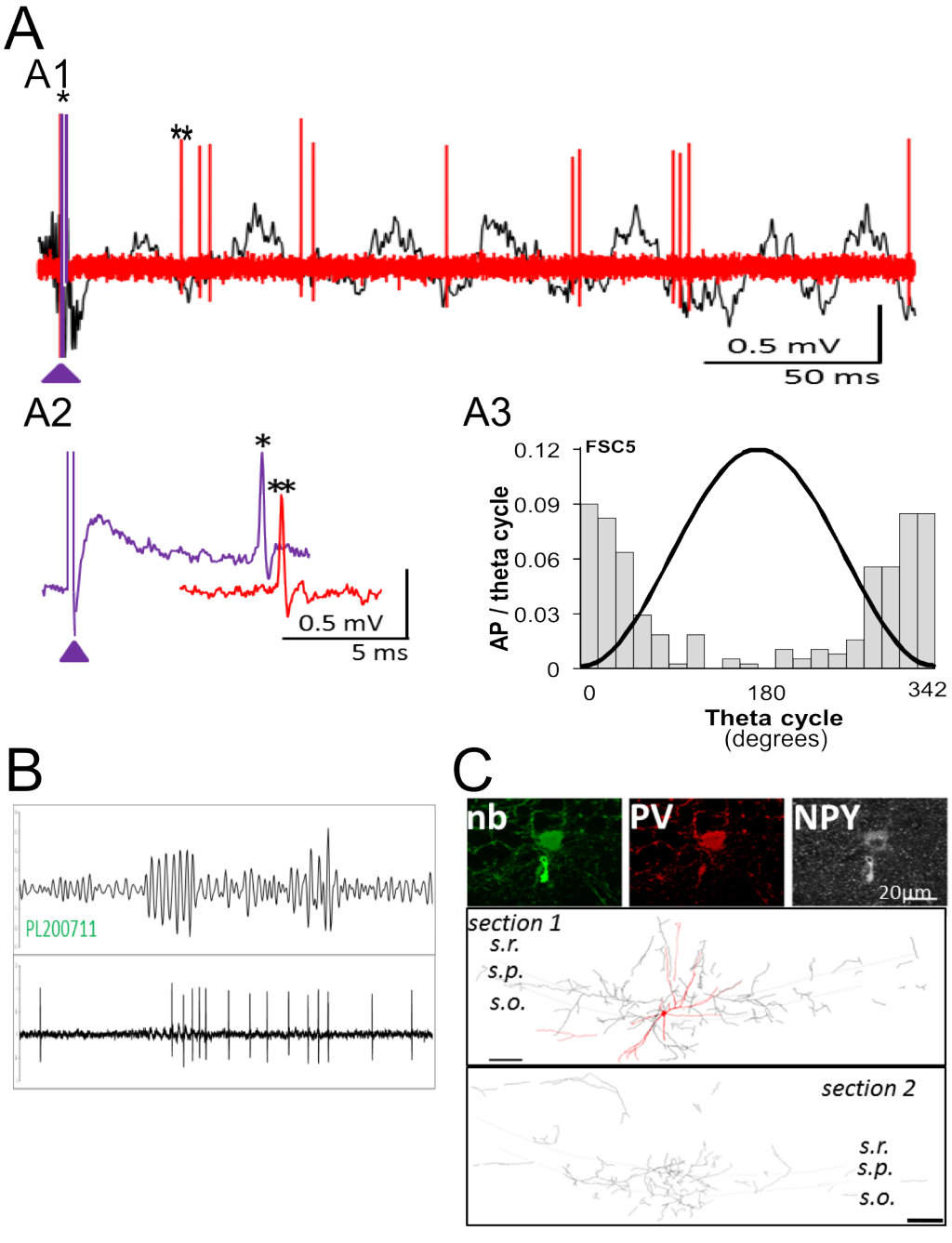

Figure 3.6. Identification of postsynaptic bistratified cell PL200711. (A1) Superimposed traces of LFP (black trace) and the cell firing (red trace) during theta oscillation. Characteristic of bistratified cells, this cell discharges during consecutive theta cycles. (A2) Cell shows fast kinetics of juxtacellularly recorded postsynaptic action potential (half-width 1 ms). Red trace shows spontaneous spike, purple trace illustrates a stimulus-evoked postsynaptic spike with stimulus artefact on left. (A3) Theta oscillation coupling analysis shows action potential firing preference at trough of a theta oscillation cycle.

(B) Occasionally sharp wave ripple events were detected (LFP band-passed filtered 90-200 Hz) (above). The cell fires (below) vigorously throughout the ripples. Intense firing activity during these events in urethane anaesthetised rat is characteristic of fast-spiking CA1 bistratified cells (Klausberger et al., 2004).

(C) Confocal images show immunopositivity of the neurobiotin (nb, streptavidin-alexa488) - labelled cell for PV (secondary antibody in Cy3) and NPY (Cy5). Below is a reconstruction of DAB labelled somatodendritic (red) and axonal (black) structure of the recorded cell. Co-expression of PV and NPY in the CA1 area is a hallmark of bistratified cells (Klausberger et al., 2004). Scale Bars, 20 μm for micrographs and 100 μm for reconstruction.

Figure 3.7.

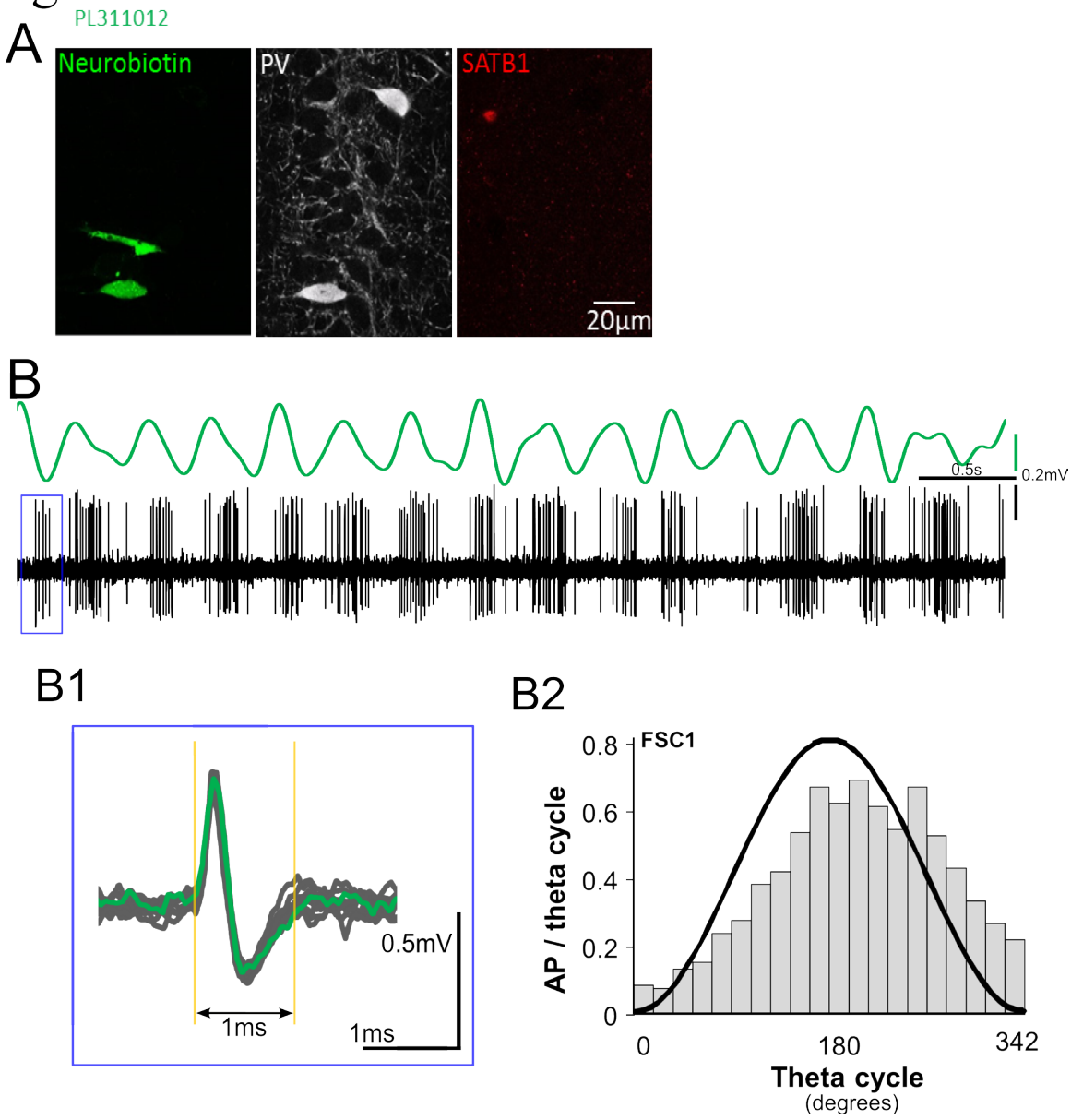
PL311012
A
Neurobiotin
PV
SATB1
20µm
B
0.5s
0.2mV
B1
0.5mV
1ms
1ms
B2
FSC1
AP / theta cycle
0.8
0.6
0.4
0.2
0
0
180
342
Theta cycle
(degrees)

Figure 3.7. Identification of postsynaptic PV+ axo-axonic cell PL311012. (A) Confocal images show immunpositivity of neurobiotin (Alexa488, Green) -filled recorded cell for cytoplasmic PV (Cy5, white) and immunonegativity for transcription factor SATB1 (Cy3, red). The recorded cell is PV+, but SATB1- although nearby PV+ cell show nuclear positive signal for SATB1. Scale bar, 20 μm. This combination is characteristics of axo-axonic cells in the CA3 area (Viney et al., 2013).

(B1) Local field potential (green) during theta oscillation and spontaneous action potential firing of the cell (black). Scale bars as shown. (B2) Spike shows characteristic rapid kinetics of fast-spiking PV+ cells (1 ms spike width). (B3) Cell shows peculiar spike firing preference at the peak of theta oscillation cycle, characterised only in PV+ axo-axonic cells in the CA1 area (Somogyi and Klausberger, 2005).

Figure 3.8.

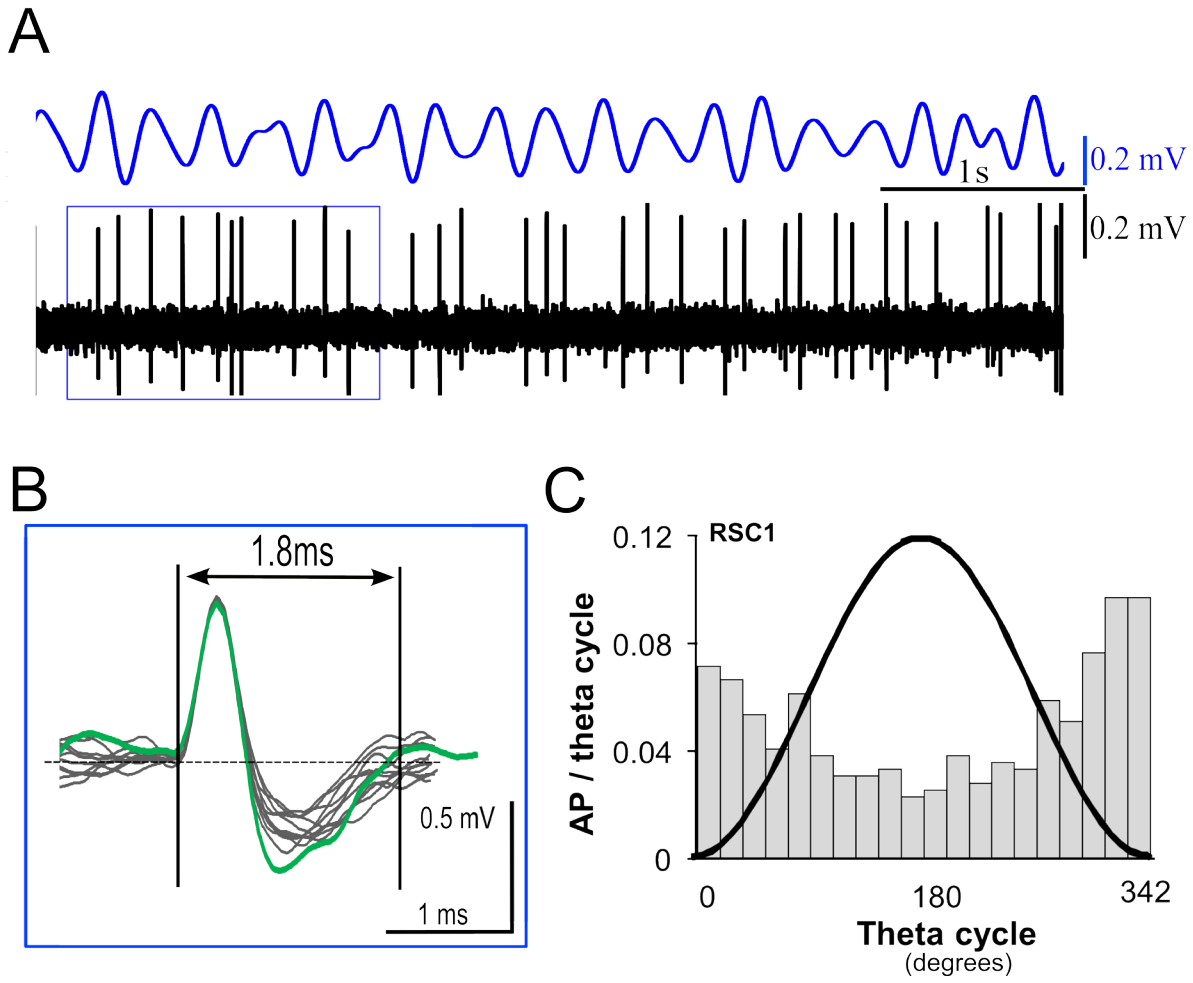

Figure 3.8. Identification of postsynaptic CA1 area ivy cell PL170412 (anatomically confirmed, not shown). (A) Sample traces of spontaneous action potential firing of the cell (black trace) and LFP (blue) during theta oscillation. The cell shows regular rhythmic firing during theta which is a common characteristic for interneurons in the CA1 area and different to pyramidal cells (Somogyi and Klausberger, 2005). (B) Superimposed spontaneous extracellular action potentials from the cell show slow kinetics (spike width 1.8 ms) typical of ivy cells (Fuentealba et al., 2008). (C) Histogram shows firing during theta cycles with superimposed one theta cycle (black). PL170412 fires at all phase of theta oscillations, without clear preference although more firing occurs towards the trough.

Figure 3.9.

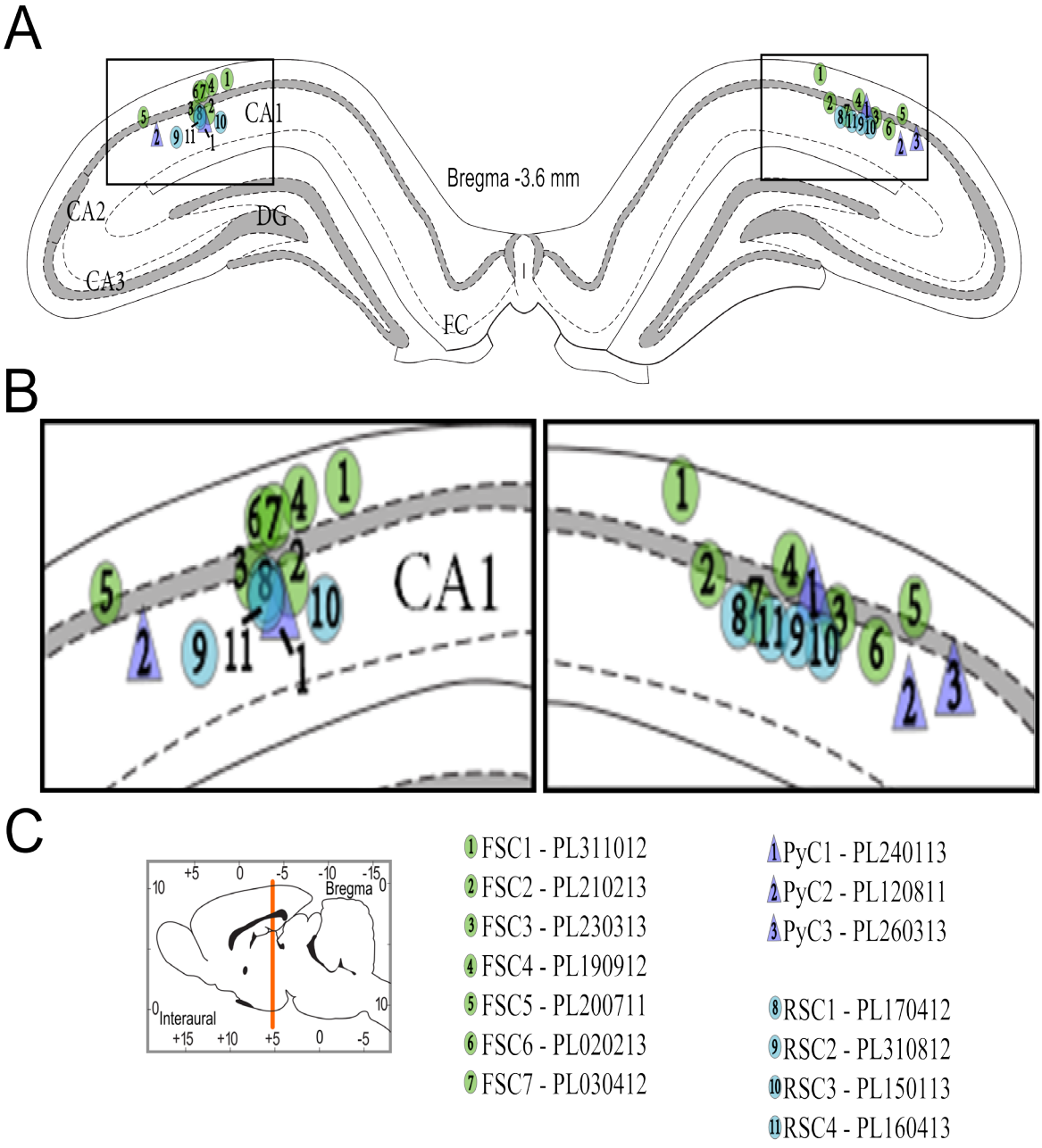
A
CA1
CA2
CA3
DG
FC
Bregma -3.6 mm
B
CA1
C
Bregma
Interaural
FSC1 - PL311012
FSC2 - PL210213
FSC3 - PL230313
FSC4 - PL190912
FSC5 - PL200711
FSC6 - PL020213
FSC7 - PL030412
PyC1 - PL240113
PyC2 - PL120811
PyC3 - PL260313
RSC1 - PL170412
RSC2 - PL310812
RSC3 - PL150113
RSC4 - PL160413

Figure 3.9. *Post hoc* analysis of stimulation and recording electrode positions in the CA1 area (rostral-caudal axis collapsed in the schematic).

A schematic drawing of hippocampal CA1 areas in left and right hemispheres showing positioning of the stimulation and recording microelectrodes for 14 experiments in this study. A) For simplicity, rostral-caudal axis (between Bregma -3.2 mm and -3.9 mm) is collapsed in the schematic and positions are shown in a one transversal hippocampal cut at Bregma -3.6mm, as described in Chapter 2.3.2. Numbered purple triangles represent *post hoc* verified stimulation sites and recording sites for pyramidal cells presented, fast spiking cells are labelled and marked in green circles, and blue circles represent regular spiking cells (as labelled in the key panel below).

B) A panel shows zoomed-in hippocampal CA1 areas corresponding to black boxed area in panel above.

C) Inset on the left shows a sagittal section with orange lines across the hippocampus corresponding to rostral-caudal stereotaxic coordinates of the recording area and collapsed schematic drawings above. A key showing individual experiments labelling and numbering is presented in right.

4. Activity-induced long-term potentiation in excitatory hippocampal fibres to CA1 area pyramidal cells *in vivo*

4.1. Introduction

In the previous chapter I demonstrated that electrical stimulation from contralateral hippocampus elicits excitatory postsynaptic responses in the right hemisphere hippocampal CA1 area neurons *in vivo*. In the experiments selected for further investigation, the stimulated pathway showed two critical characteristics of a monosynaptic excitatory connection: 1) short monosynaptic-like delay of the evoked postsynaptic action potential in the contralateral target cell, and 2) about 3 ms cycle-by-cycle variability in delay from stimulation to action potential onset (Deadwyler et al., 1975, Berry and Pentreath, 1976, Debanne et al., 1998). Next, in this and the following two chapters I will study plasticity in this excitatory pathway to identified CA1 area neurons *in vivo*. This is novel since plasticity in excitatory pathways to different identified CA1 neuron types has not been directly studied *in vivo* before. The CA1 neuron types recorded in the present study include pyramidal cells (n = 3, Chapter 4), fast spiking PV+ interneurons (n = 7, Chapter 5) and regular spiking interneurons (n = 4, Chapter 6) (see Chapter 3.2.1 and Chapter 3.2.2.).

First, I tested if a common LTP-induction paradigm elicits long-term potentiation in the "transhippocampal" pathway to identified postsynaptic pyramidal cells *in vivo* (Chapter 3.2.2.). Assuming that long-term potentiation takes place in a monosynaptic pathway, an increase in spike probability with shortened or unchanged spike delay with little effect on cycle-by-cycle variation in delay to stimulation is expected (Deadwyler et al., 1975, Berry and Pentreath, 1976, Debanne et al., 1998). Behaviour of these parameters in a potentiated

pathway would bring important additional information to either support or challenge my earlier conclusion that excitatory transmission in the studied "transhippocampal pathway" is monosynaptic rather than polysynaptic (see Chapter 3). The result indeed showed systematic increase in stimulus-evoked postsynaptic spike probability. In addition, the evoked spikes preserved short spike delay and cycle-by-cycle coherence of the spike delay. These observations would be difficult to explain with polysynaptically driven postsynaptic action potentials (Deadwyler et al., 1975, Buzsaki and Eidelberg, 1982b, Debanne et al., 1998). I have performed detailed analysis on the evoked spike probability, delay and spike cycle-by-cycle variation before and following potentiation in the results section below.

4.2. Results

4.2.1. A common LTP-induction paradigm elicits long-term potentiation of excitatory synaptic connection to CA1 pyramidal cells *in vivo*

I adjusted stimulation intensity to elicit stimulus-evoked postsynaptic action potential roughly at half-maximal (50 %) probability in the excitatory pathways to CA1 pyramidal cells mentioned above. However, the evoked spike probability moderately varies between the experiments, since an estimation of stimulation intensity for half-maximal probability was performed only by visual inspection for a few minutes before pre-TBS recording (see Chapter 4.2.1.1.). In the three experiments, electrical stimuli were delivered to the

contralateral hippocampus at 450 μA, 200 μA and 525 μA stimulation intensities to elicit postsynaptic responses in the pyramidal cells (PyC 1-3 i.e. PL240113, PL120811, and PL260313) during pre-TBS, respectively.

After setting the stimulation intensity, I collected pre-TBS baseline with afferent low-frequency (every 5 s) stimulation for at least 10 min. During this period, I also ensured stability of the recording. Recording was considered stable when extracellularly measured postsynaptic spike amplitude was large enough (at least 2 times more than noise level) and the noise level remained constant and smaller than 0.1mV to allow accurate extracellularly recorded spike analysis. I also monitored the spontaneous firing level throughout the recording and ensured it remained constant. It has been reported that if microelectrode juxtaposition was causing damage to a recorded cell, this was associated with sudden increase in spontaneous firing of the recorded neuron and elongation of spike kinetics (Pinault, 1996). Anaesthesia was maintained with intraperitoneal injection of xylazine and ketamine mixture, application of which gradually shifted the oscillation pattern in LFP from theta (4-6 Hz) activity to slow waves (see Methods Chapter 2.4.3.) (Klausberger et al., 2004, Klausberger et al., 2005). In most cases, noxious somatosensory stimuli, applied as paw or tail pinches (for 2 s) would temporarily elicit theta oscillation (Buzsaki and Eidelberg, 1982b, Klausberger et al., 2004). I aimed to record spontaneous activity of recorded cells both during theta and slow wave activity periods.

Next, an electrical stimulation paradigm, which is commonly used in acute hippocampal slices recording to elicit LTP, was applied to test long-term plasticity in the excitatory synaptic pathway to pyramidal cells. Theta-modulated high-frequency burst stimulation pattern (i.e. TBS, 5 pulses at 100 Hz, given every 200 ms and repeated 20 times) was delivered through the stimulation electrode to the "transhippocampal pathway" using the same half-maximal stimulation intensity. Then, the single pulse (every 5 s) stimulation was resumed to monitor strength of the excitatory connection to the recorded cell after TBS. I continued to collect data for at least 40 min for all recorded pyramidal cells (up to 100 min in one cell, PyC2- PL120811).

Evoked spike probability and delay in response to single shock pulse stimuli measured the strengt***h*** of the excitatory pathway, and were compared between baseline and post-TBS recording. In parallel, I quantified spontaneous firing activity of the neurons. Alterations in spontaneous firing rate may reflect changes in postsynaptic cell excitability (Klausberger et al., 2004, Klausberger et al., 2005). Hence, differences in the evoked spike probability, i.e. P(spike), was tested comparing periods with similar spontaneous firing rates when possible.

If no similar spontaneous firing rate range can be found between pre- and post- TBS, windows contains spontaneous spiking rates were selected for comparison in pre-TBS in the case of LTP, and vice versa. Evoked spike delay values were calculated from the same

selected time periods as P(Spike).

4.2.1.1. Synaptically-evoked postsynaptic action potentials during baseline and following TBS

Delivering TBS increased the single shock-evoked spike probability in all three pyramidal cells in the post-TBS period (see figures 4.1. - 4.3.). To exclude the potential influence of altered spontaneous firing rate on the increased stimulus-evoked spike probability, I compared periods with similar or reduced spontaneous firing rate during baseline and following the TBS. Spontaneous firing level well correlates with brain states characterized by LFP oscillatory pattern showing theta or slow waves (Klausberger et al., 2005). The spontaneous firing levels are quantified and shown in every LTP plot presented in this study on pyramidal cells (Figures 4.1. – 4.3) and on other neuron types later (Chapter 5 and 6). I present data on evoked spike probability and delay with quantified spontaneous firing for pyramidal cells in Figures 4.1. – 4.3. In addition, results on stimulus-evoked spike plasticity, their spontaneous firing and pyramidal cell electrophysiological identification are summarized in Table 4.1.

In PyC1, the evoked spiking probability increased from 0.47 in baseline to 0.74 ($p <$ 0.001, Chi-square test). A more substantial increase was observed in PyC3-PL260313 from

0.26 to 0.77 $p < 0.01$, Chi-square test). The TBS also elicited long-term potentiation in PyC2, with increased evoked spike probability from 0.41 to 0.99 $p < 0.01$, Chi-square test). All three cells were recorded for at least 40 min following TBS (post-TBS) and in PyC 2 (PL120811) the responses were followed for 100 min in post-TBS conditions. In all three experiments the long-term potentiation shows significant increase in the evoked spike probability throughout the post-TBS period (Figure 4.1B, 4.2B, and 4.3B).

In all three pyramidal cells, spike latency remained statistically unchanged between pre- and post-TBS recording. According to the Mann-Whitney tests, spike latency values at any stage of post-TBS period are not statistically different from baseline values in PyC1 and PyC3. In PyC2 (PL120811) the spike latency was transiently shortened initially for 15 min in parallel with increased evoked spike probability. Spike latency decreased from 11.79 ms (± 0.11 ms, mean ± S.E.M.) in the baseline to 10.54 ms (± 0.055, mean ± S.E.M.) ($p < 0.05$, Mann-Whitney test). However, no difference in spike latency was observed in later time point, in the same cell (PyC2, PL120811), even though the P(Spike) is potentiated.

Finally, I analysed if the evoked spikes during post-TBS period were more coherently or less coherently organized in time, indicating by the range between 25 % and 75 % percentile of spike delay (25 % - 75 % percentile range). I compared data points of spike delay in 15 min windows and looked into late LTP time points (30-45 min from TBS). For

PyC2, 25 % - 75 % percentile range was shortened from 1.69 ms in baseline to 0.25 ms at a late post-TBS time windows ($p < 0.05$, Kolmogorov-Smirnov test). However, no statistically significant change in spike delay data distribution was observed in the other two pyramidal cells. The evoked spike delay range (25 % - 75 % percentile range) in PyC1 was 1.07 ms in the baseline and remained statistically unchanged in late post-TBS (1.39 ms) (range from 25 % to 75 % percentile). The evoked spike range in PyC3 was 2.86 ms (from 25 %-75 % percentile range) in baseline and 1.85 ms in a late post-TBS time window, but delay value distribution was not statistically different from baseline ($p > 0.05$, Kolmogorov-Smirnov test).

It is worth stressing that contralateral stimulation-evoked spikes showed very narrow distribution temporal window in all three pyramidal cells. It is very unlikely that polysynaptic connections could generate such a temporally precise distribution that remains similar or becomes more coherent after the robust increase in the spike probability.

4.2.1.2. Pyramidal cell spontaneous firing and brain states during plasticity experiments

In parallel with stimulus-evoked action potentials, spontaneous firing of postsynaptic cells was followed and analysed throughout the experiments. Spontaneous firing was

systematically quantified for 1 s periods just before afferent single shock stimuli (applied every 5 s). In general, the pyramidal cells firing levels were low. The cells PyC1 and PyC3 fired spontaneously at average frequency of 3.82 Hz and at 2.43 Hz during baseline, respectively. The remaining cell, PyC2, fired less (1.11 Hz) in baseline, but showed the highest average spontaneous firing rate during LFP theta oscillations (2.94 Hz) (Table 4.1, Figure 4.1. – 4.3.). I have quantified and illustrated the average spontaneous firing throughout the experiments in parallel with stimulation-evoked spike data for the cells in Figures 4.1. 4uuuuuu.2. and 4.3. In addition, spontaneous firing data are summarized in Table 4.1 I have also indicated in the experiments underlying brain states identified by the LFP oscillatory pattern either as theta or non-theta. The latter occasionally comprise slow waves and slow wave activity associated with sharp wave ripple episodes. Although the spontaneous "background" firing level varied during the course of the experiment during these recordings, an altered spontaneous firing level or alternating LFP oscillatory pattern cannot explain the long-term potentiation in the evoked spike probability. Results on pyramidal cells spontaneous activity in the plasticity experiments are summarized in Table 4.1.

4.3. Discussion

In this chapter I have analysed experiments on long-term plasticity of excitatory synaptic connections to identified hippocampal CA1 pyramidal cells *in vivo* described

above in Chapter 3. In Chapter 3 I presented evidence that the transhippocampal pathway, activated by electrical stimulation in the contralateral hippocampal CA1 area, elicits "monosynaptic delay-like" action potential firing in identified postsynaptic CA1 pyramidal cells. Here I particularly tested if this connection is permanently potentiated following high-frequency stimulation applied to the synaptic pathway. The same stimulation paradigm i.e. TBS, has been reported in hippocampal slices to evoke long-term potentiation in excitatory synapses to hippocampal pyramidal cells and in addition LTP or LTD in CA1 interneurons (Larson et al., 1986, Staubli and Lynch, 1987, Otto et al., 1991, Bliss and Collingridge, 1993, Nissen et al., 2010). Although brain slice experiments have revealed details of LTP induction and expression and uncovered its molecular mechanisms, only a few studies have hitherto investigated long-term synaptic plasticity in intact hippocampus (Buzsaki and Eidelberg, 1982b, Kohl et al., 2011, Shipton et al., 2014).

4.3.1. Robust LTP in excitatory synaptic connections to CA1 pyramidal cells

Results on synaptic long-term potentiation in pyramidal cells in anaesthetised rat are important to this research project for two major reasons. First, the experiments I presented in this chapter prove that the high-frequency afferent stimulation (i.e. TBS) *in vivo* anaesthetised rat manages to reproduce results regularly reported in acute hippocampal slices on potentiation of excitatory synaptic pathways to CA1 pyramidal cells (Larson et al.,

1986, Staubli and Lynch, 1987, Otto et al., 1991, Bliss and Collingridge, 1993). Second, the successful LTP obtained from on postsynaptic CA1 area pyramidal cells mean that this experimental paradigm is a valid method to study activity-induced plasticity in excitatory synaptic pathways to other identified CA1 neuron types. LTP and LTD in the CA1 area nonpyramidal cells have been investigated in brain slices, but not in intact brain *in vivo* until now (Buzsaki and Eidelberg, 1982b, Kullmann and Lamsa, 2011).

It is noteworthy that LTP in these experiments was elicited in the presence of low dosage of NMDA receptor (NMDAR) antagonist ketamine. Although the ketamine concentration in the brain was not directly measured here, its presence in the brain was reflected by oscillatory activity in LFP, which was constantly monitored through experiments. Application of ketamine and xylazine mixture (see Methods Chapter 2.2) intraperitoneally changed the anaesthesia level of the rats and altered oscillation pattern in LFP towards non-theta states where slow waves occur in the hippocampus (Soltesz and Deschenes, 1993). Therefore, it is plausible that level of the NMDAR inhibition was higher in the brain in experiments where ketamine levels had been recently topped up and the hippocampal activity showed non-theta slow waves rather than theta activity. However, robust LTP was observed in all three pyramidal cells when the plasticity induction protocol was applied at theta (in PyC1, PL240113 and PyC2, PL120811) or in non-theta activities (PyC3, PL260313). Therefore, I conclude that although ketamine is a non-competitive NMDA receptor antagonist, its levels in the brain in these experiments was not sufficient to block LTP in CA1 pyramidal cells. However, it was shown that LTP in the CA1 pyramidal

cells requires activation of NMDARs (Bliss and Collingridge, 1993) and both ipsilateral Schaffer collaterals and contralateral commissural pathway LTP in CA1 pyramid cells depend on NMDARs (Kohl et al., 2011).

4.3.2. Synaptically-evoked spike distribution in the pre- and post-TBS supports observations on monosynaptically evoked spike

The data on synaptic plasticity experiments further support other observations (Chapter 3.2.1. and 3.2.2.) that postsynaptic spikes evoked by stimulation of contralateral pathway were elicited by monosynaptic excitation rather than polysynaptic activity. Although in most analysed post-TBS time points spike delays failed to show shortening compared to baseline, the synaptically-evoked spike delay data were organized in a compact temporal window (i.e. restricted within three millisecond range in all cells. This can be clearly seen in individual data histograms of the experiments in Figures 4.1. – 4.3.

However, perhaps even a more important result of the spike delay analysis here was the finding that following a robust increase in the evoked spike probability by TBS, the temporal distribution of evoked spike delays remained strikingly compact and cycle-by-cycle variability remained unchanged after TBS. In one of the three pyramidal cells studied, the evoked spike delay distribution became even narrower than in the baseline. As pointed

out above, such a relation between a robust increase in synaptically-evoked postsynaptic spike probability and unchanged cycle-by-cycle variability in spike delay indicate mono- rather than polysynaptically driven action potential generation in the postsynaptic cells (Deadwyler et al., 1975, Berry and Pentreath, 1976, Debanne et al., 1998).

4.4. Figures and table

Figures 4.1, 4.2. and 4.3. LTP induction paradigm elicits a long-term potentiation in the excitatory synaptic pathway to CA1 pyramidal cells in anaesthetised rats *in vivo.* Three experiments on identified postsynaptic pyramidal cells.

Figure 4.1.

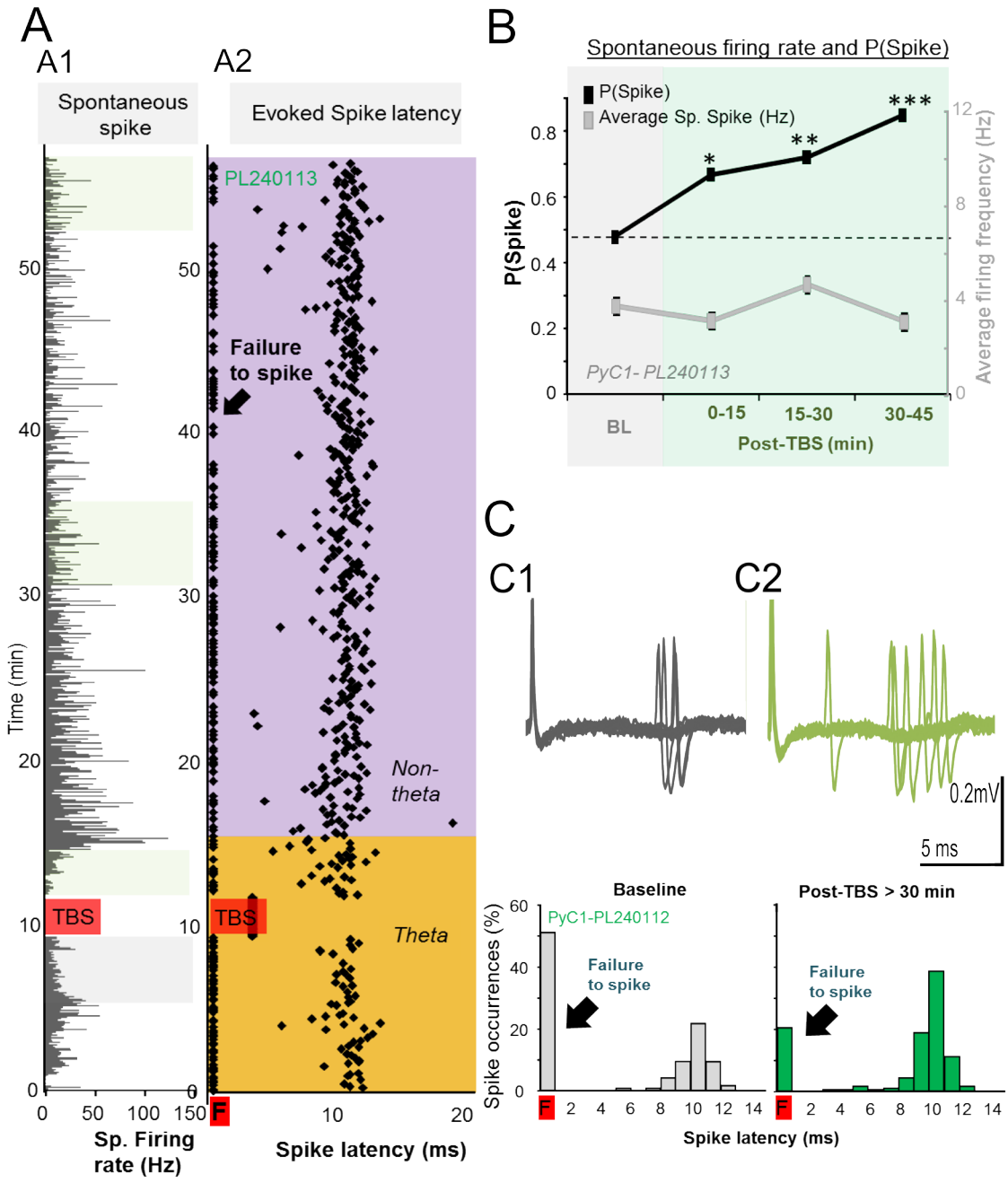

Figure 4.1. LTP in pyramidal cell PL240113. (A) Long-term potentiation in stimulation-evoked monosynaptic spike probability in pyramidal cell PL240113 by theta-modulated high frequency stimulation (TBS) of the afferent excitatory pathway. Ordinate shows time line of the recording from beginning of baseline, a delivery of TBS (timing marked in red) and > 40 min post-TBS recording. (A1) Spontaneous firing of the recorded cell ("Spontaneous spike") is illustrated as a horizontal histogram showing count of action potentials (abscissa, count per second) throughout the experiment (see Methods Chapter 2.4.4 and Results Chapter 4.2.1.2.). Time periods marked with background colour in grey and green show time windows plotted in *B* and used for statistical comparison of stimulus-evoked spike probability between baseline and post-TBS. (A2) Dot plot shows stimulus-evoked action potential probability and delay in the same cell as a function of time (ordinate as in A1). Dots represent evoked action potentials cycle-by-cycle with a delay to contralateral afferent stimulation. Failure to fire is indicated on the left as "F" (highlighted in red box). Different background colours in the dot plot indicate visually verified brain states, either theta oscillation (3-6 Hz, yellow) or non-theta in the LFP (violet).

(B) Increased average probability of the stimulation-evoked postsynaptic action potential and unchanged spontaneous firing level in the cell shown at different time points (mean ± S.E.M) colour coded in A1. Spike probability, "P(Spike)",was calculated at time windows with similar spontaneous firing level. P(Spike) values are plotted with black dots and line. (Probability scale is shown in left ordinate). Grey dots and line illustrate spontaneous mean ± SEM of firing level in same recording periods (Scaling on the right is the "average firing Hz"). Statistical significance (compared to the baseline): *, $P<0.05$; **, $P<0.01$; ***, $P<0.001$ (Chi-square test). Dotted line illustrates P(Spike) mean in baseline.

(C) Histogram and consecutive traces from original recording showing stimulation-evoked juxtacellularly recorded postsynaptic action potentials in the pyramidal cell. (C1) Traces of evoked spikes (above) and a spike occurrence histogram (below) show a short and consistent delay (small cycle-by-cycle variability) to afferent stimulation. Timing of stimulation is seen in traces as a voltage artefact at 0 -time point. Stimulation cycles with postsynaptic spike failures in the histogram are indicated in left as "Failure to spike". (C2) Evoked spikes in the cell 30 min after TBS. Above are 10 consecutive extracellular recording traces (green). Histogram below shows a significant reduction in postsynaptic spike failures ("Failures to spike" column) to stimulation following TBS (30 - 40 min) indicating LTP. In addition, note unchanged delay and cycle-by-cycle variability of spike delay although spike probability has substantially increased.

Figure 4.2.

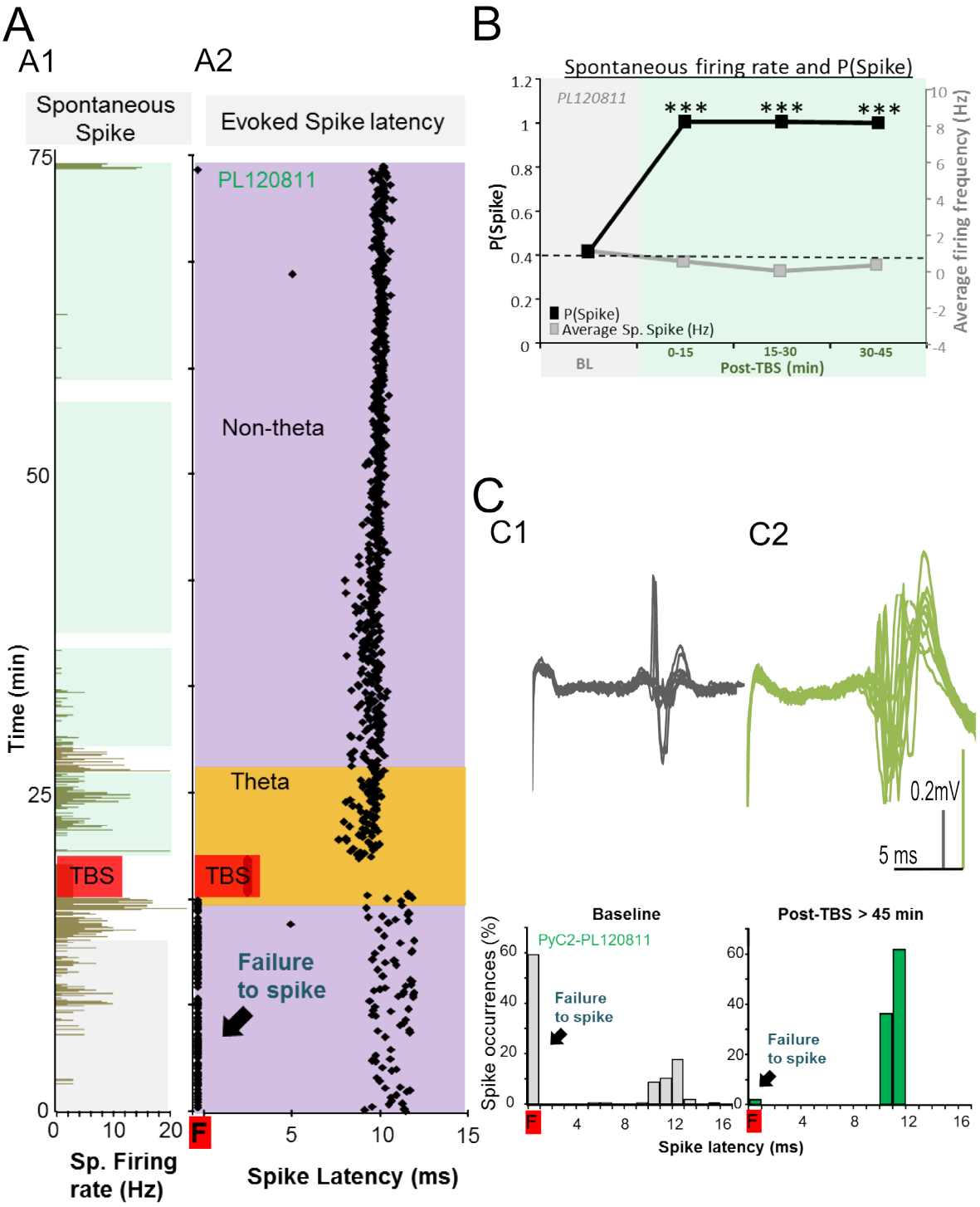
A
A1
A2
Spontaneous Spike
Evoked Spike latency
PL120811
Non-theta
Theta
TBS
TBS
Failure to spike
Time (min)
Sp. Firing rate (Hz)
Spike Latency (ms)
B
Spontaneous firing rate and P(Spike)
PL120811
P(Spike)
Average firing frequency (Hz)
P(Spike)
Average Sp. Spike (Hz)
BL
0-15
15-30
30-45
Post-TBS (min)
C
C1
C2
0.2mV
5 ms
Baseline
Post-TBS > 45 min
PyC2-PL120811
Failure to spike
Spike occurrences (%)
Spike latency (ms)

Figure 4.2. LTP in pyramidal cell PL120811. (A) Dot plot of stimulation-evoked spike probability and delay in pyramidal cell PL120811 before and following TBS (timing of TBS indicated in red). Ordinate shows time. (A1) Spontaneous firing ("Spontaneous spike") horizontal bar histogram for spike count (abscissa, count in 1 s period taken every 5 s). Time periods marked with grey and green background indicate periods in baseline and after TBS used for statistical comparison of spontaneous activity level and stimulus-evoked spike probability in panel *B*. (A2) Dot plot of stimulus-evoked action potentials as a function of time. Dots represent pyramidal cell spikes evoked by afferent stimulation cycle-by-cycle showing a delay (abscissa). Failures to spike are indicated in left as "F". Different background colours in the dot plot mark episodes with LFP theta oscillation (3-6 Hz, yellow) or non-theta (violet).

(B) Plot of increased stimulus-evoked spike probability and unchanged spontaneous firing in the cell following TBS at different time points indicated in abscissa. Time windows for the analysed data are colour-coded in *A1*. Evoked spike probability is shown in black, "P(spike)", scaling in left. Grey dots and line show mean ± SEM of spontaneous firing (scaling in right, "average firing Hz"). Dotted line illustrates P(Spike) mean in baseline. ***, $P < 0.001$ (Chi square test).

(C) Histograms and traces illustrate stimulation-evoked postsynaptic action potentials in the pyramidal cell in baseline and during LTP. (C1) In the baseline consecutive traces of evoked spikes (top) with failures and a histogram (below) of spike delay and probability. Stimulation cycles with high proportion of spike failures are shown in column "Failure to spike". (C2) Evoked spikes in the cell 30 min after TBS. Above are consecutive traces with no failures to spike, below is a histogram showing drastically reduced number of failures (in "Failure to spike") indicating LTP. In addition, note preservation of temporal coherence in cycle-by-cycle variation of the evoked spike delay after TBS.

Figure 4.3.

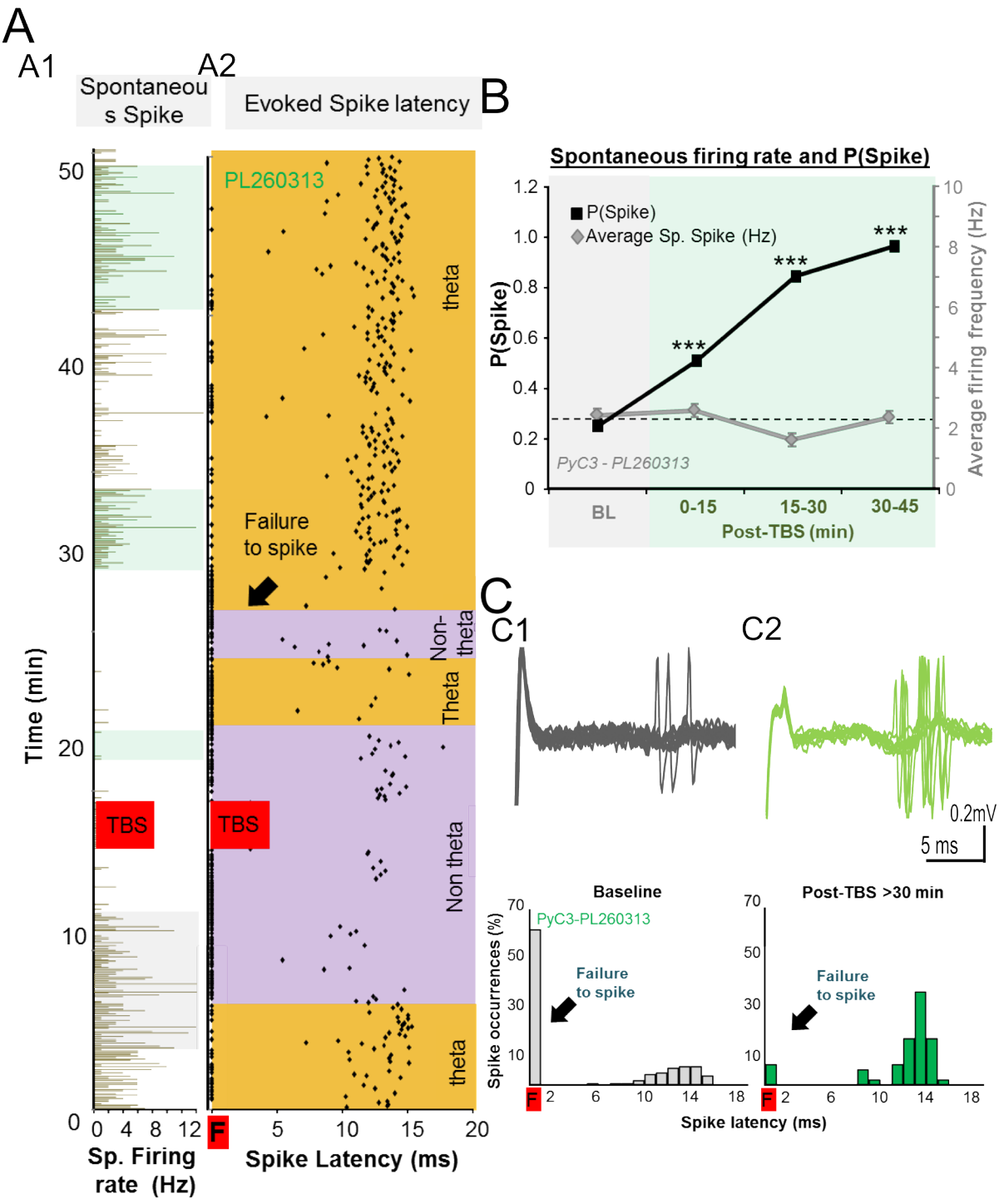
A
A1
A2
Spontaneous Spike
Evoked Spike latency
B
PL260313
theta
Failure to spike
Non-theta
Theta
Non theta
theta
TBS
TBS
Time (min)
Sp. Firing rate (Hz)
Spike Latency (ms)
F
Spontaneous firing rate and P(Spike)
P(Spike)
Average Sp. Spike (Hz)
Average firing frequency (Hz)
PyC3 - PL260313
BL
0-15
15-30
30-45
Post-TBS (min)
C
C1
C2
0.2mV
5 ms
Baseline
Post-TBS >30 min
PyC3-PL260313
Failure to spike
Spike occurrences (%)
Spike latency (ms)

Figure 4.3. LTP in pyramidal cell PL260313. (A) LTP in stimulation-evoked monosynaptic spike probability and unchanged spontaneous firing in pyramidal cell PL260313 following TBS. Ordinate shows time line. (A1) Spontaneous firing of the recorded cell ("Spontaneous spike") shown as a horizontal bar histogram for spike count (abscissa, 1 s period taken every 5 s). Time windows marked in grey or green background indicate periods with similar spontaneous firing level in baseline and in LTP. These were used to compare stimulus-evoked spike probability in Figure *B*. (A2) Dot plot of stimulus-evoked action potentials as a function of time. Dots represent spikes evoked cycle-by-cycle showing a delay to stimulation. Failures are indicated in "F". Marked background colours (yellow and violet) show episodes with LFP theta oscillation (4-6 Hz, orange) or non-theta.

(B) LTP shown of stimulus-evoked spike probability in the cell at different time points after baseline as indicated in abscissa (background colour-coded as in *A1*). The evoked spike probability is shown in black, "P(spike)", scaling in left. Grey dots and line show mean ± SEM of unchanged spontaneous firing (scaling in right "average firing Hz"). Dotted line illustrates P(Spike) mean in baseline. ***, $P<0.001$ (Chi-square test).

(C) Histogram and consecutive recording traces show LTP in probability of stimulation-evoked postsynaptic action potentials in the pyramidal cell and unchanged cycle-by-cycle variability of the evoked spike delay. (C1) In baseline the traces of evoked spikes (top) with many failures and a histogram (below) of spike occurrence illustrating spike probability and delay to stimulation. Stimulation cycles with failures to elicit postsynaptic action potential in histogram are shown in vertical bar "Failure to spike". (C2) Evoked spikes in the cell 30 min after TBS. Above are consecutive traces, below is a histogram showing data in LTP. Note massive reduction in the evoked spike failures ("Failure to spike") in parallel with preservation of coherent cycle-by-cycle variation in spike delay.

Cell ID	Spontaneous spiking properties				Stimulus evoked spikes and plasticity during selected time points								
	(1) Spontaneous firing frequency during theta (Hz)	(2) Mean angle - phase log to theta (deg) ± Mean angular deviation	(3) Depth of modulation i.e. *r* (no. of theta cycles counted)	(4) Spike half width / spike width (ms) ± s.d.	(5) Evoked spike rate			(6) Average Spike latency (ms) ± S.E.M.			(7) Averaged Spontaneous spiking rate (Hz) ± S.E.M.		
					Baseline	Post TBS 0 - 15 min	Post TBS 30 - 45 min	Baseline	Post TBS 0 -15 min	Post TBS 30-45 min	Baseline	Post TBS 0 - 15 min	Post TBS 30 - 45 min
PL240113	3.29	34.23 ± 48.72	0.64 (n = 852)	0.82 ± 0.020 / 1.90 ± 0.039	0.48	0.64 *	0.85 ***	10.01 ± 0.16	9.64 ± 0.26	10.05 ± 0.23	3.78 ± 0.29	3.15 ± 0.76	3.12 ± 0.69 ***
PL120811	2.94	83.83 ± 63.64	0.38 (n = 34)	1.17 ± 0.018 / 1.98 ± 0.040	0.41	1.00 ***	0.99 ***	11.79 ± 0.11	10.17 ± 0.055 ***	11.06 ± 0.03 ***	1.11 ± 0.17	1.78 ± 0.45	0.32 ± 0.14 ***
PL260313	2.96	357.66 ± 39.94	0.76 (n = 833)	0.59 ± 0.021 / 1.41 ± 0.042	0.26	0.51 ***	0.96 ***	12.35 ± 0.48	13.51 ± 0.29	12.78 ± 0.23	2.43 ± 0.31	0.12 ± 0.06 ***	2.36 ± 0.29

Table 4.4. Activity-induced LTP measured in evoked spikes and properties of spontaneous firing of recorded CA1 pyramidal cells.

A table summarising electrophysiological properties of the three CA1 pyramidal cells recorded *in vivo*. (Left panel) Spike properties used for electrophysiological identification of the cell as described in 3.2.1. and 3.2.2. Critical parameter show (1) spontaneous firing frequency during theta, 2) spike preference phase of LFP theta cycles, 3) depth of modulation (*r*) with number of theta cycles it represents, and 4) the AP waveform half width and the width in milliseconds. The half width (upper) was measured from the onset to the trough, and the spike width (lower) from the onset to the end of the waveform. (Right panel) Stimulus-evoked spike properties in the pyramidal cells recorded in the plasticity experiments. 5 – 6) Data presented are from the baseline and two post-TBS windows (i.e post-TBS 0-15 min and 30 – 45 min) that represent short- and long-term plasticity, respectively. 7) Averaged spontaneous spiking level (Hz) of the cells is summarised on the right.

5. Afferent excitatory pathway long-term plasticity in CA1 fast-spiking PV+ interneurons

5.1. Introduction

Having established that CA1 pyramidal cells exhibit long-term potentiation in the "transhippocampal" excitatory synaptic pathway (Chapter 4.), I tested a similar experimental plasticity-induction paradigm in the excitatory pathway to other postsynaptic CA1 neuron types. As I described in Chapter 3, various GABAergic inhibitory CA1 interneurons also received a monosynaptic-like excitatory input from contralateral hippocampus. Some of these cells I was already able to recognise as interneurons and partially identify as interneurons by their electrophysiological properties at an early stage of experiment (Chapter 3.2.3.). In acute slice preparation there is cumulating evidence that many CA1 area GABAergic interneurons also exhibit use-dependent activity-induced long-term plasticity in their excitatory glutamatergic afferents (Kullmann and Lamsa, 2007, Nissen et al., 2010, Kullmann and Lamsa, 2011). However, hitherto such plasticity in identified GABAergic interneurons afferents has only been investigated in acute brain slices, and has yet not been studied in the intact brain *in vivo*.

An important advantage in my project, when compared to an early pioneering study which provisionally explored interneuron plasticity *in vivo*, is that I have used electrophysiological and anatomical analyses of recorded cells to identify interneuron types (Buzsaki and Eidelberg, 1982b). Identification of cell type is critically important because GABAergic interneurons form a diverse group of neurons and in the CA1 area at least 21 different inhibitory interneuron types have been characterised in the rat (Klausberger et al.,

2005). Different interneuron types emerge ontogenically from distinct precursor cells so that GABAergic cells expressing mutually exclusive neurochemical markers in mature hippocampus often have their developmental origin in different embryonic brain regions, and cells are "born" at different times (i.e. their last mitosis as neuroblasts take place at different times during brain development) (Anastasiades and Butt, 2011, Kepecs and Fishell, 2014). The 21 interneuron types characterised in the CA1 area are structurally specific and innervate cellular domains of pyramidal cells and other interneurons in a cell type-specific way (Freund and Buzsaki, 1996).

Studies on acute hippocampal slices (Perez et al., 2001, Lamsa et al., 2005, Camire and Topolnik, 2014) have also revealed that distinct CA1 area GABAergic cell types can exhibit LTP very differently in their glutamatergic synapses (Topolnik et al., 2006, Kullmann and Lamsa, 2007, Lamsa et al., 2007b, Kullmann and Lamsa, 2011, Le Roux et al., 2013). An induction protocol that consistently elicits LTP in one anatomically identified cell type is unsuccessful in other CA1 cell types (Oren et al., 2009, Nissen et al., 2010, Szabo et al., 2012). A recent study by Nissen et al. (2010) demonstrated a fundamental difference in long-term plasticity between CA1 interneurons expressing mutually exclusive neurochemical markers parvalbumin (PV+) or cholecystokinin (CCK+). PV-expressing interneurons consistently generated LTP following high-frequency afferent glutamatergic pathway stimulation, whereas CCK+ postsynaptic cells failed to show plasticity in similar conditions. An early study by Buzsaki and Eidelberg (1982b) reported that roughly about half of CA1 area unidentified interneurons exhibited LTP in their experiments. The authors did not

address the question of whether plasticity properties differ between distinct CA1 interneuron types. My project provides the first results *in vivo* to directly address this question.

5.2. Results

5.2.1. Long-term plasticity study in fast-piking postsynaptic PV+ interneurons

Experimental conditions in interneuron experiments were very similar to the recordings from pyramidal cells (Chapter 4.2.1.). I aimed to set stimulation intensity so that single shock stimuli (every 5 s) evoked a postsynaptic spike with approximately 50 % probability. Fast-spiking PV+ interneurons show characteristic electrophysiological properties such as occasionally high frequency spontaneous firing and firing preference for a specific phase of the LFP theta oscillation cycle, which differ from pyramidal cell firing (as described in Chapter 3.2.3.1.). However most distinctively, PV+ fast-spiking interneurons show very fast kinetic action potentials that differentiates them from other CA1 neuron types allowing their identification as a group relatively easily even in extracellular recordings (Klausberger et al., 2005, Somogyi and Klausberger, 2005) (Method Chapter 3.2.3.1. and Figures 3.1.). The average action potential duration in fast spiking cells recorded in this study was 1.02 ms (± 0.048 ms, SEM.). These cells responded to afferent stimulation with phase-locked monosynaptic-like delay at 9.71 ms ± 0.62 ms (measured in 7 cells in baseline conditions). I

collected a baseline response to afferent stimulation (interval 5 s) for at least 10 minutes under the same criteria as in pyramidal cell recordings described earlier (Chapter 4.2.1.). Baseline recording was started when extracellularly measured postsynaptic spike amplitude was large enough (at least 3 times above the noise or 0.3 mV) to allow confident identification of the spike, analyses of the spike kinetics and measurement of its delay to any stimulation artefact. I continuously monitored the brain state via the local field potential (LFP) throughout the plasticity recording (Klausberger et al., 2004, Klausberger et al., 2005). After collecting the baseline, I applied a theta-modulated high-frequency burst stimulation pattern (i.e. TBS, 5 pulses at 100 Hz every 200 ms, repeated 20 times) to the pathway via the stimulation electrode. Stimulation with single pulse (every 5 s) was then resumed and continued to collect data for at least 30 min (n = 7), but in some cases up to 8 hours (n = 1, FSC5 – PL200711). I used juxtacellular labelling at the end of the recording that aims to label the postsynaptic cell with neurobiotin as described in Methods Chapter 2.3.2. In four of seven cells studied here, labelling was successful for visualization of the soma and proximal dendrites of the cell. Postsynaptic cell structures were visualized with fluorophore-conjugated streptavidin. Cells with visualized soma and (or) dendrites were immunohistochemically tested for the expression of relevant marker proteins, important for their cell type identification (Somogyi and Klausberger, 2005). All four cells were positive for parvalbumin (PV+). Additional immunoreactions were performed for some cells to further identify their cell type (see below). In these four cells I was also able to clearly visualize the axonal structures using DAB conversion. All these criteria together with electrophysiological analyses were used to fully identify PV+ CA1 area interneuron type.

Immunoreaction results are reported in table 5.2. Immunohistochemical reactions are described in detail in Methods Chapter 2.5.3. and Table 2.3 and 2.4). The laminar distribution of visualised axon in either *stratum pyramidale* (PL190912, PL311012 and PL230313) or *strata radiatum* and *oriens* (PL200711) were used to categorise the cells as perisoma- or dendrite targeting PV+ cells.

5.2.2. Plastic change in synaptically evoked postsynaptic action potentials following TBS

Given that fast-spiking interneurons can be readily distinguished by their unique spiking properties as described above (Chapter 3.2.3.), I first analysed plasticity results in this interneuron population identified by their narrow spike kinetics (≤ 1 ms action potential width). I found that delivery of TBS after baseline significantly changed single shock stimulation-evoked spike probability in six of seven postsynaptic CA1 area fast-spiking interneurons (see table 5.2. for details). The plasticity results in the seven cells showed a bimodal data distribution, since four of seven fast-spiking cells exhibited significant LTP with initial spike probability increase (FSC 1, 2, 5, 6, and 7) and two cells showed LTD (FSC 3 and 4). One fast-spiking cell (FSC1) failed to show any change in evoked spike probability during 30 min following TBS. For simplicity, I abbreviate the cells in this chapter as FSC1-7 (i.e. fast-spiking cell 1-7) as shown below in table 5.1. Cells showing potentiation or

depression in the evoked spike probability following TBS are shown in red and blue, respectively.

Table 5.1. Experimental codes for the fast spiking interneurons in the study.

FSC1	PL311012
FSC2	PL210213
FSC3	PL230313
FSC4	PL190912
FSC5	PL200711
FSC6	PL020213
FSC7	PL030412

In the four experiments with LTP, average P(Spike) increased from 0.66 ± 0.03 to 0.86 ± 0.04 (mean ± SEM, n = 4) in the post-TBS period ($p < 0.05$, one sample t-test). Long-term depression in the two cells (FSC 3 and 4) was observed as spiking probability decrease from 0.42 ± 0.10 in the baseline to 0.26 ± 0.075, following TBS (mean ± S.E.M., n = 2).

As I described in Chapter 4, spike probability and delay to single-shock stimulus were the major measures of transmission strength in the stimulated synaptic pathway. One cell (FSC 5) showed moderate shortening of spike delay after TBS ($p < 0.05$, Mann-Whitney test). Spike latency shortening was also observed in FSC2, although transiently present only for the first 30 min after TBS ($p < 0.05$, Mann -Whitney test). In the remaining five cells, spike delay

was not significantly altered ($p < 0.05$, Unpaired t-test with Welch's correction, Mann-Whitney test). Details on fast-spiking CA1 interneurons plasticity, electrophysiological and structural (axon distribution) features and immunohistochemical properties are presented in table 5.2..

5.2.2.1. Spontaneous firing properties of postsynaptic PV+ cells in the plasticity experiments

Spontaneous firing activity in fast spiking cells was higher than in pyramidal cells except in all but one cell, FSC5 – PL200711 (refer to Chapter 4 for comparison). Average spontaneous firing rate of the fast-spiking cells varied from 13.23 Hz to 21.07 Hz, except in FSC5, 0.59 Hz). Variation in spontaneous activity can at least be partially explained by fluctuating brain states between theta and non-theta, and differences of firing activity of distinct cell-types (Klausberger et al., 2004, Klausberger et al., 2005). In general, fast spiking cells show a high spontaneous spiking rate during LFP theta oscillation pattern compare to other non-fast spiking cells (Klausberger et al., 2004, Klausberger et al., 2005) (Table 5.2.). In addition, the very low firing level cell (FSC5) exhibited only non-theta activity in the LFP, which in general is associated with lower level of discharge than theta (Klausberger et al., 2003).

Although the spontaneous firing level in individual experiments varied during the course of the recordings, this was an unlikely reason for explaining the TBS-elicited long-term changes in evoked spike probability in the experiments. I have plotted stimulus-evoked spike data in parallel with quantified spontaneous firing of the postsynaptic cell throughout the experiment for all seven fast-spiking cells. To compare stimulus-evoked spike probability and delay values, I have selected time windows in pre- and post-TBS episodes where the spontaneous firing levels and brain states are similar or akin (or change in opposite direction).

In the four studied cells that exhibit LTP in stimulus-evoked spike probability, two show reduction of spontaneous firing level (FSC2 and 6). In FSC2, spontaneous spiking decreased from 17.98 Hz (± 1.08 Hz) to 13.61 Hz (± 0.89 Hz, post-TBS mean ± SEM), while the evoked spike mean probability simultaneously increased from 0.73 to 0.88 ($p < 0.001$, Chi-square test). A similar pattern was observed in FSC6 where evoked mean P(Spike) increased from 0.61 to 0.86 ($p < 0.001$, Chi-square test), while spiking rate decreased from 12.76 Hz to 10.42 Hz (± 0.60 Hz, post-TBS mean ± SEM). In FSC 7, spontaneous firing rate remained statistically unchanged with significant LTP in evoked spike probability raised from 0.69 to 0.83 ($p < 0.001$, Chi-square test). In the remaining cell FSC5 with stimulus-evoked spike LTP, spontaneous spiking rate was unchanged, and evoked spike probability showed potentiation after TBS from 0.61 to 0.80 ($p < 0.01$, Chi-square test).

Significant LTD was observed in two cells (FSC 3 and 4). In the case of FSC3, stimulus-evoked spike probability decreased from 0.52 to 0.33 ($p < 0.001$, Chi-square test), and from 0.32 to 0.18 in the case of FSC4 ($p < 0.001$, Chi-square test). However, LTD in these cells occurs in parallel with a decrease in spontaneous spiking level during the post-TBS period.

5.2.2.2. Identification of postsynaptic fast-spiking interneuron types in plasticity experiments

Analysing spontaneous electrophysiological spiking properties allows discrimination of perisoma-targeting and dendrite-targeting CA1 fast-spiking PV+ interneurons (Chapter 3.2.3.) (Somogyi and Klausberger, 2005). In the urethane anaesthetised rat brain theta oscillations are regularly generated in the hippocampus, therefore by analysing an average fast-spiking cell action potential firing preference during a LFP theta oscillation cycle can reveal the PV+ cell type (Klausberger et al., 2004, Klausberger et al., 2005). Specifically, CA1 fast-spiking cells which prefer to spike close to LFP theta cycle peaks (measured in or close to *stratum pyramidale*) are perisoma-targeting interneurons such as basket- or axo-axonic cells (Somogyi and Klausberger, 2005). In contrast, fast-spiking cells that innervate dendritic domains (i.e. bistratified cell and oriens-lacunosum moleculare i.e. O-LM cells) prefer to spike close to the LFP theta cycle trough (Klausberger et al., 2004, Klausberger et al., 2005). I analysed spike preferences in these cells during LFP theta (described in Chapter 3.2.3.2.) to

electrophysiologically identify the two PV+ cell subpopulations, and looked at plasticity experiments with information on cell identities.

In addition, anatomical features were revealed in the four cells successfully visualised following juxtacellular labelling. Soma and dendrites in these cells, and axonal branches in three of them, were analysed after strepavidin-alexa 488 visualisation and following conversion of the sections with DAB chromogen staining (Methods Chapter 2.5.3.5.). In the presence of a peroxidase enzyme, DAB will produce dark precipitate that is insoluble in alcohol, and can be dehydrated through ethanol. These provided additional anatomical and immunohistochemical data for cell type analyses. Hence, I was able to identify four fast-spiking postsynaptic interneuron as perisoma-targeting axo-axonic cells (n = 2) or basket cells (n = 2). One cell was identified as a dendrite-targeting bistratified cell. The two remaining cells were inconclusive regarding cell type identification (see discussion Chapter 5.3.1.).

5.2.2.3. Plasticity in identified perisomatic-targeting PV+ basket- and axo-axonic cells

Four fast-spiking postsynaptic cells studied in the plasticity experiments were categorised as perisomatic-targeting. This definition includes here both basket and axo-axonic cells, although axo-axonic cells exclusively innervate axon initial segments of pyramidal cells

(Somogyi et al., 1983a, Somogyi et al., 1983b). Both these two cell types show distinctive spontaneous firing characteristics during theta oscillation as compared to other characterised CA1 neuron types, preferring to spike close to LFP theta cycle peaks. Axo-axonic cells prefer to fire close to 180° in LFP theta cycles and basket cells usually fires at a descending phase between peak (180°) and though (360°) (Klausberger et al., 2004, Klausberger et al., 2005). In three cells I was able to visualise the soma and partial axons innervating *stratum pyramidale*. All three cells showed immunopositivity for PV in soma or dendrites. Two cells were identified as axo-axonic cells by their mean firing preference at 213° ± 65°, and 238° ± 71° **(**mean ± angular deviation**).** One of the two axo-axonic cells was successfully visualised and confirmed immunohistochemically with negative reaction in nucleus for transcription factor SATB1 (Viney et al., 2013) (Table 5.2.). Two cells with mean firing preferences at 305° ± 75°, and 302° ± 64°, were identified as PV+ basket cells. (Table 5.2.).

In addition I found that the two axo-axonic cell had firing that was strongly coupled to their favoured phase at theta cycles, while basket cells had less clearly phase-locked firing preferences (Klausberger et al., 2004, Klausberger et al., 2005). This result was visible in spike firing preference plots illustrated for the four cells in Figures 5.2. and 5.6.. Rayleigh test indicated the depth of modulation; results for each FSC were shown in table 5.2.

The axo-axonic PV+ cell FSC1 (PL311012) failed to show statistically significant plasticity either in spike probability or delay, whereas another putative axo-axonic cell

(FSC2-PL210213) showed significant LTP in stimulation-evoked postsynaptic spike probability following the TBS. Mean spiking probability for afferent single-shock stimulation increased in FSC1 and FSC2 from 0.69 to 0.73 (averaged post-TBS, $p > 0.05$, Chi-square test) and 0.727 to 0.884 (averaged post-TBS, $p < 0.05$, Chi-square test). The two basket cells exhibited long-lasting depression LTD from 0.519 to 0.327, and 0.316 to 0.177 (average post-TBS, $p < 0.05$, Chi-square test).

5.2.2.4. Plasticity in other fast-spiking PV+ interneurons

One fast-spiking postsynaptic interneuron (FSC5 - PL200711) was identified as a dendrite-targeting bistratified PV+ cell. Its firing preference during theta oscillation was close to the trough (0° or 360°) of the LFP theta cycle. Immunohistochemical analysis showed positive reactions for PV and neuropeptide-Y (NPY) and the visualized axon was mainly detected in *strata radiatum* and *oriens*. These features are specific for CA1 bistratified cells (Freund and Buzsaki, 1996, Klausberger et al., 2004, Somogyi and Klausberger, 2005, Tukker et al., 2007, Shepherd and Grillner, 2010). The bistratified cell has been illustrated earlier in Chapter 3 in Figure 3.6. as an example of a fully identified postsynaptic CA1 interneuron. The cell has a strong preference to spike at the trough showing phase preference at 358° ± 48° with depth of modulation of 0.643 (n = 377, Rayleigh test).

In addition, two recorded postsynaptic cells (FSC6 - PL020212 and FSC7 - PL030412) also exhibited fast spike kinetics and were labelled with neurobiotin, but their identity was not established. The two cells showed spike preference during theta cycle at $311^{o} \pm 67^{o}$ and $337^{o} \pm 75^{o}$ (mean ± angular deviation) respectively. Depth of modulation for FSC 6 and 7 were 0.311 (Rayleigh test, n = 2171) and 0.133 (Rayleigh test, n = 5589) respectively. In comparison to the strong modulation observed early in identified cells FSC5 – PL200711 (r = 0.64, Rayleigh test, n = 377) and weak modulation in FSC3 – PL230312 (r = 0.139, Rayleigh test, n = 1321), FSC7 was basically not coupled to theta oscillations and FSC6 was weakly coupled to theta cycles. However, these results as such are insufficient for identification of the cell type. Detailed electrophysiological and anatomical characteristics of the cells are presented in table 5.2. Both FSC6 and 7 showed robust LTP in stimulus-evoked postsynaptic spike probability following the TBS. The potentiation persisted throughout post-TBS recording period. Plasticity result for FSC6 is illustrated in Figures 5.7.

5.3. Discussion

My results show that like pyramidal cells, CA1 area PV+ fast-spiking interneurons also show activity-induced long-term plasticity in their monosynaptic excitatory afferents *in vivo*. LTP has been previously reported in fast-spiking cells in acute brain slices in the hippocampus, dentate gyrus as well as various neocortical regions (Kullmann and Lamsa, 2011). Furthermore, acute hippocampal slice experiments have reported, in line with my

findings here, that some CA1 area fast spiking cells can generate long-term depression instead (Nissen et al., 2010, Peterfi et al., 2012). In addition, the studies on slices have reported failures to generate LTP in a subpopulation of perisoma-targeting axo-axonic cells (Nissen et al., 2010). The results here show that plasticity result reported previously in slices showing LTP and LTD in PV+ CA1 area interneurons are reproducible in the intact brain *in vivo* (Kullmann and Lamsa, 2011).

5.3.1. Plasticity in identified PV+ cell types *in vivo*

Interestingly, results here differ from earlier studies on acute slices in one important aspect; the *in vivo* results failed to reproduce an identical cell type-specific plasticity in the CA1 fast-spiking cells with high-frequency (100 Hz) stimulation in hippocampal slices (Nissen et al., 2010). The study by Nissen et al. (2010) using brain slices showed that perisoma-targeting PV+ CA1 interneuron types, basket and axo-axonic cells, systematically generate LTP in response to high-frequency stimulation of glutamatergic afferents, or occasionally fail to elicit plasticity at all. That study did not report LTD in perisoma-targeting cells. Although 4 PV+ cells here showed LTP including one axo-axonic cell, two basket cells generated LTD. I will discuss possible reasons for this below (Chapter 5.3.2.).

In acute slice experiments LTP has also been thoroughly reported in CA1 area dendrite-targeting O-LM cells (Perez et al., 2001, Topolnik et al., 2006, Oren et al., 2009, Szabo et al., 2012). However CA1 dendrite-targeting PV+ bistratified cells reported by Nissen et al. (2010) generated LTD in slices. In my *in vivo* experiments the only identified bistratified neuron showed robust LTP. In slices, bistratified cells have not been reported to show LTP.

Discrepancy between basket and bistratified cells *in vivo* and *in vitro* regarding direction of high-frequency stimulation-induced long-term plasticity is important. The results suggest that the *in vivo* system with its intact circuits is more complex as an experimental model than the simplified acute slice circuitry. I proposed that *in vivo* circumstances have more regulatory elements to modulate plasticity than in acute brain tissue biopsies. Such "state dependent" transition from LTD to LTP and *vice versa* has been characterised in hippocampal CA3 interneurons in brain slices (Pelkey et al., 2008). Endogenous neuromodulators released in intact brain might at least partially be responsible for the transition from LTP to LTD and *vice versa* in PV+ cells. Indeed, activity-induced release of endocannabinoids has been shown to cause LTD at glutamatergic synapses to CA1 PV+ and non-fast-spiking interneurons (Edwards et al., 2012, Peterfi et al., 2012). The release of endocannabinoids is activity-dependent and occurs from postsynaptic cells during their action potential firing (Chen et al., 2003, Katona and Freund, 2008).

5.3.2. Possible factors affecting polarity of long-term plasticity in PV-expressing interneurons

Although my results in this chapter confirm that CA1 fast-spiking interneurons exhibit use-dependent long-term plasticity in their excitatory afferents *in vivo*, the inconsistency of the plasticity results with earlier *in vitro* experiments needs explanation. There are various possible explanations for this. First, as I mentioned above, the intact *in vivo* brain is likely to have more intact endogenous regulatory mechanisms, which can be compromised in brain slices. As an example, co-activation of fibres releasing other transmitters and neuromodulators could differently contribute to plasticity of glutamatergic circuits *in vitro* and *in vivo*. Good candidates for such an interaction are monoaminergic and cholinergic projection pathways, which both innervate hippocampus Although co-operation of glutamatergic and monoaminergic, endocannabinoid or cholinergic transmission in interneuron plasticity in this case is speculation. It is noteworthy that *in vitro* slice studies have demonstrated a strong effect of nicotinic receptors on NMDAR-independent LTP in some hippocampal CA1 area interneurons (Nakauchi and Sumikawa, 2012, Griguoli et al., 2013). Cannabinoid receptors were also related to NMDAR-independent LTP in in hippocampal PV+ cells (Peterfi et al., 2012). Alterations in the cholinergic transmission are associated with different brain states (Zhang et al., 2010). In my experiments the brain states, as determined by LFP oscillatory patterns, did not explain the polarity of glutamatergic plasticity in PV+ cells. Both LTP and LTD were induced in perisoma-targeting population when TBS was delivered at theta activity (see Figures 5.1. – 5.5).

Finally, during TBS postsynaptic spontaneous firing, which reflects the general excitation level, could also determine plasticity strength or even shift its polarity (Lamsa et al., 2007b, Le Duigou and Kullmann, 2011, Le Roux et al., 2013, Camire and Topolnik, 2014). I have analysed postsynaptic firing levels during TBS stimulation in all seven fast-spiking cells, and I found that between LTP cells and the LTD perisoma-targetting cell there was no significant difference in number of postsynaptic spikes generated during TBS (see Chapter 7 for details).

In summary, in this chapter I have demonstrated that fast-spiking PV+ CA1 interneurons exhibit long-term plasticity in their glutamatergic excitatory afferents as has been reported previously in studies using brain slices (Nissen et al., 2010, Peterfi et al., 2012, Le Roux et al., 2013). In addition, the polarity of plasticity (i.e. LTP or LTD) in PV+ cells can be determined by various possible factors. I have discussed and speculated why slice experiments could give more stereotypic plasticity result in a single identified postsynaptic cell type and propose that in the intact brain, heterosynaptic regulation of use-dependent plasticity is more likely to take place. Several mechanisms for such long-term plasticity strength and direction modulation have been reported in CA1 interneurons *in vitro* (Pelkey and McBain, 2008, Peterfi et al., 2012, Griguoli et al., 2013). Yet, actual mechanisms responsible for LTP *versus* LTD shift in PV+ cells *in vivo* remain still open.

5.4. Tables and figure

Spontaneous spiking properties				Anatomical sturcture	Properties of stimulus evoked spikes and plasticity during selected time points							
					(6) Evoked spike rate		(7) Average Spike latency (ms) ± S.E.M.			(8) Averaged Spontaneous spiking rate (Hz) ± S.E.M.		
Cell ID	(1) Spontaneous firing frequency during theta (Hz)	(2) Mean angle - phase log to theta (deg) ± Mean angular deviation	(3) Depth of modulation (no. of theta cycles counted)	(4) Spike half width / spike width (ms) ± s.d.	(5) IIHC	Baseline	Post TBS 0-15 min	Post TBS > 20 min	Baseline	Post TBS 0 - 15 min	Post TBS > 20 min	Baseline	Post TBS 0-15 min	Post TBS > 20 min
PL311012	35.35	213.14 ± 65.10	0.36 (825)	0.45 ± 0.01 / 0.96 ± 0.02	SATB1-, PV+; soma, dendrites and axon visible in Strep. Alexa 488	0.69	0.70	0.78	12.04 ± 0.28	11.12 ± 0.29*	11.78 ± 0.35	21.07 ± 1.35	21.21 ± 0.80	14.69 ± 0.60*
PL210213	21.61	238.81 ± 70.63	0.24 (1804)	0.56 ± 0.011 / 1.07 ± 0.01	DAB shows aspiny structure around str.rad.	0.73	0.90***	0.86*	9.05 ± 0.07	9.22 ± 0.05	8.79 ± 0.09*	17.98 ± 1.08	11.47 ± 0.85***	15.16 ± 0.55***
PL230313	14.90	305.24 ± 75.18	0.14 (4947)	0.45 ± 0.003 / 0.88 ± 0.03	PV+ soma, NPY- axon ; soma, dendrites and axon visible in strep. Alexa 488	0.520	0.39*	0.35***	9.11 ± 0.46	9.34 ± 0.33	8.14 ± 0.38	15.90 ± 0.45	14.27 ± 0.62	15.1 ± 0.54
PL190912	20.13	302.59 ± 63.84	0.38 (1842)	0.46 ± 0.01 / 1.11 ± 0.02	PV+, NPY- ; soma, dendrites and axon visible in strep. Alexa 488	0.32	0.19**	0.19**	7.04 ± 0.82	7.00 ± 0.70	7.36 ± 0.58	19.82 ± 1.45	13.89 ± 0.49 ***	12.87 ± 0.75 ***
PL200711	2.25	357.80 ± 48.40	0.64 (243)	0.34 ± 0.01 / 1.08 ± 0.03	PV+, NPY+ ; soma, dendrites and axon visible in strep. Alexa 488	0.61	0.69*	0.80***	11.40 ± 0.16	10.49 ± 0.12 ***	10.08 ± 0.15 ***	0.59 ± 0.09	0.57 ± 0.09	0.40 ± 0.20 ***
PL020213	14.01	310.58 ± 67.27	0.31 (7114)	0.38 ± 0.02 / 0.83 ± 0.06	DAB shows dendrites and axons around stra.ori. and str. rad, a few axon around str. pyr.	0.61	0.87***	0.81***	9.38 ± 0.24	9.45 ± 0.25	9.19 ± 0.25	12.76 ± 0.52	11.26 ± 0.77 *	9.39 ± 0.49 ***
PL030412	13.23	337.17 ± 75.46	0.13 (18579)	0.67 ± 0.01 / 1.17 ± 0.03	DAB shows aspiny structure at str. ori., pyr., and rad.	0.69	0.93***	0.93***	9.94 ± 0.46	9.95 ± 0.35	9.89 ± 0.12	12.65 ± 0.76	14.7 ± 0.74	12.67 ± 0.27

Table 5.2. Spontaneous firing properties and stimulation-elicited spike plasticity in CA1 fast-spiking PV+ interneurons.

A table summarises electrophysiological properties (left in "Spontaneous spiking properties") used for identification of fast-spiking PV+ interneurons in the experiments. In right "stimulus-evoked spike properties and plasticity" are summarized. First two columns show cell experiment code (Cell ID) and identified type (Cell type). Left category shows **1)** spontaneous firing frequency of the neurons during LFP theta oscillation, **2)** phase coupling of action potential to LFP theta cycle, **3)** depth of this modulation during theta oscillation and **4)** the AP waveform half width and the width in milliseconds. The half width (upper) was measured from the onset to the trough, and the spike width (lower) calculated from the onset to the end of the waveform. **5)** Immunohistochemical reactions (IHC) in fluorophore-streptavidin – visualized somatodendritic structure of cell (positive +, negative -). When visualization with fluorophore was unsuccessful, DAB reaction results are shortly summarized. Right category shows **6)** single-shock stimulus-evoked spikes rate (probability) in baseline, and immediately (0 – 15 min) as well as > 20 min after TBS. Statistical significance (*versus* baseline) is indicated by asterisks. In **7)** values for evoked spike latency (delay) are given, **8)** Shows average spontaneous firing rate (mean ± SEM) in baseline and after TBS at time points indicated. *, $P < 0.05$; **, $P < 0.01$; **, $P < 0.001$ (Chi-square test , Unpaired t-test or Mann Whitney test where appropriate).

Figure 5.1., 5.2. 5.3. and 5.4. Illustrated experiments on excitatory input plasticity in fast-spiking perisoma-targeting PV+ axo-axonic cell and basket cell.

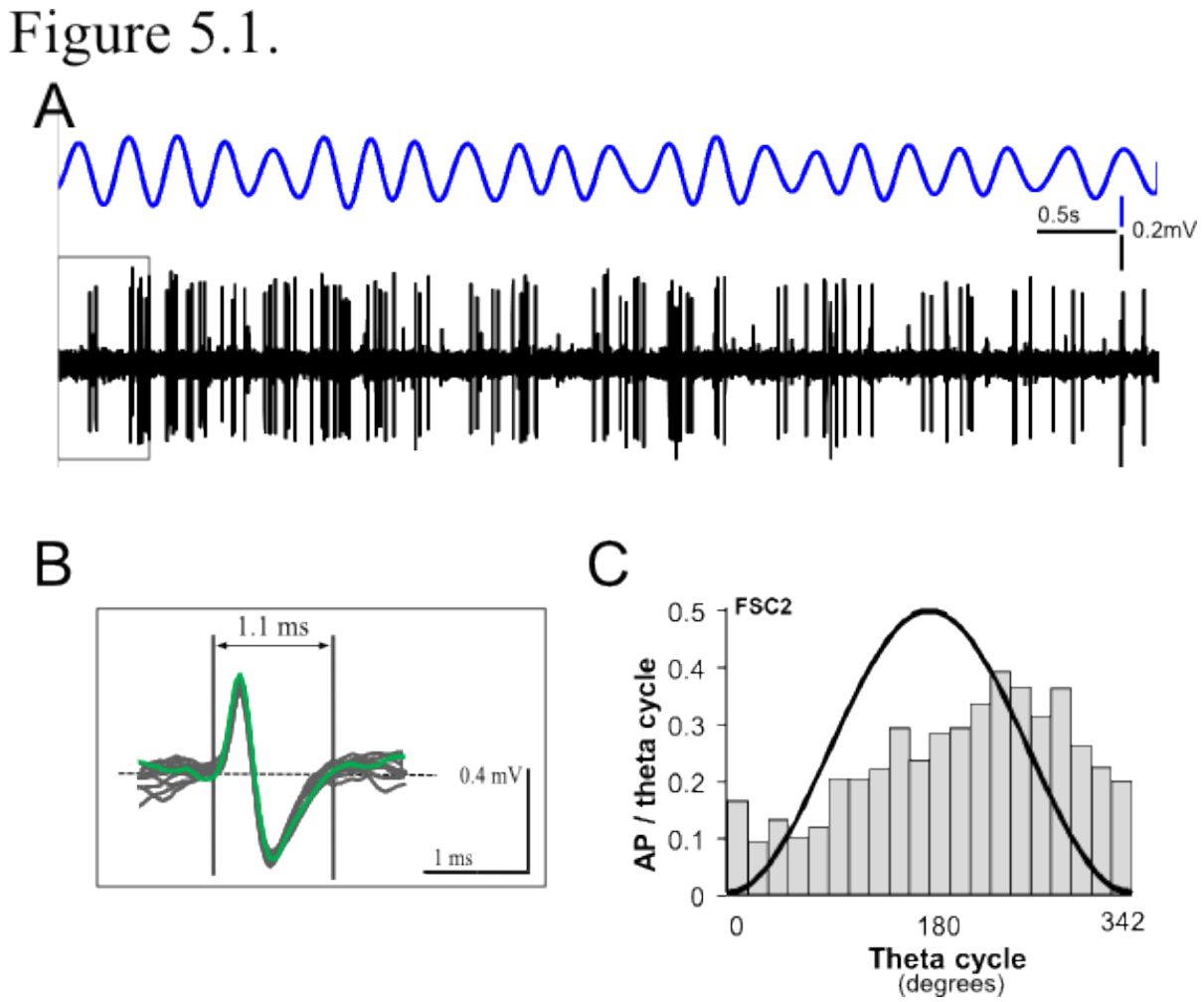

Figure 5.1. Spontaneous spiking properties reveal fast-spiking perisoma-targeting PV+ axo-axonic cell (PL210212 – FCS2). (A) Juxtacellularly recorded spontaneous firing of during LFP theta oscillation (4.46 Hz ± 1.14 Hz, mean ± SEM). (B) *Above;* LFP theta oscillation shown in blue. *Below*; band-pass filtered unit recording showing rhythmic spontaneous firing (average 35.35 Hz during theta oscillations detected at baseline). (B) Superimposed consecutive action potentials (n = 10) in *A* (square) and afferent stimulation elicited action potential highlighted in green. Evoked spike waveform is identical to spontaneous spikes with narrow wavelength of < 1 ms. (C) Histogram (in grey) showing spontaneous firing preference during a theta cycle (binned in 30 degrees, a theta cycle shown in black). Firing preference is at 238° ± 70°.

Figure 5.2.

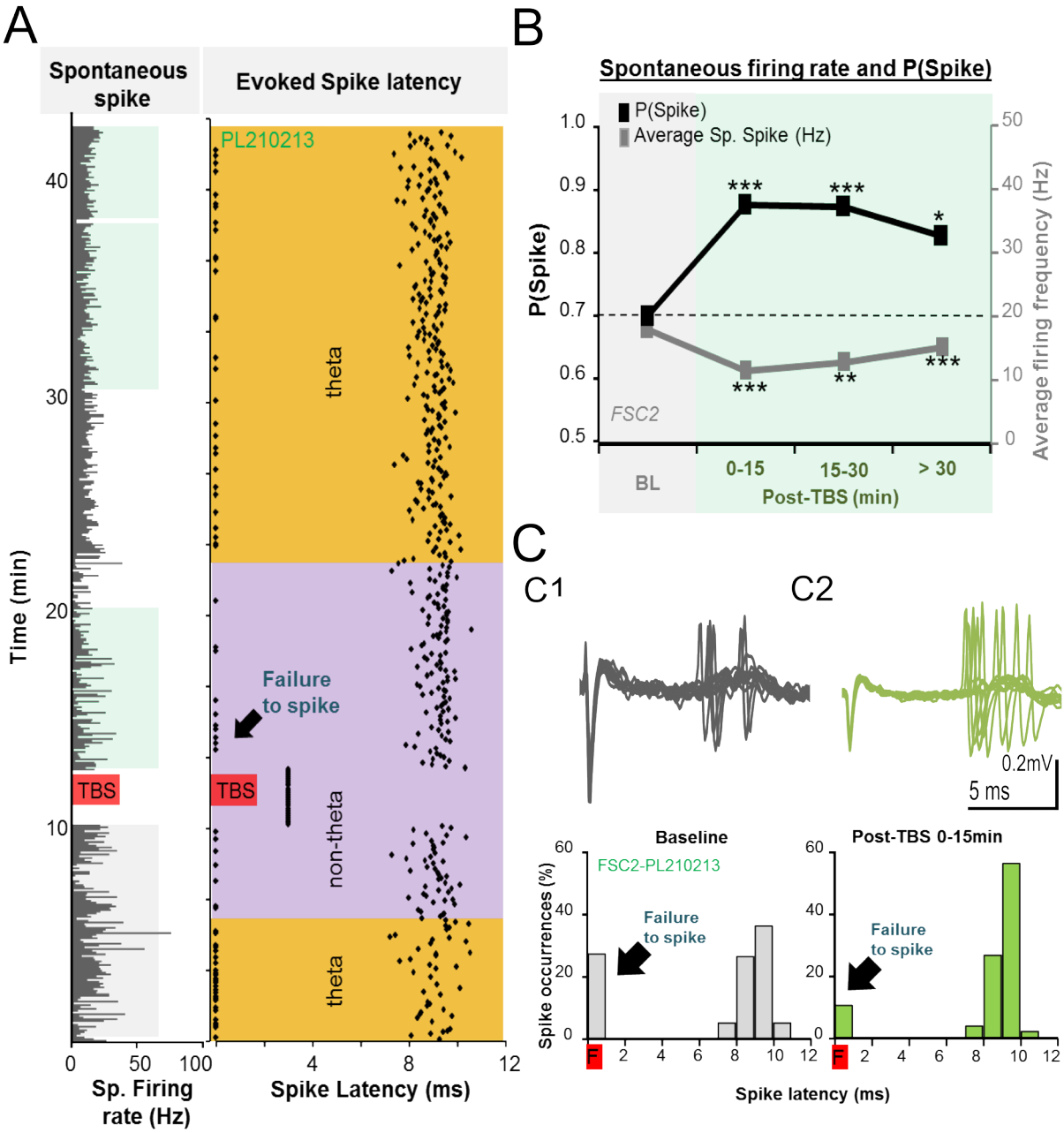
A
Spontaneous spike
Evoked Spike latency
PL210213
theta
non-theta
theta
Failure to spike
TBS
TBS
Time (min)
Sp. Firing rate (Hz)
Spike Latency (ms)
B
Spontaneous firing rate and P(Spike)
P(Spike)
Average Sp. Spike (Hz)
FSC2
BL
0-15
15-30
> 30
Post-TBS (min)
Average firing frequency (Hz)
C
C1
C2
0.2mV
5 ms
Baseline
Post-TBS 0-15min
FSC2-PL210213
Failure to spike
Spike occurrences (%)
Spike latency (ms)

Figure 5.2. Excitatory synaptic input to same cell (axo-axonic cell PL210212 – FSC2) with LTP.

(A) Spontaneous and stimulus-evoked spikes, ordinate shows time. (A1) Horizontal bar histogram shows spontaneous action potential frequency (abscissa, Hz). Shaded areas (grey in baseline, and green post-TBS) show time windows used for statistical comparison in plot B. (A2) A dot plot shows probability and delay of stimulus-evoked postsynaptic action potential in the cell, same ordinate as in A1. A TBS (indicated in red) evokes immediately a potentiation in evoked spike probability that lasts at least 30 min. Stimulation cycles that failed to elicit spike are shown in "F". Yellow background shows LFP theta (3-6 Hz) episodes and violet indicates non-theta.

(B) Average stimulus-evoked postsynaptic spike probability, P(Spike), show significant potentiation after TBS (Chi-square test). Average spontaneous spiking (Spont., mean ± SEM) drops after baseline (Mann-Witney test). Ordinate scaling for P(Spike) and Spont. are shown on left and right, respectively. Dotted line indicate baseline mean. Statistical significance compared to baseline: *, $P<0.05$; **, $P<0.01$.; ***, $P<0.01$ (Chi-square test).

(C) Traces showing consecutive responses to afferent pathway stimulations in the baseline and post-TBS. (C1) During the baseline. *Above*: superimposed traces (10) showing postsynaptic spikes and cycles with spike failures. *Below;* histogram summarising the evoked spike probability and delay. "F" indicates cycles that fail to elicit spike. (C2) Up to 15 min after TBS. *Above;* consecutive sample traces superimposed. *Below;* histogram showing delay and probability for evoked spikes. Decrease in failures (in "F") indicates potentiation of transmission in the stimulated pathway.

Figure 5.3.

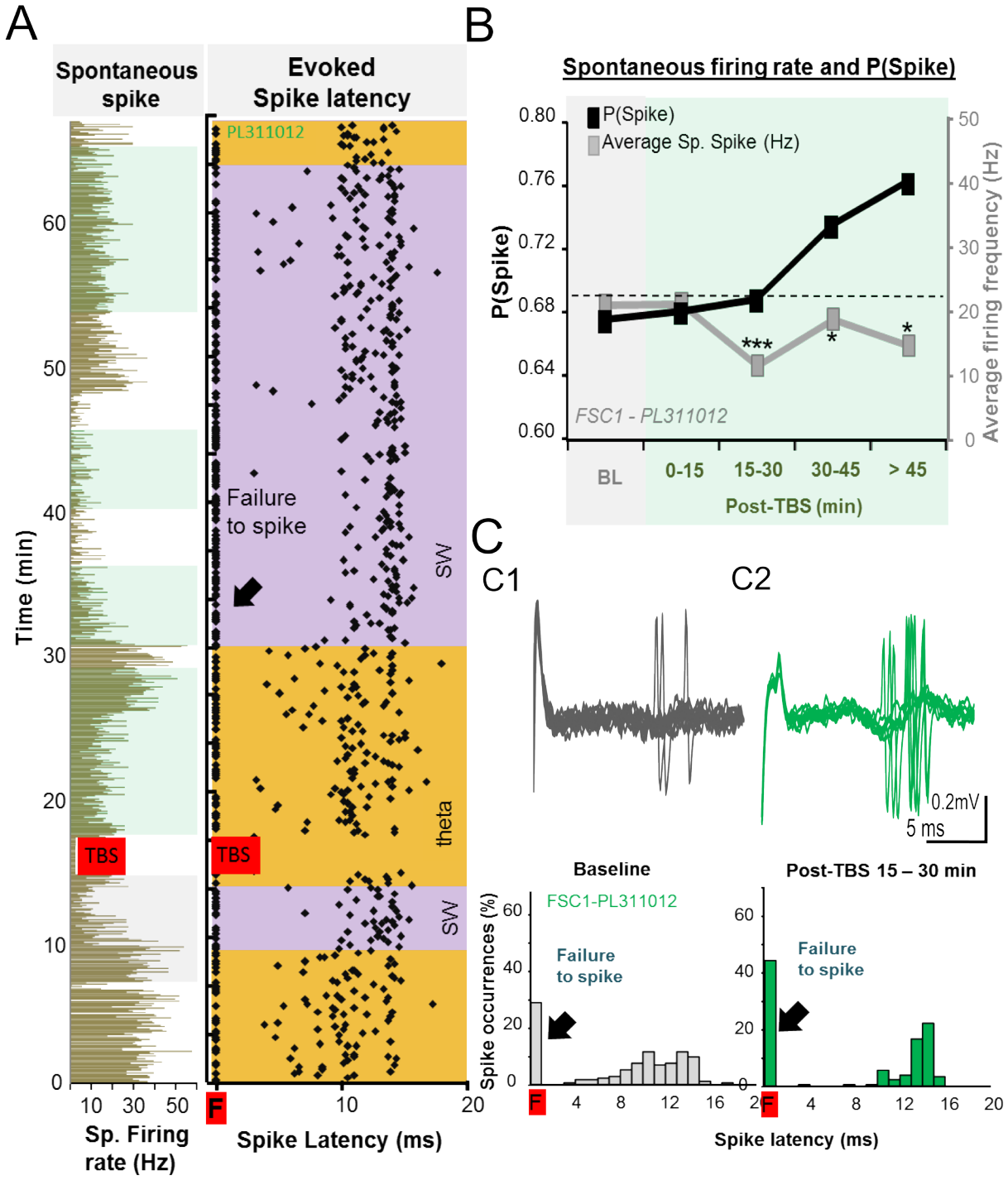
A
Spontaneous spike
Evoked Spike latency
PL311012
Failure to spike
SW
theta
SW
TBS
TBS
Time (min)
Sp. Firing rate (Hz)
Spike Latency (ms)
B
Spontaneous firing rate and P(Spike)
P(Spike)
Average Sp. Spike (Hz)
FSC1 - PL311012
BL
0-15
15-30
30-45
> 45
Post-TBS (min)
Average firing frequency (Hz)
C
C1
C2
0.2mV
5 ms
Baseline
Post-TBS 15 – 30 min
FSC1-PL311012
Failure to spike
Spike occurrences (%)
Spike latency (ms)

Figure 5.3. Unchanged excitatory synaptic input to identified axo-axonic cell (PL311012 – FSC1) initially after TBS with moderate delayed potentiation.

(A) Spontaneous and stimulus-evoked spikes, ordinate shows time. (A1) Horizontal bar histogram shows spontaneous action potential frequency throughout the experiment (abscissa, Hz). Shaded areas (grey in baseline, and green post-TBS) show time windows used to calculate averages shown in plot B1. (A2) A dot plot shows probability and delay of stimulus-evoked postsynaptic action potential in the cell, same ordinate as in A1. The TBS (indicated in red) elicits permanent increase in the monosynatic-delay spike probability. Stimulation cycles that failed to elicit spike are shown next to "0" time point in "F". Yellow background colour indicates LFP with theta (3-6 Hz) and brown non-theta.

(B) Dot plot shows stimulus-evoked average postsynaptic P(Spike). Probability (black dots and line) remained unchanged till 30 min after TBS, whereupon it significantly increased. In parallel, spontaneous spiking level (Spont., mean ± SEM) significantly drops. Grey dots and line illustrate firing level. Statistical significance compared to baseline: *, $P<0.05$; ***, $P<0.001$ (the Chi-square test P(Spike), Unpaired t-test or Mann Whitney test for spontaneous firing).

(C) Evoked spike traces and histogram in baseline and post-TBS. (C1) During baseline. *Above;* superimposed consecutive sample traces (10) of stimulus-evoked postsynaptic spikes and failures. *Below;* a histogram summarising evoked spike probability and delay. "F" indicates count of cycles failed to elicit spike. (C2) > 45 min after TBS induction. *Above;* sample traces (10) superimposed. *Below;* histogram showing delay and probability for stimulus-evoked spikes.

Figure 5.4.

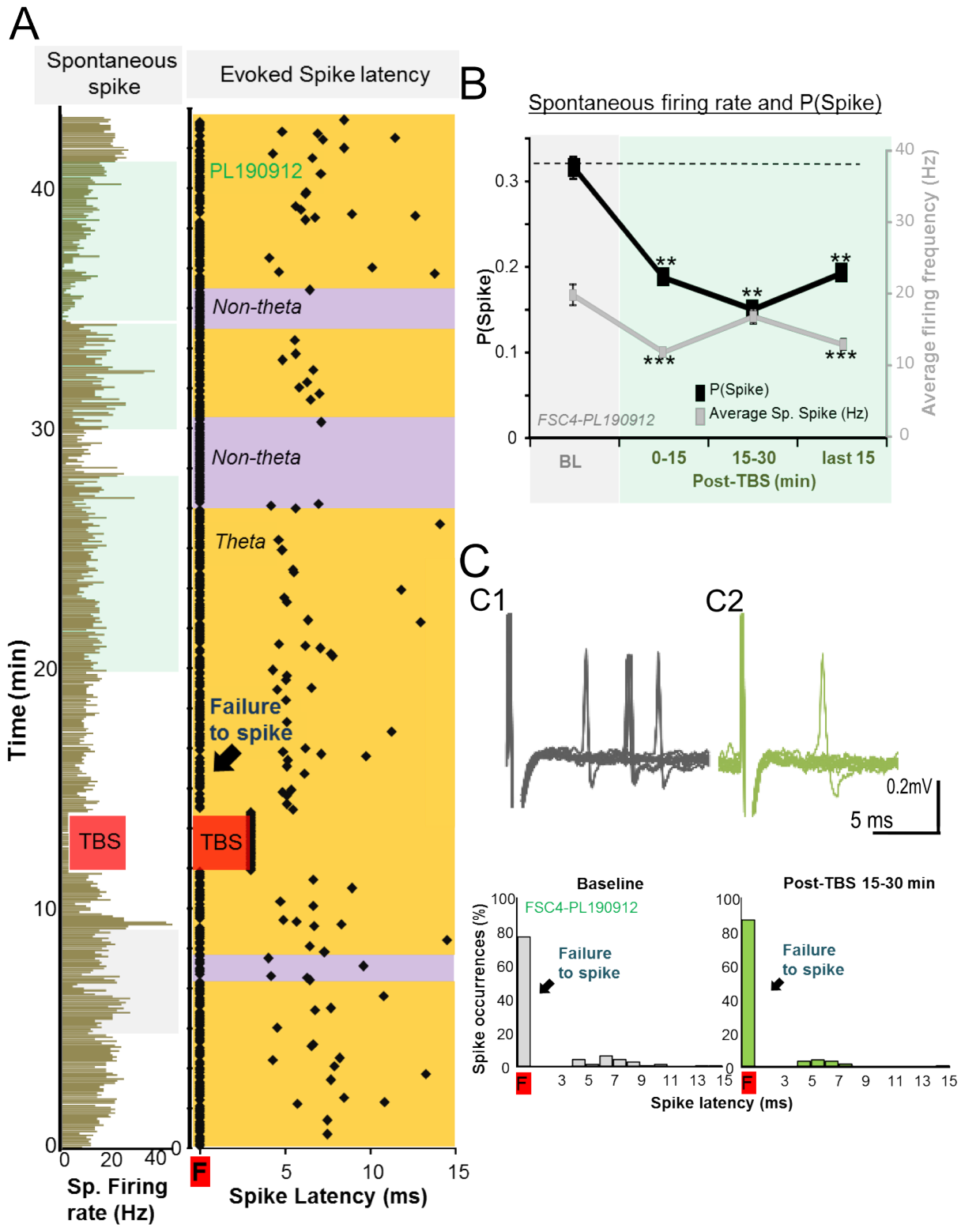
A
Spontaneous spike
Evoked Spike latency
PL190912
Non-theta
Non-theta
Theta
Failure to spike
TBS
TBS
Time (min)
Sp. Firing rate (Hz)
Spike Latency (ms)
B
Spontaneous firing rate and P(Spike)
P(Spike)
Average firing frequency (Hz)
FSC4-PL190912
P(Spike)
Average Sp. Spike (Hz)
BL
0-15
15-30
last 15
Post-TBS (min)
C
C1
C2
0.2mV
5 ms
Baseline
Post-TBS 15-30 min
FSC4-PL190912
Failure to spike
Failure to spike
Spike occurrences (%)
Spike latency (ms)

Figure 5.4. Excitatory synaptic input to PV+ basket cell (PL190912 – FSC4) with depression following TBS (Spontaneous spiking illustrated in Chapter 3).

(A) Spontaneous and stimulus-evoked spikes, ordinate shows time. (A1) Horizontal bar histogram shows spontaneous action potential frequency (abscissa, Hz). Shaded areas (grey and brown) shows data windows plotted in B. (A2) A dot plot shows probability and delay of stimulus-evoked postsynaptic action potential. TBS (indicated in red.) evokes long-lasting decrease in stimulus-evoked spike probability. Stimulation cycles that failed to elicit spike are shown in "F". Yellow background indicates LFP theta and brown shows non-theta.

(B) Average P(Spike) is reduced after TBS (Chi-square test). Spontaneous spiking (Spont. Hz) reduces in parallel (Mann-Witney test). P(Spike) black dots and line, spontaneous firing (Spont. Hz) in grey color. Dotted line indicates average in baseline. Statistical significance compared to baseline: **, $P < 0.005$; ***, $P < 0.001$. the Chi-square and Mann-Witney tests.

(C) Evoked spike traces and histograms in baseline and post-TBS. (C1) During the baseline. *Above:* consecutive sample traces (10). *Below;* a histogram summarising P(Spike) and delay. Column next to "0 ms" delay time point indicates stimulus cycles with failures to elicit a spike. (C2) 15 to 30 min after TBS. Above; sample traces (10) of spikes superimposed. *Below;* histogram showing delay and probability for evoked spikes. Increase in failures (F) indicates reduced transmission strength in the stimulated pathway.

Figure 5.5., 5.6. and 5.7. Excitatory input plasticity to other than fast-spiking perisoma-targeting PV+ cells.

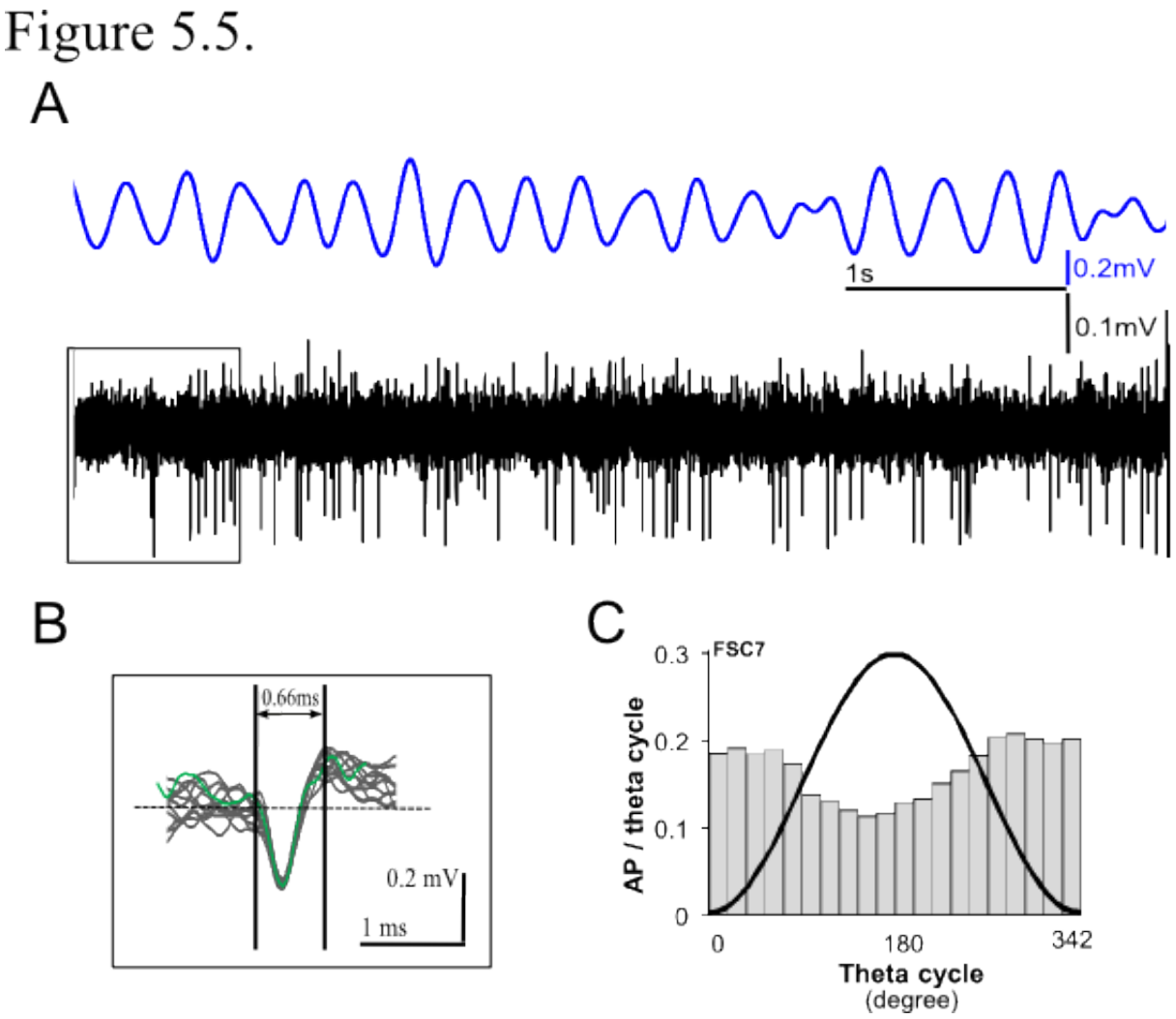

Figure 5.5. Spontaneous spiking properties reveal putative dendrite-targeting PV+ cells. (A) Juxtacellularly recorded spontaneous firing of PL030412 (FSC7) during LFP theta oscillation. *Above;* trace showing LFP theta (blue). *Below;* band-pass filtered unit recording show rhythmic spontaneous firing. Spikes in boxed area are shown in B. (B) Superimposed consecutive spontaneous spikes (10, black) from A with an afferent stimulation-evoked spike superimposed (blue). (C) Histogram show spontaneous firing preference during a theta cycle close to though at 337° ± 75°.

Figure 5.6.

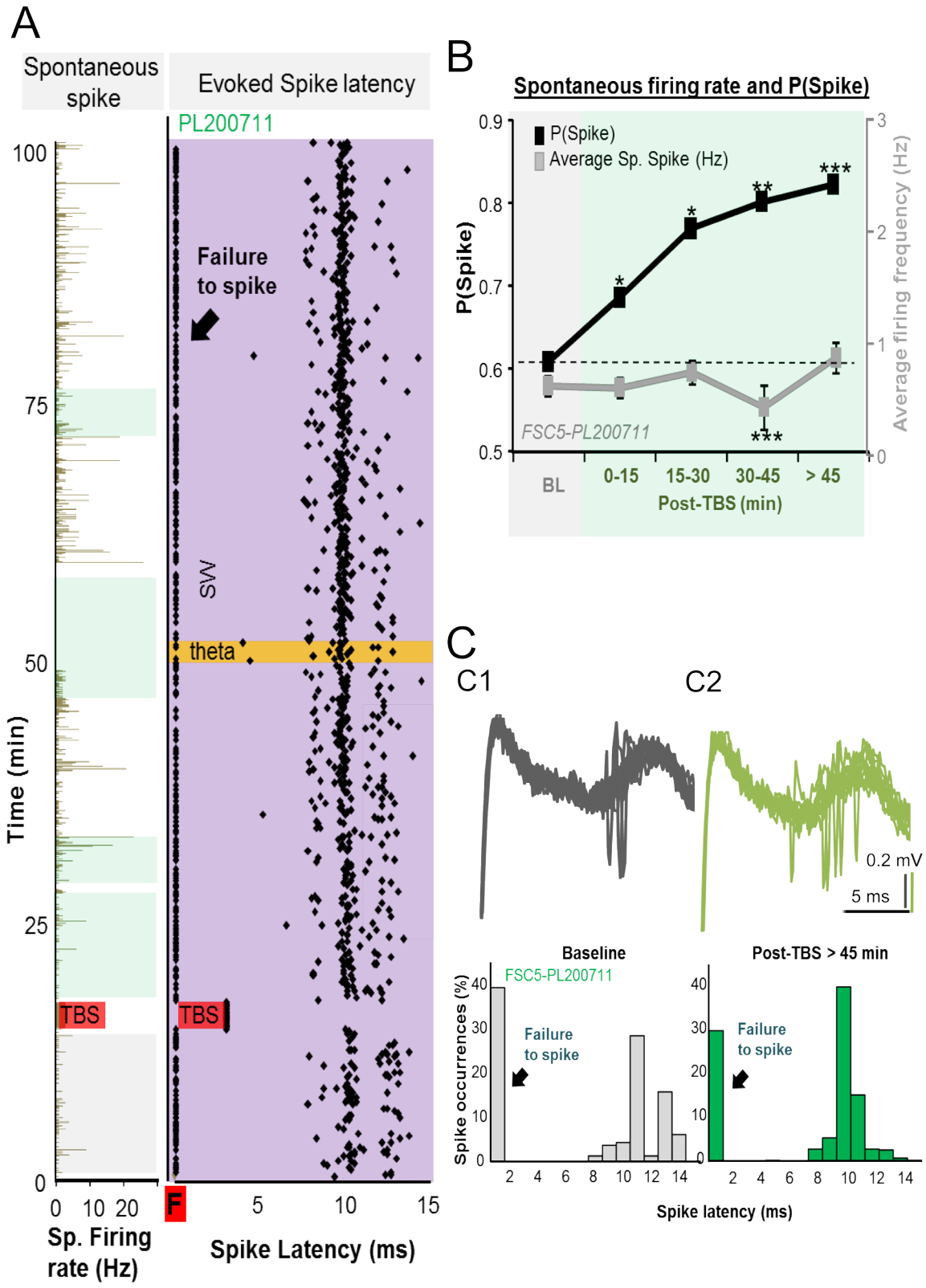
A
Spontaneous spike
Evoked Spike latency
PL200711
Failure to spike
SWs
theta
TBS
TBS
Time (min)
100
75
50
25
0
0 10 20
Sp. Firing rate (Hz)
F
5
10
15
Spike Latency (ms)
B
Spontaneous firing rate and P(Spike)
P(Spike)
Average Sp. Spike (Hz)
FSC5-PL200711
BL
0-15
15-30
30-45
> 45
Post-TBS (min)
Average firing frequency (Hz)
C
C1
C2
0.2 mV
5 ms
Baseline
Post-TBS > 45 min
FSC5-PL200711
Failure to spike
Failure to spike
Spike occurrences (%)
Spike latency (ms)

Figure 5.6. Excitatory synaptic input to an identified bistratified cell (PL200711 – FSC5) with LTP (spontaneous spiking illustrated in Chapter 3).

(A) Spontaneous and stimulus-evoked spikes, ordinate shows time. (A1) Horizontal bar histogram shows spontaneous action potential frequency. Shaded grey and green areas show data windows plotted in B. (A2) A dot plot shows probability and delay of stimulus-evoked postsynaptic action potential. TBS (in red.) evokes long-lasting increase in P(Spike). Stimulation cycles that failed to elicit spike are shown in "F". Yellow background shows LFP theta and violet indicates non-theta.

(B) Stimulus-evoked postsynaptic spike probability, P(Spike), shows potentiation after TBS (black dot and lines, Chi-square test). Spontaneous spiking (Spont. Hz) remains unchanged after baseline although transiently drops at 30-45 min following post-TBS (grey, Mann-Witney test). Dotted line indicates average in baseline. Statistical significance compared to baseline: *, $P < 0.05$; **, $P < 0.01$; ***, $P < 0.001$.

(C) Evoked spike traces and histograms. (C1) During the baseline. *Above:* consecutive traces (10) of stimulus-evoked responses. *Below;* a histogram summarising evoked spike probability and delay. "F" indicates failures to elicit spike. (C2) 45 min after TBS. *Above;* sample traces (10). *Below;* histogram showing delay and probability for evoked spikes. Decrease in failures indicates potentiation of transmission in the stimulated pathway.

Figure 5.7.

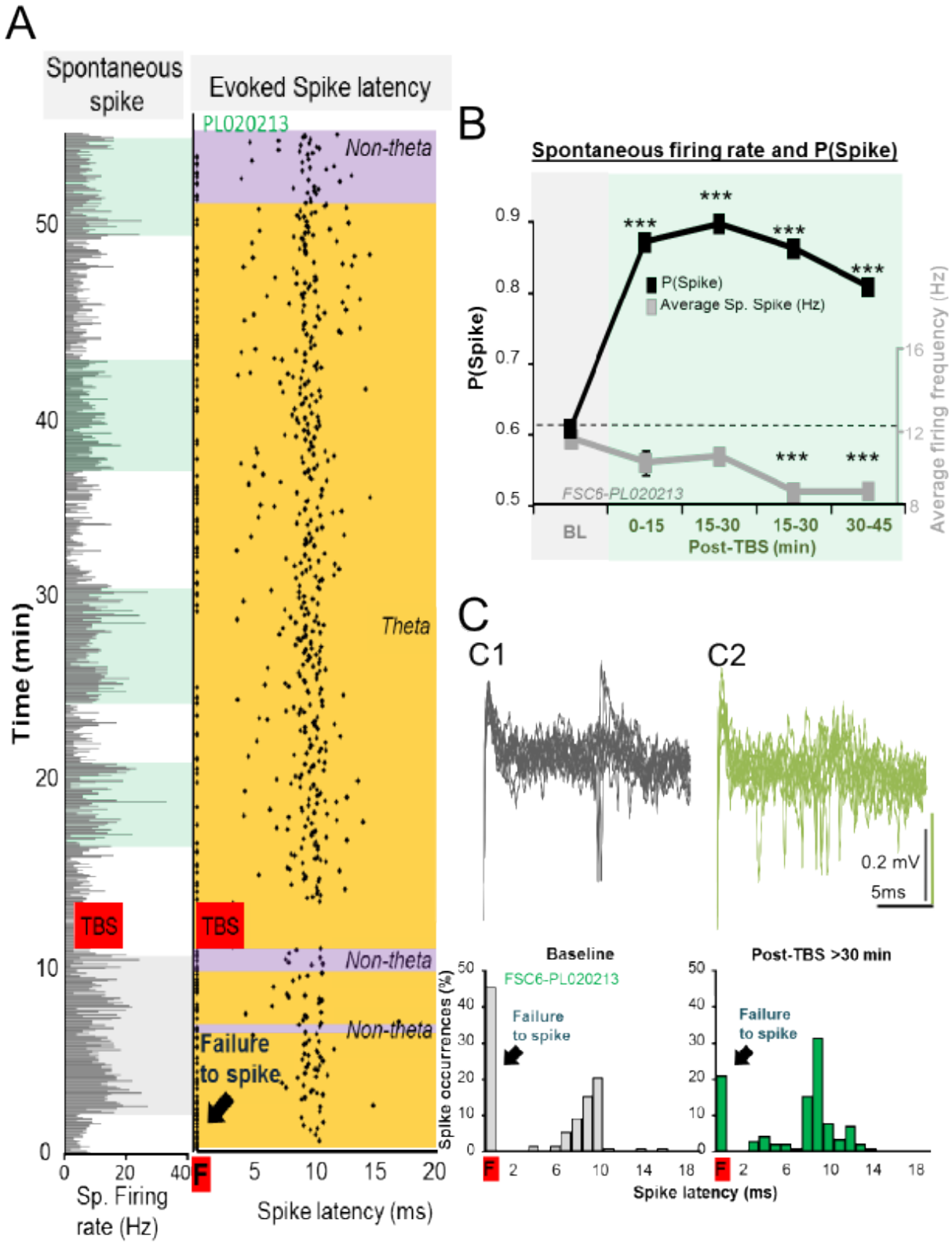
A
Spontaneous spike
Evoked Spike latency
PL020213
Non-theta
Theta
Non-theta
Non-theta
TBS
TBS
Failure to spike
Time (min)
Sp. Firing rate (Hz)
Spike latency (ms)
B
Spontaneous firing rate and P(Spike)
P(Spike)
Average Sp. Spike (Hz)
FSC6-PL020213
BL
0-15
15-30
15-30
30-45
Post-TBS (min)
Average firing frequency (Hz)
C
C1
C2
0.2 mV
5ms
Baseline
Post-TBS >30 min
FSC6-PL020213
Failure to spike
Spike occurrences (%)
Spike latency (ms)

Figure 5.7. Excitatory synaptic input to an unidentified fast-spiking cell (PL020213 – FSC6) with LTP.

(A) Spontaneous and stimulus-evoked spikes. (A1) Horizontal bar histogram illustrates spontaneous action potential firing (abscissa, Hz). (A2) A dot plot shows probability and delay of stimulus-evoked postsynaptic action potential. A TBS (in red) evokes long-lasting increase in spike probability. Stimulation cycles that failed to elicit spike are shown in "F". Yellow background shows LFP theta and non-theta periods are shown in brown.

(B) Average stimulus-evoked postsynaptic spike probability, P(Spike), is increased after TBS (black line and symbols, the Chi-square test). Spontaneous spiking level (Spont. Hz, grey line and symbols) remains initially unchanged, but decrease after 30 min. Dotted line indicates baseline mean. Statistical significance compared to baseline: ***, $P < 0.01$.

(C) Evoked responses and histograms in baseline and post-TBS. (C1) During the baseline. *Above:* sample traces (10) of stimulus-evoked responses with spikes and failures. *Below;* a histogram summarising evoked spike probability and delay, "F" indicates cycles with a failure to elicit spike. (C2) 30 min after TBS. *Above;* sample traces (10). *Below;* histogram showing delay and probability for evoked spikes. Decrease in failures indicates robust potentiation of transmission in the stimulated pathway.

6. Excitatory pathway long-term plasticity to other CA1 neuron types

6.1. Introduction

Although long-term synaptic plasticity in hippocampal pyramidal cells and fast-spiking interneurons has been investigated and reported in slices, studies on "non-fast spiking" interneuron long-term plasticity in the hippocampus are very rare (Lamsa et al., 2005, Edwards et al., 2012, Szabo et al., 2012). One obvious reason for the shortage of plasticity data on these neurons is that these neurons are challenging to identify (Somogyi and Klausberger, 2005). Recognising electrophysiological features for regular-spiking interneurons is less distinctive than for the other two neuronal populations studied above because of lack of distinctive features. However, my experimental set up *in vivo* anaesthetised brain provides a valuable opportunity to investigate plasticity in these cells because in some cases electrophysiological firing properties during LFP oscillations help to recognise "non-fast spiking interneurons (Klausberger et al., 2005, Fuentealba et al., 2008). In this Chapter 6, I have analysed results from plasticity experiments carry out on other CA1 postsynaptic neuron types than pyramidal cells or fast-spiking PV+ interneurons. As I reviewed in Chapter 5.1.. GABAergic interneurons comprise a diverse population of inhibitory neurons, which in the hippocampal CA1 are classified into 21 different types (Freund and Buzsaki, 1996, Somogyi and Klausberger, 2005). Each interneuron type has its own specialised structural and chemical features that reflect specialisation of their role in the brain (Freund and Buzsaki, 1996, Shepherd and Grillner, 2010). Importantly, most CA1 interneurons are not fast-spiking PV+ interneurons, in fact only about 20 % hippocampal GABAergic interneurons express PV (Bezaire and Soltesz, 2013). However, the electrophysiological features of many of the non-fast spiking interneuron types, in particular when recorded extracellularly *in vivo*, are not

distinctively different from pyramidal cells. This makes it challenging to find and identify them without *post hoc* anatomical studies. Many GABAergic CA1 area interneuron types have the "regular spiking" action potential firing pattern (Klausberger et al., 2005, Bezaire and Soltesz, 2013) and action potential kinetics close to that of pyramidal cells (Buzsaki and Eidelberg, 1982b, Csicsvari et al., 1999). However, some of these cells, such as CCK-expressing (CCK+) perisoma-targeting basket cells display distinctive spike firing behaviour during different brain states *in vivo* (Klausberger et al., 2005). These interneurons prefer to fire at the ascending phase of the LFP theta cycles, closer to the peak than the trough, meaning that together with other (PV-expressing) perisoma-targeting cells they fire out of phase when compared to pyramidal neurons (Nyiri et al., 2001, (Klausberger et al., 2005). In addition, some non-fast spiking interneurons have moderately faster action potential kinetics than pyramidal cells (Csicsvari et al., 1999, Fuentealba et al., 2008). However, most non-fast spiking CA1 interneurons fire with discernibly lower frequency during hippocampal oscillations when compared PV-expressing cells (Somogyi and Klausberger, 2005). Hence, non-PV+ GABAergic interneurons are often called "regular spiking" interneurons. Some of these cells can be recognised, although not fully identified by their electrophysiological features during extracellular recording.

Another common "regular-spiking" interneuron type in the CA1 area is the ivy cell. Ivy cells innervate basal and oblique dendrites of pyramidal cells with fine and dense axons (Fuentealba et al., 2008, Armstrong et al., 2012, Somogyi et al., 2012, Szabo et al., 2012). These cells show a very low spontaneous firing rate in an anaesthetized rat during theta, sharp

wave-associated ripples, and non-theta/ non-sharp wave- associated ripple oscillations, although spiking rate can vary considerably in the same cell (Fuentealba et al., 2008). Plasticity in CA1 area ivy cells and CCK+ interneurons has been studied *in vitro* slice preparations and ivy cells have been shown to exhibit activity-induced long-term potentiation (Nissen et al., 2010, Szabo et al., 2012). Yet, there is no evidence that these neurons exhibit similar plasticity *in vivo*.

In this Chapter I have analysed plasticity in experiments where the postsynaptic cell was identified as a non-fast spiking CA1 interneuron by its electrophysiological and anatomical features.

6.2. Results

6.2.1. Long-term plasticity in anatomically analysed non-fast spiking CA1 interneurons

Regular spiking or "non-fast spiking" CA1 area GABAergic interneurons exhibit action potential kinetics which are close to those of pyramidal cells (Klausberger et al., 2005). In extracellular recordings here, postsynaptic spike width (from onset to end) for three regular-spiking interneurons was 1.60 ± 0.09 ms (mean ± SEM), which is comparable to earlier reports of non-fast spiking cells (Csicsvari et al., 1999, Klausberger et al., 2004, Klausberger

et al., 2005, Fuentealba et al., 2008). Because spike kinetics alone is not a sufficient feature to discriminate these cells from pyramidal cells, additional parameters for their identification were needed. Most importantly, spontaneous firing rate and pattern during hippocampal oscillatory theta oscillation can reveal non-fast spiking interneurons (Klausberger et al., 2005, Fuentealba et al., 2008). I have reviewed identification of interneurons earlier in Chapter 3.2.3.1 and 3.2.3.2. Compared to pyramidal cells, non-fast spiking interneuron firing is characterized by lack of complex spikes (described in Chapter 3.2.2.4.), and higher spontaneous rate than in pyramidal cells (Chapter 3.2.3.2.). In this study, I successfully filled two regular-spiking interneurons with neurobiotin using juxtacellular labelling technique, and their *post hoc* visualization revealed their somato-dendritic structure with aspiny dendrites.

6.2.1.1. LTP in an ivy cell

Cellular structures of PL170412 and PL310812 were uncovered by Alexa488-streptavidin visualization of neurobiotin. The cell PL170412 showed characteristic ivy cell features with a small somata and spiny radially oriented dendrites in *str. rad.*. The cell had a dense local axon cloud in the *str. rad.* (Fuentealba et al., 2008, Szabo et al., 2012) and immunopositive for NPY but nNOS negative (Fuentealba et al., 2008, Bezaire and Soltesz, 2013). The cell is not shown here as the section containing the soma was accidentally lost in the process of a follow-up immunohistochemical reaction. The ivy cell preferred to fire

spontaneous action potentials at the trough of LFP theta cycles with the highest probability at $352^{o} \pm 69^{o}$ (mean ± angular deviation). These findings are in line with what has been reported earlier on CA1 area ivy cell extracellular recording (Fuentealba et al., 2008). The cell is presented earlier in Chapter 3 as an example of a fully identified regular-spiking interneuron (Figure 3.8.). Delivering TBS to the contralateral afferent excitatory pathway after baseline (15 min) elicited an increase in evoked-spike probability from 0.24 in baseline to 0.46 and 0.52 (0 -15 and >15 min time windows post-TBS, respectively). The P(Spike) increase was significant throughout post-TBS recording ($p < 0.001$, Chi-square test). It is noteworthy that in addition to the spontaneous firing level of the cell increased moderately after TBS ($p < 0.001$, Mann-Whitney test). However, as shown earlier in Chapter 5, alterations in spontaneous firing rate when the LFP oscillation pattern changes from non-theta to theta do not generally explain the change to the stimulus-evoked spike probability changes. The plasticity experiment and spontaneous firing activity results of the identified ivy cell are illustrated in Figure 6.1.

6.2.1.2. LTD in unidentified regular-spiking CA1 interneuron

For cell PL310812, analysis of the spontaneous firing showed that during theta oscillation, it preferred to fire close to the trough of LFP theta cycle. A lack of complex spikes in the spike autocorrelogram suggested a non-fast spiking interneuron (see Figure 6.2. when visualized the PL310812 showed somato-dendritic interneuron structure with soma in *str. rad.*

and smooth aspiny dendrites in the same layer. However, visualization only recovered the somato-dendritic structure of the cell and no axon was detected by fluorescence imaging. Alexa488-streptavidin visualized cell soma was immunonegative for a common regular-spiking cell marker protein precursor of cholecystokinin (pro-CCK) (Klausberger et al., 2005). The lack of more detailed anatomical analyses, and due to the fact that electrophysiological features of the cell fit with various CA1 interneuron types, the cell identity of this neuron was not possible (Somogyi and Klausberger, 2005).

Following TBS, single shock-evoked spike probability decreased from 0.48 (in baseline) to 0.03 and 0.10 (at post-TBS 0 – 15 min and late post-TBS after 45 min, respectively) ($p < 0.05$, Chi-square test). At the same time, the spontaneous firing of the cell increased moderately ($p < 0.001$, one sample *t*-test and $p < 0.001$, Mann-Whitney test). This means that the cell showed LTD in its afferent excitatory input after TBS. The results for the cell PL310812 are illustrated in Figure 6.2.

6.2.1.3. LTD in CA1 non-fast spiking interneurons lacking anatomical analysis and cell type identity

The two non-fast spiking interneurons studied here in plasticity experiments remained without any interneuron type categorisation (other than non-fast spiking interneuron). One

reason for this is that detailed in electrophysiological behaviour of these cell types is less well characterised compare to pyramidal cells or fast-spiking neuron types (Klausberger et al., 2005). This means that although many non-fast spiking cells recorded were distinguished from pyramidal cells by their spontaneous electrophysiological firing pattern during hippocampal theta or non-theta oscillations, these neurons remained without complete cell type identification because cell labelling failed to reveal any cell structures for further analyses and identification. Major electrophysiological features distinguishing these two cells from CA1 pyramidal cells are distinctively high spontaneous firing rate at average frequency of 17.69 Hz of cell PL150113 in baseline (Table 6.1.). The cell PL160413 exhibited theta cycle-coupled firing phase preference very different to that of CA1 pyramidal cell (Somogyi and Klausberger, 2005).

Cell PL150113 and cell PL160413 showed preferred spike firing at $1^{o} \pm 71^{o}$ and $99^{o} \pm 58^{o}$ (mean angle-phase ± angular deviation). Depth of modulation measured by the Rayleigh test was 0.24 (n = 772) and 0.48 (n = 2450), respectively. The analyses show that the recorded cells prefer to fire at LFP theta cycle trough and at the ascending phase, respectively. Firing in the ascending phase is common to CCK-expressing interneurons in the CA1 area of anaesthetised rats (Klausberger et al., 2005). Cell PL150113 was weakly modulated by theta oscillation (depth of modulation 0.242 the Rayleigh test) (Klausberger et al., 2005). The cell PL160413 showed theta-cycle coupled firing phase preference which resembles what has been reported in some CCK+ CA1 interneurons (Klausberger et al., 2005).

I analysed the full plasticity recording and juxtacellular labelling experiment on the two postsynaptic non-fast spiking CA1 neurons that were distinguished from pyramidal cells by their electrophysiological activity. PL150113 showed significant ($p > 0.001$, Chi-square test) decrease in evoked spike probability throughout the post-TBS time (0 – 45 min post-TBS), and spontaneous firing rate also reduced in after TBS ($p < 0.001$, Student's *t*-test and Mann-Whitney test). However, like it has been presented in Chapter 4 and 5, the spontaneous firing level in these experiments alone is unlikely to be sufficient to explain the long-term plasticity observed in recorded cells (see also Chapter 7).

PL160413 showed long-term depression following TBS. The TBS delivered after a baseline (10 min), induced a significant and persistent (at least up to post-TBS 45 min time point) depression of the stimulus-evoked excitatory pathway spike probability ($p > 0.001$, Chi-square test). This was associated with a moderate increase in the spontaneous firing rate. Results for slow-spiking cells PL150113 and PL160413 are illustrated in Figures 6.3. and 6.4., respectively.

6.3. Discussion

6.3.1. Diversity of long-term plasticity results in non-fast spiking CA1 interneurons *in vivo*

Although the non-fast spiking interneuron pool in the plasticity experiments here is fairly small and comprise of only four neurons, of which only two were confirmed anatomically, the experiments add important information on interneuron plasticity results *in vivo*. First, long-term potentiation in an identified ivy cell in this work supports earlier reports on LTP in CA1 area ivy cells in acute brain slice preparation (Szabo et al., 2012). Second, results on having either LTP or LTD in non-fast spiking interneurons show that not only pyramidal cells or PV+ interneuron express diverse synaptic plasticity forms *in vivo*. Potentiation and depression of the stimulus-evoked short-delay postsynaptic action potential probability induced by TBS in the three distinct CA1 neuron populations also strongly support the conclusion that excitation is mediated via a monosynaptic pathway (see Chapter 3). The TBS elicited robust depression in most regular-spiking interneurons, other than ivy cells. This finding is in line with *in vitro* slice experiments which have reported LTD commonly in the excitatory afferents onto non PV+ interneurons in the CA1 area (Edwards et al., 2012, Brown et al., 2013).

However, the plasticity result from putative CCK+ interneuron differs from acute brain slice results on CCK+ CA1 interneuron types that fail to express either LTP or LTD in their glutamatergic afferents by high-frequency stimulation (Nissen et al., 2010). The number of regular-spiking cell type plasticity in these experiments is low, and results to confirm the cell type specific plasticity rules will require more experiments in the future. Importantly, these experiments on regular spiking cells further strengthen the earlier conclusion made in this research project that various different CA1 interneurons exhibit long-term plasticity also *in*

vivo. An important another conclusion made from the regular-spiking interneuron plasticity results here is that transmission during the "monoysnaptic delay' stimulation-evoked postsynaptic spike is indeed likely to be mediated via a monosynaptic pathway. Otherwise the cell type-specific plasticity rules and occurrence of both LTP and LTD with the same stimulation pattern in different cell subpopulation would be difficult to explain by plasticity in polysynaptic excitatory pathways (Maccaferri et al., 1998, Lamsa et al., 2005).

Spontaneous spiking properties					Properties of stimulus evoked spikes and plasticity during selected time points								
Cell ID	(1) Spontaneous firing frequency during theta (Hz)	(2) Mean angle-phase log to theta (deg) ± Mean angular deviation	(3) Depth of modulation (no. of theta cycles counted)	(4) Spike half width / spike width (ms) ± s.d.	(5) Evoked spike rate			(6) Average spike latency (ms)			(7) Averaged Spontaneous spiking rate (Hz) ± S.E.M.		
					Baseline	Post TBS 0-15 min	Post TBS >20 min	Baseline	Post TBS 0 - 15 min	Post TBS >20 min	Baseline	Post TBS 0-15 min	Post TBS >20 min
PL170412	4.04	351.72 ± 68.73	0.28 (388)	0.72 ± 0.02 / 1.49 ± 0.02	0.24	0.47***	0.52***	11.30 ± 0.47	11.29 ± 0.28	10.12 ± 0.47	3.83 ± 0.18	5.47 ± 0.26 ***	14.97 ± 0.88 ***
PL310812	1.45	34.39 ± 66.36	0.33 (346)	0.94 ± 0.01 / 1.88 ± 0.02	0.48	0.03***	0.06***	9.48 ± 0.22	9.84 ± 1.63	11.23 ± 1.50 *	2.18 ± 0.17	3.30 ± 0.13 ***	3.57 ± 0.20 ***
PL150113	17.69	1.16 ± 70.57	0.24 (3052)	0.81 ± 0.01 / 1.49 ± 0.02	0.75	0.57***	0.44***	8.30 ± 0.18	8.55 ± 0.23	8.84 ± 0.19 *	16.46 ± 0.59	15.34 ± 0.45	9.50 ± 0.39 ***
PL160413	4.45	99.28 ± 58.43	0.48 (2332)	0.73 ± 0.02 / 1.54 ± 0.04	0.44	0.16***	0.23***	8.16 ± 0.13	8.77 ± 0.53	8.05 ± 0.31	4.08 ± 0.25	7.71 ± 0.63 ***	5.51 ± 0.33 ***

Table 6.1. Activity-induced plasticity in the monosynaptic delay excitatory pathway to non-fast spiking CA1 area interneurons. *Left:* A table summarises electrophysiological features in "Spontaneous spiking properties" for the four cells. *Right;* "stimulus-evoked spike properties and plasticity" are summarized. Left category shows 1) average spontaneous firing frequency of the interneurons during LFP theta oscillation, 2) phase coupling of the cell action potential to LFP theta cycle, 3) depth of modulation to theta cycle (± angular deviation), and 4) the AP waveform half width and the width in milliseconds. The half width (upper) was measured from the onset to the trough, and the spike width (lower) from the onset to the end of the waveform. Right category shows 5) Probability of single-shock stimulus-evoked spike measured during baseline, and immediately (0 - 15 min) as well as > 20 min post-TBS. In 6) values for evoked spike delay (ms) to stimulation are given (mean ± SEM). Columns in 7) show mean ± SEM of spontaneous firing rate (Hz) during baseline and at the two time points where evoked spike plasticity was measured.

Figure 6.1.

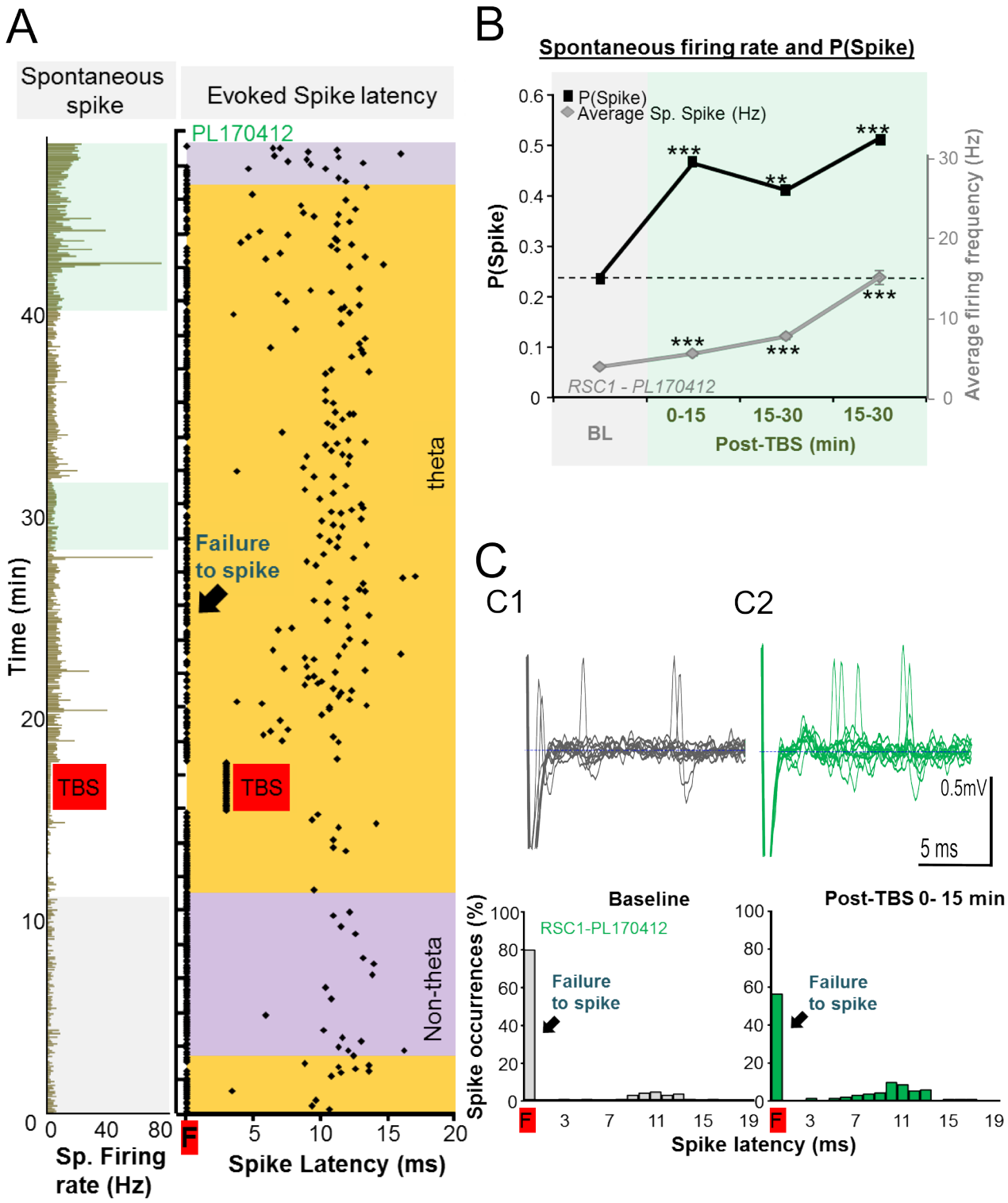
A
Spontaneous spike
Evoked Spike latency
PL170412
Time (min)
TBS
TBS
Failure to spike
theta
Non-theta
Sp. Firing rate (Hz)
Spike Latency (ms)
B
Spontaneous firing rate and P(Spike)
P(Spike)
Average Sp. Spike (Hz)
RSC1 - PL170412
BL
0-15
15-30
15-30
Post-TBS (min)
Average firing frequency (Hz)
C
C1
C2
0.5mV
5 ms
Baseline
Post-TBS 0- 15 min
RSC1-PL170412
Failure to spike
Failure to spike
Spike occurrences (%)
Spike latency (ms)

Figure 6.1. Excitatory synaptic input to Ivy cell (PL170412) shows lasting potentiation following TBS.

(A) Spontaneous and afferent stimulation-evoked spikes in PL170412 in baseline and after TBS. (A1) *Left:* Horizontal histogram shows spontaneous action potential firing (Hz, abscissa, spontaneous firing rate) during experiment. Ordinate shows time. Timing of TBS is marked in red. Shaded background area (grey, green) defines time windows for data in plot B. (A2) Dot plot illustrates stimulation-evoked postsynaptic spike probability and delay, same ordinate as in (A1). Stimulation cycles with failure to elicit a spike is shown in 'F". Yellow background indicates theta episodes in LFP, non-theta activity is shown in brown.

(B) Plot shows probability of stimulation-evoked postsynaptic spike and average spontaneous firing frequency (mean ± SEM) in baseline and at distinct time points following TBS. The cell shows an increase in stimulation-evoked spike probability following TBS (dots and line in black). Spontaneous firing from same time windows (grey dots and line). Note that although stimulus-evoked spike probability increased (Chi-square test), so did the spontaneous firing level (Mann-Witney test). Statistical significance: **, $P < 0.01$; ***, $P<0.001$.

(C) Consecutive traces with success and failures to evoke postsynaptic spike (n = 10) and histograms showing P(Spike) and delay in baseline (left) and following TBS (right). Decrease in failures ("F", marked as red in ordinate) after TBS indicates increased probability to fire an action potential.

Figure 6.2.

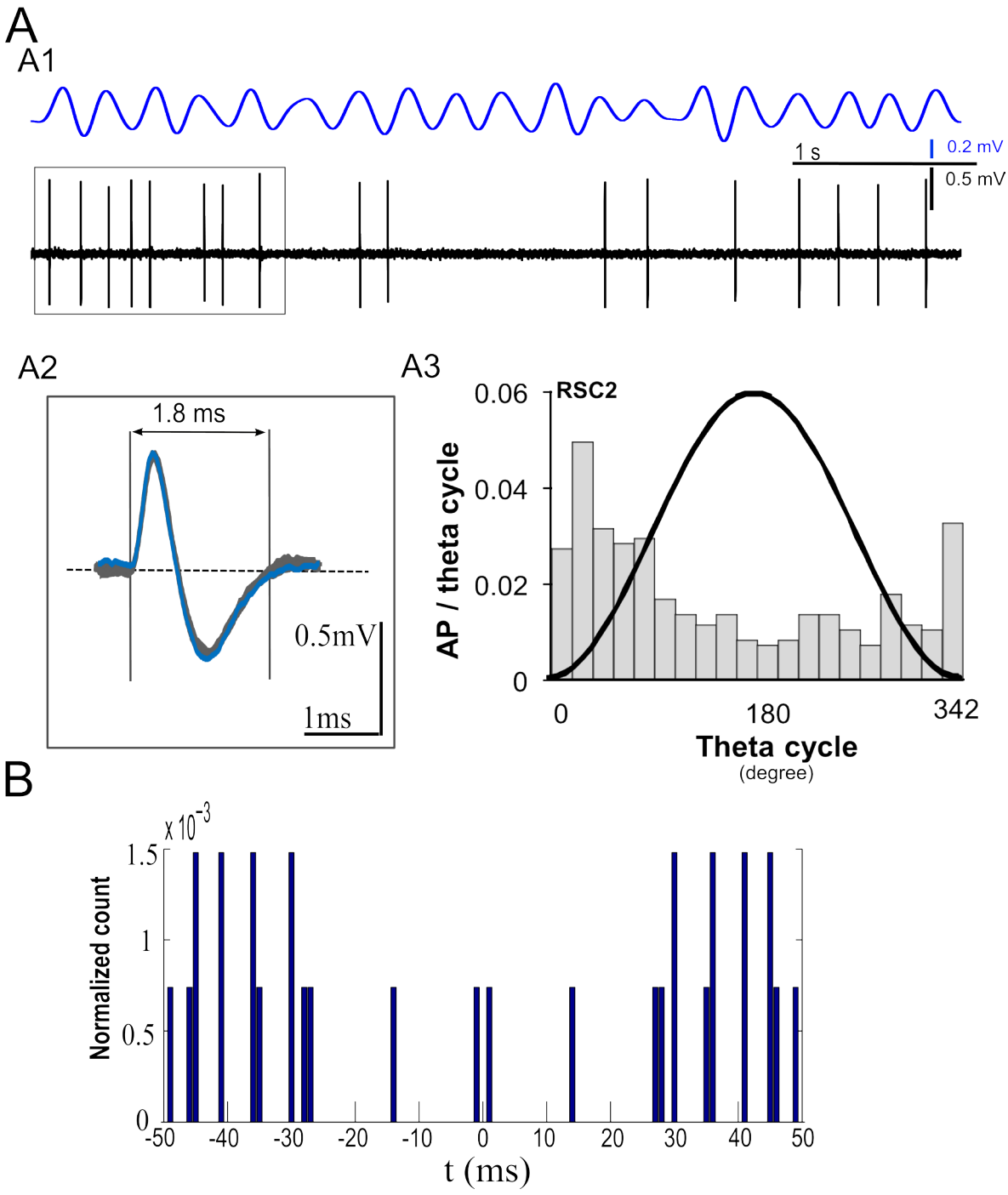
A
A1
1 s
0.2 mV
0.5 mV
A2
1.8 ms
0.5mV
1ms
A3
RSC2
AP / theta cycle
0.06
0.04
0.02
0
0
180
342
Theta cycle
(degree)
B
x 10^-3
Normalized count
1.5
1
0.5
0
-50
-40
-30
-20
-10
0
10
20
30
40
50
t (ms)

Figure 6.2.

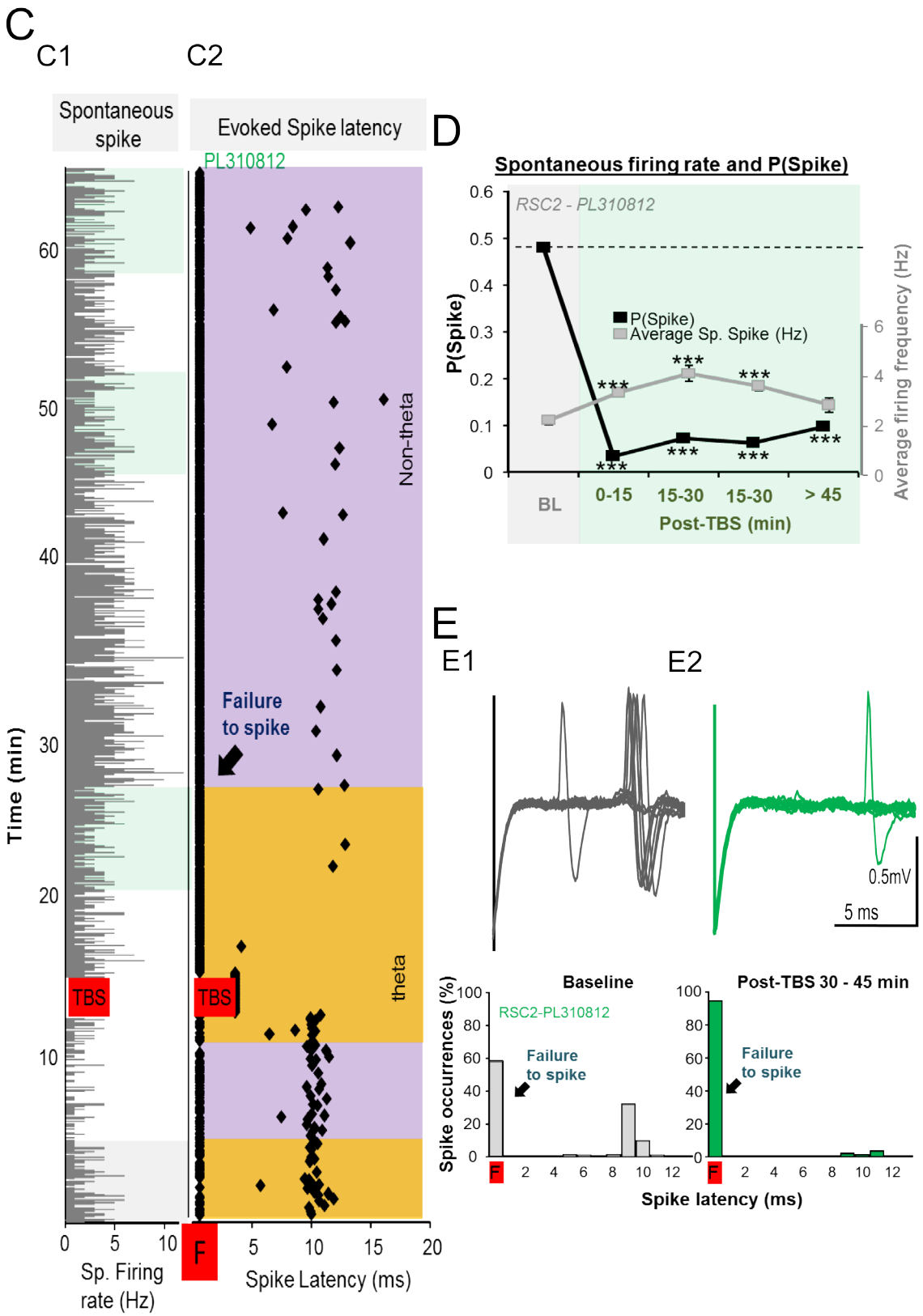
C
C1
C2
Spontaneous spike
Evoked Spike latency
PL310812
Time (min)
Non-theta
theta
Failure to spike
TBS
TBS
F
Sp. Firing rate (Hz)
Spike Latency (ms)
D
Spontaneous firing rate and P(Spike)
RSC2 - PL310812
P(Spike)
Average Sp. Spike (Hz)
Average firing frequency (Hz)
BL
0-15
15-30
15-30
> 45
Post-TBS (min)
E
E1
E2
0.5mV
5 ms
Baseline
Post-TBS 30 - 45 min
RSC2-PL310812
Failure to spike
Spike occurrences (%)
Spike latency (ms)

Figure 6.2. Electrophysiological activity and LTD in excitatory synaptic inputs to a non-fast spiking interneuron (PL310812).

(A1) A sample trace shows LFP (blue) and action potential firing of the cell (black). Spikes in boxed area are illustrated in next plot. (A2) Juxtacellularly recorded spikes exhibit slow action potential kinetics (duration 1.8 ms). Superimposed spontaneous spikes (black) and one stimulus-evoked postsynaptic spike (blue). No complex spikes with fixed short inter-spike intervals were observed. (A3) Histogram of the cell spontaneous firing phase preference during the LFP theta cycle. The cells firing preference is at $35^{o} \pm 66^{o.}$

(B) Inter-spike interval histogram of the cell spontaneous spiking measured in LFP theta during baseline recording. Spontaneous firing does not show a peak at short intervals, indicating lack of complex spikes. The cell is a typical regular-spiking non-pyramidal cell.

(C) Spontaneous and stimulation-evoked spikes. (C1) *Left:* Horizontal histogram showing spontaneous firing level (abscissa). Ordinate shows time. Timing of TBS is marked in red. Shaded background (grey and green) define time windows for data in plot D. (C2) Dot plot shows postsynaptic spike probability and delay, ordinate as in (C1). "F" (marked in red) shows stimulation cycles with failure to elicit a postsynaptic spike. Yellow background indicates LFP theta, non-theta is shown in violet.

(D) Probability of stimulus-evoked postsynaptic action potential in baseline and at defined time points following TBS (black dots and line). The cell shows robust decrease in P(Spike) following TBS (Chi-square test). Dots and line in grey show an increase in the average (mean ± SEM) spontaneous firing rate (Mann-Witney test). Dotted line in the plot indicates average in baseline for P(Spike). Statistical significance ***, $P<0.001$.

(E) Consecutive traces of juxtacellularly recorded responses (10) with evoked spike and histograms showing evoked spike probability and delay. (E1) Baseline and (E2) following TBS. Increase in failures ("F") after TBS indicates weakened transmission in the studied excitatory pathway to the cell.

Figure 6.3.

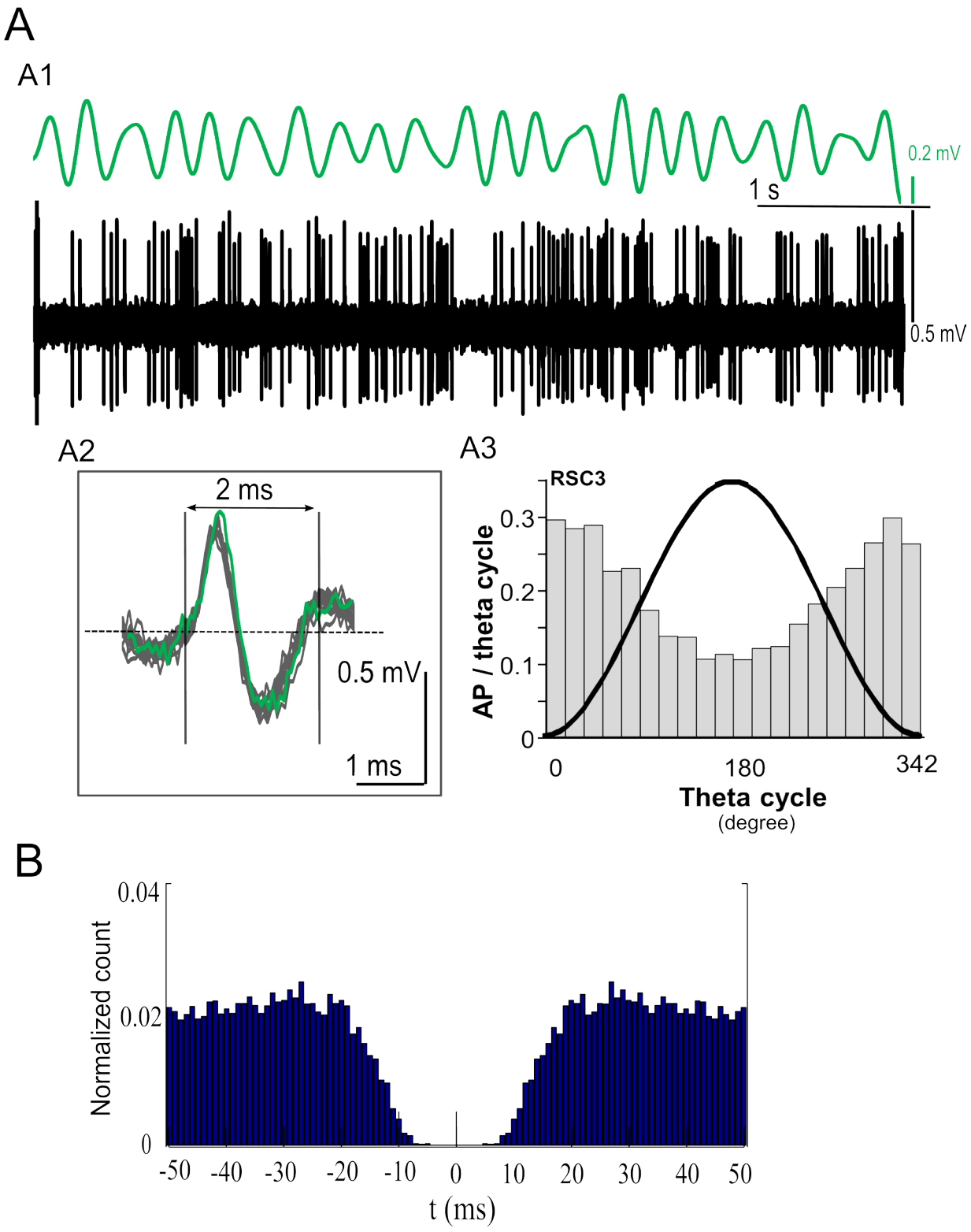
A
A1
0.2 mV
1 s
0.5 mV
A2
2 ms
0.5 mV
1 ms
A3
RSC3
AP / theta cycle
0.3
0.2
0.1
0
0
180
342
Theta cycle
(degree)
B
0.04
0.02
0
Normalized count
-50
-40
-30
-20
-10
0
10
20
30
40
50
t (ms)

Figure 6.3.

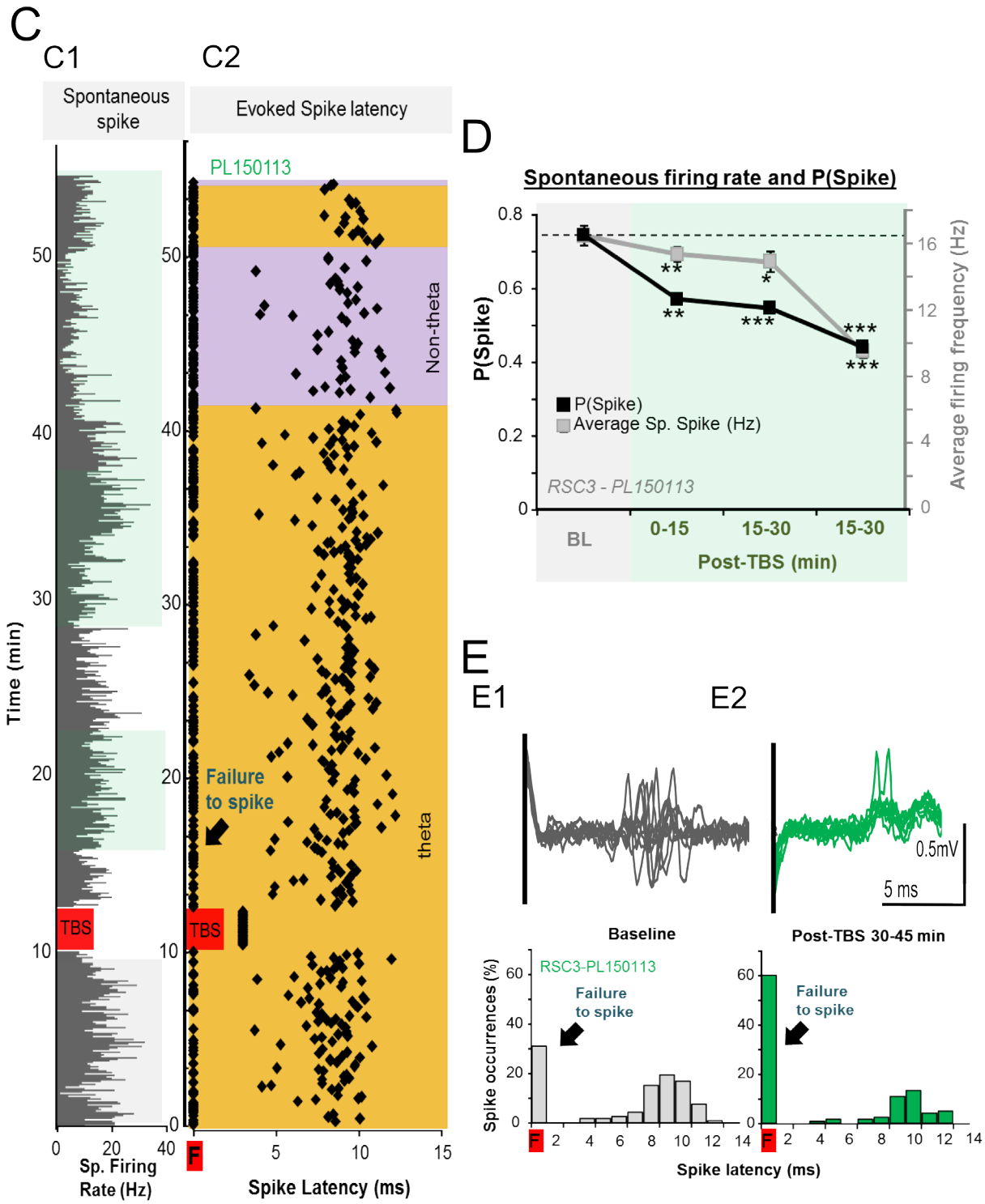
C
C1
C2
Spontaneous spike
Evoked Spike latency
PL150113
Non-theta
theta
Failure to spike
TBS
TBS
Time (min)
Sp. Firing Rate (Hz)
Spike Latency (ms)
F
D
Spontaneous firing rate and P(Spike)
P(Spike)
Average Sp. Spike (Hz)
Average firing frequency (Hz)
RSC3 - PL150113
BL
0-15
15-30
15-30
Post-TBS (min)
E
E1
E2
0.5mV
5 ms
Baseline
Post-TBS 30-45 min
RSC3-PL150113
Failure to spike
Failure to spike
Spike occurrences (%)
Spike latency (ms)

Figure 6.3. Electrophysiological activity and depression in excitatory input strength in an unidentified non-fast spiking interneuron (PL150113).

(A1) A sample trace showing LFP (green) and juxtacellularly recorded action potential firing (black) during theta oscillation. (A2) Superimposed spontaneous spikes (black) and one stimulus-evoked postsynaptic spike (green). Spikes show identical waveform and have slow kinetics (duration 2 ms). No complex spikes were observed. (A3) Histogram of spontaneous firing phase preference of the cell during LFP theta cycle. The cell firing preference is close to through. at $1^{o} \pm 71^{o}$.

(B) Statistical analysis of inter-spike interval (ISI) of spontaneous firing does not show a peak at short intervals indicating lack of complex spikes, although the cell is a regular firing CA1 cells.

(C) Spontaneous and stimulation-evoked spikes. (C1) *Left:* Horizontal bar histogram of spontaneous action potential firing throughout the experiment. Ordinate shows time, timing of TBS is highlighted red. Shaded areas in background (grey and green) show time windows for data analysed in plot D. (C2) Dot plot shows postsynaptic spike probability and delay. "F" shows stimulation cycles with a failure to produce postsynaptic spike. Yellow background indicates theta and non-theta activity is shown in violet.

(D) Average P(Spike) of stimulation-evoked postsynaptic action potential and spontaneous firing level at time points indicated. The cell shows decrease in afferent stimulation-evoked spike probability following the TBS (black dots and line, Chi-square test). Spontaneous firing from same time windows (grey, mean ± SEM, Mann-Witney test). Dotted line shows averages in baseline. Statistical significance *, $P<0.05$; **, $P<0.01$; ***, $P<0.01$.

(E) Consecutive juxtacellularly recorded responses (10) showing evoked postsynaptic spike and cycles with failures. Histogram shows the evoked spike probability and delay in baseline (E1) and following TBS (E2). Increase in failures ("F") after TBS indicates attenuated transmission in the excitatory input pathway.

Figure 6.4.

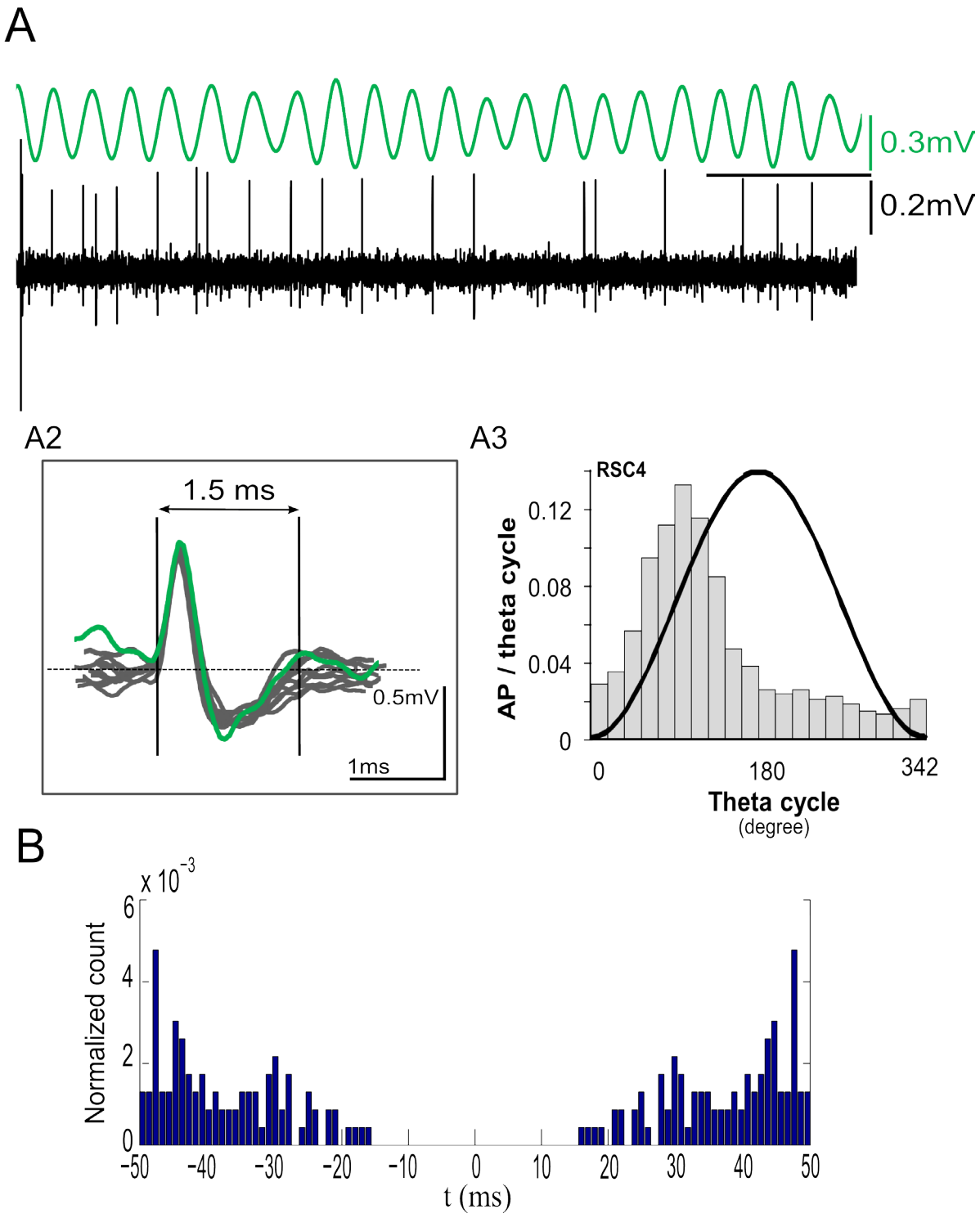
A
0.3mV
0.2mV
A2
1.5 ms
0.5mV
1ms
A3
RSC4
AP / theta cycle
0.12
0.08
0.04
0
0
180
342
Theta cycle
(degree)
B
x 10^-3
Normalized count
6
4
2
0
-50
-40
-30
-20
-10
0
10
20
30
40
50
t (ms)

Figure 6.4.

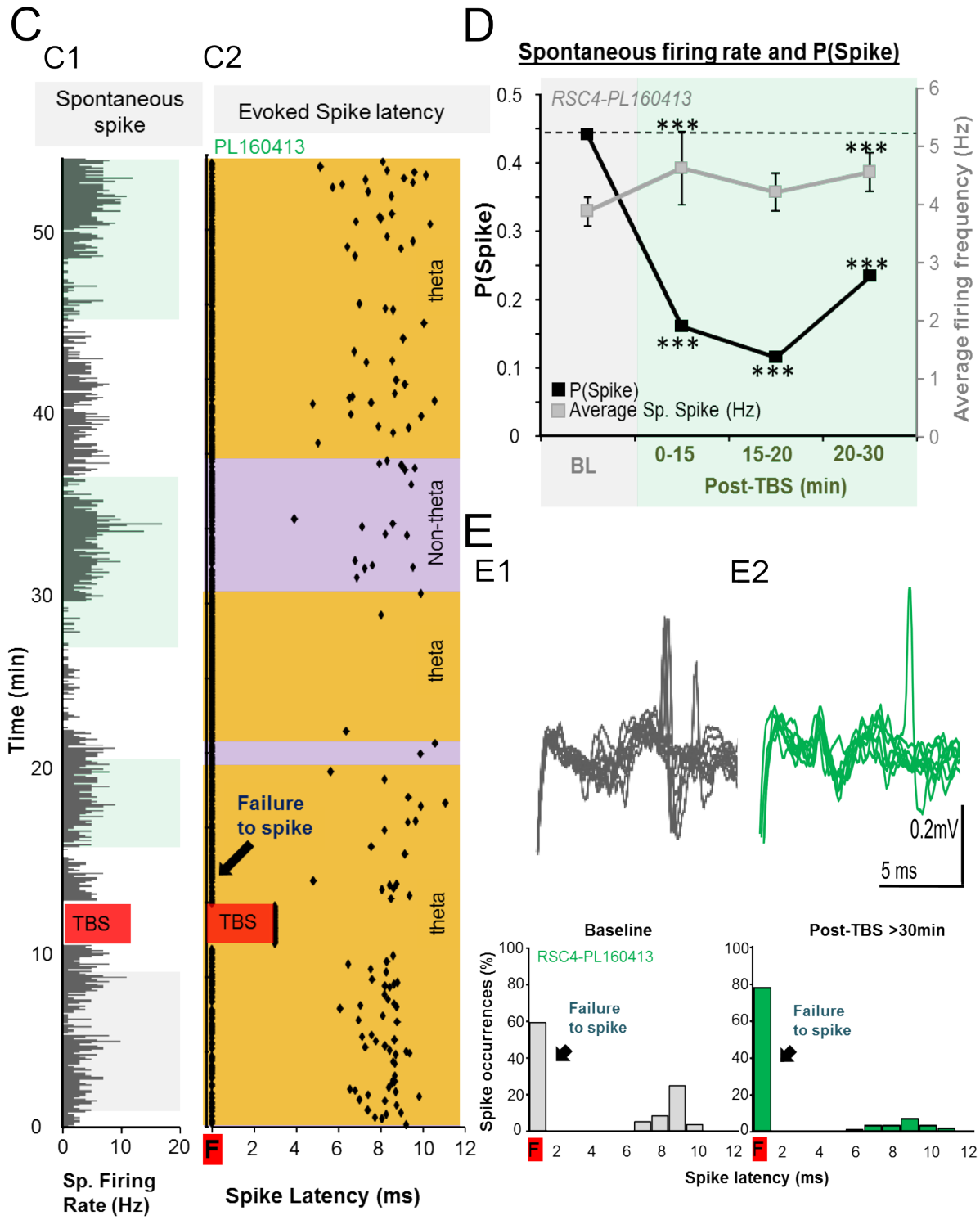
C
C1
C2
Spontaneous spike
Evoked Spike latency
PL160413
theta
Non-theta
theta
theta
Failure to spike
TBS
TBS
Time (min)
Sp. Firing Rate (Hz)
Spike Latency (ms)
D
Spontaneous firing rate and P(Spike)
RSC4-PL160413
P(Spike)
Average Sp. Spike (Hz)
Average firing frequency (Hz)
BL
0-15
15-20
20-30
Post-TBS (min)
E
E1
E2
0.2mV
5 ms
Baseline
Post-TBS >30min
RSC4-PL160413
Failure to spike
Failure to spike
Spike occurrences (%)
Spike latency (ms)

Figure 6.4. Electrophysiological activity and LTD in excitatory synaptic input to a non-fast spiking interneuron (PL160413).

(A1) Traces show LFP (green) and juxtacellularly recorded action potentials of the cell (black). (A2) Spontaneous spikes (black) and one stimulus-evoked postsynaptic spike (green) superimposed. Spikes show slow action potential kinetics (duration 1.5 ms). No complex spikes were observed. (A3) Histogram showing spontaneous spiking phase preference during LFP theta cycle. The cell prefers to fire at the ascending phase of LFP theta cycle at $99^{o} \pm 58^{o}$ (Klausberger et al., 2005).

(B) Inter-spike interval (ISI) of spontaneous firing does not to show a peak at short intervals indicating lack of complex spikes in a regular firing cell.

(C) Spontaneous and stimulation-evoked spikes. (C1) *Left:* Horizontal bar histogram of spontaneous action potential firing throughout the experiment. Ordinate shows time. TBS is indicated in red. Shaded areas (grey and green) show time windows for data analysis in plot D. (C2) Postsynaptic spike probability and delay. "F" shows stimulation cycles with failures to elicit postsynaptic spike. Yellow background indicates theta and violet non-theta activity in LFP.

(D) P(Spike) in baseline and at time points following TBS as indicated in abscissa. The TBS is followed by a decrease in afferent stimulation-evoked spike probability. Spontaneous firing from the same time points (grey dots and lines, mean ± SEM, Student's *t*-test). Dotted line in the plot indicates averages in baseline. Statistical significance: ***, $P<0.001$, the Chi-square test.

(E) Consecutive traces (10) of evoked spikes with occasional failures and histogram showing spike probability and delay to stimulation in baseline (E1) and following TBS (E2). Increased spike failures ("F") after TBS indicate lasting depression in the stimulated pathway.

7. Contribution of brain state and postsynaptic firing level to plasticity in the CA1 area neurons

7.1. Introduction

Finally, I tested the hypothesis whether plasticity was affected by the underlying brain state, strength of afferent excitatory fibre input or postsynaptic cell firing level in these experiments. *In vivo* experiments such as recordings from an anaesthetized rat brain allow only limited control of postsynaptic cell spontaneous firing and postsynaptic discharge during high-frequency (plasticity inducing) excitatory afferent pathway stimulation (Blackstad, 1956, Buzsaki and Eidelberg, 1982b, Debanne et al., 1998, Andersen et al., 2007). Both spontaneous firing rate and TBS-elicited firing depend on postsynaptic cell excitability and regulated by brain states. As I reviewed earlier, local field potential (LFP) activity patterns and spontaneous firing rate of hippocampal neurons vary between wakefulness *versus* sleep, and alertness *versus* inattentiveness (O'Keefe and Nadel, 1978). Specific patterns of synchronous network oscillations in the hippocampus are observed during different behavioural activities (O'Keefe and Nadel, 1978, Buzsaki, 2005, Somogyi and Klausberger, 2005). These variations in hippocampal activity states are physiological function that controlled by subcortical brain areas through monoaminergic and cholinergic innervation (O'Keefe and Nadel, 1978, Chrobak and Buzsaki, 1996, 1998, Popa et al., 2010). Interestingly, many of the hippocampal oscillatory patterns observed in drug-free animals, are also observed in anaesthesia animals (Chrobak and Buzsaki, 1998, Buzsáki, 2003, Klausberger et al., 2003, Lapray et al., 2012).

Among these, most relevant to the present study are theta (4 – 8 Hz in awake rats)

oscillations, which can be observed in the hippocampus during cognitive task performances and learning such as during exploratory behaviour with recall and update of hippocampus-based spatial memory in drug free animals (Chrobak and Buzsaki, 1998, Klausberger et al., 2003). Theta oscillations are prominent during rapid-eye-movement sleep episodes and active exploration (O'Keefe and Nadel, 1978, Chrobak and Buzsaki, 1998). Hippocampal theta and sharp wave ripple high frequency oscillations are closely associated with hippocampus-based spatial memory consolidation (Buzsaki, 1998, Reiner et al., 2014). In urethane-anaesthetized rats, theta activity often spontaneously emerges in the hippocampus although its average frequency is slightly slower (3 – 6 Hz) than in awake animals (Ognjanovski et al., 2014). Intraperitoneal injection of ketamine/xylazine mixture to urethane-anaesthetized rats typically shifts brain state from theta oscillatory activity towards the non-theta state, in which slow-waves (1 Hz) can also occur (Vanderwolf, 1988). During the non-theta state, theta oscillations can be periodically generated by noxious somatic stimuli that increase alertness (Buzsaki and Eidelberg, 1982b).

7.2. Results

In this chapter I have analysed parameters related to the underlying brain states and quantified spontaneous firing level of the postsynaptic cells and compared these with their long-term plasticity results reported earlier in Chapter 4 and 5. In these analyses I have concentrated on pyramidal cells and fast-spiking interneurons, in which plasticity is well

characterized in acute brain slices and both represent electrophysiologically relative homogeneous groups (Somogyi and Klausberger, 2005).

7.2.1. Potential impact of postsynaptic cell spontaneous firing level and hippocampal brain state on the excitatory pathway long-term plasticity

Although in this study postsynaptic PV+ interneurons showed long-term plasticity is response to afferent TBS stimulation *in vivo*, plasticity results qualitatively differed from what has been reported of TBS in PV+ cells in acute brain slices (i.e. *in vivo* two fast-spiking basket cells generated LTD and a bistratified cell showed LTP, see Chapter 5.2.1.). In addition, TBS failed to elicit either immediate potentiation or depression in one axo-axonic cell (see Chapter 5.2.1.). Although a failure to elicit plasticity in cell types that typically show plasticities reported in brain slice studies, reasons for such behaviour are unknown (Oren et al. 2009, Nissen et al. 2010). Most synaptic long-term plasticity mechanisms reported in the hippocampus depend on postsynaptic neuron membrane potential, which can be indirectly quantified by the cells spontaneous firing level (Klausberger et al., 2003, Kullmann and Lamsa, 2007). In general, during theta oscillation plasticity is facilitated and promoted in the hippocampal circuits (Huerta and Lisman, 1993, Lubenov and Siapas, 2009). Therefore, I analysed here the recorded neurons spontaneous firing level and LFP oscillation pattern during TBS, and compared the results with the plasticity outcome in the cells.

7.2.1.1. Spontaneous firing level of postsynaptic cells in the plasticity experiments

First, I asked if the spontaneous action potential firing level during experiments has an effect on long-term plasticity in the group of cells studied. As I described earlier (see figures in Chapters 4-6), I have analysed spontaneous discharge of all cells in this study by selecting a 1s time windows every 5 seconds just prior to the single-shock electrical stimulation of afferent fibres (see Chapter 4.2.1.2.).

I found that general spontaneous spiking activity is unlikely to explain the direction of plasticity elicited, since both LTP and LTD were seen in the fast-spiking interneurons (n = 7) in cells with similar spontaneous firing levels. Five of seven fast-spiking cells showed spontaneous firing between 10 Hz and 20 Hz at the time of TBS, and of them two cells showed LTP (FSC6 and FSC7) and two cells generated LTD (FSC3 and FSC4). One cell (FSC1) failed to show plasticity during 30 min post-TBS although its spontaneous discharge level was similar to the other two. Figure 7.1. summarizes results on the spontaneous firing and plasticity in PV+ cells.

7.2.1.2. Brain states during the TBS determined by LFP oscillations

Next, I compared plasticity results with brain states defined by the LFP oscillation

patterns at the time point when TBS was applied. I found that in identified pyramidal cells robust LTP was generated in all three experiments although the brain states during TBS were different. At the time of plasticity induction (i.e. delivering TBS) LFP in one pyramidal cells showed non-theta activity, whereas in the other two cells the activity pattern was clear theta oscillation. Hence, I can conclude that the underlying brain state (identified as theta *versus* non-theta) during TBS in these experiments is unlikely to govern the directions of plasticity (i.e. LTP versus no plasticity) in the pyramidal cells.

In addition, LTP with a similar magnitude was generated in PV+ fast-spiking cells with either the underlying theta or non-theta activity at the time of TBS. Although sample sizes in these experiments are fairly small, the occurrence of both LTP and LTD in thePV+ population showing theta activity during the TBS protocol makes it unlikely that "theta *versus* non-theta" determines the direction of the plasticity observed. Results are illustrated in Figure 7.2.

7.2.2. Postsynaptic cell excitation level and action potential discharge during the TBS

The general firing level of postsynaptic cells depends on their intrinsic excitability, which varies between brain states (Klausberger et al., 2003), but as I reviewed earlier in Chapter 3, the strength of afferent fibre stimulation (i.e. number of glutamatergic synapses activated) also affects the number of evoked postsynaptic spikes (see Chapter 3.2 and 3.3.). I

found that although the postsynaptic firing level elicited by TBS stimulation also varied between experiments in PV+ cells (see Chapter 7.2.2.1.), this is unlikely to explain why LTP, LTD or no plasticity was induced in PV+ cells. Results of the analyses are presented below.

7.2.2.1. Quantifying postsynaptic cell action potential firing during the TBS

I quantified the postsynaptic firing triggered by afferent TBS stimulation in the postsynaptic cell. Figure 7.3. shows sample traces of TBS-associated postsynaptic firing in two PV+ fast-spiking cells with a very different number of spikes. Figure 7.4. quantifies TBS-associated postsynaptic firing in all studied cells is shown and plot this against their baseline-normalized plasticity (n = 14).

Overall the cells studied here varied substantially regarding their firing during the TBS. This variation is difficult to explain simply by cell type-specific differences in discharge properties, because some pyramidal cells and fast-spiking PV+ interneurons showed a similar TBS-elicited firing level in the experiments. In addition, the TBS-associated firing level in PV+ cells is unlikely to explain qualitative differences in the plasticities (i.e. LTP versus LTD) because PV+ cells with similar prominent postsynaptic firing during the TBS showed either no plasticity (n = 1), LTP (n = 4), or LTD (n = 3).

7.2.2.2. Comparison of afferent pathway strength and plasticity

Finally, I compared plasticity and the excitatory pathway strength defined by a probability to evoke postsynaptic spikes by low-frequency afferent stimulation during baseline. Results show that in pyramidal cells the lowest baseline probability resulted in the highest proportional potentiation, which is expected because the lowest starting probability can allow the largest relative increase. In fast-spiking cells, there was an interesting tendency that the two cells with the lowest spiking probability (0.31 and 0.52, in FSC4 and 3, respectively) generated LTD, whereas the other five cells showed LTP or no plasticity (other > 0.6). However, the difference in the evoked spike probability values between LTD and LTP fast spiking cells is relatively small but the small sample size (n = 2) of fast-spiking cells with LTD does not allow statistical testing of the hypothesis on weak pathway strength favouring LTD. Results from the comparison of the two parameters are illustrated in Figure 7.5.

7.3. Discussion

The results in this chapter show two relevant features on hippocampal excitatory connection plasticity in the CA1 area neurons. First, in the present experimental conditions *in vivo* the CA1 pyramidal cells exhibit robust LTP independent of variation between two common brain states, defined by the underlying LFP oscillatory activity as theta or non-theta. Second, results on pyramidal cells and fast-spiking interneurons indicate that postsynaptic cell

type is the strongest factor to explain LTP and LTD in these plasticity results. Differences in postsynaptic spiking level and excitability do not explain the induction of LTP, LTD or no plasticity in the studied cells.

7.3.1. Robust brain state-independent plasticity in pyramidal cells

Theta burst-modulated high-frequency stimulation (i.e. TBS) robustly potentiated synaptically-evoked spike probability in all three pyramidal cells recorded although brain states during LTP induction were different in these experiments. In addition, spontaneous and TBS-evoked firing levels varied substantially in the cells and so did the stimulated pathway strength (measured as single-shock evoked spike probability in baseline). Although it is well established that hippocampal brain state showing theta activity facilitates learning-related synaptic plasticity and LTP in pyramidal cells (Buzsaki, 1998), the robust LTP in all neurons here may indicate that our LTP induction paradigm is strong enough to elicit plasticity either during theta or non-theta. Postsynaptic cell excitability and firing level have been demonstrated to regulate LTP in pyramidal cells *in vitro* (Park et al., 2014), but in my experiments here the sample size is too small to study a hypothesis on modulation of the pyramidal cell plasticity by spontaneous firing rate *in vivo*.

As a summary, results shown here demonstrated that a plasticity induction protocol

commonly used in acute brain slices (i.e. TBS), can elicit equivalent and strong LTP *in vivo*, independent of brain state. In addition, the experiments on three identified pyramidal cells demonstrate that the model I used here to study plasticity in anesthetized rat brain is stable and well suited to address basic questions on use-dependent plasticity of the excitatory inputs to CA1 neuron types. Thus, electrical stimulation with defined properties of the monosynaptic pathway (see Chapter 3) provides a valid method to investigate general features of the glutamatergic pathway plasticity in rodent brains *in vivo*.

7.3.2. Qualitative differences in the interneuron plasticity are poorly explained by brain states or target cell firing level

Fast-spiking PV+ interneurons provide a relatively homogeneous neuron population regarding many electrophysiological properties (Hu et al., 2014). Although CA1 PV+ cells vary regarding anatomical features, and in slices PV+ cell types may show differences in plasticity, most fast-spiking neuron types in acute hippocampal slice preparation generate LTP following delivery of high frequency stimulation to afferent glutamatergic connections (Nissen et al., 2010, Le Roux et al., 2013). For anatomically analysed PV+ basket, axo-axonic and bistratified -cells consistent plasticity results in slice preparation have been reported (Nissen et al., 2010, Le Roux et al., 2013). However, recent studies have shown that CA1 PV+ interneurons, which often show LTP in slices, can in other conditions generate LTD (Bodor et al., 2005, Peterfi et al., 2012). One of the aims of my project was to study if some

general *in vivo* recorded parameters, such as brain state and brain-state associated firing level could clearly regulate plasticity direction in the CA1 area PV+ cells. The *in vivo* preparations are more optimal for such a study, since they conserve intact brain circuits, physiological temperature and lack traumatizing and ischemic pre-treatment (which inevitably have side effects due to the preparation of brain slices). This allows more physiologically relevant conditions to study plasticity compare to brain slices where results may vary depending on the preceding tissue slicing procedure and slice thickness, slice storage and super-fusion conditions as well as the solutions used for perfusion and intracellular recording (Isaac et al., 1996, Lamsa et al., 2005, Hajos et al., 2009).

Interestingly *in vivo* experiments I performed here show that LTD appears commonly in PV+ basket cells, whereas in other identified and unidentified PV+ cells LTP was seen with the same afferent stimulation paradigm. Although a number of experiments on identified PV+ cell types here is small, it is large enough to conclude that fluctuation in urethane anaesthesia between theta and non-theta oscillation does not determine whether LTP or LTD in these cells is induced (Kullmann and Lamsa, 2007). In addition, the postsynaptic spiking level before or during TBS failed to divide PV+ cells to LTP- and LTD -expressing cells. Only the cell type (i.e. basket cell *versus* others) and stimulation pathway intensity (measured as evoked spike probability in baseline) showed any potential to predict whether LTP or LTD was generated by TBS in PV+ cells. Unfortunately the data in this study is too little to statistically test this hypothesis. However, it is intriguing to speculate that weak pathway stimulation prefers LTD, whereas strong pathways generate LTP. Such a rule is commonly recognized in plasticity

rules in pyramidal cells (Frey and Morris, 1997, Fonseca et al., 2004, Andersen et al., 2007). One speculative explanation of such behaviour is that low strength pathways fail to recruit mechanisms needed for LTP and engage LTD-inducing machinery instead (Kullmann and Lamsa, 2007). Whether this hypothesis is correct remains to be tested, and if it is, possible mechanisms will need to be investigated. Cannabinoid receptors (Katona and Freund, 2008, Camire and Topolnik, 2014), calcium-permeable AMPARs (Lamsa et al., 2007b) and NMDARs (Poncer et al., 1995) would be good candidates to be involved.

7.4. Figures

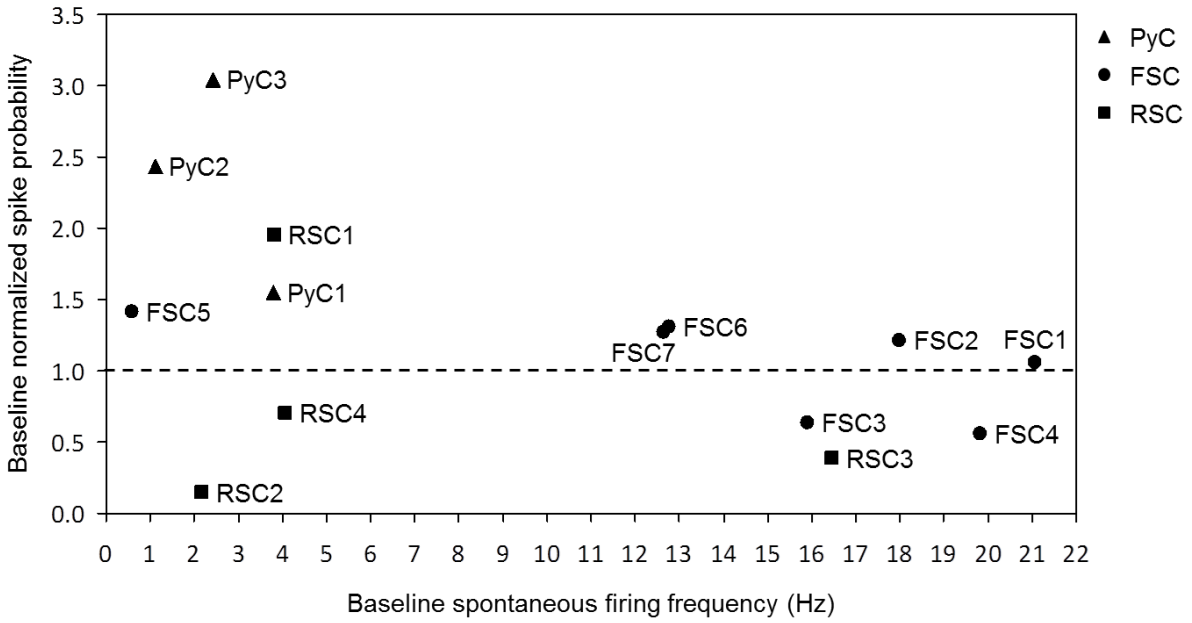

Figure 7.1. Spontaneous postsynaptic cell firing level and long-term plasticity.

Baseline-normalised stimulus-evoked spike probability after TBS (in ordinate, dotted line indicates normalised baseline mean 1) in all recorded cells plotted against their spontaneous firing level during baseline (abscissa, Hz). The three cell populations are indicated by specific symbols on the right. All three pyramidal cells (PyC, triangles) showed robust LTP and low spontaneous firing level (1-4 Hz). Fast-spiking PV+ cells (FSC, circles) showed the highest spontaneous firing rate, but firing frequency varied substantially between individual cells (from <1 to > 20 Hz). Spontaneous firing level poorly explains polarity of the plasticity (i.e. LTP vs. LTD) in PV+ cell population, since cells with LTP and LTD are seen with 10 – 20 Hz spontaneous firing level. Firing level also varied between individual regular-spiking interneurons (RSC, rectangles), and their firing on average was in between pyramidal cells and FS-interneurons. Most RSCs, except one identified ivy cell showed LTD.

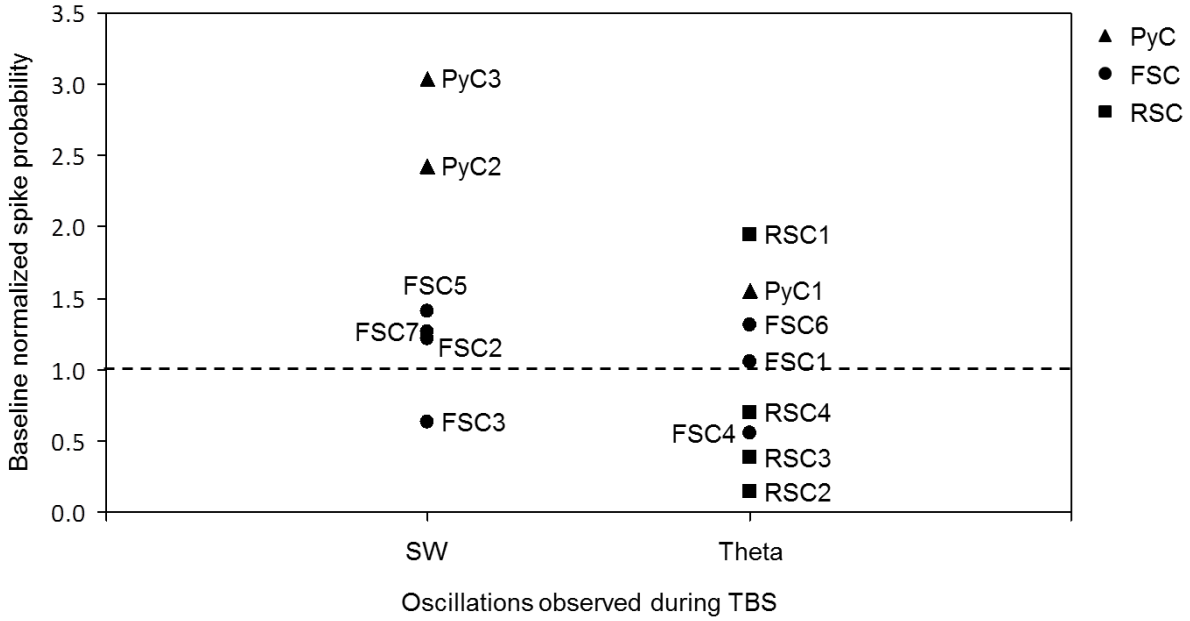

Figure 7.2. LFP brain state and long-term plasticity.

Baseline-normalised afferent stimulation-evoked spike probability after TBS (in ordinate, dotted line is cells baseline mean 1) in all cells sorted by brain state as LFP theta or non-theta (abscissa). The three distinct cell populations are indicated by symbols as shown on the right. Robust LTP in pyramidal cells (triangles) was seen in experiments with either LFP non-theta or theta during TBS. Fast-spiking PV+ cells (circles) with LTP and LTD are seen in experiments exhibiting either non-theta or theta. All experiments on regular-spiking interneurons (rectangles) were stimulated with TBS during LFP theta activity; both cells with LTD and one cell with LTP were seen in this group. As a conclusion, the underlying LFP theta or non-theta activity during TBS poorly explains polarity of the plasticity in the

interneurons.

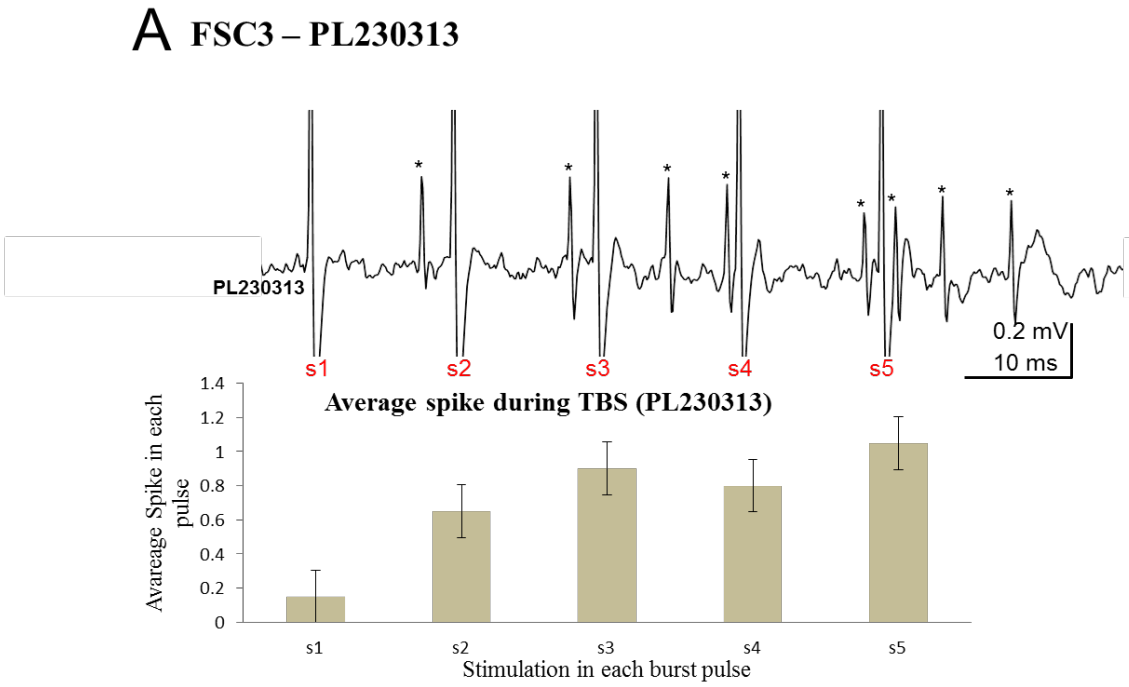

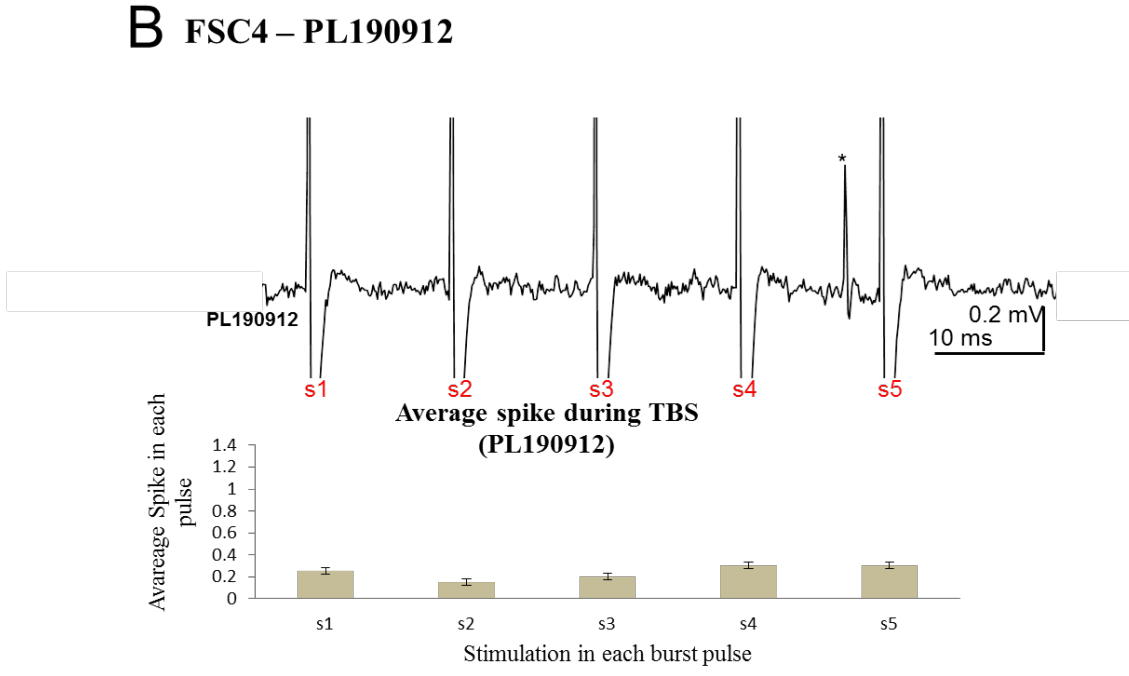

Figure 7.3. Quantification of postsynaptic action potential firing during TBS.

Sample traces showing juxtacellularly recorded postsynaptic firing of two fast-spiking PV+ interneurons during afferent TBS. Traces show response to one stimulation cycle (5 pulses) in two PV+ cells. (In total 20 cycles with 200 ms interval were delivered in TBS). Histograms below report mean ± sd of postsynaptic spikes evoked in these cells during 20 stimulation cycles. (A) Prominent firing of fast-spiking PV+ interneuron PL230313 (FSC3, identified as PV+ BC) during TBS. *Above;* a juxtacellularly recorded response showing postsynaptic spiking during one 5-pulse stimulation cycle. *Below;* histogram shows mean ± sd of action potentials evoked by stimuli 1-5 (s1-s5) during all 20 cycles in this cell (spikes counted in 10 ms time window from stimulation).

(B) Fast-spiking PV+BC, FSC4-PL190912, shows much less discharge during TBS. Trace and histogram as above.

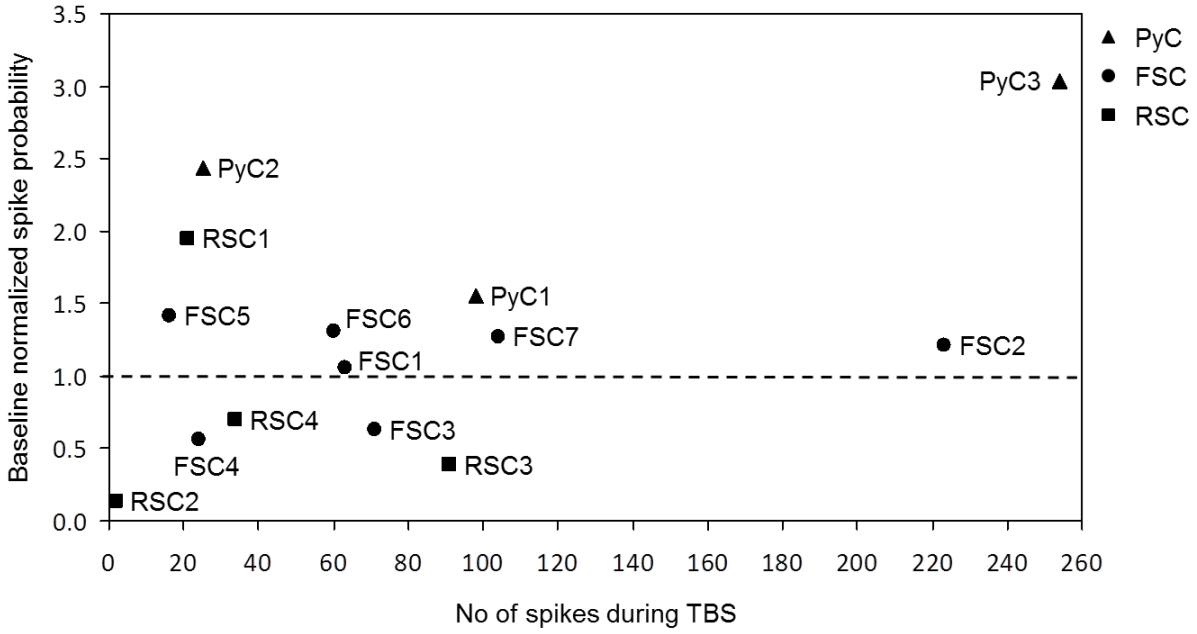

Figure 7.4. Postsynaptic action potential firing during TBS and long-term plasticity.

Baseline-normalised spike probability in the stimulated pathway after TBS (ordinate, dotted line shows normalised baseline mean 1) plotted against quantified postsynaptic firing of the cells during TBS (abscissa). The three cell populations are identified with symbols shown on the right. Although pyramidal cells (triangles) were different in the TBS-associated spiking level, they all show robust LTP. Fast-spiking PV+ (circles) and regular-spiking interneurons (rectangles) showed variability in TBS-evoked discharge too. Postsynaptic firing level poorly explains polarity of plasticity (i.e. LTP vs. LTD) in the interneurons, since FSCs with similar discharge levels (20 – 100 spikes) show either LTP or LTD.

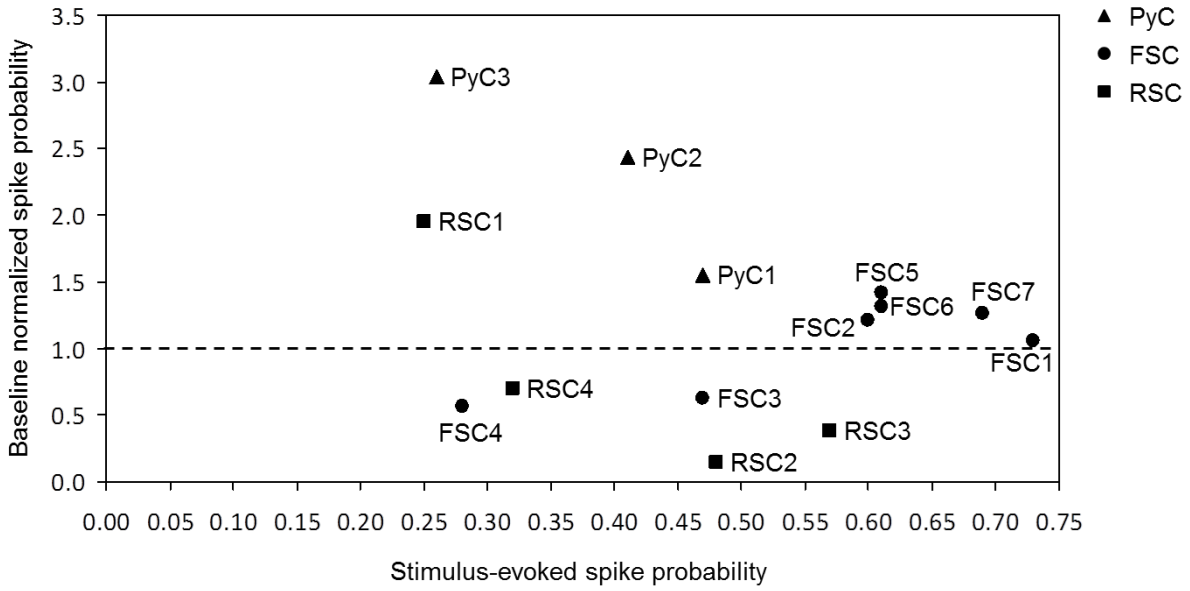

Figure 7.5. Afferent pathway excitation strength and long-term plasticity.

Baseline-normalised evoked spike probability after TBS (ordinate, dotted line is normalised baseline mean 1) plotted against the stimulated pathway strength (measured as average spike probability evoked by stimuli in baseline, abscissa). Cell populations shown on the right with specific symbols: triangle, circle and rectangle, for pyramidal, fast spiking, and regular spiking cells. Range of evoked-spike probability was from 0.25 to 0.73. Although the distribution of data points fails to show clear relation between plasticity polarity (i.e. LTP *versus* LTD) and stimulated pathway strength, fast-spiking interneurons show interestingly that LTD was generated in two cells with the lowest afferent pathway strength.

8. General Discussion

8.1. Summary of findings

In the present study, I have investigated induction and expression of activity-induced long-term plasticity in excitatory synaptic pathways to identified CA1 interneuron types *in vivo*. Use-dependent long-term potentiation and depression in glutamatergic synapses to cortical pyramidal cells, including hippocampus, are well established (Hebb, 1949, Bliss and Lomo, 1973, Mcnaughton et al., 1978, Buzsaki and Eidelberg, 1982b). In addition, LTP and LTD in excitatory pathways to some hippocampal GABAergic interneurons have been previously reported in experiments utilizing acute brain slice preparations and organotypic slice cultures (Pelletier and Lacaille, 2008, McBain and Kauer, 2009, Galvan et al., 2011, Kullmann and Lamsa, 2011, Ran et al., 2012). A recent study also suggested that hippocampus-based spatial learning is associated with permanent changes in the CA1 area pyramidal and interneuron communication, measured as their correlated sequential spiking as "a pre- and postsynaptic neuron" (Dupret et al., 2013). However, it has been unknown whether activity of excitatory synaptic connections is able to similarly cause permanent changes in hippocampal pyramidal cell – interneuron spike coupling in the CA1 area *in vivo*.

I have demonstrated here that contralateral electrical stimulation of excitatory synaptic connections provides a good model to investigate long-term plasticity in glutamatergic pathways to identified hippocampal CA1 area neurons. Single-shock electrical stimulation from the left hemisphere CA1 area elicited a phase-locked short-delay field EPSP in the right

hippocampal CA1 area. Phase locking of the postsynaptic response onset (both fEPSP and postsynaptic spike) to afferent stimulation with only a millisecond-range cycle-by-cycle variation indicates a monosynaptic excitatory transmission in the CA1. In addition, stimulating and recording from contralateral the CA1 area avoids antidromic action potentials in the recorded cells (Andersen et al., 2007, Witter, 2007).

Importantly, the fEPSPs were detected in recordings where postsynaptic cell firing was recorded in identified CA1 pyramidal cells. In two of three juxtacellular recordings experiments from a postsynaptic pyramidal cell with "half-maximal" spike generation probability, the field EPSP was simultaneously generated. In both recordings the postsynaptic pyramidal cell spike was elicited close to the peak of fEPSP, which is characteristic of monosynaptic transmission. Furthermore, in most recordings from postsynaptic CA1 interneurons fEPSP was not elicited. This is in line with earlier *in vivo* studies reporting that CA1 interneurons are excited by a lower stimulation intensity than pyramidal cells, presumably because they are innervated by a higher density of excitatory fibres and have a lower threshold for spiking than CA1 pyramidal cells (Buzsaki and Eidelberg, 1982a, b). Postsynaptic cells with the monosynaptic excitatory input were recognised (see Chapter 3.1) when the evoked postsynaptic spikes were phase-locked to stimulations with short monosynaptic delays with little cycle-by-cycle variations (Deadwyler et al., 1975, Buzsaki and Eidelberg, 1982b). With elevated stimulation intensity or following TBS-elicited potentiation of evoked spike probability, the postsynaptic spike probability increased with a minor change in spike delay. All these results indicate that the 14 hippocampal CA1 neurons

in this study were excited by activation of monosynaptic glutamatergic pathway. Postsynaptic spike probability measurement provides a stable experimental protocol *in vivo* to measure excitatory synaptic pathway strength and plasticity in identified cells in rat brain. However, it is reasonable to admit that my experimental approach had fairly low yield, since just 14 of more than 300 extracellularly recorded postsynaptic CA1 area cells responded to the contralateral stimulation that matched the monosynaptic connection criteria and were stable enough to be studied in the experiments lasting for at least an hour (see chapter 3.1.).

First, I established that LTP can be induced by the afferent TBS in excitatory input to identified postsynaptic pyramidal cells (measured as increased evoked spike probability). Interestingly, LTP was robust in pyramidal cells although ketamine was co-applied with xylazine to maintain anaesthesia during the recordings. Ketamine is a non-competitive NMDAR antagonist, and in high concentrations blocks LTP in pyramidal cells (Yamakura et al., 1993, Hara and Harris, 2002, Morgan et al., 2004). However, systemically applied low ketamine levels in urethane-anesthetized rats (30 mg/kg, i.p.) are unlike to cause full NMDAR receptor blockade (Soltesz and Deschenes, 1993, Salami et al., 2000, Hara and Harris, 2002). For the interneuron plasticity experiments, the presence of NMDAR antagonist is less relevant, since in most CA1 GABAergic interneurons LTP and LTD are independent of NMDARs (Kullmann and Lamsa, 2011). The presence of ketamine may have reduced polysynaptic NMDAR-dependent plasticity generating polysynaptic spikes in these experiments (Maccaferri et al., 1998).

My experiments showed long-lasting potentiation in most PV+ fast-spiking postsynaptic interneurons, and LTD-like depression in synaptic connections to identified PV+ basket cells. These results show that LTP- and LTD-like use-dependent long-term changes take place in excitatory connections to various PV+ interneuron types, as has been demonstrated previously in acute slice preparations (Nissen et al., 2010, Peterfi et al., 2012, Campanac et al., 2013, Le Roux et al., 2013). However, my results *in vivo* also differ from the plasticity results in slices; in acute slice preparations both axo-axonic and basket cells showed LTP or no plasticity following theta-burst high frequency stimulation of glutamatergic fibres, while bistratified cells showed LTD (Nissen et al., 2010, Campanac et al., 2013, Le Roux et al., 2013). In experiments here, I found that although axo-axonic cells again either showed potentiation or no LTP, two of the identified basket cells exhibited LTD and one of the identified bistratified cell showed moderate LTP.

What might explain the differences between *in vitro* and *in vivo* experiments? Both in experiments using slice preparations and *in vivo* recordings, minimally invasive postsynaptic recording method of excitatory pathway input strength was used. Hence dialysing of postsynaptic cell cytoplasmic content can be excluded(Isaac et al., 1996, Lamsa et al., 2007a). In slice recordings a perforated patch measurement of EPSP was utilised, and here I measured excitatory pathway input strength with extracellular recording of postsynaptic spike probability. One possible explanation of the difference is that urethane-based anaesthesia which might affect synapses and plasticity, however there is no evidence in the literature for such changes (Hara and Harris, 2002). Another possible explanation could be that only partial

blockade of NMDARs *in vivo* experiments with ketamine was achieved, whereas in most *in vitro* plasticity tests NMDARs have been pharmacologically fully blocked (Kullmann and Lamsa, 2011). Although it is not straight-forward to speculate how the different NMDAR activity levels could lead to a switch of long-term plasticity in hippocampal interneurons, it is possible that there are presynaptic NMDARs affecting plasticity through release probability in excitatory synapses on PV+ interneurons (Buchanan et al., 2012). Yet, an equally likely possibility is that in the experiments *in vivo* with contralateral afferent stimulation, the glutamatergic anatomical pathways tested for plasticity are different from the slice recordings and that CA1 interneurons show pathway-specific plasticity properties (Sambandan et al., 2010). However, the relative proportion of activated the ipsi- and contralateral CA3 pyramidal cell fibres have not been analysed neither in previous slice experiments nor in experiments here. It was shown recently that optogenetic selective excitation of commissural and associative glutamatergic fibres in slices result in different long-term plasticity results in postsynaptic CA1 pyramidal cells (Kohl et al., 2011). In interneurons there is no evidence that distinct afferent pathways in the same postsynaptic CA1 area cell would exhibit LTP or LTD, although distinct pharmacological features of LTP between afferent pathways have been reported in some interneurons (Walker et al., 2002, Le Roux et al., 2013).

I tested a hypothesis whether different brain state, defined as spontaneous postsynaptic cell firing level or LFP oscillation pattern, correlates with plasticity results. Yet, because in all studied PV+ cell types here these parameters were similar, I conclude that in the present experimental conditions these are unlikely to explain alternative expression of LTD or LTP in

interneurons. Whatever mechanism underlies the regulation or switch of long-term plasticity polarity in the excitatory synaptic inputs to PV+ cells in urethane anaesthetized rat hippocampus remains unknown. Experiments here show for the first time that in the intact brain the excitatory synaptic pathways exhibit LTP and LTD in specific interneuron types in parallel with LTP in CA1 area pyramidal cells. In addition to PV+ interneurons, I tested plasticity in four non-fast spiking CA1 interneurons. As far as my limited data pool allows interpretion, the results in these experiments give similar results to previous experiments in acute slice preparations. I identified an ivy cell with LTP-like potentiation *in vivo*. These cells have been reported to exhibit glutamatergic afferent LTP in slices (Szabo et al., 2012). However, like most non-fast spiking CA1 area interneurons studied in slice experiments, most regular-spiking interneurons studied *in vivo* here showed LTD (McBain and Kauer, 2009).

8.2. Functional implications of use-dependent LTP and LTD in excitatory input to interneurons

These findings show that activity patterns in excitatory hippocampal pathways that elicit LTP or LTD in CA1 area interneuron acute slice preparations, also generate changes in excitatory input strength to the same interneuron types *in vivo* in anaesthetized rat brain. However, an important question remains that what possibly is the role of these use-dependent plasticity contributes to function of the brain. Could similar use-dependent potentiation and

depression be triggered by intrinsic brain activities, and what role do these plastic changes play in the hippocampal function?

8.2.1. Possible role in hippocampus-based learning and spatial memory

A recent study from Dupret et al. (2013) demonstrated that when the hippocampus-based cognitive map of spatial memory is updated in a novel environment, establishment of new place cells is also associated with permanent changes in "causal" connectivity from CA1 area pyramidal cells to fast-spiking (putative PV+) interneurons. Although the major message of their study was to stress how cellular level place representations of old and new spatial information gradually fade and strengthen during the spatial learning process, they also made an additional, important and original discovery showing dynamic recruitment of interneurons during this process. Using tetrode recordings in combination with behavioural spatial learning tests in rats, the authors demonstrated that old and new place cells show some LTD or LTP – like permanent depression or potentiation of fast-spiking interneurons in correlative pre-and-post spike coupling during the learning process. The authors also report that newly-formed place cells can either increase or decrease their causally-related spike coupling to interneurons. Although they were unable to identify the fast-spiking CA1 interneuron types in these plasticity processes because they used tetrode recordings, the results show for the first time that a specific type of learning and storage of new memories in the hippocampal CA1

area is associated with long-term changes in connectivity between the presynaptic excitatory neuron and its postsynaptic interneuron.

Such changes could be interpreted in many ways. One possible explanation is that learning-associated firing of hippocampal neurons and novel place cell formation in the CA1 area drives long-term plasticity in synaptic connections from the excitatory pyramidal cells to fast-spiking interneurons (Kullmann and Lamsa, 2007). My findings presented here support this hypothesis showing that such LTP and LTD-like long-term potentiation in excitatory connections to these (fast-spiking) interneurons is possible and indeed readily takes place in the intact brain hippocampal CA1 area.

How would pyramidal – interneuron plasticity be relevant to learning and memory? For the time being this remains unknown. However, as previous work on acute slice preparations demonstrated, the plasticity of inhibitory neuron input-output transformation regulates CA1 pyramidal cell input integration (Pouille and Scanziani, 2001). Slice experiments have shown that parallel potentiation of feed-forward inhibition with LTP in glutamatergic synapses is required to maintain fast input-output transformation in CA1 pyramidal cells. In other words, plasticity in interneurons demonstrated here for the first time *in vivo*, is theoretically capable of regulating a temporal resolution of pyramidal cells input-output function (Lamsa et al., 2005). Thus, through interneuron LTP and LTD, the CA1 pyramidal cells can regulate temporal windows to sum up EPSPs for spike generation in their mutual communication, a

feature which can be important in coordination of firing in place cell combinations that discharge coherently in special locations of the hippocampus-based spatial cognitive map (O'Keefe and Nadel, 1978).

8.2.2. Interneuron LTP and LTD in pathological processes

In addition to specific physiological roles, activity-induced permanent changes in synapses that drive inhibitory interneuron activity can be triggered in pathological processes. Experimental disease models in rodents suggest that excitatory synapses in interneurons undergo long-term changes in conditions with non-physiological synchronous activity (Jefferys, 2014). Epileptogenesis is associated with a gradually developing an imbalance between neuronal excitation and inhibition, and the progression of spontaneous hypersynchronous discharges that also cause cell death (Whittington et al., 1995, Bragin et al., 2000). The progression of epilepsy can be partly explained by the activation of synaptic plasticity mechanisms such as NMDAR-dependent LTP in pyramidal cells, it evolved to be recruited by relevant physiological activity patterns, but hijacked by epileptiform bursts. The LTP and LTD- like plasticity in excitatory connections to hippocampal inhibitory interneurons can potentiate and depress local inhibition during epileptogenesis. Given that high-frequency stimulation patterns of excitatory axons here resulted in a long-term changes in recruitment of CA1 area interneurons in anaesthetized rat brain, it is likely that similar

changes occur at some stage in hippocampus showing epileptic activity (Jefferys, 2014). Given that most known interneuron LTP and LTD forms are independent of NMDARs and require mGluRs and the transcription factor CREB1 (Ran et al., 2012), it might be possible to study the effect of the interneuron plasticity in the progression of epilepsy in animal models using genetic manipulations that ablate LTP and LTD specifically in fast-spiking PV+ interneurons (see 8.4.).

Moreover, alterations in inhibitory interneuron function have been recently associated with neuropsychiatric diseases (Lewis et al., 2005, Benini and Avoli, 2006, Lodge et al., 2009, Belforte et al., 2010, Pavlov et al., 2011, Rotaru et al., 2011, Lewis et al., 2012, Krook-Magnuson et al., 2013, Liu et al., 2013, Pavlov and Walker, 2013). An emerging hypothesis suggests that abnormal development of inhibitory GABAergic interneurons could lead to a dysfunctional rhythmogenetic cortical clockwork, causing disruptions in coordinated interneuron activity and resulting in cognitive impairment (Buzsaki et al., 1983, Blatow et al., 2003, Vierling-Claassen et al., 2010, Allene et al., 2012). Such changes could be reflected only as subtle changes in cortical EEG. Neurological or neuropsychiatric symptoms emerge from the developmental disorder of inhibitory interneurons have given rise to the term "interneuronopathy". In this case a developmental failure in long-term plasticity in pyramidal cell - interneuron connectivity represents one possible mechanism for an interneuronpathy and behavioural symptoms (see Chapter 8.4.).

8.3. Other mechanisms contributing to long-term changes in CA1 interneurons input-output function

Although synaptic long-term plasticity in excitatory afferents onto PV+ CA1 interneurons offers a good candidate mechanism to explain the activity-induced potentiation and depression of excitatory connections to these cells as reported here, other mechanism can be involved in the observed changes. Experiments on hippocampal slice preparations have demonstrated that high-frequency local stimulation can also result in an increase in intrinsic excitability of interneurons (Ross and Soltesz, 2001, Campanac et al., 2013). In parallel with activity-induced LTP of the excitatory synaptic current, the postsynaptic cell input resistance can increase through alteration in K+ channel-mediated conductance in CA1 area PV+ cells (Campanac et al., 2013). This change is mediated via mGluR5 activation and it is caused by down regulation of Kv1 channel activity. A similar increase in input resistance has been reported in interneurons in the dentate gyrus, which exhibit increased input resistance following high-frequency local stimulation with a stimulation electrode (Ross and Soltesz, 2001). However it is noteworthy that in hippocampal slice experiments electrical stimulation is usually located close to the recording site and it is unclear to what extent direct electrical stimulation of postsynaptic cells and neighboring glial cells contribute to the changes observed. One advantage of our experimental design with stimulation from the contralateral site is that it avoids non-synaptic effects of electrical stimulation. However, at this stage I am unable to measure intrinsic excitability and its contribution to induced postsynaptic spike probability changes in the *in vivo* experiments. Increased membrane resistance is always

associated with the elongation of the membrane time constant, which would lengthen the synaptic delay in the potentiated synapses, and shortening in the depressed synapses. However, my experiments did not show such a relationship between evoked spike probability and delay. These findings suggested that the activity-induced input resistance changes in the recorded cells are not responsible for the effects demonstrated. One potential mechanism that can also increase evoked postsynaptic spike probability is polysynaptic LTP between glutamatergic synapses of pyramidal cells. This has been commonly reported in hippocampal CA3 associative circuitry by high-frequency stimulation (Maccaferri et al., 1998). However, this is unlikely to explain the plasticity of evoked spike probability detected in the 13 experiments in this study (one studied cell failed to show plasticity), since in most of these postsynaptic neurons the probability change was associated with no change or a negligible change in spike delay. In addition, in all experiments cycle-by-cycle variation of the evoked spike delay remained similar to baseline while evoked probability changed. These results indicate spike generation by monosynaptic rather than polysynaptic EPSPs. Polysynaptically evoked spikes are characteristically associated with large cycle-by-cycle variation in (poly)synaptic delay, and a probability decrease (e.g. by reduced stimulation intensity) substantially increases a delay and its cycle-by-cycle variation (Deadwyler et al., 1975, Berry and Pentreath, 1976, Andersen et al., 2000).

8.4. Future directions

Although possible roles of use-dependent LTP and LTD in hippocampal PV+ interneuron excitatory afferents has been speculated here, direct evidence for their contribution to behaviour and behaviour-associated electrical activity would be required to judge their relevance in hippocampal function. One exciting and realistic approach is to use knock-down of critical genes or proteins specifically involved in the interneurons plasticity. *In vitro* studies in CA1 area interneurons have revealed specific genes and gene products critical for LTP and LTD in the CA1area interneurons (Lamsa et al., 2007a, Ran et al., 2012, Le Roux et al., 2013, Camire and Topolnik, 2014).

1) Metabotropic glutamate group I receptors mGluR1 and mGluR5 would provide a useful target for suppression or prevention of LTP and LTD in most CA1 interneurons (Perez et al., 2001, Le Duigou et al., 2011, Le Duigou and Kullmann, 2011, Campanac et al., 2013). Silencing critical genes with oliginucleotide antisense specifically in CA1 area interneurons using adeno-associated virus transduction and Cre-LoxP-dependent expression in Cre-expressing cells could be used to reveal a role of specific interneuron subpopulation plasticity in learning indexed by relevant behavioural tests (Dupret et al., 2013).

2) In addition, a recent publication reported that interneuron LTP consolidation requires activation of transcription factor cyclic-AMP response element-binding protein (CREB) (Ran et al., 2012), and targeted knock-down of CREB1 gene or its product, using a similar strategy as described above, would elucidate a role of interneurons long-term plasticity in behavioural studies.

In addition, intracellular recordings from interneurons *in vivo* are needed to confirm LTP and LTD in synaptic excitatory inputs to PV+ interneurons. Such experiments could be most practically done in the CA1 area neurons using sharp electrode recordings, which easily penetrate through an overlaying neocortical mantle without causing prominent damage and compression of tissue. However the yield of such experiments from identified PV+ interneurons with long-term stability is expected to be relatively low.

Finally, certain differences in plasticity experiments between experiments *in vitro* and *in vivo* require explanation. Analyses of hippocampal brain state and hippocampal neurons spontaneous firing level failed to explain induction of LTP or LTD in PV+ interneurons. My favourite hypothesis to explain the plasticity difference here and *in vitro* experiments is activation of distinct anatomical pathways with different plasticity properties and selectivity to cannabinoid receptors in these experiments (Peterfi et al., 2012). Plasticity in associative and commissural pathways can be studied using selective optogenetic stimulation of contra-

or ipsilateral CA3 pyramidal cells transduced with the channelrhodopsin gene, and fibres tested for plasticity in *in vitro* slice preparation (Kohl et al., 2011).

8.5. Final conclusions

The results of this thesis demonstrated that specific CA1 area interneuron types, in particular those expressing PV, exhibited use-dependent long-term plasticity in their afferent excitatory glutamatergic fibres. The results were in line with earlier experiments in hippocampal brain slices, but also showed some novel features of the plasticity in the intact brain. *In vivo* experiments confirmed that PV+ basket cells in the intact brain can undergo LTD and a bistratified cell expressed LTP in response to the same afferent stimulations. Similar LTP was observed in a regular-spiking identified ivy cell similar to the results in brain slices. Similar to the results shown in slice recordings, most non-fast spiking interneurons here show LTD. Bidirectional modulation of synaptic strength in neuronal circuits is expected. Long-term plasticity experiments with identified pyramidal cells demonstrate that the experimental configuration provides a stable paradigm to measure synaptic excitatory pathway plasticity in dorsal hippocampal CA1 area identified neurons *in vivo*.

9. Reference

Allene C, Picardo MA, Becq H, Miyoshi G, Fishell G, Cossart R (2012) Dynamic changes in interneuron morphophysiological properties mark the maturation of hippocampal network activity. The Journal of neuroscience : the official journal of the Society for Neuroscience 32:6688-6698.

Andersen P, Morris RG, Amaral DG, Bliss T, O'Keefe J (2007) The hippocampus book. Oxford ; New York: Oxford University Press.

Andersen P, Soleng AF, Raastad M (2000) The hippocampal lamella hypothesis revisited. Brain research 886:165-171.

Armstrong C, Krook-Magnuson E, Soltesz I (2012) Neurogliaform and Ivy Cells: A Major Family of nNOS Expressing GABAergic Neurons. Frontiers in neural circuits 6:23.

Belforte JE, Zsiros V, Sklar ER, Jiang Z, Yu G, Li Y, Quinlan EM, Nakazawa K (2010) Postnatal NMDA receptor ablation in corticolimbic interneurons confers schizophrenia-like phenotypes. Nature neuroscience 13:76-83.

Benini R, Avoli M (2006) Altered inhibition in lateral amygdala networks in a rat model of temporal lobe epilepsy. Journal of neurophysiology 95:2143-2154.

Berry MS, Pentreath VW (1976) Criteria for distinguishing between monosynaptic and polysynaptic transmission. Brain research 105:1-20.

Bezaire MJ, Soltesz I (2013) Quantitative assessment of CA1 local circuits: knowledge base for interneuron-pyramidal cell connectivity. Hippocampus 23:751-785.

Blackstad TW (1956) Commissural connections of the hippocampal region in the rat, with special reference to their mode of termination. The Journal of comparative neurology 105:417-537.

Blatow M, Rozov A, Katona I, Hormuzdi SG, Meyer AH, Whittington MA, Caputi A, Monyer H (2003) A novel network of multipolar bursting interneurons generates theta frequency oscillations in neocortex. Neuron 38:805-817.

Bliss TV, Lomo T (1973) Long-lasting potentiation of synaptic transmission in the dentate area of the anaesthetized rabbit following stimulation of the perforant path. The Journal of physiology 232:331-356.

Bodor AL, Katona I, Nyiri G, Mackie K, Ledent C, Hajos N, Freund TF (2005) Endocannabinoid signaling in rat somatosensory cortex: laminar differences and involvement of specific interneuron types. The Journal of neuroscience : the official journal of the Society for Neuroscience 25:6845-6856.

Bragin A, Wilson CL, Engel J, Jr. (2000) Chronic epileptogenesis requires development of a network of pathologically interconnected neuron clusters: a hypothesis. Epilepsia 41 Suppl 6:S144-152.

Brown TE, Chirila AM, Schrank BR, Kauer JA (2013) Loss of interneuron LTD and attenuated pyramidal cell LTP in Trpv1 and Trpv3 KO mice. Hippocampus 23:662-671.

Buchanan KA, Blackman AV, Moreau AW, Elgar D, Costa RP, Lalanne T, Tudor Jones AA, Oyrer J, Sjostrom PJ (2012) Target-specific expression of presynaptic NMDA receptors in neocortical microcircuits. Neuron 75:451-466.

Buzsáki (2003) Hippocampal network patterns of activity in the mouse.

Buzsaki G (1998) Memory consolidation during sleep: a neurophysiological perspective. Journal of sleep research 7 Suppl 1:17-23.

Buzsaki G (2005) Theta rhythm of navigation: link between path integration and landmark navigation, episodic and semantic memory. Hippocampus 15:827-840.

Buzsaki G, Eidelberg E (1982a) Convergence of Associational and Commissural Pathways on Ca1 Pyramidal Cells of the Rat Hippocampus. Brain research 237:283-295.

Buzsaki G, Eidelberg E (1982b) Direct afferent excitation and long-term potentiation of hippocampal interneurons. Journal of neurophysiology 48:597-607.

Buzsaki G, Leung LW, Vanderwolf CH (1983) Cellular bases of hippocampal EEG in the behaving rat. Brain research 287:139-171.

Camire O, Topolnik L (2014) Dendritic calcium nonlinearities switch the direction of synaptic plasticity in fast-spiking interneurons. The Journal of neuroscience : the official journal of the Society for Neuroscience 34:3864-3877.

Campanac E, Gasselin C, Baude A, Rama S, Ankri N, Debanne D (2013) Enhanced intrinsic excitability in basket cells maintains excitatory-inhibitory balance in hippocampal circuits. Neuron 77:712-722.

Chrobak JJ, Buzsaki G (1996) High-frequency oscillations in the output networks of the hippocampal-entorhinal axis of the freely behaving rat. The Journal of neuroscience : the official journal of the Society for Neuroscience 16:3056-3066.

Chrobak JJ, Buzsaki G (1998) Gamma oscillations in the entorhinal cortex of the freely behaving rat. The Journal of neuroscience : the official journal of the Society for Neuroscience 18:388-398.

Csicsvari J, Hirase H, Czurko A, Mamiya A, Buzsaki G (1999) Oscillatory coupling of hippocampal pyramidal cells and interneurons in the behaving Rat. The Journal of neuroscience : the official journal of the Society for Neuroscience 19:274-287.

Deadwyler SA, West JR, Cotman CW, Lynch G (1975) Physiological studies of the reciprocal connections between the hippocampus and entorhinal cortex. Experimental neurology 49:35-57.

Debanne D, Gahwiler BH, Thompson SM (1998) Long-term synaptic plasticity between pairs of individual CA3 pyramidal cells in rat hippocampal slice cultures. J Physiol-London 507:237-247.

Dupret D, O'Neill J, Csicsvari J (2013) Dynamic reconfiguration of hippocampal interneuron circuits during spatial learning. Neuron 78:166-180.

Edwards JG, Gibson HE, Jensen T, Nugent F, Walther C, Blickenstaff J, Kauer JA (2012) A novel non-CB1/TRPV1 endocannabinoid-mediated mechanism depresses excitatory synapses on hippocampal CA1 interneurons. Hippocampus 22:209-221.

Fonseca R, Nagerl UV, Morris RG, Bonhoeffer T (2004) Competing for memory: hippocampal LTP under regimes of reduced protein synthesis. Neuron 44:1011-1020.

Freund TF, Buzsaki G (1996) Interneurons of the hippocampus. Hippocampus 6:347-470.

Frey U, Morris RG (1997) Synaptic tagging and long-term potentiation. Nature 385:533-536.

Fuentealba P, Begum R, Capogna M, Jinno S, Marton LF, Csicsvari J, Thomson A, Somogyi P, Klausberger T (2008) Ivy cells: a population of nitric-oxide-producing, slow-spiking GABAergic neurons and their involvement in hippocampal network activity. Neuron 57:917-929.

Galvan EJ, Cosgrove KE, Barrionuevo G (2011) Multiple forms of long-term synaptic plasticity at hippocampal mossy fiber synapses on interneurons. Neuropharmacology 60:740-747.

Hajos N, Ellender TJ, Zemankovics R, Mann EO, Exley R, Cragg SJ, Freund TF, Paulsen O (2009) Maintaining network activity in submerged hippocampal slices: importance of oxygen supply. The European journal of neuroscience 29:319-327.

Hara K, Harris RA (2002) The anesthetic mechanism of urethane: the effects on neurotransmitter-gated ion channels. Anesthesia and analgesia 94:313-318, table of contents.

Hebb DO (1949) The organization of behavior; a neuropsychological theory. New York,: Wiley.

Hu H, Gan J, Jonas P (2014) Interneurons. Fast-spiking, parvalbumin(+) GABAergic interneurons: from cellular design to microcircuit function. Science 345:1255263.

Isaac JT, Hjelmstad GO, Nicoll RA, Malenka RC (1996) Long-term potentiation at single fiber inputs to hippocampal CA1 pyramidal cells. Proceedings of the National Academy of Sciences of the United States of America 93:8710-8715.

Jefferys JG (2014) Are changes in synaptic function that underlie hyperexcitability responsible for seizure activity? Advances in experimental medicine and biology 813:185-194.

Katona I, Freund TF (2008) Endocannabinoid signaling as a synaptic circuit breaker in neurological disease. Nature medicine 14:923-930.

Klausberger T, Magill PJ, Marton LF, Roberts JD, Cobden PM, Buzsaki G, Somogyi P (2003) Brain-state- and cell-type-specific firing of hippocampal interneurons in vivo. Nature 421:844-848.

Klausberger T, Marton LF, Baude A, Roberts JD, Magill PJ, Somogyi P (2004) Spike timing of dendrite-targeting bistratified cells during hippocampal network oscillations in vivo. Nature neuroscience 7:41-47.

Klausberger T, Marton LF, O'Neill J, Huck JH, Dalezios Y, Fuentealba P, Suen WY, Papp E, Kaneko T, Watanabe M, Csicsvari J, Somogyi P (2005) Complementary roles of cholecystokinin- and parvalbumin-expressing GABAergic neurons in hippocampal network oscillations. The Journal of neuroscience : the official journal of the Society for Neuroscience 25:9782-9793.

Kohl MM, Shipton OA, Deacon RM, Rawlins JN, Deisseroth K, Paulsen O (2011) Hemisphere-specific optogenetic stimulation reveals left-right asymmetry of hippocampal plasticity. Nature neuroscience 14:1413-1415.

Krook-Magnuson E, Armstrong C, Oijala M, Soltesz I (2013) On-demand optogenetic control of spontaneous seizures in temporal lobe epilepsy. Nature communications 4:1376.

Kullmann DM, Lamsa KP (2007) Long-term synaptic plasticity in hippocampal interneurons. Nature reviews Neuroscience 8:687-699.

Kullmann DM, Lamsa KP (2011) LTP and LTD in cortical GABAergic interneurons: emerging rules and roles. Neuropharmacology 60:712-719.

Lamsa K, Heeroma JH, Kullmann DM (2005) Hebbian LTP in feed-forward inhibitory interneurons and the temporal fidelity of input discrimination. Nature neuroscience 8:916-924.

Lamsa K, Irvine EE, Giese KP, Kullmann DM (2007a) NMDA receptor-dependent long-term potentiation in mouse hippocampal interneurons shows a unique dependence on Ca(2+)/calmodulin-dependent kinases. The Journal of physiology 584:885-894.

Lamsa KP, Heeroma JH, Somogyi P, Rusakov DA, Kullmann DM (2007b) Anti-Hebbian long-term potentiation in the hippocampal feedback inhibitory circuit. Science 315:1262-1266.

Lapray D, Lasztoczi B, Lagler M, Viney TJ, Katona L, Valenti O, Hartwich K, Borhegyi Z, Somogyi P, Klausberger T (2012) Behavior-dependent specialization of identified hippocampal interneurons. Nature neuroscience 15:1265-1271.

Le Duigou C, Holden T, Kullmann DM (2011) Short- and long-term depression at glutamatergic synapses on hippocampal interneurons by group I mGluR activation. Neuropharmacology 60:748-756.

Le Duigou C, Kullmann DM (2011) Group I mGluR agonist-evoked long-term potentiation in hippocampal oriens interneurons. The Journal of neuroscience : the official journal of the Society for Neuroscience 31:5777-5781.

Le Roux N, Cabezas C, Bohm UL, Poncer JC (2013) Input-specific learning rules at excitatory synapses onto hippocampal parvalbumin-expressing interneurons. The Journal of physiology 591:1809-1822.

Lewis DA, Curley AA, Glausier JR, Volk DW (2012) Cortical parvalbumin interneurons and cognitive dysfunction in schizophrenia. Trends in neurosciences 35:57-67.

Lewis DA, Hashimoto T, Volk DW (2005) Cortical inhibitory neurons and schizophrenia. Nature reviews Neuroscience 6:312-324.

Liu G, Gu B, He XP, Joshi RB, Wackerle HD, Rodriguiz RM, Wetsel WC, McNamara JO (2013) Transient inhibition of TrkB kinase after status epilepticus prevents development of temporal lobe epilepsy. Neuron 79:31-38.

Lodge DJ, Behrens MM, Grace AA (2009) A loss of parvalbumin-containing interneurons is associated with diminished oscillatory activity in an animal model of schizophrenia. The Journal of neuroscience : the official journal of the Society for Neuroscience 29:2344-2354.

Maccaferri G, Toth K, McBain CJ (1998) Target-specific expression of presynaptic mossy fiber plasticity. Science 279:1368-1370.

McBain CJ, Kauer JA (2009) Presynaptic plasticity: targeted control of inhibitory networks. Current opinion in neurobiology 19:254-262.

Mcnaughton BL, Douglas RM, Goddard GV (1978) Synaptic Enhancement in Fascia Dentata - Cooperativity among Coactive Afferents. Brain research 157:277-293.

Morgan CJ, Mofeez A, Brandner B, Bromley L, Curran HV (2004) Acute effects of ketamine on memory systems and psychotic symptoms in healthy volunteers. Neuropsychopharmacology : official publication of the American College of Neuropsychopharmacology 29:208-218.

Morino P, Herrera-Marschitz M, Castel MN, Ungerstedt U, Varro A, Dockray G, Hokfelt T (1994) Cholecystokinin in cortico-striatal neurons in the rat: immunohistochemical studies at the light and electron microscopical level. The European journal of neuroscience 6:681-692.

Nissen W, Szabo A, Somogyi J, Somogyi P, Lamsa KP (2010) Cell type-specific long-term plasticity at glutamatergic synapses onto hippocampal interneurons expressing either parvalbumin or CB1 cannabinoid receptor. The Journal of neuroscience : the official journal of the Society for Neuroscience 30:1337-1347.

O'Keefe J, Nadel L (1978) The hippocampus as a cognitive map. Oxford New York: Oxford University Press.

Ognjanovski N, Maruyama D, Lashner N, Zochowski M, Aton SJ (2014) CA1 hippocampal network activity changes during sleep-dependent memory consolidation. Frontiers in systems neuroscience 8:61.

Park P, Volianskis A, Sanderson TM, Bortolotto ZA, Jane DE, Zhuo M, Kaang BK, Collingridge GL (2014) NMDA receptor-dependent long-term potentiation comprises a family of temporally overlapping forms of synaptic plasticity that are induced by different patterns of stimulation. Philosophical transactions of the Royal Society of London Series B, Biological sciences 369:20130131.

Pavlov I, Huusko N, Drexel M, Kirchmair E, Sperk G, Pitkanen A, Walker MC (2011) Progressive loss of phasic, but not tonic, GABAA receptor-mediated inhibition in dentate granule cells in a model of post-traumatic epilepsy in rats. Neuroscience 194:208-219.

Pavlov I, Walker MC (2013) Tonic GABA(A) receptor-mediated signalling in temporal lobe epilepsy. Neuropharmacology 69:55-61.

Pelletier JG, Lacaille JC (2008) Long-term synaptic plasticity in hippocampal feedback inhibitory networks. Progress in brain research 169:241-250.

Perez Y, Morin F, Lacaille JC (2001) A hebbian form of long-term potentiation dependent on mGluR1a in hippocampal inhibitory interneurons. Proceedings of the National Academy of Sciences of the United States of America 98:9401-9406.

Peterfi Z, Urban GM, Papp OI, Nemeth B, Monyer H, Szabo G, Erdelyi F, Mackie K, Freund TF, Hajos N, Katona I (2012) Endocannabinoid-mediated long-term depression of afferent excitatory synapses in hippocampal pyramidal cells and GABAergic interneurons. The Journal of neuroscience : the official journal of the Society for Neuroscience 32:14448-14463.

Poncer JC, Shinozaki H, Miles R (1995) Dual modulation of synaptic inhibition by distinct metabotropic glutamate receptors in the rat hippocampus. The Journal of physiology 485 (Pt 1):121-134.

Popa D, Duvarci S, Popescu AT, Lena C, Pare D (2010) Coherent amygdalocortical theta promotes fear memory consolidation during paradoxical sleep. Proceedings of the National Academy of Sciences of the United States of America 107:6516-6519.

Pouille F, Scanziani M (2001) Enforcement of temporal fidelity in pyramidal cells by somatic feed-forward inhibition. Science 293:1159-1163.

Ran I, Laplante I, Lacaille JC (2012) CREB-dependent transcriptional control and quantal changes in persistent long-term potentiation in hippocampal interneurons. The Journal of neuroscience : the official journal of the Society for Neuroscience 32:6335-6350.

Reiner M, Rozengurt R, Barnea A (2014) Better than sleep: theta neurofeedback training accelerates memory consolidation. Biological psychology 95:45-53.

Ross ST, Soltesz I (2001) Long-term plasticity in interneurons of the dentate gyrus. Proceedings of the National Academy of Sciences of the United States of America 98:8874-8879.

Rotaru DC, Yoshino H, Lewis DA, Ermentrout GB, Gonzalez-Burgos G (2011) Glutamate receptor subtypes mediating synaptic activation of prefrontal cortex neurons: relevance for schizophrenia. The Journal of neuroscience : the official journal of the Society for Neuroscience 31:142-156.

Salami M, Fathollahi Y, Esteky H, Motamedi F, Atapour N (2000) Effects of ketamine on synaptic transmission and long-term potentiation in layer II/III of rat visual cortex in vitro. European journal of pharmacology 390:287-293.

Sambandan S, Sauer JF, Vida I, Bartos M (2010) Associative plasticity at excitatory synapses facilitates recruitment of fast-spiking interneurons in the dentate gyrus. The Journal of neuroscience : the official journal of the Society for Neuroscience 30:11826-11837.

Shepherd GM, Grillner S (2010) Handbook of brain microcircuits. New York: Oxford University Press.

Soltesz I, Deschenes M (1993) Low- and high-frequency membrane potential oscillations during theta activity in CA1 and CA3 pyramidal neurons of the rat hippocampus under ketamine-xylazine anesthesia. Journal of neurophysiology 70:97-116.

Somogyi J, Szabo A, Somogyi P, Lamsa K (2012) Molecular analysis of ivy cells of the hippocampal CA1 stratum radiatum using spectral identification of immunofluorophores. Frontiers in neural circuits 6:35.

Somogyi P, Klausberger T (2005) Defined types of cortical interneurone structure space and spike timing in the hippocampus. The Journal of physiology 562:9-26.

Szabo A, Somogyi J, Cauli B, Lambolez B, Somogyi P, Lamsa KP (2012) Calcium-permeable AMPA receptors provide a common mechanism for LTP in glutamatergic synapses of distinct hippocampal interneuron types. The Journal of neuroscience : the official journal of the Society for Neuroscience 32:6511-6516.

Vanderwolf CH (1988) Cerebral activity and behavior: control by central cholinergic and serotonergic systems. International review of neurobiology 30:225-340.

Vierling-Claassen D, Cardin JA, Moore CI, Jones SR (2010) Computational modeling of distinct neocortical oscillations driven by cell-type selective optogenetic drive: separable resonant circuits controlled by low-threshold spiking and fast-spiking interneurons. Frontiers in human neuroscience 4:198.

Viney TJ, Lasztoczi B, Katona L, Crump MG, Tukker JJ, Klausberger T, Somogyi P (2013) Network state-dependent inhibition of identified hippocampal CA3 axo-axonic cells in vivo. Nature neuroscience 16:1802-1811.

Walker HC, Lawrence JJ, McBain CJ (2002) Activation of kinetically distinct synaptic conductances on inhibitory interneurons by electrotonically overlapping afferents. Neuron 35:161-171.

Whittington MA, Traub RD, Jefferys JG (1995) Synchronized oscillations in interneuron networks driven by metabotropic glutamate receptor activation. Nature 373:612-615.

Witter MP (2007) Intrinsic and extrinsic wiring of CA3: indications for connectional heterogeneity. Learning & memory 14:705-713.

Yamakura T, Mori H, Masaki H, Shimoji K, Mishina M (1993) Different sensitivities of NMDA receptor channel subtypes to non-competitive antagonists. Neuroreport 4:687-690.